SLAC-340
UC-28
(A)

OPTICAL TUNING IN THE ARCS AND FINAL FOCUS SECTIONS OF THE STANFORD LINEAR COLLIDER*

Philip Sébastien Bambade

Stanford Linear Accelerator Center
Stanford University
Stanford, California 94309

March 1989

Prepared for the Department of Energy
under contract number DE-AC03-76SF00515

Printed in the United States of America. Available from the National Technical Information Service, U.S. Department of Commerce, 5285 Port Royal Road, Springfield, Virginia 22161. Price: Printed Copy A08, Microfiche A01.

* Ph.D. thesis.

OPTICAL TUNING OF THE ARCS AND FINAL FOCUS SECTION OF THE STANFORD LINEAR COLLIDER (SLC)

In this thesis, we present the experimental tuning procedures developed for the Arcs and for the Final Focus Section of the Stanford Linear Collider (SLC). Such tuning is necessary to maximize the luminosity, by minimizing the beam size at the interaction point, and to reduce backgrounds in the experiment.

In the final Focus Section, the correction strategy must result from the principles of the optical design, which is based on cancellations between second order aberrations, and on the ability to measure micron-size beams typical of the SLC.

In the Arcs, the corrections were designed after the initial commissioning, to make the system more error-tolerant, through a modification in the optical design, and to enable adjustments of the beam phase-space at the injection to the Final Focus System, through a harmonic perturbation technique inspired from circular accelerators. Although the overall optimization of the SLC is not entirely finished, an almost optimal set-up has been achieved for the optics of the Arcs and of the Final Focus Section.

Beams with transverse sizes close to the nominal ones, of a few microns, have been obtained at the interaction point. We present and discuss our results and the optical limits to the present performance.

ACKNOWLEDGEMENTS

I would first like to warmly thank my third cycle thesis advisor, Jean Buon, who encouraged and helped me to get into the fascinating field of accelerator physics.

After my third cycle thesis, I had the opportunity to work on part of the design and commissioning of the first linear collider for high energy physics, at SLAC, Stanford, and clearly, it is SLAC, for its hospitality during my years as a visiting physicist, and my friends and colleagues, whom I want to thank the most. These four years were both extremely exciting and interesting.

Among the numerous people whom I worked and interacted with, I would like to thank especially Burt Richter and Rae Stiening, who encouraged me and made me work hard, Karl Brown, Andrew Hutton, Witold Kozanecki, David Ritson, and Nobu Toge, with whom I had the opportunity to collaborate, and from whom I learned an enormous amount, and the many physicists and engineers working on the SLC.

I present this thesis on the methods which we developed to commission a part of this new machine: the arcs and the final focus section. At the beginning of my stay at SLAC, and during most of my work, the lack of documentation resulting from our hectic schedules was often a big impediment. One of the motivations of my thesis is to contribute to this documentation.

Jacques Haïssinski has accepted to direct my work from Orsay, and his advise on the organization and writing of the manuscript was of great help to me. During his stay at SLAC, we also had the opportunity to be "on shift" together. The clarity of his thinking and his enthousiasm were often a guide for me. I would like to express all my gratefullness to him.

I would also like to thank Michel Davier for having presided my thesis committee, Karl Brown and Wolfgang Schnell for having travelled to be part of it, respectively from Stanford and from Genève, and Jean Buon and Bernard Grossetête, also for being part of it.

Finally, I am very grateful to Jocelyne Brosselard, Nicole Mathieu, and Annie Pottier, from the scientific secretariat, for their efficient help in putting my thesis together, Bruno Mazoyer, for his help on the figures, Alain Coueslan and Jacques Pennec, for the speed at which they got it printed.

Table of Contents

IV. SLC TURN-ON PROGRAM

V. OVERVIEW OF OPTICAL TUNING IN THE ARCS AND FINAL FOCUS

VI. REPORTS AND PUBLICATIONS ON OPTICAL CORRECTIONS IN THE ARCS

VII. REPORTS AND PUBLICATIONS ON OPTICAL CORRECTIONS IN THE FINAL FOCUS

List of Figures

List of Tables

I. INTRODUCTION

I.1 LINEAR COLLIDER APPROACH AND BASIC NOTIONS

In the past twenty years, electron-positron colliders have established themselves as powerful tools for studying high-energy particle physics.

Until now, electrons and positrons have been collided by confining particle bunches in storage rings. This approach can however not be extrapolated as desired to very high energy because of the rapid increase in synchrotron radiation emitted in the bending magnets. The energy loss per turn to synchrotron radiation scales as E^4/R, where E is the beam energy and where R is the average radius of the storage ring. It can be shown[1] that because of this, both the size and the cost of a storage ring with an optimized design scale as E^2. This law is illustrated in Fig. 1, where the average radius of most electron-positron storage rings is shown as a function of their energy.

An alternate method for producing electron-positron collisions consists of colliding beams of two opposed linear accelerators[2]. In this case there is no significant synchrotron radiation except in the vicinity of the collision point, and thus more favorable scaling with energy may be possible.

In order to be a useful tool for particle physics, an electron-positron collider must in addition to high energy also provide high luminosity - or event rate for a process with unit cross-section. The luminosity can be expressed as a function of the frequency of the collisions f, the number of particles per bunch N, and the effective transverse area A over which the collisions take place:

$$\mathcal{L} = \frac{fN^2}{A}. \tag{1}$$

Present technology limits the repetition rate of linear accelerators to a few hundred Hz. This is much less than the frequencies of several hundred KHz at which bunches circulate in typical storage rings. Also, the bunch population is usually higher in a storage ring than in a linear accelerator. In order to reach comparable or higher luminosity, the transverse area of the beams at the collision point of a linear collider must be made substantially smaller than that typical of storage rings*.

The collision point area A is conveniently expressed as a function of ϵ, the transverse emittance of the beam, defined as the area of the phase-space occupied by the particles divided by π, and of β^*, which we define as the second moment of the transverse particle distribution at the collision point normalized to this emittance*. If these two parameters

---

* *Stronger space-charge effects arise in the collision of beams with very small areas, but the resulting disruption to the particle trajectories is not as severe a limitation as in storage rings since the beams of linear colliders are not saved for future collisions after each crossing.*

* *The β-parameters of a beam imaged through a focusing array can more generally be interpreted*

are the same in each transverse plane, one obtains for A[3]:

$$A = 4\pi\beta^*\epsilon. \tag{2}$$

The factor 4 in (2) arises through the overlap of the particle distributions, assumed to be gaussian in this calculation.

To produce a small interaction area A, both the emittance and the β^*-parameter must be small. The emittance can only be made small at the source, or through radiation damping, which can be used to cool the beams in a dedicated storage ring. Such a storage is referred to as a "damping ring". The β^*-parameter can only be reduced by focusing the beam to the smallest possible size. This is achieved in a dedicated optical system immediately upstream of the collision point, which must in general be corrected for chromatic aberrations. This optical system is referred to as a "final focus system".

Besides the basic design of the components of a linear collider, the handling of imperfections in the long open structure involved presents conceptually new problems. Such handling must be folded into both the detailed design of the individual components and into the overall system optimization. Considerable effort is in fact required at several stages of the system to preserve the carefully damped emittance and to precisely monitor and control beam parameters. Both are necessary conditions for the final focusing to work properly and to minimize backgrounds in the experimental apparatus from secondaries produced by the beam halo and by the tails which are typical of linear accelerators. Solving such issues at reasonable cost appears to be a crucial element in the development of linear colliders which must be factored into basic scaling and feasibility arguments.

I.2 THE STANFORD LINEAR COLLIDER

The Stanford Linear Collider (SLC) is the first linear collider presently operating. It was conceived and built with the double motivation of[4]:

1. Producing high luminosity electron-positron collisions with a center of mass energy of about 92 GeV, to study the physics of the intermediate vector boson Z^0.

2. Providing the first practical test of the linear collider approach towards high energy electron-positron machines.

A schematic of the SLC is shown in Fig. 2. In the case of the SLC, one single linear accelerator - the Stanford linear accelerator - is used rather than two opposing systems

---

as the values taken by an envelope function $\beta(s)$. This function describes the evolution through the array of the square of the beam size corresponding to a phase-space with emittance unity. More on the correspondance between these two definitions can be found in section VI.1

as was described in I.1, to accelerate both electron and positron beams. The beams are then aimed into collision by means of two arcs. The collision point beam size required to achieve significant luminosity is nominally a few microns.

More specifically, at the begining of each cycle, two electron bunches are generated and co-accelerated to 1.116 GeV in the injector and in the first sector of the linear accelerator[5]. At 200 MeV, they are joined by a positron bunch. The three are then injected for cooling into two damping rings[6], from which they are extracted before the next linac pulse. They are then reinjected into the linear accelerator and co-accelerated up to energies of 50 GeV[7]. The 6 mm equilibrium ring bunch-length is compressed to 1.5 mm before reinjecting into the linear accelerator to minimize wake-field effects produced in the accelerator wave-guide structure by the intense bunches. The last electron bunch is ejected onto a target at 33 Gev, to produce positrons[8]. These are returned along the length of the Linac to the 200 Mev point in the injector. At the end of the linear accelerator, electrons and positrons are bent around and into collision through two arcs[9]. The final focus system, straddling the interaction area, provides the necessary optical demagnification and steers the beams into collision[10].

The main parameters of the SLC are shown in Table 1. Column one lists the design parameters, and column two lists presently achieved parameters. As can be seen the luminosity reaches unfortunately only a thousandth of the nominal value. Also, the operating efficiency for achieving peak luminosity with acceptable background in the experimental apparatus (not listed in Table 1) was lower than 5% in the last cycle of luminosity runs during the summer of 1988.

The discrepancy between expected and achieved performance results partly from insufficient emphasis, during the early phases of the project, on the design of systematic diagnostic and correction schemes to control the beams adequately at each stage of the system, on the development of a global integrated tuning strategy, and on hardware reliability and stability. Tuning and correction methods were in most cases developed empirically and added-on to each of the components of the SLC after the basic optics and geometry had been fixed, or sometimes in response to specific difficulties encountered in the commissioning phase. In several cases, the methods developed were therefore imperfect, and their improvement is the centerpoint of the ongoing effort to bring the SLC towards its design performance. The experience gained with the SLC, which is the first linear collider to be brought into operation, will be very useful to the design of future linear colliders.

I.3 SCOPE AND OUTLINE OF THESIS

In this thesis, we present the procedures developed to correct and to tune the optics in two parts of the SLC complex: the arcs and the final focus sections. The methods which we

describe were conceived and developed in preparation for and during the commissioning of the SLC, mainly between 1984 and now. They are presented through a selection of technical notes, conference articles and publications describing in detail their design and the operational experience which has been acquired. Although the entire SLC complex has not yet reached its nominal performance, these methods have enabled to achieve a close to optimized optical transport in these two sections, and to characterize the optical limitations to the SLC performance.

We introduce these papers in an overall presentation where we:

1. Review the basic principles of the optical designs of the arcs and final focus sections, on which our tuning methods are based.

2. Study the effect of focusing errors in the system on the luminosity and on the background. These errors can result in both recoverable and unrecoverable distortions of the beam phase-space. We give order of magnitudes for resulting tolerances and characterize the different cases in terms of their effect on the phase-space and of their correctability.

3. Describe the context of the SLC commissioning, and the evolution of the global tuning strategy, from which the optimization of the arcs and final focus can not be entirely isolated. Some of the methods were developed in preparation for the commissioning, while others were conceived in response to specific difficulties encountered during the first tests.

We then introduce each of the papers presented, show its relevance to the subject of this thesis, and outline its original components.

In the case of the arcs, the papers presented describe essentially:

1. A method for correcting long FODO arrays in a compact and economical way. This method is inspired from harmonic correction techniques common to circular accelerators. Its application to an open beam-line is new. We have designed and implemented this method in the last portion of the arc beam-line, to enable tuning the phase-space at the entrance to the final focus section. Such tuning has turned out to be crucial to minimize backgrounds resulting in the experimental apparatus from secondary particles. Such secondaries are generated when edges or tails of mismatched beams get scraped off in the final focus system, where the aperture (normalized to the nominal beam size) is significantly smaller than in the arcs.

2. The study of the partial modification of the arc lattice. To follow the terrain of the SLAC site, the arcs were designed in three dimensions: in addition to the horizontal bending, the beam-line is deflected vertically by rotating the bending magnets about their axis. In the initial design, these rotations were introduced abruptly. The coupling between the horizontal and vertical betatron motions was suppressed by grouping these rotations in long-range cancelling pairs. This strategy, however, made the system sensitive to systematic errors. It has been possible to modify the design to produce smoother transitions. These new transitions almost entirely suppress the sensitivity to systematic errors, and

render the overall optical transport much more tolerant.

In the case of the final focus, the papers presented describe essentially:

1. The elaboration of the interaction point beam size minimization procedure. This procedure consists of the sequential application of ten corrections in the different optical modules of the final focus section, following a strategy which must take into account the ability to measure very small beam sizes and to resolve the various distortions, as well as the specificity of the final focus optics. The final focus design is in effect based on balancing several higher order optical aberrations which can individually dominate the minimum beam size if the system is not adjusted correctly. It is now possible to adequately control the interaction point beam size, starting with a very distorted phase-space at the entrance to the system.

2. The practical implementation of this procedure and the operational experience which has been acquired, along with the present optical factors which limit the SLC luminosity. As we explain, these optical limits result principally from the requirement to minimize backgrounds in the experimental apparatus, and from a somewhat larger than nominal emittance at the exit to the SLAC linear accelerator.

Finally, we include, in an appendix, papers on the development and on the initial performance of one of the three measurement techniques, based on electromagnetic space-charge effects occuring in the collisions between the two beams, which were conceived to diagnose the beams at the interaction point: the "beam-beam deflection" technique. The two other methods which were developed are based on "beamstrahlung", or synchrotron radiation from the space-charge forces, and on "disruption". Such methods are particularly important to diagnose the beams at the interaction point, but do not belong directly to the subject of this thesis.

II. OPTICS IN THE ARCS AND FINAL FOCUS

II.1 OPTICS IN THE ARCS[11]

II.1.1 Overview

The arcs are the only part of the SLC which will not be required in linear colliders of the future. They are needed in the SLC system, which uses the same linear accelerator to accelerate both beams, to bend each beam around 270^0, and into frontal collision. Because of the limited size of the SLAC site, they have a short bending radius of 279 meters. They are intended to behave passively and to produce a close to exact optical image of the electron and positron beams injected from the linear accelerator. The optics is therefore designed to be an optical identity from the beginning point to the exit. A schematic of the two arcs is shown in Fig. 3. Two physical mechanisms must be counteracted to prevent the beam phase-space from being enlarged as it is imaged through: synchrotron radiation emittance dilution and filamentation effects from the natural chromaticity of the lattice and from the fact that the beam has a finite energy spread.

II.1.2 Synchrotron Radiation

Synchrotron radiation photons are emitted at random and cause energy fluctuations. Lower energy particles are bent more and follow curves with shorter average radius. This disperses their trajectories incoherently which in turn dilutes the phase-space in the plane of the bending. Such trajectories execute betatron oscillations in the quadrupole lattice. To minimize the growth, both the photon emission rates and the oscillation amplitudes must be small. This is achieved by making the bending radius large and the betatron period short, through tight focussing. It can be shown that the growth is proportional to T_β^3/ρ^4, where T_β is the betatron period and ρ the average radius[4]. The transport therefore uses the lowest possible field compatible with the size of the SLAC site, and a strong focusing alternating gradient lattice, with optical parameters chosen to minimize the average invariant amplitude of the dispersed oscillations. For a FODO array, the optimum cell phase-shift[12] to minimize emittance growth is near 135^0. For reasons explained below, the design in fact uses 108^0. The packing factor is in addition maximized by using combined function magnets.

At 50 Gev, the emittance added in one passage is $1.3\ 10^{-10}$ rad-m (or one half of the design value at the entrance) in the horizontal plane, and $0.5\ 10^{-10}$ rad-m in the vertical plane[4]. The emittance growth occurring in the vertical plane arises because of vertical dispersion introduced by the rolls (described later).

II.1.3 "Chromatic Filamentation"

The second mechanism for phase-space growth arises through residual energy spread resulting from the bunch-length and the accelerating linear accelerator RF. Because of the energy dependance in the focussing, or chromaticity, optical distortions at the injection to the arc, or arising from gradient errors within the arc lattice, are not imaged coherently. For example an off-energy slice of a mismatched phase-space is transmitted with a phase-shift $\Delta\psi = 2\pi N_\beta \frac{d\phi}{dG}\delta_E$ where δ_E is the relative energy error, N_β is the number of betatron periods, and $\frac{d\phi}{dG} \simeq 1.5$ is the ratio of phase change to excitation change in the arc lattice. For large phase-shifts, the overall mismatch averaged over all energies looses its phase relation to the input. The effective volume occupied by the observable phase-space is thereby enlarged. This effect is referred to as "chromatic filamentation". Unlike the phase-space dilution resulting from synchrotron radiation, this enhancement of the effective volume does not violate Liouville's Theorem. The volume of the full six-dimensional phase-space $(x, x', y, y', \frac{\delta E}{E}, z)$ is in fact not changed, but acquires a complicated internal structure corresponding to a second order correlation.

The arc beam-lines have $N_\beta = 69$ betatron periods. For a fractional energy spread of $\sigma_E/E \simeq 0.5\%$, the spread in betatron phases at the output is about $\sigma_\psi \simeq \pi$. In order to assure coherent imaging of focusing errors injected into the arc or generated along the beam-line, over an energy band-pass of $\pm 0.5\%$, the design uses sextupoles to cancel the first-order chromaticity of the lattice.

II.1.4 Chromatic Correction

The sextupoles are introduced by shaping the combined function magnet poles[7]. For the horizontal optics, the vertical component of the magnetic field on the horizontal axis $(y = 0)$ is:

$$B_y(x) = B_{yo}(1 - \frac{Q}{\rho}x + \frac{S}{\rho^2}x^2), \tag{3}$$

where Q and S are the strengths of the quadrupole and sextupole components respectively, and ρ is the bending radius. The sextupole provides additional focusing for off-energy and off-axis rays with $x = \delta x + \delta_E \eta$, where η is the dispersion function, which suppresses the chromaticity if $2S\eta = Q\rho$. Since sine and cosine-like components are equivalent modulo $\pi/2$ in a repetitive lattice, only one family per plane is needed. Additional terms in x^2 and δ^2 for rays solely off-axis or off-energy are suppressed by grouping the cells to produce cancellations as locally as possible. Second order achromats achieve this by pairing the sextupoles π phase-shift apart and by requiring at least four-fold sequential symmetry[13]. This is done by grouping the cells into achromatic superperiods with the smallest possible multiple of 2π compatible with the cell phase-shift. In the SLC arcs, each such superperiod - or achromat - spans a 6π phase-advance and consists of ten 108^0 cells. This is a compromise between achromat compactness, best with 90^0, and quantum dilution, smallest near 135^0. The resulting lattice functions β and η are shown in Fig. 4.

II.1.5 General Layout

The whole arc consists of 23 such achromats. In addition, as shown in Fig. 3, special matching sections are used at the inflexion points (reverse bends sections) and between the linear accelerator and the main arc (beam switchyard section). The matching sections needed at the exit of the arcs are described in the section on the final focus.

Finally, for economical reasons, the arc beam-lines are required to follow the terrain of the SLAC site, and are therefore not planar. To provide the necessary vertical deflections, the achromats are rolled relative to each others. The distribution of rolls for the north and south arcs are shown in Fig. 5.

II.2 OPTICS IN THE FINAL FOCUS[14]

II.2.1 Overview

The final focus is the last section of beam-line in the SLC before the interaction point. Its main function is to focus the beam to a transverse size of less than 2μm at the collision point.

Schematically the final focus consists of a demagnifying telescope, similar to a low-β insertion in a circular machine, with a special section at its entrance to match the arc lattice parameters. Because of the finite emittance and momentum spread in the beam, a 2μm beam spot cannot be obtained without carefully minimizing higher order chromatic and geometric aberrations. The dominant optical aberration is the first order chromaticity - or momentum dependance of the focusing - of the demagnifying telescope. Physically, this first order chromaticity causes particles with different energies to be imaged into longitudinally displaced focal points at the interaction point. The magnitude of this effect is easy to estimate by considering solely the variation with energy of the focal length of the last focusing elements. Since this focal length, computed as the distance from the interaction point to the principal planes of the final lens system in each plane, is about 5 meters, and because the depth of focus of the optical system, measured by the linear β-function at the interaction point is required to be about 0.5 centimeters, we see that particles with energy errors of a few parts per thousand are totally out of focus (See Fig. 6)

II.2.2 First Order Chromaticity

More quantitatively, we use TRANSPORT[15] to compute the rate of change F of the interaction point beam size with the fractional energy error δ_E. We have:

$$\sigma^2(\delta_E) = \epsilon\beta^*(\delta_E) = \epsilon\beta_0^* + \frac{\epsilon}{\beta_0^*}F^2\delta_E^2, \tag{4}$$

where $\beta_0^* = \beta^*(\delta_E = 0)$ represents the nominal value of the β^* parameter, and where ϵ is the emittance. One obtains $F \simeq 15$ m. where $F \simeq 15$ meters, where β_{eff}^* and β_{lin}^* are the effective and linear β-functions at the interaction point,

The presence of this first order* chromatic term in (4) leads one to define an energy band-pass over which the demagnifying telescope will perform its function. This band-pass is shown in Fig. 7a. As can be seen it is much smaller than the minimum fractional energy spread of 0.002 which can presently be obtained[s] at the end of the linear accelerator.

An effective value could be calculated for the β^* parameter, by averaging equation (4) over the particle's energy distribution. This parameter would however not represent the new particle distribution very well since this new distribution is more peaked than a gaussian, and has tails. Rather than calculating this new distribution explicitly, we will directly estimate the effect on the luminosity, by averaging the usual expression over the two beam's energy distributions, which we take to be equal and square. One obtains:

$$\mathcal{L}(\beta^*, \sigma_E) = \frac{fN^2}{2\pi{\sigma_E}^2}\int_0^{\sigma_E}\int_0^{\sigma_E}\frac{d\delta_E^+ d\delta_E^-}{2\epsilon\beta^* + \frac{\epsilon}{\beta^*}F^2(\delta_E^{+2} + \delta_E^{-2})} \tag{5}$$

The result is shown in Fig. 8 for different energy spreads and allows to determine an optimum β^*. Since this energy band-pass scales as β^* from (4), and because the optimum occurs when the band-pass is matched to the energy spread, one expects the optimum β^* to scale roughly linearly with the energy spread in Fig. 8. This can indeed be verified.

II.2.3 Chromaticity Compensation and 2^{nd} Order Distortions[14,4]

The first order chromaticity is corrected by introducing a special chromatic correction section upstream of the demagnifying telescope (see Fig. 9). This chromatic correction section consists of two $-I$ telescopes, combined with dipoles at their foci, to generate significant energy dispersion at the quadrupoles. Sextupoles, where the focusing strength varies linearly with excursion, are put near the quadrupoles, to provide additional focusing proportional to energy. This compensates for the intrinsic first order chromaticity. Additional first-order perturbations to the imaging produced by each sextupole are made to cancel over the length of the section by pairing the sextupoles π betatron phase-shift apart

* *The chromatic term in question appears to be a second order term in (4), but it is really does correspond to a first order term in the optical transfer since (4) gives the behaviour of the square of the beam size.*

and by imposing sequential symmetry for the dispersion function. In this way, all residual perturbations to the focusing are pushed to second order. The parameter β^* can thus now be written:

$$\beta^* \simeq \beta_0^* + \kappa_1^2 \frac{\delta_E^4}{\beta_0^*} + \kappa_2^2 \epsilon \frac{\delta_E{}^2}{\beta_0^{*2}} + \kappa_3^2 \frac{\epsilon^2}{\beta_0^{*3}}, \tag{6}$$

where κ_1, κ_2 and κ_3 measure the magnitudes of the residual second order perturbations to the focusing.

II.2.4 Origin and Scaling Laws for 2^{nd} Order Distortions

Because the SLC is designed for round beams at the collision point, with equal emittances and β-functions in each plane, the linear chromaticity must be corrected in both planes, and two families of sextupoles must be used. In order to save space, a single chromatic correction section, with interleaved families for correction in each plane, is used. The second order perturbations to the focusing come in most part from coupling between these two interleaved families. This consideration allows to develop approximate scaling laws for these terms[16].

Since the largest contribution to the first order chromaticity comes from the final demagnifying telescope, we can find a nearly exact scaling law for the strengths of the sextupoles by neglecting the first order chromaticity introduced by the telescopes which make up the chromatic correction section: the scaling law is obtained by equating the first order chromatic contributions to the variation of the interaction point angular spread, from the intrinsic first order chromaticity of the final demagnifying telescope and from the sextupoles. We obtain:

$$S \propto \frac{l^*}{l_{ccs}^2} \frac{1}{B}, \tag{7}$$

where S is the strength of the sextupoles, l^* is the distance from the interaction point to the principal planes of the last lenses, B is the angle of bending in the chromatic correction section, and l_{ccs} is the length of the chromatic correction section (see Fig. 9).

Next, because the dominant second order perturbations to the focusing in (6) come from the cross-coupling of the sextupole families used to correct in each plane, we can neglect the final demagnifying telescope in the scaling laws for these second order terms. We find in this case:

$$\begin{cases} \kappa_1 \propto S^2 l_{ccs}^3 B^2, \\ \kappa_2 \propto S^2 l_{ccs}^3 BM, \\ \kappa_3 \propto S^2 l_{ccs}^3 M^2, \end{cases} \tag{8}$$

where $M = l^*/L$ is the magnification of the final demagnifying telescope, and where L is the distance between the lens and the "source" in Fig. 9.

By substituting in (8) for the sextupole strength needed to correct the first order chromaticity in (7), we find the following scaling laws for the three contributions to the

interaction point beam size which arise from the second order terms in (6):

$$\begin{cases} \sigma_{\kappa_1} \propto \frac{l^{*2}}{l_{ccs}} \delta_E^2 \sqrt{\frac{\epsilon}{\beta^*}}, \\ \sigma_{\kappa_2} \propto \frac{l^{*2}}{l_{ccs}} \frac{M}{B} \delta_E \frac{\epsilon}{\beta^*}, \\ \sigma_{\kappa_3} \propto \frac{l^{*2}}{l_{ccs}} (\frac{M}{B})^2 (\frac{\epsilon}{\beta^*})^{\frac{3}{2}}. \end{cases} \tag{9}$$

It can in addition be noted that scaling l^* at constant $M = l^*/L$ is equivalent to scaling the full length of the final demagnifying telescope*. Thus if we scale the whole length l_{tot} of the final focus system, we expect all terms in (9) to scale linearly.

The dependence of these three limiting residual second order terms on the design variables: B, l_{ccs}, l^* and l_{tot} has been checked with TRANSPORT, by scaling the SLC final focus design. The results of such calculations are shown in Fig. 10a,b,c,d.

As can be seen the scaling is not perfect. This arises mainly because the first order chromaticity of the lenses in the chromatic correction section is not, as was pointed out, included in the scaling argument. Because of this, the reduction of the magnitude of these terms when increasing the length l_{ccs} of the chromatic correction section is less than linear and eventually saturates, in particular for the geometric term σ_{κ_3}. Similarly, the reduction of their magnitude when decreasing l^* is less than quadratic. The actual simulated power dependances are given in the figure captions.

II.2.5 Limits on Chromatic Correction Bend Angle

As can be seen from (9), there is a lower limit on the angle B of the bending in the chromatic correction section, from both the chromatic term in κ_2 and from the geometric term in κ_3. We will return to this point in the next section.

In addition, there is a sharp upper limit on this bend angle from synchrotron radiation emittance dilution, which increases as the fifth power of the bend angle and of the beam energy. For the SLC final focus, the limit occurs[14] when this bend angle B is of the order of about one degree, which corresponds to an emittance growth of about 20% at 50 GeV.

II.2.6 Optimization Procedure

The scaling laws given in (9) allow one to understand the different procedures which can be followed to optimize the optical design. A full description of the optimization process can be found in Ref. [16].

* *By length of the telescope, we intend the distance between the image and the source*

Several points of views can be taken. Here, we will show one of them, which consists in considering that the emittance ϵ and the energy spread δ_E have been set in the overall system specification, that a given β^* is desired, and that one wishes to choose the lengths l_{tot}, l_{ccs} and l^*, and the bend angle B in an optimal way*.

A reasonable procedure would go as follows:

1. Set the bend angle B to the maximum possible consistent, from the point of view of the synchrotron radiation emittance dilution, with the chosen minimum beam size $\sigma^* = \sqrt{\beta_0^* \epsilon}$.

2. Set the magnification M such that all terms in (9) be about equal, for the given emittance and energy spread, and for the chosen β_0^*. When this has been done, it can be seen from the two first equations in (9) that the betatron and chromatic angular spreads at the input to the chromatic correction section are about equal.

3. Decrease the ratio l^{*2}/l_{ccs} until the second order aberration terms and the linear term in (6) are about equal. This determines a minimum for β^* in (6). As we will also see, this optimum can also be interpreted as the point for which the energy band-pass of the corrected system is matched to the energy spread δ_E of the beam.

Implicit in this is the fact that the sextupole strengths are free parameters. Also, the magnification M of the final demagnifying telescope is in general not sufficient to demagnify the input β-function to the desired β_0^*, and an initial demagnifying section is needed upstream of the chromatic correction section. Therefore, when M, the magnification of the final demagnifying section, is varied, we assume that this initial demagnifying section can be adjusted to keep the overall magnification of the beam-line (and thus β_0^*) constant, and that over this adjustment range, this initial section does not contribute significantly to the chromaticity of the overall beam-line.

In practice, the minimum distance l^* between the interaction point and the principal planes of the last focusing elements is set by the maximum gradient available in those focusing elements, and by the requirement to leave sufficient space for components of the experimental apparatus. In the case of the SLC final focus system, $l^* \simeq 5m$. The optimization led to introducing a demagnification of a factor four in both planes for the final telescope, and of factors eight and three in the horizontal and vertical planes respectively for the initial telescope. Besides initiating the demagnification, the initial transformer also serves to match the final focus and arc betatron lattices[14]. This results, given an energy

---

* *Two different points of view would consist in asking:*

1. For given constraints on the lengths l_{tot} and l^*, what are the requirements on the emittance and on the energy spread to reach a given β^* ?

2. For a given emittance and energy spread, and for given constraints on the lengths l_{tot} and l^*, what is the minimum β^* that can be reached ?

spread of $\delta_E \simeq 0.002$ and an emittance of $\epsilon \simeq 3\ 10^{10}$ rad-m, to about a $\beta^*_{min} \simeq 4$ mm (this is also illustrated in II.2.8). The bend angle B is set to about one degree as was mentionned above.

II.2.7 Optical Bandpass

The overall effect of the chromatic correction is to broaden the energy band-pass, described above, over which rays are imaged to the same interaction point focal point. From (6), the width of this band-pass scales roughly as $\sqrt{\beta^*_0}$ (if only the term in κ_1 from (6) is used). The bandpass is shown in Fig. 7b. Defining it quantitatively as the band of energy deviations for which $\beta^* \leq 1.25\beta^*_0$, it is $\pm 0.5\%$ for $\beta^*_0 = 16$ mm and $\pm 0.22\%$ for $\beta^*_0 = 4$ mm.

II.2.8 Optimum β^*

Much as in the case without chromatic correction described above, the luminosity is maximized by matching this enlarged band-pass, defined by β^*, to the beam energy spread. This is illustrated in Fig. 11, where the luminosity loss is computed as a function of β^* for two different energy spreads, using the raytracing code MURTLE[17]. The solid lines indicate the luminosity loss as a function of β^* for the chromatically corrected system, and the dashed lines, reproduced from Fig. 8, show for comparison the loss which occurs without the chromatic correction. As can be seen the wider band-pass produced by the chromatic correction results in a smaller optimum for β^*.

II.2.9 General Layout

The whole system is shown in Fig. 12. It includes, in addition to the two telescopes and to the chromatic correction, a section to match the arc dispersion function. Also the extraction of the spent beam is built in to the upper telescope, using a kicker and septum magnet.

III. IMPERFECTIONS AND TOLERANCES

III.1 INTRODUCTION

The goal in this chapter is to describe the effect of errors on the beam phase-space, in order to define tolerances and a global strategy for adjusting the SLC or an SLC-like system. We give this description at a qualitative level, and we give only orders of magnitude for the tolerances.

We first determine the evolution of the phase-space from the different kinds of errors, and in the different cases. We then analyse the effect of the distortions induced by these errors on the performance of the system – i.e. on the luminosity and on the backgrounds in the experimental apparatus, and the ability to correct them. As we shall see, this analysis enables to classify the different kinds of errors in terms of their consequences and in terms of the type of correction they require (local or at the end) and to split up the tuning of the machine sequentially into several pieces. This then allows to define criteria for setting tolerances, and to outline a global commissioning strategy.

This thought-process results from our accumulated experience in learning to operate the SLC. The actual commissioning strategy which was followed differed initially from the prescription we give here. We briefly describe this initial strategy in the next chapter.

Ideally, such conceptual analysis would be carried through at an early enough stage so as to be able to incorporate its most important implications into the basic design and architecture of the optics and of the control system.

III.2 EFFECTS FROM IMPERFECTIONS

III.2.1 Errors in the Guide-Field and Betatron Oscillations

Static dipole errors along the entire system cause spurious kicks to the beam, which then as a result executes betatron oscillations in the quadrupole lattice. Such dipole errors arise from misalignments of the lenses in the focusing lattice, or from field errors in the bending magnets of the transport. This is illustrated in Fig. 13a. The frequency of the betatron oscillation is referred to as the betatron frequency.

III.2.2 Errors in Focusing-Field and Phase-Space Distortions

III.2.2.1 Regular Focusing Field Errors and Betatron Mismatch

Static quadrupole - or focusing - errors perturb the beam phase-space ellipse as shown in Fig. 14. Such focusing errors arise from gradient errors in the focusing lenses of the system, or, if the lattice uses sextupole magnets, from horizontal misalignments of the beam in these sextupoles. Because the quadrupole error will kick particles in this ellipse proportionally to their excursion in the quadrupole, its effect is the stretching of the ellipse shown in Fig. 14. The ellipse will then rotate in the coordinate system as it is imaged through the rest of the system. The beam envelope, or the projection of this ellipse on the horizontal axis, will therefore beat along the optical array. Because the ellipse is invariant under rotation of π, the beating which is generated has twice the betatron frequency. This is illustrated in Fig. 13b.

III.2.2.2 Skew Focusing Field Errors and Cross-Plane Coupling

If sextupoles are used in the transport, as in the arcs and final focus sections, or if the system does not satisfy mid-plane symmetry, such as the arcs, where the beam-line is rolled about the axis to allow following the terrain, then another type of focusing error can arise, which couples the horizontal and vertical planes. Such cross-plane coupling arises from vertical misalignments of the beam in the sextupoles, or from the imaging of beats in the beam envelope, generated by the regular focusing errors described above, across the rolls. In this case, the projections of the - coupled - four-dimensional phase-space onto the horizontal and vertical planes are in general not preserved and can result, if left uncorrected, in larger effective emittances.

III.3 EVOLUTION OF PERTURBATIONS – CORRECTIBILITY

III.3.1 Case of Chromaticity Corrected Optical Lattice

In parts of the system where the first order chromaticity of the lattice is corrected, such as the arcs or the final focus sections, the distortions of the envelope, from both regular and skew quadrupole errors, and the coherent oscillation of the beam generated by dipole errors, are transmitted with the same frequency for all energies within the optical band-pass of the chromaticity-corrected optics. In this case, the effects of these errors can be corrected further downstream in the system. This is in particular the case for the arcs.

III.3.2 Case of Lattice Not Corrected for Chromaticity

In parts of the system which do not have chromatically corrected optics, such as the

linear accelerator, both these errors will gradually loose their coherence, due to the finite energy spread in the beam.

III.3.2.1 Incoherent Propagation of Betatron Oscillations – Beam Dispersion

The propagation of a dipole error will generate linear correlations between the energy and the transverse coordinates, which we refer to as beam dispersion. After the phase-shift accumulated between particles with maximum positive and negative energy errors has reached π, the effective phase-space area containing the beam will become as large as the phase-space trajectory described by the betatron oscillation induced by a dipole error. This occurs without violating the conservation of the six-dimensional $(x, x', y, y', \frac{\delta E}{E}, z)$ phase-space volume. However this phase-space volume has become correlated, and its projection on one of the (x, x') or (y, y') planes corresponds to an enlarged area. We illustrate this mechanism in Fig. 15a,b.

Such beam dispersion is correctable downstream, through adjustments in a purposely designed matching section.

III.3.2.2 Incoherent Propagation of Betatron Mismatch – Chromatic Filamentation

Similarly, the propagation of a quadrupole error will cause second order correlations - or aberrations - of energy to transverse coordinates. In this case, the quadrupole error generates an anomalous correlation between positions and angles in the transverse (x, x') or (y, y') phase-space. This correlated ellipse then rotates in phase-space with different speeds for different energy slices in the beam, as was described in II.1.3. Also here, when the accumulated phase-shift between slices with opposite and maximal energy error has reached π, the ensemble of trajectories composing the beam will be contained in an effective area as large as the circle in which the distorted phase-ellipse in inscribed. The actual area occupied by the trajectories is not enlarged, but acquires a complicated smeared structure. This effect, usually referred to as chromatic filamentation, is illustrated in Fig. 16.

In this case, the distortions cannot be corrected downstream and must be corrected locally. This is particularly the case for the linear accelerator, and is important to minimize the effective emittance at the injection to the arcs.

III.3.3 Frequency Analysis

The effects from the accumulation of these two errors will in general only be significant if they add in phase. In the case of the dipole errors, subsequent kicks of the same sign and separated by 2π phase-advance will add up and cause a betatron oscillation with increasing amplitude. In the case of the quadrupole errors, the beats in the beam envelope will grow

if errors with the same sign are separated by π phase-advance. In general, since the errors are random, their Fourier component, at the betatron frequency for the dipole errors, and at twice the betatron frequency for the quadrupole errors, is not more significant statistically than other components in the frequency spectrum of the errors. Also, the specific distribution of the errors can be such that cumulative effects occur in one section of the array and not in the others.

We will examine the case of focusing errors in more detail.

III.3.3.1 Average Growth from Random Focusing Errrors

In a repetitive FODO array, and for an ensemble of error distributions, the average fractional growth $\langle \frac{\Delta A}{A} \rangle$ of the beam phase-space which occurs at the end, in any of its dimensions, is related to the magnitude of the errors in the following way:

$$\langle \frac{\Delta A}{A} \rangle \simeq e^{\lambda \epsilon_R \sqrt{N}}, \tag{10}$$

where ϵ_R is the standard deviation of the random errors, N is the number of cells in the array, and λ is a parameter or order unity, which characterizes the lattice. For the arc lattice, we find through simulation that $\lambda \simeq 2$. In this case, the exponential law arises because the differential growth of the beam size is proportional to the beam size and to the cell number for a quadrupole error at twice the betatron frequency. The $\sqrt{N}$ in the exponent arises from the fact that the one standard deviation statistical expectation value for the magnitude of any given component in the spectrum of random quadrupole errors is $\epsilon_R/\sqrt{N}$.

Growth occuring through the accumulation of random errors can in some cases be corrected globally, by deliberate introduction of a perturbation at the resonant frequency. This is explored in more detail in sections VI.3 and 4 for the case of focusing errors in the arc lattice.

When chromatic filamentation effects are negligible, the induced distortions remain coherent and can also be corrected downstream, in a purposely designed matching section. Such a matching section has been developed in the final focus (see chapter VII)

III.3.3.2 Bandwidth Limits from Discontinuities in the Focusing Lattice

It is not uncommon that there be a rather large component in the spectrum of random errors at zero frequency, from systematic errors in the calibration of the magnets or in the knowledge of the energy (if the lattice is not chromatically corrected). For a truly repetitive lattice, such errors are harmless and simply cause the betatron frequency to be shifted.

This is however no longer the case if the lattice includes discontinuities, as is the case for the arcs, where large rolls of up to ten degrees were introduced to enable following

the terrain (see section II.1.5). These rolls were matched in pairs, to produce long-range cancellations of the distortions induced on the phase-space. This arrangement produced a relatively strong artificial sensitivity to systematic errors (see also section VI.2).

The distortions of the phase-space are correctable, either globally, through systematic adjustments of the focusing elements, or further downstream, in the same conditions as in III.3.3.1.

III.3.4 Electromagnetic Coupling to the Environment – Wake-Field Effects[18]

Electromagnetic coupling of the beam charge distribution to the environment can result in correlations between transverse and longitudinal coordinates. Orbit excursions of the beam, caused by dipole errors, induce in general asymmetries in the image-currents on the inner walls of the vacuum chamber, or of any other structure seen by the beam. For large enough current, these asymmetries can result in significant transverse fields – or wakefields – affecting the trailing part of the bunch, and thus causing a growth of the effective emittance.

The most sensitive part of the system is the linear accelerator, where large wakefield effects are generated in the RF waveguide structure, for typical SLC beams. Beam trajectory errors must be corrected locally and launch parameters must be stabilized at the entrance for minimization. Such wakefield effects, pertinent to the dynamics of the linear accelerator, are not considered further in this Thesis.

III.3.5 Number of Free Parameters of Transverse Phase-Space

It is important to know the number of independent phase-space distortions which can be corrected downstream, in order to enable designing appropriate correction schemes. We will evaluate this number in the case of the transverse phase-space, and include also the four dispersion terms. We will include in our counting neither correlations to the longitudinal coordinate from wakefields, nor second order correlations between energy and transverse coordinates, from chromatic filamentation effects, both of which must be corrected locally.

III.3.5.1 Optical Transfer Matrix

The optical transfer is described through a four by four matrix R (transport matrix), relating the four input coordinates $\vec{X}_{in}$ to the four output coordinates $\vec{X}_{out}$:

$$\vec{X}_{out} = R\vec{X}_{in} \tag{11}$$

Since the particle motions are governed by Hamilton's equations, this transfer matrix is constrained to be symplectic, which means that:

$$R^t S R = S, \quad \text{where} \quad S = \begin{pmatrix} 0 & -1 & 0 & 0 \\ 1 & 0 & 0 & 0 \\ 0 & 0 & 0 & -1 \\ 0 & 0 & 1 & 0 \end{pmatrix}, \tag{12}$$

is the symplectic matrix in four dimensions. It can be shown[19] that (12) results in six independent constraints on the matrix R, which has therefore a total of ten independant parameters.

III.3.5.2 Beam Phase-Space Matrix

The phase-space is described through a symmetrical four by four variance matrix σ, describing the correlations between the four x, x', y and y' beam excursions. For a linear transformation of the coordinates described by R, this matrix is mapped through similarity transformation as follows:

$$\sigma_{out} = R \sigma_{in} R^t. \tag{13}$$

III.3.5.3 General Case of Unequal Input Emittances

The σ-matrix is fully specified through ten terms. However, only eight of these terms can be perturbed through a perturbation satisfying Hamilton's equations. This comes about because in general, Hamiltonian systems with two degrees of freedom can be shown to possess two canonical invariants[20]. Including the four linear dispersions, the phase-space can thus in general be perturbed in twelve independent ways.

III.3.5.4 Special Case of Equal Input Emittances

In the case of equal input emittances, it is possible to show, using the symplectic constraint of (12), that two additional constraints exist on the beam phase-space, restricting the total number of independent distortions, including the four linear dispersions, to ten. The proof, which we outline below, is straightforward. What is lacking, however, is a physical understanding of the mechanism by which this symmetry between the emittances can generate these two new constraints.

Proof: The proof consists of showing that because the transport matrix is symplectic, the σ-matrix transformed through this transport matrix will also be symplectic, if the emittances are equal in each plane at the input point. This then imposes two additional conditions on the elements of the σ-matrix. Consider an input phase-space with the two (x, x') and (y, y') planes decoupled. The σ-matrix σ_{in} representing this phase-space is block-diagonal. The emittance in each plane is given by the square root of the determinant of each two by two

block. Since we assume that these two emittances are equal, we scale each two by two block by this common value ϵ for the square root of the determinants. We can thus write:

$$\frac{1}{\epsilon^2}\sigma_{in}S\sigma_{in} = S \tag{14}$$

Next we multiply (14) by R from the left and by R^t from the right, and use (12). In the rest of this proof, we will in additon set $\epsilon = 1$. We have:

$$RSR^t = R\sigma_{in}R^tSR\sigma_{in}R^t. \tag{15}$$

In (15), we recognize σ_{out}, given by (13). We have thus:

$$RSR^t = \sigma_{out}S\sigma_{out}. \tag{16}$$

To show that the output phase-space matrix σ_{out} is also symplectic, we need to show that the left hand side of (16) is equal to S. To do so, we start with (12) and take its inverse, go through the following manipulations, and note that $S^2 = -I$, where I is the identity matrix. We have:

$$S^{-1} = R^{-1}S^{-1}(R^t)^{-1}, \tag{17}$$

$$RS^{-1}R^t = S^{-1}, \tag{18}$$

$$-RSR^t = -S. \tag{19}$$

Thus the output σ-matrix σ_{out} is symplectic. Writing out the conditions explicitly at a point where positions and angles are simultaneously uncorrelated within each plane, as occurs for example at the collision point, after a waist has been obtained there in each plane, i.e. where $\sigma_{12} = \sigma_{34} = 0$, we obtain:

$$\begin{cases} \sigma_{11}\sigma_{22}(1 - r_{13}^2 - r_{14}^2) = 1, \\ \sigma_{33}\sigma_{44} = \sigma_{11}\sigma_{22}, \\ r_{23} = r_{14}, \\ r_{24} = -r_{13}. \end{cases} \tag{20}$$

where we have defined the normalized correlations: $r_{ij} = \sigma_{ij}/\sqrt{\sigma_{ii}\sigma_{jj}}$. Thus there is a total of four constraints restricting the distortions of the phase-space if the input emittances in each of the two transverse planes are equal. In this case, there is a total of ten independent distortions, including the four linear dispersion terms.

III.3.6 Classification of Phase-Space Perturbations

The different cases described in this section are summarized in Table 2, where we list, for each basic type of perturbation, the consequences on the beam phase-space if a correction is not applied until the very end, as a function of each location in the SLC, downstream of the damping rings. In each case, we then ask if the distortion is in principle correctable at the very end.

Distortions correctable in principle may however not be tolerable in practice because of the requirement to minimize backgrounds in the experimental apparatus. As we shall explain in the next section, such requirements impose much more stringent constraints on the distortions which can be allowed to accumulate to the very end. We do not attempt to incorporate such requirements in Table 2

For completeness, we have also included the emittance dilution effects from synchrotron radiation which occur in the arcs.

III.4 CONSEQUENCES ON PERFORMANCE AND SENSITIVITIES

III.4.1 Sensitivities Pertinent to the Luminosity

III.4.1.1 Phase-Space Distortions

The luminosity which can be obtained depends strongly on the ability to correct the distortions of the beam phase-space which we have described. The distortions which are uncorrectable at the very end, such as the correlations of transverse to longitudinal coordinates and chromatic filamentation effects, are translated into a larger effective emittance, and affect the beam size directly through (2) if they are not taken care of locally at their source. For the ten distortions which, in the case of equal emittances in both planes, can be corrected at the very end, the SLC is equiped with a special matching section just downstream of the arcs. This matching section serves as a buffer section to absorb the distortions. Because the beam size at the interaction point is produced by carefully balancing higher order chromatic and geometric aberrations, all of these ten distortions must be corrected to fully optimize the luminosity. Allowable distortions are of the order of one half to one standard deviations of the optimum parameters at the collision point, for reasonable luminosity to be maintained.

III.4.1.2 Beam Jitter

Maintaining the luminosity also requires that the beams remain in collision. The luminosity reduction for an offset corresponding to q standard deviations of the beam can be calculated by perturbing the overlap integral performed to obtain (1) and (2). One obtains, in the case of round beams:

$$\mathcal{L}(q) = \mathcal{L}_0 \epsilon^{-\frac{q^2}{4}}, \qquad (21)$$

where $\mathcal{L}_0$ is the luminosity for an offset $q = 0$. From (21) can be seen that the maximum offset between the two beams which can be tolerated is about $q \leq 1$ standard deviations.

In the SLC, the main source of pulse to pulse jitter in the beam position resides in the kicker magnets used to extract the beams from the damping rings. This pulse to pulse jitter causes variations in the beam trajectory along the whole machine, and as mentionned in III.3.5, such variation can blow up the emittance through transverse wake-field effects. Therefore, at high intensity, the tolerance to beam position jitter is in fact not set by the requirement to maintain the beams in collision, but rather by the requirement to minimize these wakefield effects. With large local energy spread (several percent) introduced on purpose along the bunch to reduce the build-up of wake-field tails (so-called BNS Damping), the tolerance to launch jitter is of the order of a tenth of a standard deviation of the transverse beam distributions, at 5 10^{10} particles per bunch.

III.4.1.3 Intensity Dependance

More generally, the entire system enters a new regime at high intensity. Because of the wake-field effects, tolerances for maintaining a nominal phase-space at the end of the linear accelerator become more stringent with increasing intensity. It is therefore expected that the effective emittance at the collision point will be a growing function of the beam intensity, and that the gain in the luminosity from raising the current will not be as rapid as that implied through (1).

III.4.2 Sensitivities Pertinent to Backgrounds in the Experimental Apparatus

III.4.2.1 Introduction

Beyond the goal of maximizing the luminosity, the beam phase-space must also be stabilized to minimize backgrounds in the experimental apparatus. Such backgrounds arise when tails of the beam generated by wakefields in the linear accelerator strike apertures near the interaction point, causing electromagnetic showers into the detector, or further upstream in the final focus beam-line, where they produce muons which can reach the detector.

Such beam tails are clipped by using collimators at the exit of the linac and in the arcs. Ideally, such collimation would be perfect and define a full-proof beam stay-clear, allowing to precisely shadow the critical apertures in the final focus.

III.4.2.2 Principle of Collimation

The basic principle of a collimation system is illustrated in Fig. 17, as an example. Simplistically, a minimum of three collimators is used to enclose a three-dimensional $(X, X', \frac{\Delta E}{E})$ phase-space volume in the horizontal plane. The two first ones are upstream of a bending magnet, and serve mostly to define the spatial and angular dimensions. The

third one is downstream. It serves mainly to define the energy.

If the two spatial and angular dimensions of this volume are defined at reference point (0) by $X(0)$ and $X'(0)$, and if the desired cut on the energy is $\frac{\Delta E}{E}$, then the settings of the collimators is obtained by inverting the three linear equations relating the parameters of this volume at the reference point to the spatial coordinates $X(1), X(2)$ and $X(3)$ of the beam at each collimator. If $R^{(i)}$, for $i = 1, 2$ and 3, represent the optical transfer matrices between the reference point and the three collimators, then these three relations can be writen:

$$X(i) = R_{11}^{(i)} X(0) + R_{12}^{(i)} X'(0) + R_{16}^{(i)} \frac{\Delta E}{E}. \tag{22}$$

Similar equations can be writen for the vertical plane.

In order that the equations in (22) be far from degeneracy, it is important to choose the locations of the two first collimators with about a $\pi/2$ betatron phase-advance separation, and the third collimator where the natural dispersive size of the beam is significantly larger than its betatron size. Moreover, with high current small emittance beams, it is desirable to collimate the beams at relatively high values of the β-parameter, so as to minimize the power deposition on the collimators*.

In many cases, a more sophisticated collimation system is usually required, of which the arrangement described above is only the first stage. There are two basic reasons for this. The first is that the equations in (22) fully define the specified phase-space volume only to the extent that the optics between them is independent of energy over the specified $\pm\frac{\Delta E}{E}$ range. To minimize such chromatic effects it is important to place the collimators as close to each other as possible. The second perhaps more important reason is that each collimator impinged by the beam will reradiate some fraction of the incident beam through edge-scattering. For this reason, it is often desirable to add a fourth collimator $\pi/2$ phase-advance upstream of the first one in Fig. 17. With this redundant collimator, the two following ones can also serve to clean up large angle debris, and the last one to catch components of this debris with large energy errors.

Even with this extra collimator, the scheme we have described will not enable to entirely suppress particles from forbidden regions beyond the specified beam-stay-clear, and there will be a certain probability for transmitting particles into such regions. This probability can be reduced by adding more stages to the collimation system.

III.4.2.3 Beam-Stay-Clear Requirements

In relation to the nominal beam size, the tighest aperture in the system are the quadrupoles near the collision point. Although these quadrupoles only represent one betatron phase, it is appropriate to define a full phase-space volume corresponding to their

* *With very small emittances and a large β-parameter, one must also begin to worry about wakefields from the discontinuities in the beam-pipe generated by the collimators.*

aperture. The reason is that the phase relation between the collimation and these apertures is not well defined for typical tail particles with large energy errors, if the collimators are far upstream in the system. For nominal emittance and with the optics in the final focus adjusted to minimize the beam size at the collision point, this aperture, and therefore the phase-space volume to be defined by the collimators, corresponds to about five standard deviations of the beam phase-space distribution*.

III.4.2.4 Constraints on Performance from Partial Collimation

(1) Requirements on Beam Stability

During initial commissioning, the collimation scheme available at the SLC was insufficient. Only a primary cut was being made, and, in addition, the different dimensions of phase-space were cut non-orthogonally and sometimes a significant betatron phase-distance apart. As a result, not only could secondaries be transmitted, but also primary particles from corners of phase-space which are significantly correlated. Consequently, the beam stay-clear defined by these collimators was far from full-proof and was very sensitive to the detailed shape of the phase-space at the end of the linear accelerator. This generated an abnormally stringent tolerance on the stability of the phase-space. Small variations would often cause the collimator configuration to no longer be optimal and backgrounds to rise in the experimental apparatus.

With ideal collimation, the end of the linear accelerator would provide a break-point in the accumulation of errors, separating the minimization of backgrounds produced by the errors in the sections upstream of the arcs from tuning in the arcs and final focus to maximize or simply maintain the luminosity. The fraction of particles outside of the beam stay-clear defined by the collimators would then be small enough not to generate backgrounds, independent of variations in the beam phase-space upstream of this break-point. Variations would of course still need to be stabilized within this (five standard deviation) beam stay-clear, in order to maintain the luminosity. As we described in III.4.1, such stabilization must be done roughly at the level of one half to one standard deviations.

Short of such a well defined break-point, the tolerance to changes in the beam shape at the end of the linear accelerator is very tight. In the initial commissioning of the system, it was of the order of a tenth of a standard deviation, which was very hard to maintain. The collimation scheme is at present being upgraded with additional collimators. This is expected to reduce this sensitivity substantially.

---

* *This comes about from the fact that for the optimum β^* of about 0.5 cm required at the interaction point to optimize the luminosity, the one standard deviation value of the beam size in the last lenses reaches a maximum of about three milimeters, and from the fact that the aperture of these last lenses is about two centimeters. Thus, since one must allow for off-centering from misteering of about one standard deviation, the useful aperture is about seventeen millimeters or just over five standard deviations of the beam size.*

(2) Requirement to Operate with Detuned Optics

Operationally, in order to reduce the requirement for a good full-proof five standard deviation cut on the phase-space, the optical demagnification in the final focus is reduced by about a factor two. This reduces the natural beam size in all the high-β quadrupoles near the interaction point by a factor two, and lowers the probability that stray particles which have been transmitted through the collimation at the end of the linear accelerator, wander outside of the beam stay-clear specified by the aperture. This is however costly in overall performance since the beam size at the collision point is thereby enlarged, and thus the luminosity reduced.

(3) Requirements on Phase-Space at the Arc Exit

The sensitivity to insufficiently collimated beam-tails was in addition enhanced, initially, because the apertures of the final focus beam-line, upstream of the correction elements used as part of the optical buffer section for phase-space distortions (described in III.4.1), are tighter than those in the arcs, by factors of five to ten, after normalising to the nominal beam size. For this reason, otherwise correctable phase-space distortions could cause scraping off this aperture. This in turn would generate muons which could reach the detector. The tolerance to beam loss along the final focus beam-line was of the order of 10^7 particles per crossings, or one part per thousand of a beam with 10^{10} particles per bunch. This was a very stringent tolerance, which required that the beam phase-space be nearly matched at the arc exit. To meet this tolerance special optical controls within the arc lattice had to be designed, to enable controlling the beam size and shape at the end. More recently, special magnetic shielding has in addition been installed in the final focus tunnel, to relax tolerance to beam loss there by almost an order of magnitude.

III.5 TOLERANCES AND TUNING: THREE MAJOR PIECES

III.5.1 Introduction

It is appropriate to evaluate tolerances to errors and a global strategy for adjusting the system by dividing up the SLC in three major pieces, and in terms of their overall effect on performance, described in III.4.

The three major pieces are:

1. The parts of the SLC which are upstream of the damping rings: the electron and positron sources, the injector and first sector of the linear accelerator, and the transport

lines feeding the beams into the damping rings,

2. The parts of the SLC which are between the damping rings and the end of the linear accelerator: the transport lines connecting the damping rings to the the linear accelerator, and the linear accelerator,

3. And the parts of the SLC which are between the end of the linear accelerator and the collision point: the arcs and final focus sections.

III.5.2 Sources and Injector

The damping rings, thanks to the radiation damping, will "standardize" virtually anything* that is injected into them. Therefore, errors in the sections upstream of the damping rings matter only if the distortions generated become larger than the available aperture, in which case the transmission into the rings is derated. The detailed shape of the beam and its emittance are not very important as long as the beams makes it into the rings without getting scraped off. The tolerances are therefore relatively loose on the transport, as long as the phase-space generated at the source is not abnormally large. This is true both of static and dynamic errors. In this way, except for possible losses in beam current, errors and tuning upstream and downstream of the damping rings are independent of each-other. The damping rings provide a breakpoint in the overall accumulation of errors, where the beam "looses memory" of what perturbed it before.

III.5.3 Ring to Linear Accelerator Section and Linear Accelerator

Errors in the ring to linear accelerator section and in the linear accelerator will cause a combination of effective emittance growth and betatron mismatch. The effective emittance

---

* *This is strictly true only for a storage time large compared with the damping time. If the storage time, which is equal to the time between pulses in the linear accelerator, is T, and the damping time is τ, then output emittance can be written*[21]*:*

$$\epsilon_{out} = \epsilon_{eq}(1 - \epsilon^{-\frac{2T}{\tau}}) + \epsilon_{in}\epsilon^{-\frac{2T}{\tau}}, \qquad (23)$$

where $\epsilon_{eq} \simeq 2\ 10^{-5}$ mrad is the normalized equilibrium emittance of the ring. For the initial specification of the SLC at 120 Hz, $T = 8.3$ms. The damping time is $\tau \simeq 3$ms. This allows to calculate the maximum emittance or distortion ϵ_{in}^{max} of the phase-space at the injection to the damping rings which will be damped to the desired normalized emittance value of $\epsilon_{out}^{des} = 3\ 10^{-5}$ mrad. We find, using (23): $\epsilon_{in}^{max} \simeq 85\ \epsilon_{out}^{des}$. This sets a theoretical tolerance on the input phase-space at injection. As can be seen it is a rather comfortable tolerance. The practical tolerance set by the aperture of the injection lines is in fact more stringent.

growth is uncorrectable and affects the luminosity that can be achieved directly. The mismatch of the phase-space will if left uncorrected combine with the mismatch generated in the arcs and final focus. As long as such errors are static, this is not a major problem for the luminosity. The effects from, and sensitivity to such mismatch, from the point of view of the luminosity, was described in III.4.1.

The static tolerances must be specified to avoid significant emittance growth. If the collimation system at the end of the linear accelerator is close to perfect, and defines a full-proof beam-stay-clear, as described in III.4.2, then these tolerances must be determined to maintain a stable phase-space at the end of the accelerator to one half to one standard deviations of the nominal parameters. In this case, the tolerances in the linear accelerator are of the order of 100μm for the orbit errors, and of the order of half a percent for the focusing errors, in order to assure emittance growth below a factor 1.5*. The tolerance on the focusing errors is not difficult to meet for the quadrupole strengths. It is however quite difficult to know the energy of the gradually accelerated beam, locally, to that precision.

In addition, because this energy depends on the population of klystrons used to generate the RF power which is fed to the beam, and on the correct phasing of this RF at each station, and because both these are not entirely stabilized, the phase-space mismatch and effective emittance growth are not necessarily stable. It is therefore most often unreasonable to allow them to accumulate and combine with residual errors in the arcs and final focus, because as we will see, the tuning procedures for the final focus are complex and lack orthogonality, which means that a full reoptimization can be required even for modest changes. In general, this second part of the system can be considered the "active" part of the SLC. Stabilization is still an ongoing effort.

In the case of the ring to linear accelerator transport line, a chromaticity corrected optical system, the tolerances are determined by the requirement to minimize higher order aberrations. This is similar to the requirements in the final focus which we describe in chapter VII. Work on this is also ongoing.

III.5.4 Arcs and Final Focus: Range of Optical Buffer Section

Because the arc lattice is achromatic, the errors are transmitted coherently to the end, and can therefore be corrected optically in the final focus. The final focus is equipped with special optical matching elements to perform such corrections. Because the SLC has nominally equal emittances in both transverse planes, this optical matching is designed to correct the ten possible independent phase-space distortions, and uses therefore ten variable elements. The correction range allows to match phase-spaces distorted by as much as four standard deviations of the nominal parameters, and in any of its dimensions.

---

* *As we described in III.4.2.4, the tolerances in the linear accelerator were initially much more stringent, due to the fact that the collimation system was insufficient.*

If the beam phase-space is close to matched at the exit of the linear accelerator, and if for a moment we do not consider the background problems, then the tolerances to errors in the arcs are in principle set by the correction range available in the final focus. We can then estimate the tolerances through (10), by calculating the standard deviation ϵ_R of the random errors compatible with the factor four correction range. We find, since the number of cells is $N = 230$, and if require a 98% confidence level: $\epsilon_R \simeq 0.023$.

This is a rather loose tolerance. Initially the system was much more sensitive, for the two following reasons.

1. As already mentionned in III.3.3.2, the discontinuities introduced into the arc lattice by the rolls of the achromats resulted before the modification of the roll transitions in a severe tolerance to systematic errors, of the order of 0.005 (see section VI.2)

2. As already mentionned in III.4.2.4, the smaller normalized apertures in the final focus beam-line required initially that the beam phase-space be negligeably mismatched at the end of the arc. The tolerances to random errors were in this case also of the order of $\epsilon_R \simeq 0.005$.

III.5.5 Global Tuning Strategy

The above considerations on the tolerances and on the tuning in the SLC are summarized in Fig. 18. Both static and dynamic random errors naturally cause an average growth of the phase-space with the exponential of the square root of the distance. Two breakpoints exist, where the beam is in principle reset to its nominal condition. These breakpoint separate the tuning in the three parts of the SLC which they define. The first breakpoint, the damping rings, re-standardizes the beam perfectly. The second breakpoint, consisting of the collimators at the end of the linear accelerator, serves to separate tuning related to maximizing the luminosity from the requirement to minimize backgrounds in the experimental apparatus. The settings of the collimators are determined by the optical set-up arrived at in the arcs and final focus. This set-up results from tuning both these sections to maximize the luminosity at the interaction point. After this, the second breakpoint - the collimators - decouples the backgrounds in the detector from tuning in the upstream sections. The tolerable error level and performance of feedback corrections and tuning are determined at each stage by the "capture-range" defined by each of these breakpoints.

Much of the present challenge in optimizing the overall tuning strategy of the SLC is the definition of the second breakpoint, by improving the collimation at the end of the linear accelerator, and the tuning of the beam in the second part of the SLC: the ring to linear accelerator and linear accelerator sections. Once this is done, the optics in the arcs and final focus can be adjusted to optimize the luminosity independent of background considerations.

IV. SLC TURN-ON PROGRAM

IV.1 INTRODUCTION

What was described above is the current status and understanding of the commissioning of the SLC. Both result from our accumulated experience with this machine[22]. The initial program proceeded in a rather different way, as we were learning to operate this new kind of machine.

Commissioning and tests of successive stages of the SLC were an ongoing enterprise since the fall of 1981, and throughout the construction period (fall 1984 to spring 1987). Subsequently, and for a little over one year, much dedicated work was devoted to the newly installed arcs and final focus sections, with continuing improvements in the upstream parts. This last half-year, the full extent of the overall tuning problems of the SLC have been recognized. Special efforts are now dedicated to optimize each system according to the general framework described in III.5.5.

IV.2 EARLY COMMISSIONING PHILOSOPHY

The early commissioning philosophy for the systems downstream of the damping rings consisted in transmitting the beam rapidly and as far as possible into each newly built and installed systems to enable early diagnosis of major installation and construction errors. After this was done, the program continued with an overall tuning and correction strategy which treated the final focus section as an optical buffer section for the accumulated errors in the whole machine.

The program therefore began early on trying to focus the beam to a small size at the collision point, although with little success, because of primarily two reasons: the specific problems with the arc lattice, which were not understood initially, and were discovered experimentally, and the lack of understanding and stability of the phase-space at the end of the linear accelerator, due to insufficient time spent commissioning the upstream parts of the SLC.

IV.3 OPTIMIZING THE ARC PHASE-ADVANCE[23]

After the mechanism which caused the arc lattice to distort the beam phase-space had been identified, namely the sensitivity to systematic phase errors introduced by the

rolls, the program shifted towards minimizing the distortions, through a combination of measurements of the phase-advance in each of the achromats, and partial corrections, possible in the combined function magnets, by physically moving magnets and by combining trim windings in each achromat and a global imbalance between focusing and defocusing magnets set up in a separate circuit.

IV.4 MODIFICATION OF ROLL-BOUNDARIES

A second cure which was devised consisted in modifying the roll distributions to generate transitions with a greater tolerance to systematic phase errors. The adjustments of the arc phase-advance had brought the system close to specification, and had minimized the coupling to the point where it could be handled relatively well by the optical matching sections in the final focus. It was however felt important for future operability to implement this passive cure, which made the system significantly more error-tolerant, particularly for equal or close to equal input emittances. After implementation of this modification, the arcs behaved much as arcs without rolls, and although some cross-plane coupling remained at the arc exit, the beam envelope was near its nominal size. This, and improvements made in controlling the phase-space at the end of the linear accelerator, enabled to obtain and to maintain small focused spots of about 5μm at the collision point.

IV.5 NEW AND TIGHTER CONSTRAINTS FROM BACKGROUNDS

In the next commissioning phase, the problems of minimizing backgrounds in the detector began to be included in the tuning strategy. The initial collimation strategy concentrated the primary collimation in the final focus, where nearly every accessible place on the beam-line is at the same betatron phase because of the large β-functions, and where only small fractions of the phase-space could be cut without generating excessive numbers of muons reaching the detector. Because of these two problems, a nearly matched phase-space was found to be required at the entrance to the final focus. For this reason, two additional modifications had to be introduced. Firstly the collimation strategy had to be modified, and the primary collimation redeployed to the linear accelerator to arc beam-line ("beam switchyard") and to the arc "reverse bend". Secondly, a new scheme for doing optical corrections with the combined function arc magnets, through harmonic perturbations, had to be devised to enable adjusting the beam shape at the arc exit.

IV.6 COLLIDING BEAM OPERATION

After this, the program proceeded trying to maintain stable colliding beams at the interaction point, with low backgrounds. This involved both small adjustments to the optics in the arcs and final focus and extensive use of the new collimators. In this phase, the beams were made to collide and maintained in collision for the first time by detecting beam-beam deflections, which result if the beams don't collide head-on.

The beam-beam deflection method was proposed at an early stage in the commissioning, as a way to bring the focused micron size beams into collision at the interaction point, using the electromagnetic fields produced by the charged electron and positron bunches. These fields are intense enough to deflect the opposing bunch coherently, if the collision is not head-on. The deflections can be measured with strip-line beam position monitors at the system's high β-points, where they are magnified.

This method is one of the three observable effects from the beam-beam interaction at the SLC. The two other methods are the synchrotron radiation emitted as the particles are deflected in the electromagnetic field of the opposing bunch ("beamstrahlung"), and the enlargement of the betatron angular spread at the interaction point from these same fields ("disruption").

With its strong and relatively easy to detect signals, the beam-beam deflection method has become the primary method for maintaining the beams in collision. It also provides a signal strongly correlated with the luminosity, which may in the future be used to optimize the beam sizes of the two beams at the interaction point.

IV.7 TOO MANY KNOBS

With a not fully stabilized phase-space at the end of the linear accelerator, with the presence of still some unstable pieces of hardware in the arcs and final focus, and because of insufficient and solely primary collimation, the program often became non-convergent: collimators were set-up one day for a given phase-space; then the beam phase-space would change and particles would begin to get transmitted into forbidden parts of the required beam stay-clear. The response would be a combination of re-adjustments of the collimators and of the optics in the arcs and final focus, which images the collimators. This would then require further optical adjustments to re-optimize the beam size at the interaction point and so on. It was understood that to solve this problem, the program had to begin by ascertaining a stable optical set-up in the arcs and final focus, where corrections would not be made continually to feedback on variations in the beam sizes at the collision point or to rising backgrounds, but rather as well thought out adjustments based on time-averaged observations and measurements. It was also understood that the stability of the linear accelerator is essential, and that a more full-proof collimation system is needed to separate luminosity maximization from background minimization, as described above.

Also, reliability issues began to receive more attention, as the time to reach a well optimized set-up became longer, with the ever increasing requirements put on the phase-space, and sometimes almost reached the time between hardware failures in the machine.

IV.8 PRESENT GOALS

The SLC is at present being restarted. A new collimation system is to be installed at the end of the linear accelerator. Also, special magnetic shielding has been installed in the final focus tunnel, to reduce the rate of muons generated by beam tails getting scrapped off the vacuum chamber of the early parts of the final focus. This, combined with the already existing slits, will enable beam tails to be cut more efficiently.

Furthermore, much attention is now given to controlling and stabilizing the beam phase-space at the end of the linear accelerator. This, coupled with improvements in handling the backgrounds, is expected to enable using the nominal rather than the detuned optical configuration in the final focus, and thus to reach a lower β^*-parameter for the beam at the interaction point.

In addition, tests are being made with larger intensities (2 and 3 10^{10} particles per bunch), to begin exploring experimentally the hich current dynamics and the possibility to reduce wakefield effects through the introduction of a large energy spread along the bunch in the early sectors of the linear accelerator (so-called BNS damping).

The combination of these improvements, and of others not mentionned here, is expected to enable producing a useful rate of detectable Z^o particles.

V. OVERVIEW OF OPTICAL TUNING IN THE ARCS AND FINAL FOCUS

V.1 INTRODUCTION

The optical tuning procedures which were devised to adjust the arcs and final focus sections of the SLC result from:

1. The basic principles of the optical design of these two sections, which were described in chapter II, and

2. The global evaluation of the sensitivity to imperfections and of the overall tuning considerations described in chapter III.

These procedure where furthermore developed in the framework of the actual strategy followed to commission the SLC, as sketched in chapter IV.

V.2 OPTICAL TUNING IN THE ARCS

The SLC arcs have an achromatic lattice consisting of a FODO array. To maximize the packing factor, combined function magnets are used. All magnets except in the "beam switchyard" and "reverse bend" are on the same power supply. The magnets are equipped with backleg windings, on a achromat by achromat basis. These backleg windings were originally introduced to provide a gradual adaptation of the magnet excitation to the beam energy, which decreases by about 1 GeV because of the synchrotron radiation emitted in the bending field. In addition, an imbalance between focusing and defocusing magnets can be set up globally over the length of the arc, through a separate circuit.

The goal of the tuning in the arcs is primarily to render the optical transfer as close as possible to an identity transformation. To some extent, tuning in the arcs is also used to supplement the tuning of the final focus, as explained in III.4.2.4, in order to correct for errors in the incoming phase-space. Three methods were devised for this purpose. The two first ones are specifically geared towards optimizing the lattice in the presence of the large discontuities introduced by the rolls. The third one is a more general method for adjusting long repetitive FODO arrays.

V.2.1 Phase-Adjustments[23]

The first one is a partial adjustment of the phase-advance per achromat in each plane, by moving magnets horizontally, by readjusting the backleg windings and by setting up the

global imbalance. This had to be done since the rolls were in the original design grouped in compensating pairs separated by one or several achromats, to adjust the phase-advance in each plane near its design value of 6π per achromat.

V.2.2 Smoothing out Roll Discontinuities

The second one is a modification to the roll distribution, enabling a smoother transition, which was shown to reduce the sensitivity of the lattice to systematic errors substantially. This was a passive correction, which reduced the need for doing precise adjustments of the phase-advance.

This modification is described in section VI.2.

V.2.3 Harmonic Corrections

The third correction is a harmonic correction. It applies more generally to FODO arrays, and allows to correct any kind of error generated in the arcs. It is designed in particular to correct for coherent build-up of the phase-space distortions due to errors at twice the betatron frequency, including both in-plane phase-space distortions and cross-plane coupling. The required trim corrections were introduced in the combined function magnets by rewiring the backleg windings in each magnet of the last seven achromats of each arc into sets, spatially modulated at twice the betatron frequency. By driving the upper and lower windings of each magnet separately, it is possible to generate both regular and skew quadrupole perturbations in the magnets. In total, the lattice can be perturbed in nine independent ways through this method. These additional adjustments allow both to take out errors in the lattice and to correct distortions of the phase-space injected into the arcs.

This method is described in sections VI.3 and 4.

V.3 OPTICAL TUNING IN THE FINAL FOCUS

The optical corrections in the final focus were designed to enable readjusting the lattice, in order to absorb phase-space distortions in beams with equal emittances in both planes at the injection to the section. The design of these adjustments and of the strategy for optimally applying them started out with an optical system which had already been optimized for the required performance of the final focus and for the available space. Because

of this, the design work had to take a pragmatic approach, and only slight modifications to the lattice were possible. As a result, some of the correction modules straddle several of the telescopes of the final focus, and are therefore strongly coupled. In addition, one of them has a practical range severely limited by perturbations to the trajectory produced on the outgoing spent beam.

The maximum adjustments of the optics which are possible enable absorbing distortions of up to a factor four in any of the orientations of the phase-space. All components of the transverse phase-space and the couplings between them must be controlled to minimize the beam size at the collision point. This involves ten independent distortions of the phase-space, and thus the correction algorithm uses ten variable quadrupoles.

The adjustments are grouped in three sets:

1. Four corrections to minimize the spatial and angular dispersion in both planes, using two pairs of quadrupoles to perturb the matching of the dispersion in the first section of the final focus. The pairs are separated by $\frac{\pi}{2}$ and consist of regular and skew quadrupole for control in each plane.

2. Three corrections to the betatron angular spread at the interaction point, by controlling the magnitude of $< x'^2 >$ and of $< y'^2 >$, and by minimizing the $< x'y' >$ correlation. This is done using the two last erect quadrupoles and a skew quadrupole in the upper telescope, where the demagnification of the final focus is initiated.

3. Three adjustments to position the waists in both planes at the interaction point, by minimizing the correlations between the positions x,y and the angles x',y' in both planes. This is done using trim windings on the next to last two quadrupoles of the final telescope, and with a skew quadrupole just upstream.

The ten variable quadrupoles used for these corrections are shown in Fig. 12. Because each correction is coupled to the ones downstream, they must be applied sequentially. A flow diagram illustrating this sequential application is shown in Fig. 19.

The seven first adjustments are strongly coupled and depend non-linearly on phase-space parameters. The final three waist corrections can be orthogonalized independent of the input phase-space. A ten-dimensional non-linear fitting program has been developed to match the lattice in the final focus to the input beam. Local orthogonal "knobs" are also defined for fine-tweaking around the initial solution, although this is not always practical because of steering from the lenses.

The optical tuning of the final focus is the subject of chapter VII.

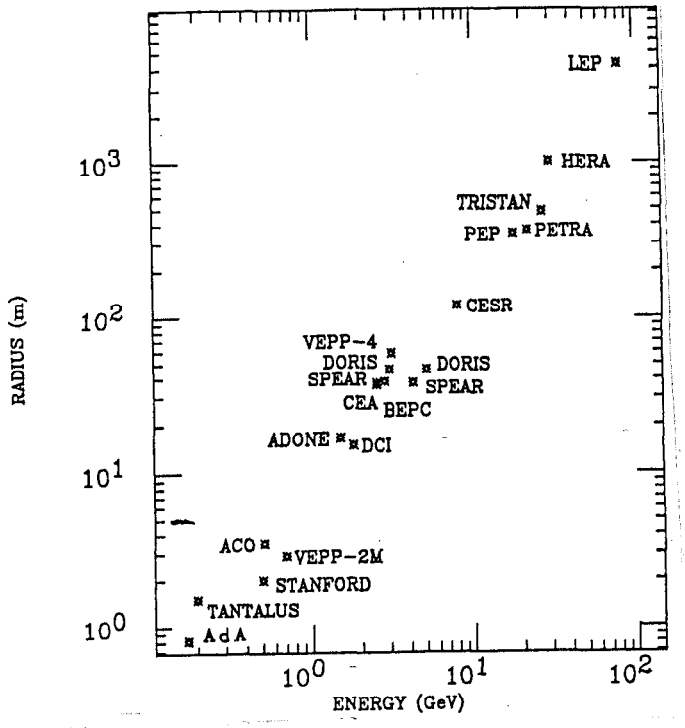

Figure 1. Average radius of the majority of the storage rings as a function of their energy. The dependance is close to quadratic.

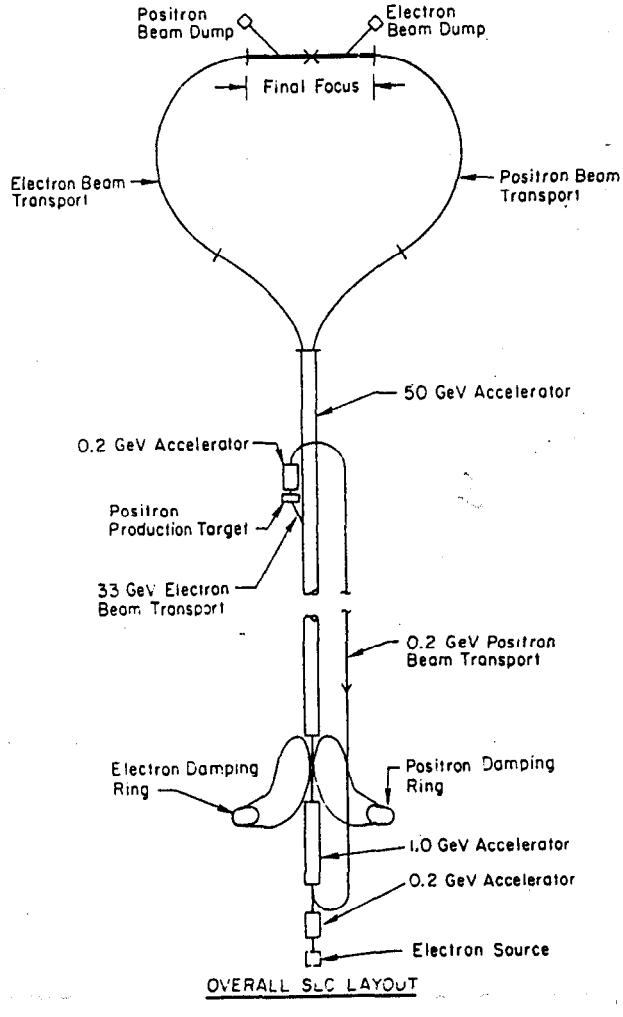

Figure 2. The Stanford Linear Collider.

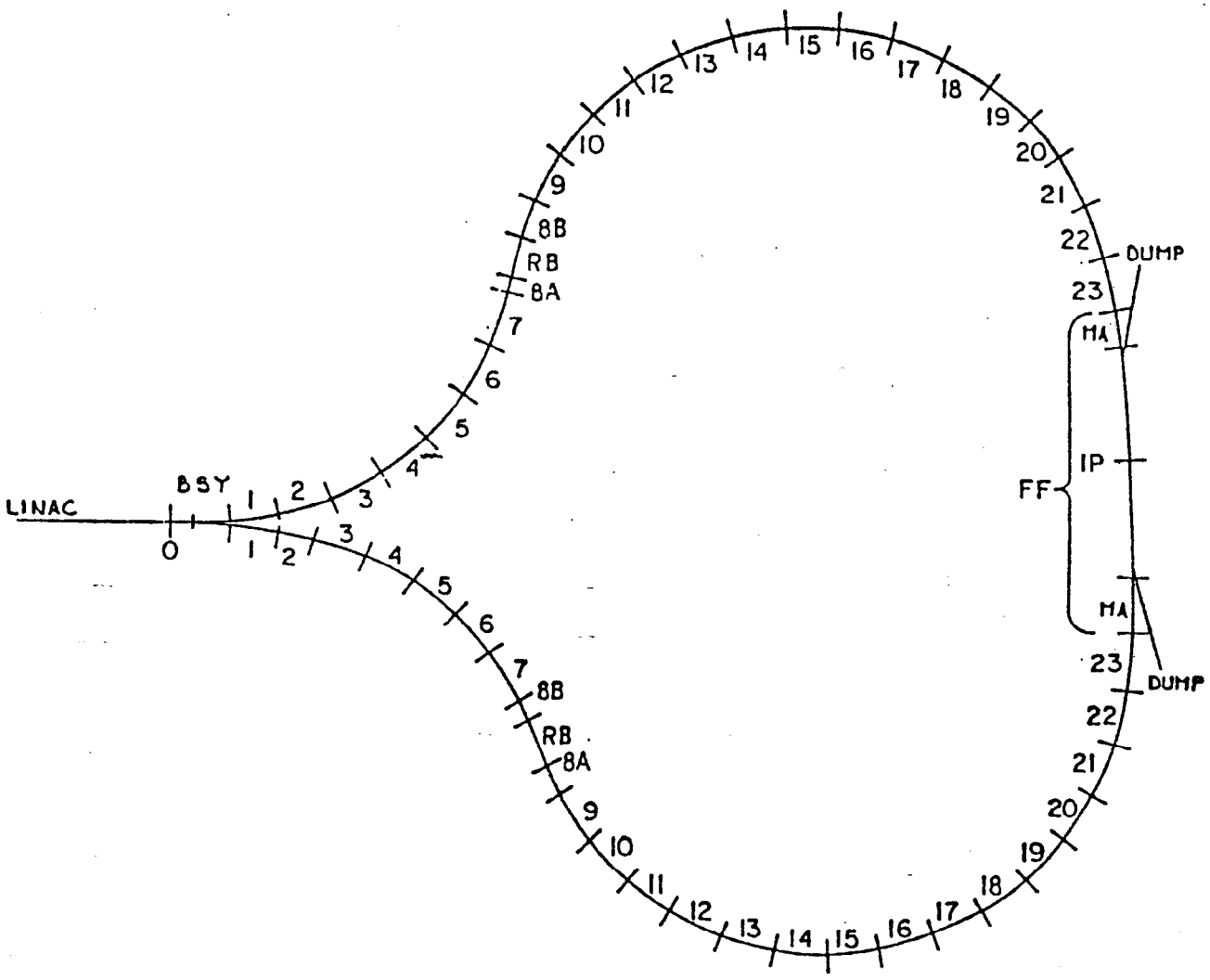

Figure 3. General layout of the arcs. The numbers refer to each achromat.

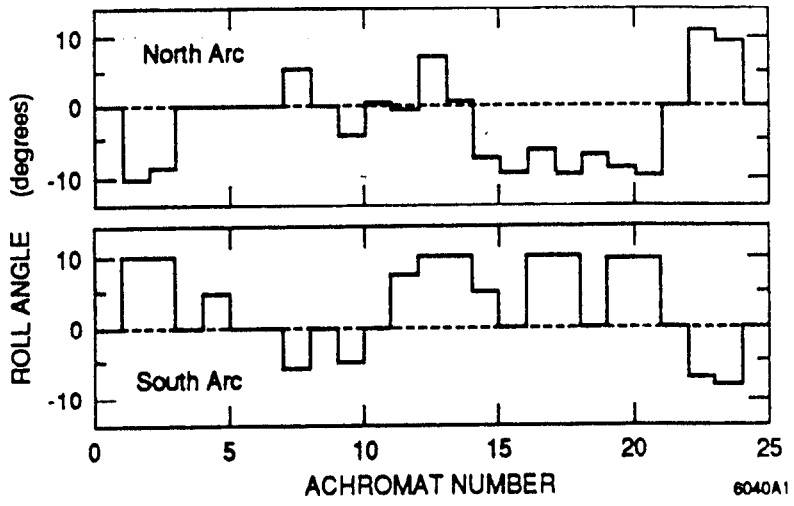

Figure 5. Rolls about axis of achromats in north and south arcs.

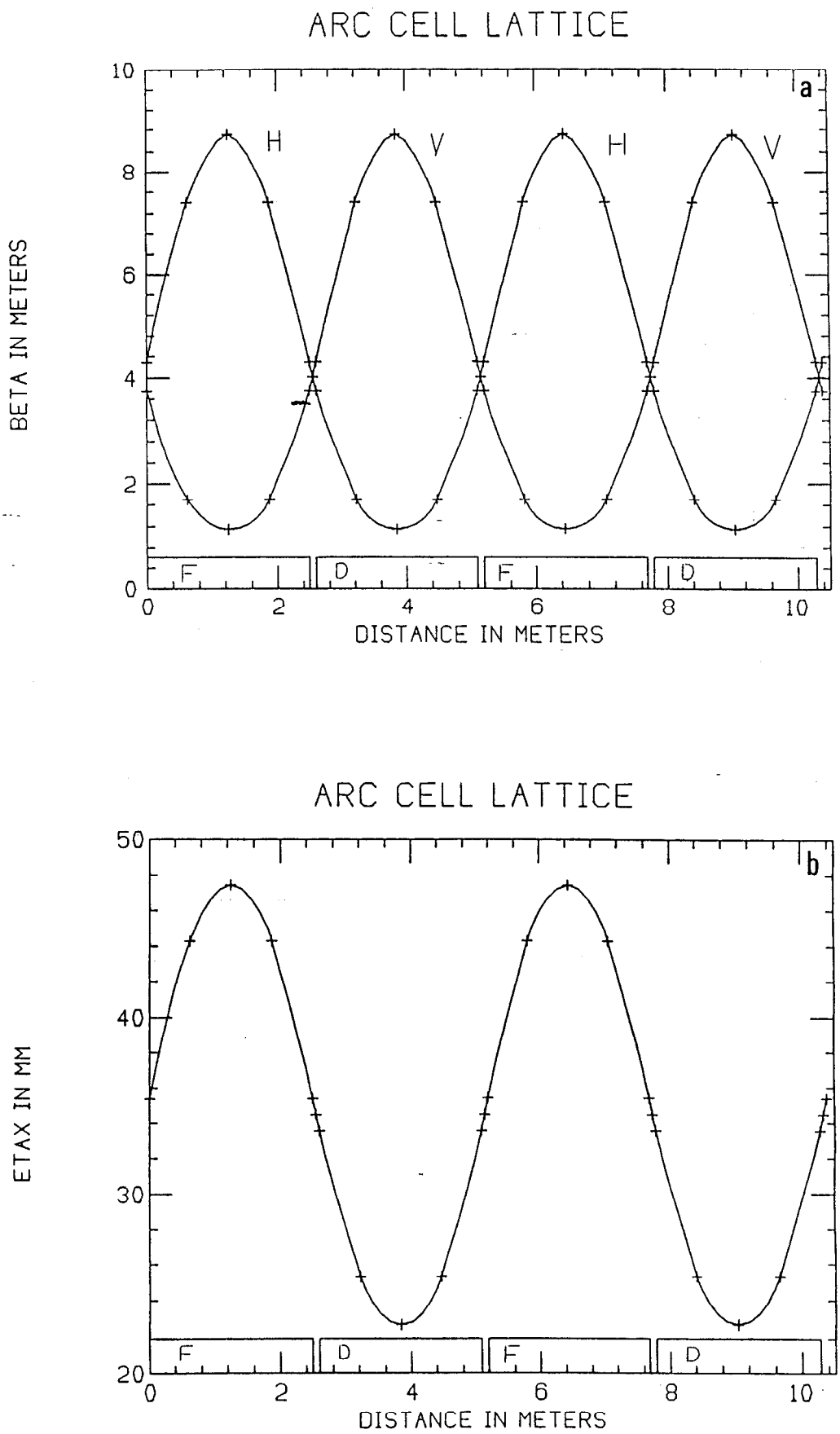

Figure 4. Optical functions of the arc lattice: in (a) the β-function, and in (b) the η-function.

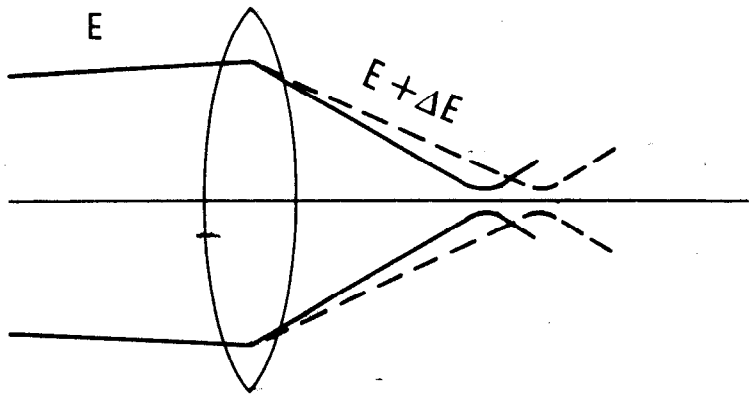

Figure 6. Longitudinal displacement of the focal point with the energy.

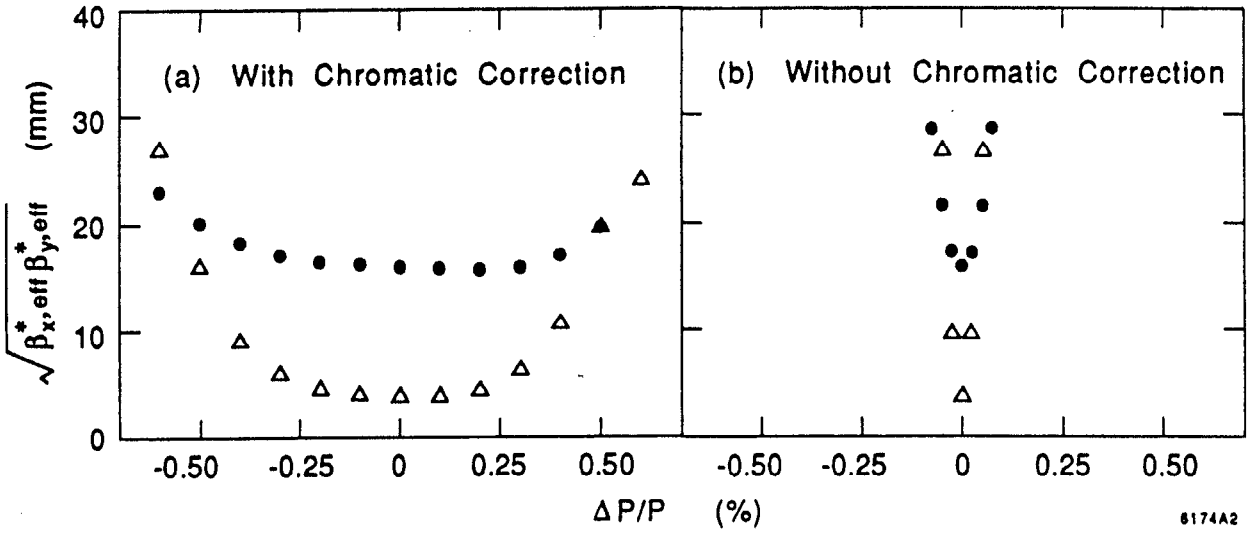

Figure 7. Variation of the β-parameter with the fractional energy error in the final focus section, with chromaticity correction (a), and without chromaticity correction (b). As can be seen, the optical bandpass of the system is enlarged by the chromaticity correction.

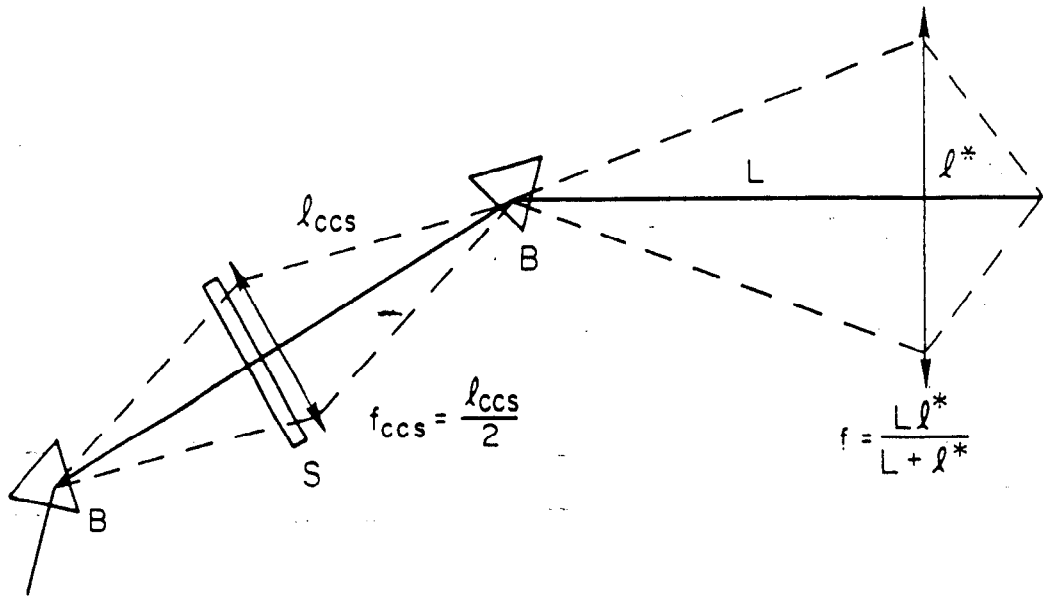

Figure 8. A simplified final focus section.

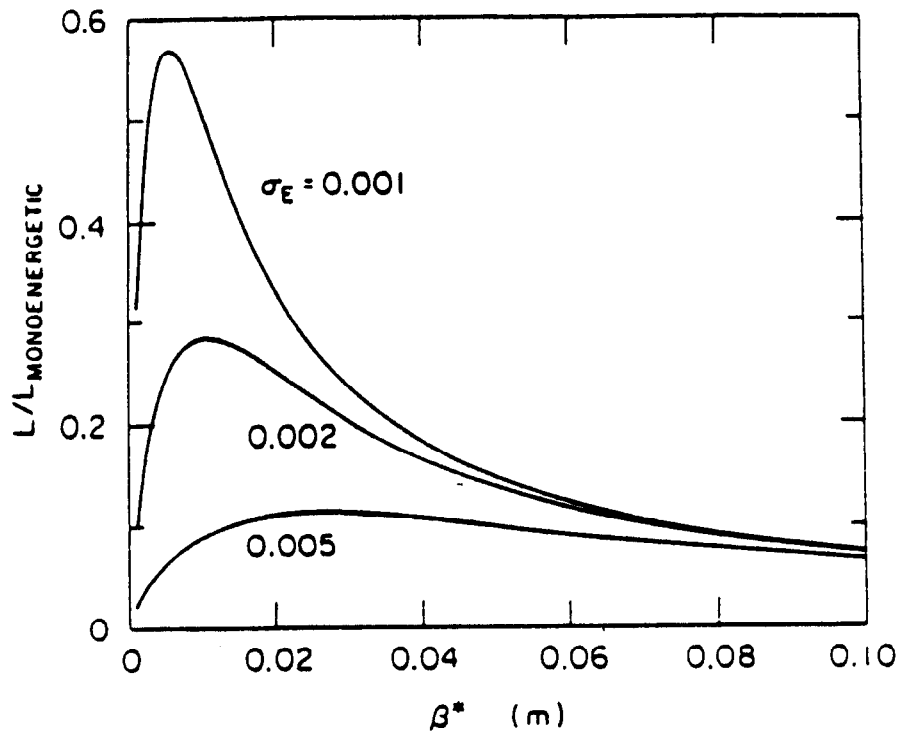

Figure. 9 Relative variation of the luminosity with the β^*-parameter in the final focus section, without chromaticity correction, and for several values of the energy spread.

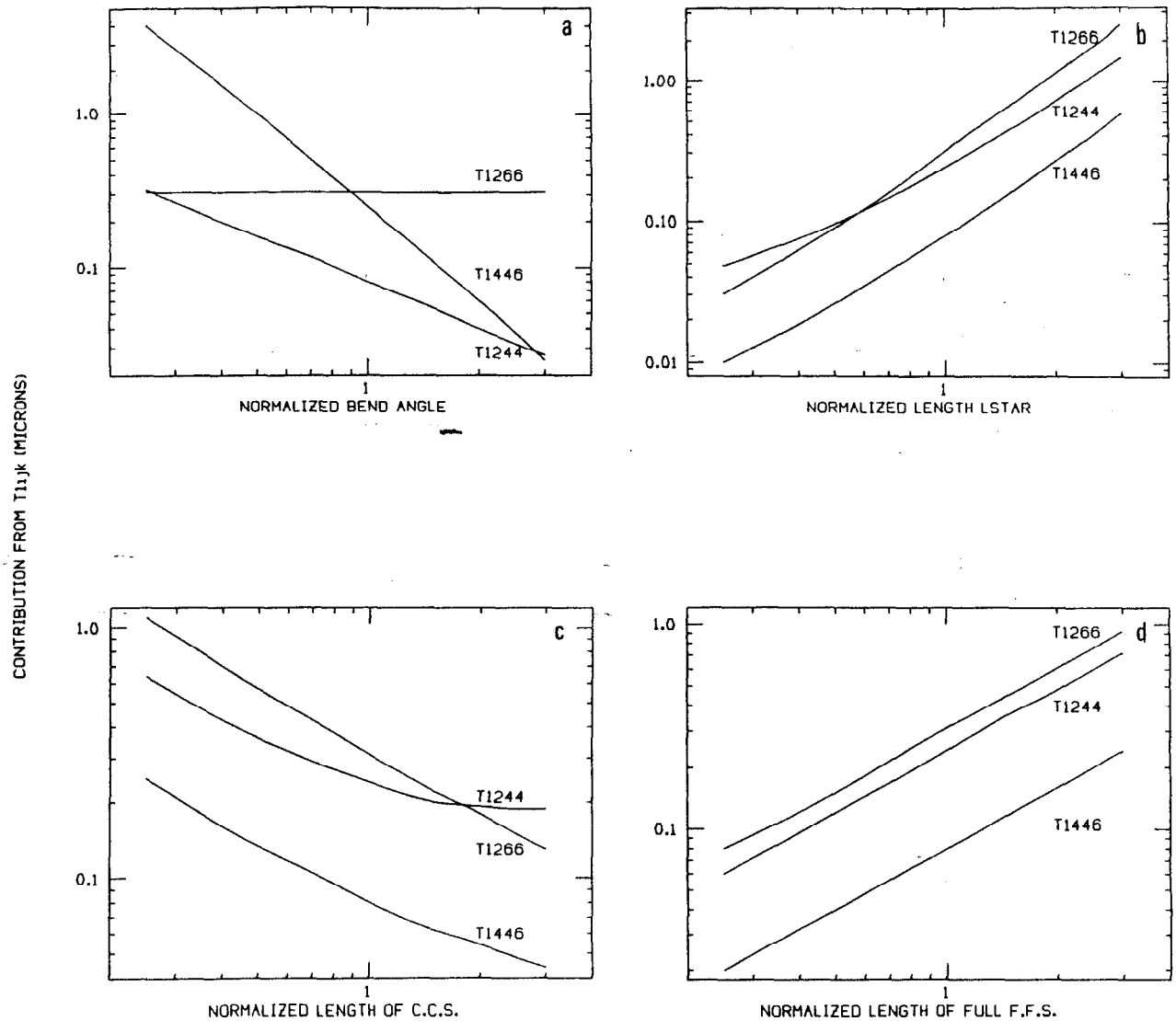

Figure. 10 Contribution to the interaction point beam size of the main second order aberrations, as a function of the bend angle of the chromatic correction section (a), of the distance between the last quadrupole and the collision point (b), of the length of the chromatic correction section (c), and of the total length of the system (d). The real power dependances for each of these aberrations are:

(a) $T_{1266} \propto B^0$, $T_{1446} \propto B^{-1}$, $T_{1244} \propto B^{-2.05}$

(b) $T_{1ijk} \propto (l^*)^{1.79}$

(c) $T_{1266} \propto (l_{ccs})^{-0.86}$

(d) $T_{1ijk} \propto (l_{tot})^{-0.98}$

In the case of (c), the power dependance is slightly weaker for T_{1244} *and for* T_{1446}*; for large values of* l_{ccs}*.*

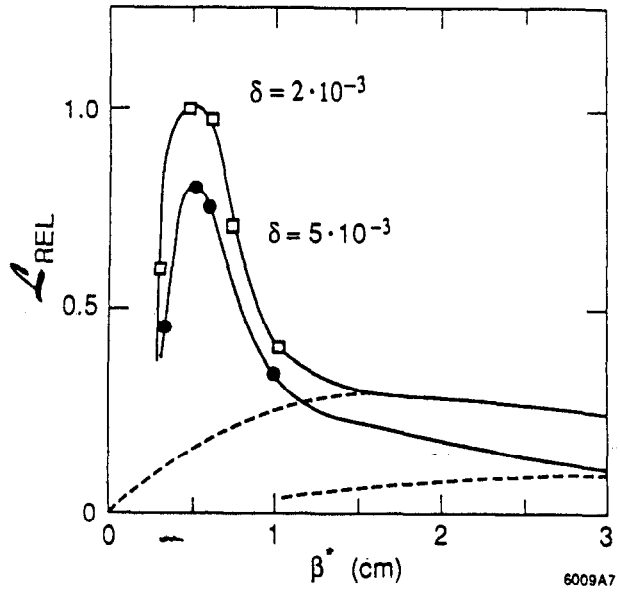

Figure. 11 Relative variation of the luminosity with the β^*-parameter, with chromatic correction (full line), and without chromatic correction (dotted line).

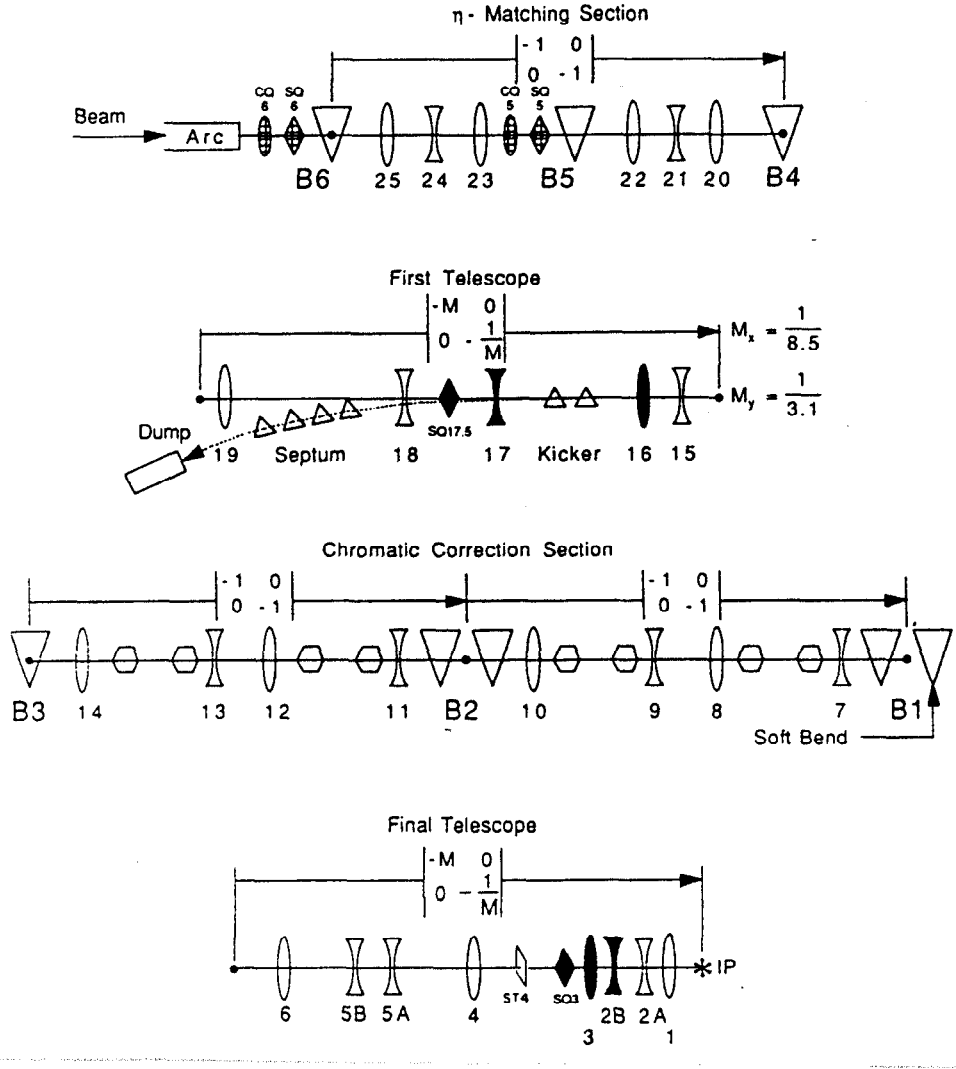

Figure. 12 Schematic of the final focus optics. Correctors for betatron matching are shown shaded, and for dispersion matching cross-hatched.

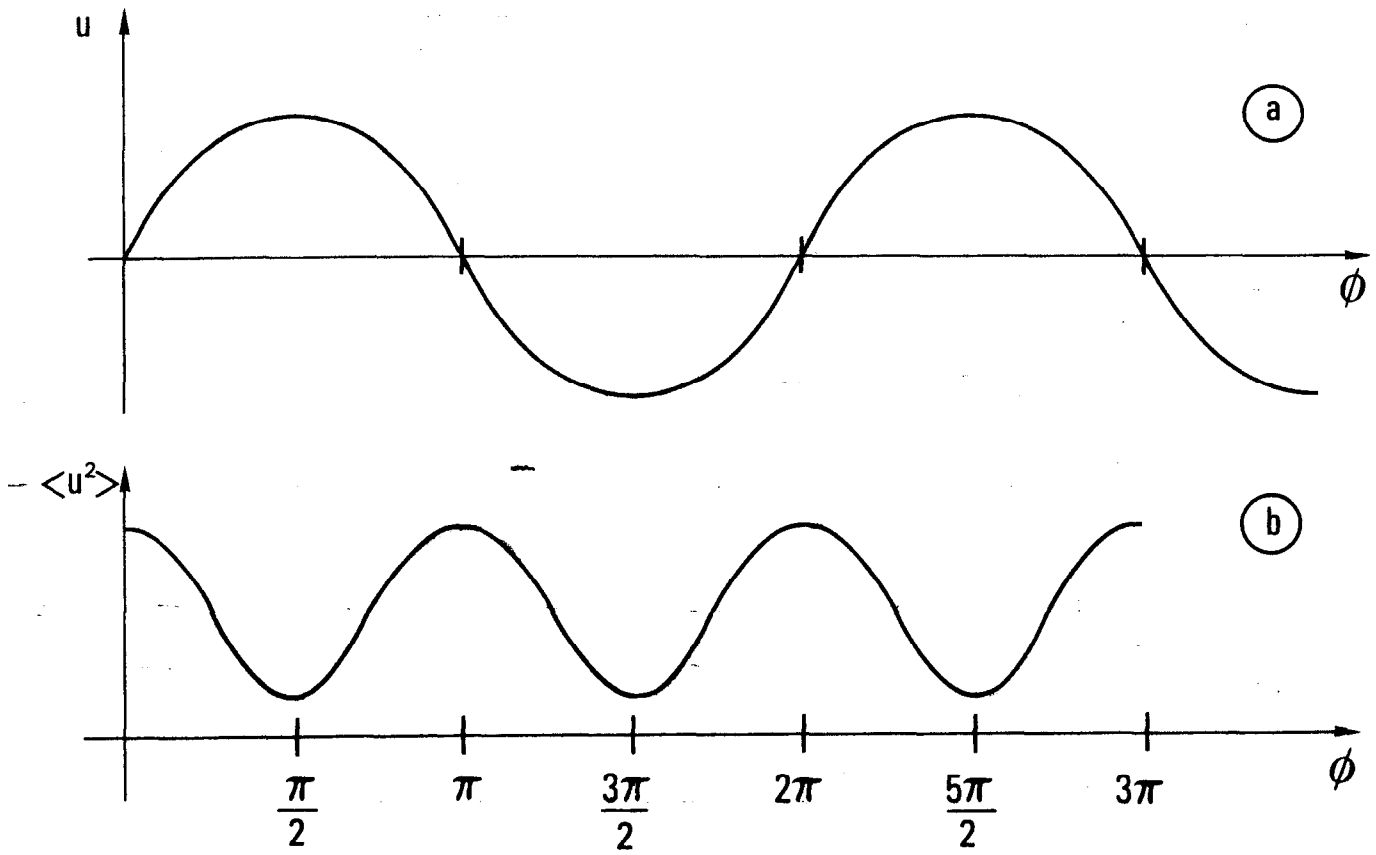

Figure. 13 Betatron oscillation (a) and oscillation of the square of the beam envelope (b) in the focusing lattice. The oscillation of the square of the envelope is at twice the betatron frequency.

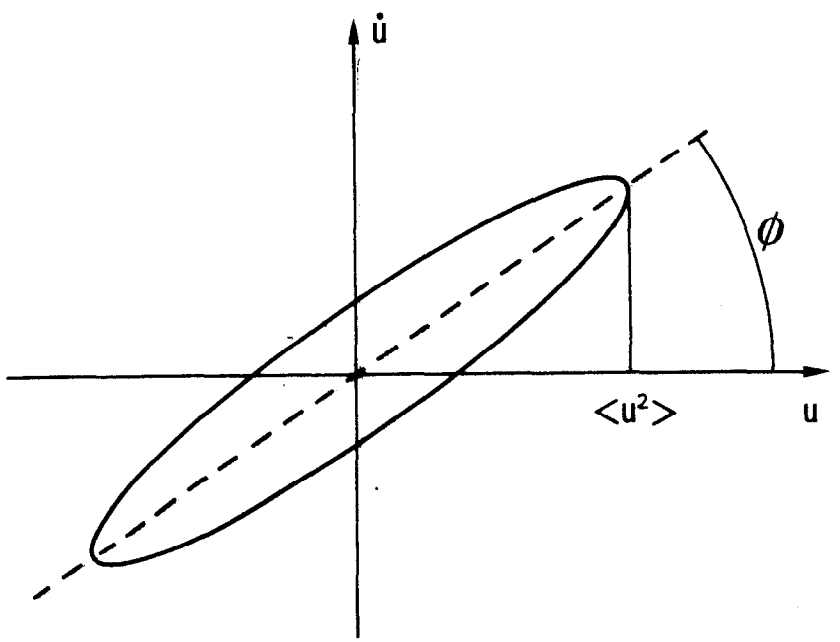

Figure. 14 Distortion and rotation of beam phase-space from a focusing error.

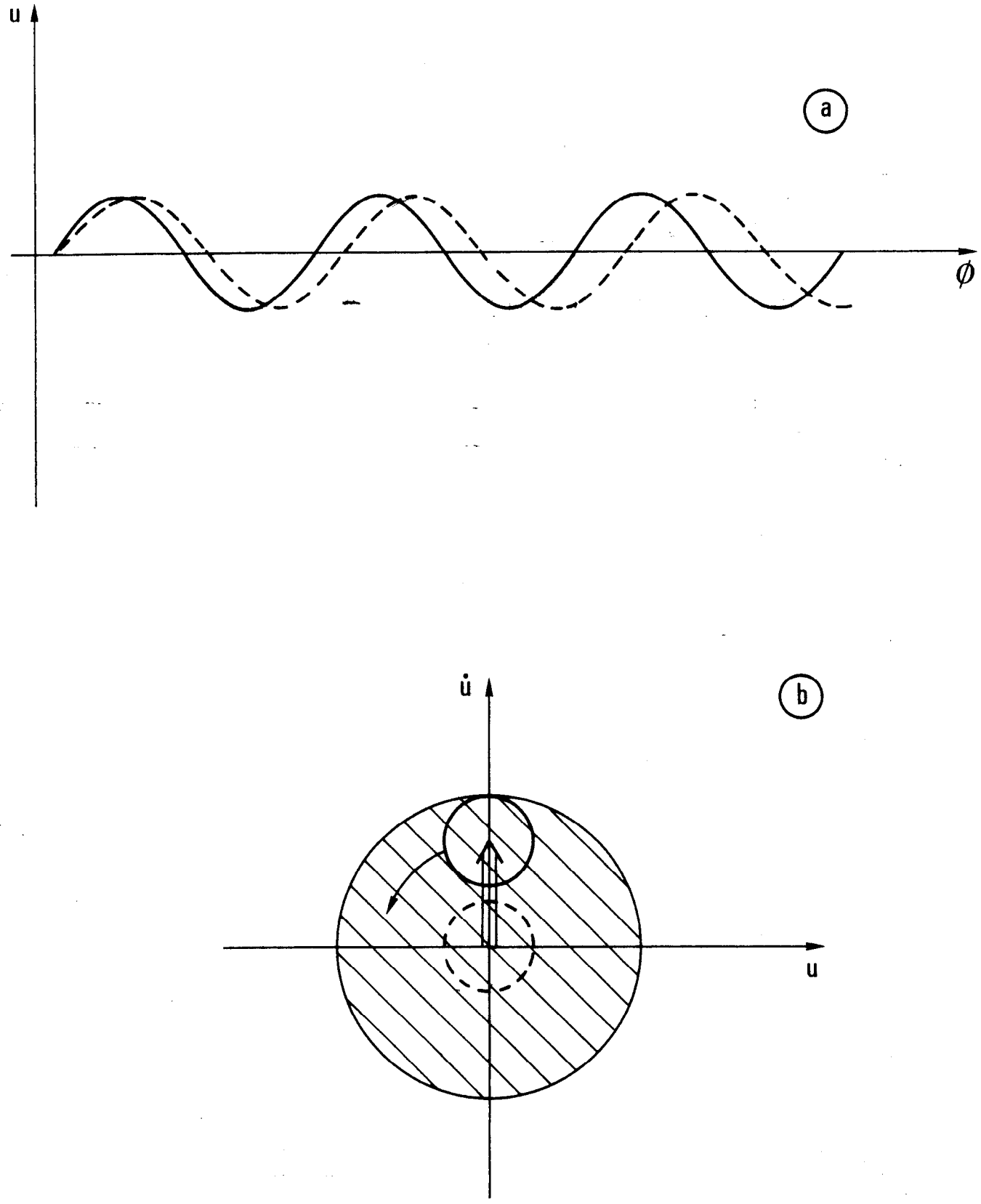

Figure. 15 Incoherent imaging of a betatron oscillation of a beam with finite energy spread (a). This results in an abnormal correlation between the transverse coordinates and the energy of the particles in the beam. The projection of the phase-space $(x, x', \frac{\delta E}{E}, z)$ *on the plane* (x, x') *is thereby enlarged.*

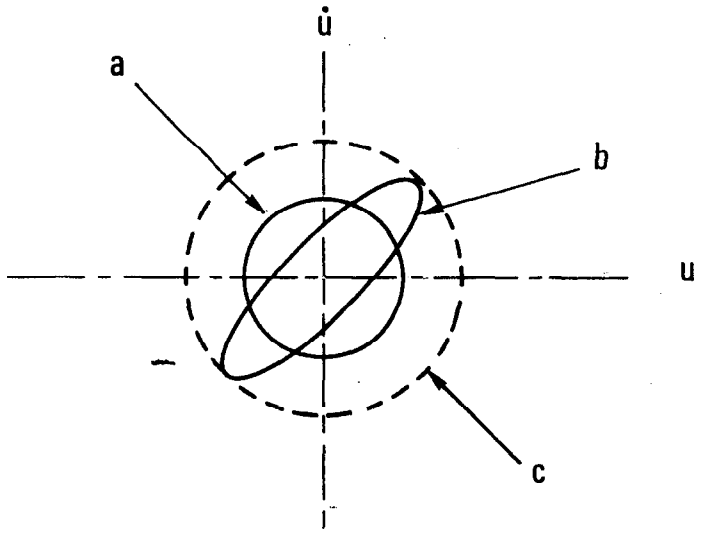

Figure. 16 Incoherent imaging of a phase-space distortion. In (a), we show the nominal phase-space, and in (b) the distortion of this phase-space from a focusing error. The incoherent imaging of this distortion generates a second order correlation between the transverse coordinates and the energy of the particles. When this correlation becomes large, the projection of the phase-space on the plane (x, x') will correspond to the larger cercle in which the ellipse is inscribed.

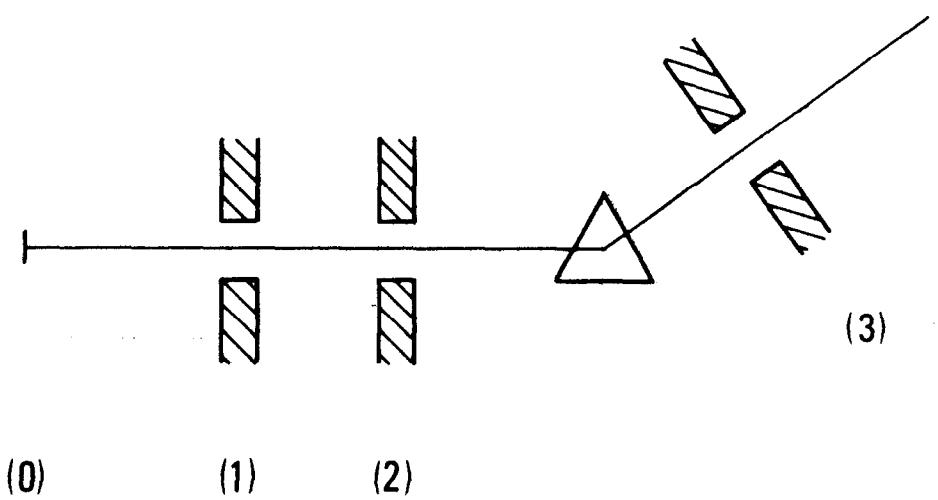

Figure. 17 Basic principle of collimation.

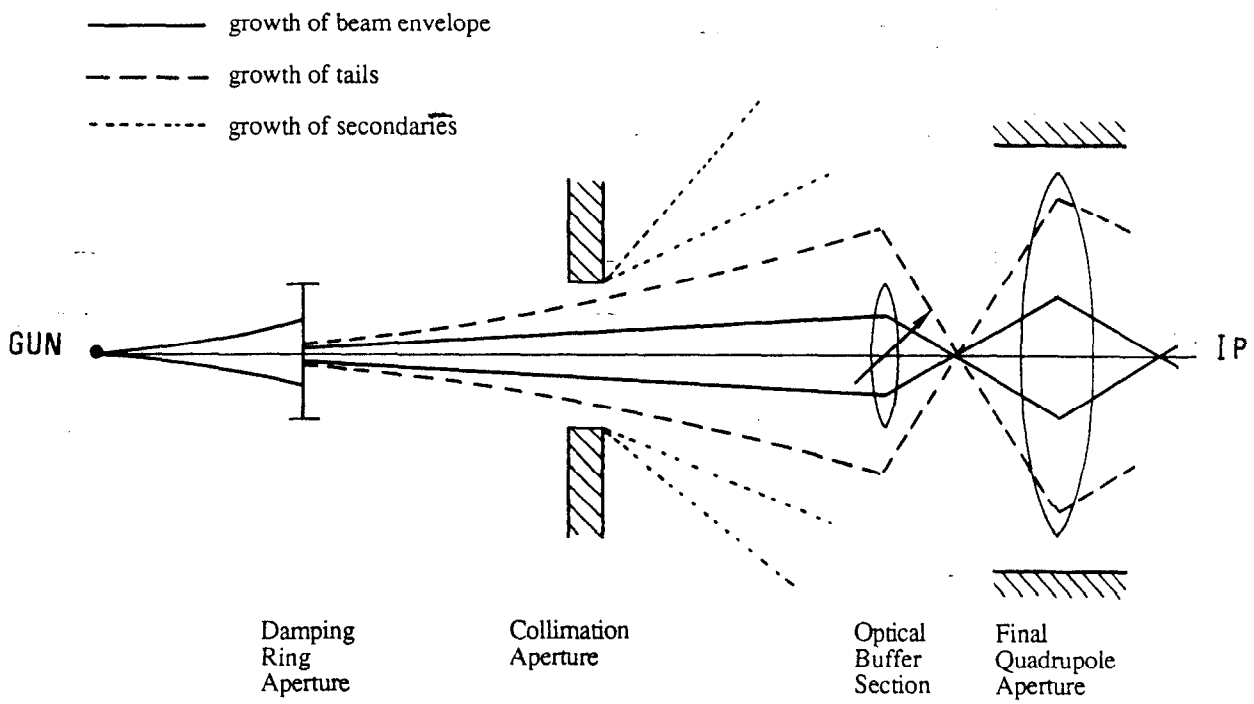

Figure. 18 Illustration of the separation in three major pieces of the tuning in the SLC. There are two breakpoints in the accumulation of the errors, from the radiation damping in the rings, and, in a more imperfect way, from the collimators at the end of the linear accelerator.

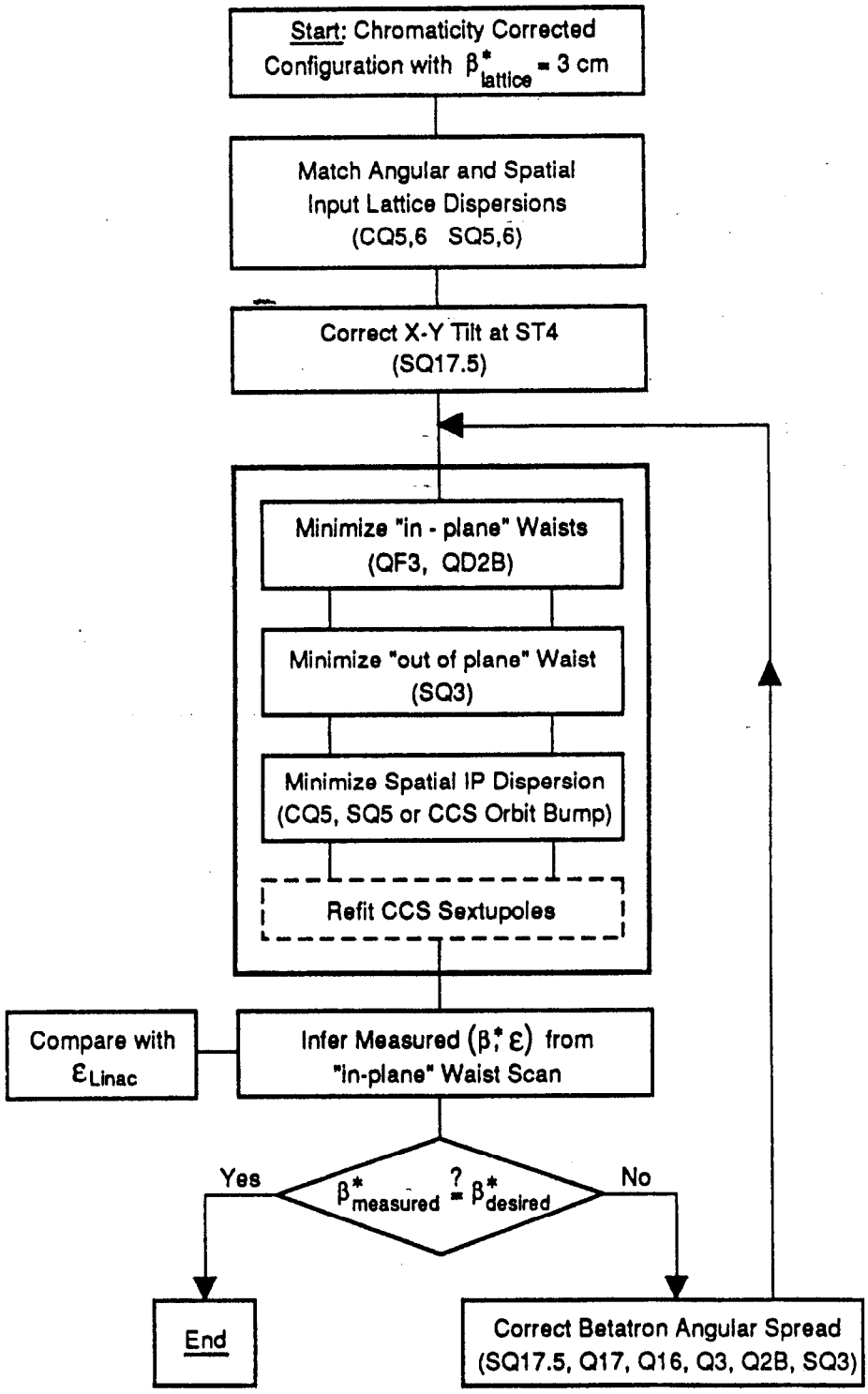

Figure. 19 Sequential application of the ten optical adjustments necessary to minimize the interaction point beam size.

	Design	Achieved	Unit
f	120 Hz	30 Hz	Hz
ε_N	3.10^{-5}	$5.4\ 10^{-5}$	m.rad.
N (e^+)	7.10^{10}	5.10^9	
N(e^-)	7.10^{10}	10^{10}	
β^*	0.75	3	cm
σ^*	1.5	4	μm
$\mathcal{L}$	$2.3\ 10^{30}$	$0.8\ 10^{27}$	$cm^{-2}\ sec^{-1}$

Table 1

	Location in SLC	Consequence on Phase-space	Downstream Correctability (Excluding Background Constraint)
Synchrotron Radiation	Arcs	Incoherent Dilution	NO
Betratron Oscillations from Errors in Guide-Field	R.T.L.	$< X_i, \frac{\delta E}{E} >$	YES
		$< X_i, Z >$	NO
	Linac	$< X_i, \frac{\delta E}{E} >$	YES
		$< X_i, Z >$	NO
	Arcs	$< X_i, Xj >$ *	YES
	Final Focus	$< Xi, Xj >$	YES
		$< X_i, \frac{\delta E}{E} >$	YES
Phase-Space Distortions from Errors in Focusing Fields	R.T.L.	$< X_i, Xj >$	YES
		$< X_i\ X_j, \frac{\delta E}{E} >$	NO
	Linac	$< X_i, X_j >$	YES
		$< X_i, X_j\ \frac{\delta E}{E} >$	NO
	Arcs	$< X_i, X_j >$	YES
	Final Focus	$< X_i, X_j >$	YES
		$< X_i, \frac{\delta E}{E} >$	YES

* The arc transfer is sensitive to steering for large steering errors.

Table 2

VI. REPORTS AND PUBLICATIONS ON OPTICAL CORRECTIONS IN THE ARCS

VI.1 "Betatron Phase-Space Diagnostic in a FODO Array"

This collider note describes one of the experimental methods used to determine the beam phase-space injected into the arcs. The method consists of:

1. Varying the phase-advance per cell in the optical lattice of the linear accelerator, in order to cause the beats in the β-parameter which result from the accumulation of focusing errors upstream of the arcs to move longitudinally, and of,

2. Measuring the beam-size on a fixed phosphor profile monitor screen.

This method is being successfully applied to monitor the phase-space at the end of the linear accelerator.

SINGLE PASS COLLIDER MEMO CN-367

AUTHOR: Philip Bambade DATE: October 2, 1988

TITLE: BETATRON PHASE-SPACE DIAGNOSTICS IN A FODO ARRAY*

I. INTRODUCTION

As has been shown[1], betatron mismatch is conveniently diagnosed in long repetitive FODO arrays by systematically varying the cell phase-shift μ and by measuring beam size at the end. For small variations, lattice parameters α and β change negligibly. This can be seen calculating[2] for example β as a function of μ in a thin lens FODO array. One gets:

$$\beta_{\pm} = \mathrm{L}\frac{1 \pm sin(\mu/2)}{sin\mu} \tag{1}$$

where $\beta_{\pm}$ are the minimum and maximum values, occurring at the D and F lens respectively, and L is the cell length. The beam-size remains therefore nearly constant *if* the phase-space is *matched* to the lattice. If it is not matched, beam parameters beat at twice the betatron frequency along the array, and the size at the end will vary as the beats are moved back and forth. A total phase-shift of π is needed to go through a full cycle of variation. In the Linac, where the total phase-advance is 60π, a $\pm 2.5\%$ systematic variation of F and D lenses is sufficient.

In this note, we show by parametrizing the mismatch in normalized coordinates, that the beam phase-space is readily determined from the measured size-variations. The parametrization given is general and applies to any transfer channel. The insensitivity of lattice parameters to systematic phase-shift applies however only in a FODO array. In addition, the calculation assumes uncoupled motion. The proposed method is therefore not applicable in the Arcs or Final Focus Sections. It is relevant however at the end of the Linac, where it enables rapid diagnostic, in both planes simultaneously, and without extensive set-up, of the beam injected into the passive part of the Collider.

*Work supported by Department of Energy Contract DE-AC03- 76SF00515.

Phase-space parameters can also be determined without varying any focussing element, through measurements at at least three different betatron phases. The four Sector-30 off-axis screens[3] may be used for this, allowing monitoring without intercepting the beam during running. Practical formulas can be derived. An approximate expression is given for the emittance as an example.

As noted[4], the spacing in betatron phase of the four screens is not regular. Also, two out of four screens are at β_{max} whereas the two others are at β_{min}. This gives about a factor two assymetry in their sensitivities, which the error analysis of this method must take into account. This, and a comparison with the traditional methods[5] is not included here.

II. NORMALIZED COORDINATES[5,6]

The transverse motion of a particle in a focussing array is governed by Hill's equation:

$$\frac{d^2z}{ds^2} + k_z(s)z = 0 \tag{2}$$

where z and $s = ct$ are the transverse and longitudinal coordinates respectively, and $k_z(s)$ represents the strength of the time-varying restoring force from the focussing array.

Introducing the *normalized* variables $\tilde{z} = \frac{z}{\sqrt{\beta}}$ and $d\phi = \frac{ds}{\beta}$, where β satisfies:

$$\frac{1}{2}\beta\frac{d^2\beta}{ds^2} - \frac{1}{4}\left(\frac{d\beta}{ds}\right)^2 + k_z\beta^2 - 1 = 0, \tag{3}$$

transforms the governing equation (2) into that of a pure harmonic oscillator:

$$\frac{d^2\tilde{z}}{d\phi^2} + \tilde{z} = 0. \tag{4}$$

Thus the solution of (2) is:

$$z = a\sqrt{\beta}cos(\phi + b), \tag{5}$$

where a and b are integration constants.

It is easily verified that:

$$\gamma z^2 + 2\alpha z z' + \beta z'^2 = a^2, \qquad (6a)$$

where $z' = \frac{dz}{ds}$, $\gamma = \frac{1+\beta'^2}{\beta}$, and $\alpha = \frac{-\beta'}{2}$. The quantity in (6a) is called the Courant-Snyder invariant[6]. It can also be written in matrix form:

$$(z, z')\mathrm{T}^{-1}\begin{pmatrix} z \\ z' \end{pmatrix} = a^2, \text{where } \mathrm{T} = \begin{pmatrix} \beta & -\alpha \\ -\alpha & \gamma \end{pmatrix} \text{and } \det(\mathrm{T}) = 1. \qquad (6b)$$

(6) defines the closed phase-space trajectory - an ellipse - of a particle with initial condition a. It also defines the envelope of the phase-space *matched* to the lattice. The Twiss parameters α, β and γ are here properties of the lattice. The area πa^2 of the ellipse is identified as π times the emittance ϵ. In the matched condition, the beam-matrix[7] $\sigma = \epsilon \mathrm{T}$.

III. PARAMETRIZATION OF MISMATCH

In the normalized coordinates $\tilde{z} = \frac{z}{\sqrt{\beta}}$ and $\tilde{z}' = \frac{d\tilde{z}}{d\phi} = \sqrt{\beta}(z' - \frac{\beta'}{2\beta}z)$, the matched phase-space is a *circle* of radius ϵ. This can be verified by direct substitution in (6a). A mismatch amounts to distorting this circle into an ellipse. We characterize the mismatch by the ratio M of the radius of the larger circle in which the ellipse is inscribed to that of the initial circle corresponding to the matched case, and by the angle ϕ_0 between its major axis and the abscissa (see Fig. 1): M and ϕ_0 can be thought of as the amplitude and phase of the mismatch.

The equation of the distorted ellipse is calculated in terms of M and ϕ_0, first in the coordinates rotated by ϕ_0 in which it is erect, and then transforming back into the unrotated coordinates. This gives:

$$\tilde{z}^2(M^2 cos^2\phi_0 + \frac{1}{M^2} sin^2\phi_0) + (\tilde{z}')^2(M^2 sin^2\phi_0 + \frac{1}{M^2} cos^2\phi_0) + 2\tilde{z}\tilde{z}' cos\phi_0 sin\phi_0 (M^2 - \frac{1}{M^2}) = \epsilon. \qquad (7)$$

The corresponding beam-matrix, written in the normalized system, is:

$$\tilde{\sigma} = \epsilon \begin{pmatrix} M^2 sin^2\phi_0 + \frac{cos^2\phi_0}{M^2} & -cos\phi_0 sin\phi_0 (M^2 - \frac{1}{M^2}) \\ -cos\phi_0 sin\phi_0 (M^2 - \frac{1}{M^2}) & M^2 cos^2\phi_0 + \frac{sin^2\phi_0}{M^2} \end{pmatrix}. \qquad (8)$$

Transforming back into real coordinates gives:

$$\begin{cases} \sigma_{11} = \beta\tilde{\sigma}_{11}, \\ \sigma_{12} = \tilde{\sigma}_{12} - \alpha\tilde{\sigma}_{11}, \\ \sigma_{22} = \frac{1}{\beta}(\tilde{\sigma}_{22} + \alpha^2\tilde{\sigma}_{11} - 2\alpha\tilde{\sigma}_{12}). \end{cases} \tag{9}$$

In the matched condition, characterized by $M = 1$, (9) reduces to (6b) as expected.

IV. PHASE-SPACE DETERMINATION

From (8) and (9), the beam-size measured at an arbitrary point at the end of the array as a function of the total induced phase-shift ϕ is:

$$\sigma^2(\phi) \simeq \frac{\epsilon\beta}{2}((M^2 + \frac{1}{M^2}) + (M^2 - \frac{1}{M^2})cos2(\phi - \phi_0)). \tag{10}$$

The period of this function is π as expected. The mismatch parameters M, ϕ_0 and the emittance ϵ are easily computed:

$$\begin{cases} \epsilon \simeq \frac{\sigma_{Min}\sigma_{Max}}{\beta}, \\ M^2 \simeq \frac{\sigma_{Min}}{\sigma_{Max}}, \\ \phi_0. \end{cases} \tag{11}$$

In (11), ϕ_0 is the difference in phase between $\sigma(\phi) = \sigma_{Max}$ and the starting point $\sigma(0)$.

The full beam-matrix can then be reconstructed from (9), using the *lattice* parameters α and β at the measurement point. Equations (10) and (11) are approximate because Twiss parameters α and β change slightly with the induced phase-shift from (1). The contribution to the error from this is however small as it is bounded by their variation over the 2.5 % phase changes which are applied.

We can also use (10) to determine the phase-space from measurements on the four off-axis screens[3], without varying any focusing element. Approximate expressions are easily written if the slight mismatch present in the design lattice is neglected† . Using[4] $\Delta\phi_{12} \simeq \Delta\phi_{34} \simeq 22.5°$, and $\Delta\phi_{23} \simeq 67.5°$, where $i = 1, 4$

† The design Linac lattice is not fully periodic. It includes deviations in quadrupole strengths required to match across sector boundaries. These local deviations can be as large as 20 %. However because the systematic strength variations induced in this method are about 2.5 %, effects from these irregularities are small. This has been checked[1] using the on-line model.

refer to the four screens, the horizontal electron emittance is:

$$\epsilon^2 \simeq (\frac{A_1 + A_2 + A_3 + A_4}{4})^2 - (\frac{A_1 - A_3}{2})^2 - (\frac{\sqrt{2}(A_2 - A_4) - (A_1 - A_3)}{2})^2, \quad (12)$$

where $A_i = \frac{\sigma_x^2(i)}{\beta_i}$, in which $\beta_{1,3} = \beta_{min} \simeq 20m.$ and $\beta_{2,4} = \beta_{max} \simeq 50m.$. The same expression applies for the vertical plane by exchanging β_{min} for β_{max}, and for the positron emittance, by exchanging horizontal for vertical electron results.

Similar expressions can be obtained in the same way for mismatch parameters M and ϕ_0.

ACKNOWLEDGEMENTS

I wish to thank K. Brown, J. Haïssinski, T. Himel, T. Lohse, J. Seeman and J. Sheppard for useful comments on this method.

REFERENCES

(1) T. Himel, Private Communication (August 1988).

(2) For Example: E. Wilson in: "Circular Accelerators - Transverse", SLAC Summer School on Physics of Particle Accelerators (July 1985), AIP Conference Proceedings 153, page 21.

(3) J. Seeman *et al.*;"Transverse Wakefield Control and Feedback in the SLC Linac", IEEE Particle Accelerator Conference, Washington, D.C.(March 1987).

(4) J. Seeman, Private Communication (August 1988)

(5) J. Rees and L. Rivkin, "On Measuring Emittances and Sigma Matrices", SLAC-PUB-3305, (March 1984), and M. Ross *et al.*, "High Resolution Beam Profile Monitors in the SLC", SLAC-PUB-3640 (April 1985).

(6) E. Courant and H. Snyder, "Theory of the Alternating Gradient Synchrotron", Annals of Physics, Vol. 3,1-48 (1958).

(7) K. Brown *et al.*, "TRANSPORT", SLAC-91, Rev. 2 (May 1977).

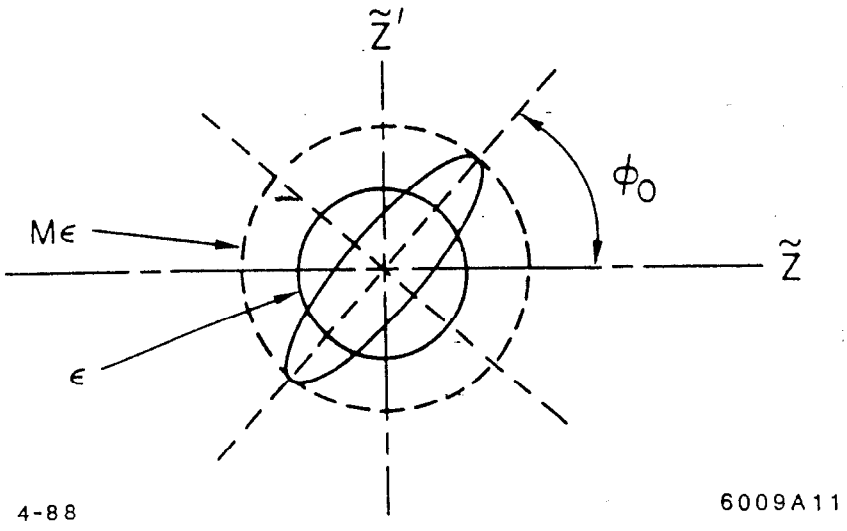

Fig. 1: Matched (inner circle) and mismatched (ellipse) phase-space in normalized coordinates.

VI.2 "Roll-fix - An Adiabatic Roll Transition for the SLC Arcs"

This conference article describes the modification of the roll transitions which were used to provide the vertical deflections necessary to follow the terrain of the SLC site. The boundary was modified into a smoother transition, which almost perfectly suppressed the coupling of horizontal lattice dispersion into the vertical plane, and substantially reduced the sensitivity of the betatron lattice to systematic focusing errors. This modification was proposed and implemented to help control the magnification and build-up of errors from the arc lattice, by making the system more error-tolerant. The paper summarizes the evaluation and performance of this scheme.

SLAC-PUB-4835 Rev.
February 1989
(A)

ROLLFIX — AN ADIABATIC ROLL TRANSITION FOR THE SLC ARCS*

P. BAMBADE,† K. BROWN, T. FIEGUTH, A. HUTTON, D. RITSON, M. SANDS and N. TOGE
Stanford Linear Accelerator Center, Stanford University, Stanford, California 94309

Contributed to the IEEE Particle Accelerator Conference, Chicago, Illinois, March 20-23, 1989.

ABSTRACT

The SLC Arcs were rolled at achromat boundaries to follow the terrain of the SLAC site. This makes the linear optics sensitive to systematic gradient errors, from which severe cross-plane coupling effects may arise. As a partial correction, a smoother roll transition was introduced which relieves much of this sensitivity. We present an evaluation of this scheme and report on the observed improvements.

INTRODUCTION

The two Arcs of the Stanford Linear Collider (SLC) are designed to bend the electrons and positrons around and into collision, without significant emittance dilution.[1] To minimize emittance growth from synchrotron radiation in the bend field, the focusing must be strong and compact and, therefore, use combined function magnets. To assure achromatic imaging, the magnets must also include sextupole components, and be grouped into sets (achromats) appropriately symmetrized for the suppression of optical aberrations.[2] In addition, for economical reasons, the two Arcs were designed to follow the terrain of the SLAC site (see Fig. 1), and thus include vertical deflections. For maximum compactness, these deflections were produced by rolling the magnets around their axis by up to 10° at achromat boundaries (see Fig. 2). To provide an overall cancellation of the induced cross-plane coupling, the rolls were grouped in pairs separated by one or several achromats, corresponding in the ideal system to an identity transfer matrix with 6 $n\pi$ phase-advance.

However, these long-range cancellations resulted in a limited bandwidth for the optical transfer, which had relatively stringent tolerances to systematic focusing errors. This fact was realized in several stages, before and during the initial beam tests. At first, a stringent tolerance to systematic horizontal displacement errors, which in the combined function magnets generate systematic focusing errors, was noticed through computer simulations. For example, see Ref. 3.

During the first beam tests, it was observed that the transfer of betatron oscillations and of the dispersion function across rolled achromat boundaries could be associated with a large magnification. A detailed calculation of the magnification associated with this transfer can be found in Ref. 4. In the initial commissioning, this magnification was observed to be as large as a factor of three over the whole length of the Arc because the systematic errors exceeded the specified design tolerances of 0.002.[5]

Although, for the case of equal input emittances (corresponding to the SLC design specification), such growth is in principle recoverable downstream, in the Final Focus, where a set of skew corrections are installed,[6] its magnitude required initial correction within the Arcs. Also, as was later found, the projected transverse emittance must in fact be close to the nominal design value at the exit to the Arcs, in order to minimize detector backgrounds induced by beam-tails striking the smaller (normalized) aperture in the Final Focus region.[7] Two basic cures were therefore devised. The first consisted of adjusting the

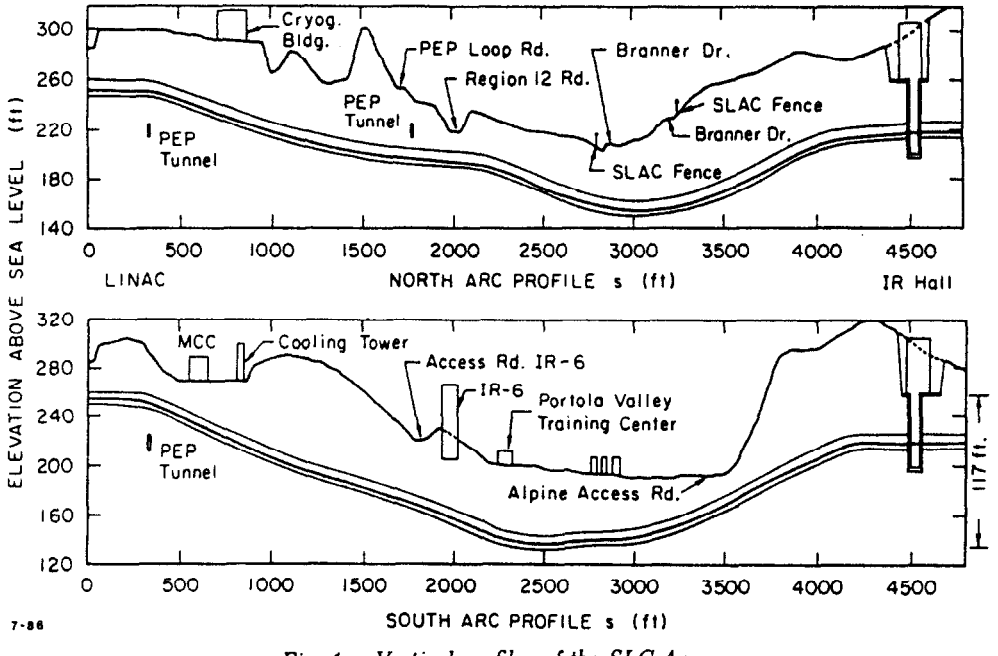

Fig. 1. Vertical profiles of the SLC Arcs.

* Work supported by the Department of Energy, contract DE-AC03-76SF00515.
† Present address: Laboratoire de l'Accélérateur Linéaire, Orsay, France.

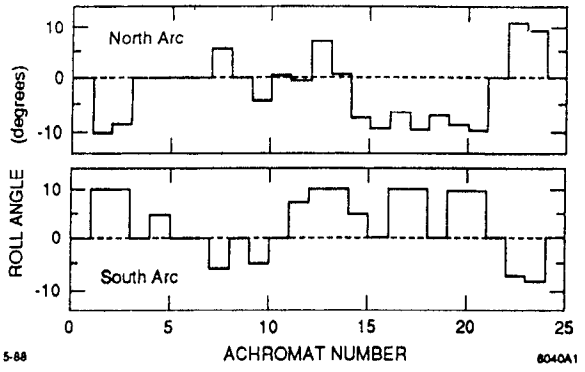

Fig. 2. Roll angle about beam axis versus achromat number for North and South Arcs.

focusing gradients, based on measurements of the phase-advance in each achromat,[8] to their nominal values. Such adjustments helped bring the growth in the betatron transfer down to within a factor of about two, but further reductions by this procedure were limited by measurement errors and by the lack of fully separate controls in each plane and in each achromat.[8]

A second cure consisted of splitting each roll over several magnets on each side of the boundaries, to yield smoother transitions having a greater tolerance to phase-advance errors, and to nearly suppress the coupling of horizontal lattice dispersion into the vertical plane. The adjustments of the phase-advance had brought the system close to specification, and had minimized the coupling to the point where it could be handled relatively well in the Final Focus. It was however felt important for future operability to implement this passive *rollfix* cure, which makes the system significantly more error-tolerant, particularly for equal or close to equal initial emittances in both planes, as was noted above.

In addition, the nearly suppressed vertical dispersion is expected to reduce synchrotron radiation induced emittance growth in the vertical plane. The scheme could be installed without major disruption to the beam-line, and resulted in some observed improvements. The reference trajectory could be kept unperturbed through small vertical displacements of the magnets involved.

In this paper, after introducing an approximate measure for the cross-plane coupling in the betatron transfer, we evaluate the sensitivity to errors in the initial and modified designs, and characterize the predicted improvements. We then report on observed improvements.

APPROXIMATE CHARACTERIZATION OF CROSS-PLANE COUPLING

The practical consequences of cross-plane coupling are different in a beam-line than in a circular machine. In a circular machine, the motion is stable only for tunes such that sum-resonances (corresponding to $p\nu_x + q\nu_y = n$), have negligible effects. Residual coupling arises in this case exclusively from difference-resonances (corresponding to $p\nu_x - q\nu_y = n$), which can be shown to result in stable beating between the two projected transverse emittances.[9] In a beam-line, distortions from cross-plane coupling can correspond both to growing and decaying solutions.[10,11] The two projected emittances can in this case both grow. It has been shown that the severity of such growth can be characterized by the determinant of the off-diagonal two-by-two submatrix C of the general four-by-four transfer matrix:[10]

$$R = \begin{pmatrix} R_{11} & R_{12} & R_{13} & R_{14} \\ R_{21} & R_{22} & R_{23} & R_{24} \\ R_{31} & R_{32} & R_{33} & R_{34} \\ R_{41} & R_{42} & R_{43} & R_{44} \end{pmatrix} = \begin{pmatrix} A & B \\ C & D \end{pmatrix} \quad . \qquad (1)$$

This can be seen from calculating the projected emittances ϵ_x and ϵ_y onto each plane of a four dimensional phase-space transfered through a fully coupled system, and by using the six symplectic conditions imposed by Hamiltonian Mechanics.[9] With the simplifying assumption of upright phase-ellipses and of beams initially uncoupled in both planes, one can show that the following inequality holds:[10]

$$\epsilon_{x,y} \geq \epsilon_{x,y}(0)|1 - \det C| + \epsilon_{y,x}(0)|\det C| \quad . \qquad (2)$$

In most cases, the inequality sign in Eq. (2) can be replaced by an equality. This has been observed in several computer simulations. An analytical attempt to show this is described in the Appendix.

From Eq. (2), we see that the most severe coupling effects arise if: $\det C < 0$, or if: $\det C > 1$. In this case, the phase-space projections will grow in both planes, irrespective of the initial emittance values. On the other hand, coupling effects with $0 < \det C < 1$ are severe only if the initial emittance values are very assymetric (and if it is desirable to preserve such an assymetry). In this case, the coupling will tend to equalize the two emittance projections. In the SLC, where the initial emittances are close to equal, coupling effects with $0 < \det C < 1$ are benign.

DESCRIPTION OF ORIGINAL AND TAPERED ROLL TRANSITIONS[13]

Figures 3(a) and (b) show the principle of the original and tapered roll transition pairs. The first transition has a total angle θ. It is matched by a second transition, with a total angle $-\theta$, located an integer number of achromats downstream. In this way, all cross-plane coupling effects cancel after the second transition, if the achromats in between are perfect, and correspond to an identity transfer matrix.

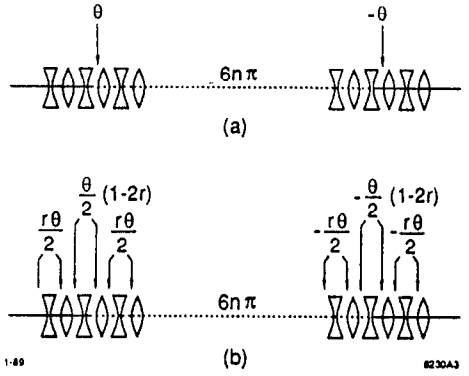

Figs. 3(a) and (b). Principle of original (a) and tapered (b) roll transition pairs. In the original set-up (a), pairs of rolls were concentrated at achromat boundaries separated by 6 nπ *betatron phase-advance. In the tapered solution (b), each roll was split about five magnets to yield a smoother transition. The optimum value for the ratio* r *of the total roll of the first cell to the total roll of the transition is near* r = 0.28.

In the original transition [see Fig. 3(a)], the full roll is concentrated at the achromat boundary. In the tapered transition [see Fig. 3(b)], the rolls are distributed across three cells around the boundary. As we will show, this tapering suppresses the most damaging component of the cross-plane coupling induced in the betatron transfer. Within each cell, the rolls are split equally across the defocussing magnet. This was found to nearly cancel the coupling of horizontal lattice dispersion into the vertical plane, and is due to the fact that the vertical phase-advance across a defocusing magnet is only about 22°, and because the angular horizontal lattice dispersion

has opposite sign at the entrance to focusing and to defocusing magnets. We define by r the ratio of the roll of the first cell to the total roll of the transition. In the original proposal, $r = 0.38$ was used, by analogy with the coefficients for a matched trajectory bump. It was later found that $r = 0.28$ gives a slightly better results.[14]

TOLERANCES WITH ORIGINAL AND TAPERED ROLL TRANSITIONS

Following the above description of cross-plane coupling effects, we use the magnitude and the sign of det C to characterize the severity of the cross-plane coupling effects which arise from errors in the Arc lattice.

The original design was especially sensitive to the total deviations $\Delta\mu_{x,y}$ from the nominal phase-advance between transition pairs. For two original roll transitions, each of angle θ, and separated by a regular FODO lattice with an integer number of betatron periods [as in Fig. 3(a)], it can be shown that after the second transition:

$$\det C = \sin^2(2\theta)\left[\sin^2\left(\frac{\Delta\mu_x - \Delta\mu_y}{2}\right) - \alpha^2 \sin\Delta\mu_x \sin\Delta\mu_y\right], \quad (3)$$

where α is the usual Twiss parameter at the transition (in the Arc, $\alpha = 2.65$).

For phase-advance errors with the same sign in each plane, det C < 0, while for phase-advance errors with opposite sign, det C > 0. The magnitudes of det C, computed with a simulation[15] to confirm Eq. (5), are shown in Fig. 4 as a function of $(1/2)(\Delta\mu_x \pm \Delta\mu_y)$, for a typical transition with $\theta = 10^0$. As expected, the maximum value for $|\det C|$, which is close to one, is reached for $(1/2)(\Delta\mu_x \pm \Delta\mu_y) = \pm 90^0$. The same quantity is shown in Fig. 5 for the tapered transition. As can be seen, the onset of a negative det C is nearly suppressed by the tapered transition, and the onset of a positive det C is reduced by a factor of two.

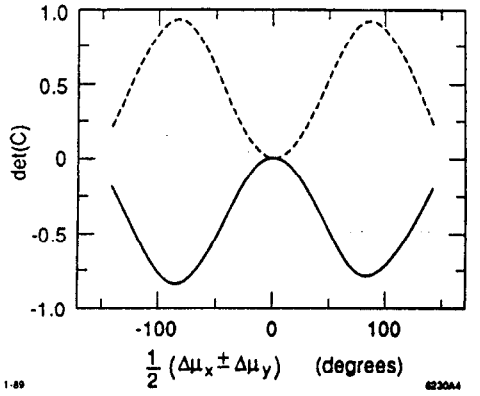

Fig. 4. det C *as a function of systematic phase-advance errors of equal sign (dashed line) and of opposite sign (solid line), between two original roll transitions.*

The actual roll distributions in the two Arcs are more complicated (see Fig. 2), but are superpositions of the basic ones shown in Fig. 3. We therefore expect the same overall features as for the simple examples examined above. To verify this, we show in Figs. 6 and 7, the same quantities as in Figs. 4 and 5, under the same conditions — but for the whole North Arc, as a function of the fractional phase-advance deviations $(1/2)[(\Delta\mu_x/\mu_x) \pm (\Delta\mu_y/\mu_y)]$. As can be seen in Fig. 6 (solid line), the tolerance to systematic phase-advance errors, for negligible coupling to occur, was about ± 0.006 in the original North Arc.

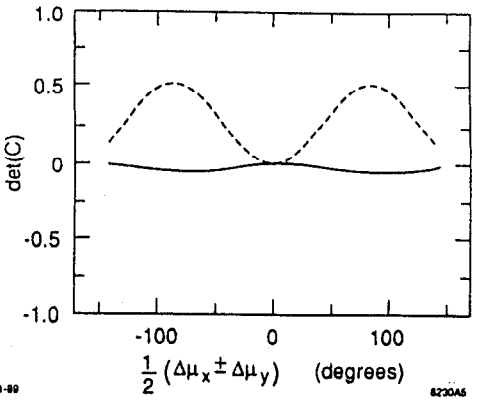

Fig. 5. det C *as a function of systematic phase-advance errors of equal sign (dashed line) and of opposite sign (solid line), between two tapered roll transitions.*

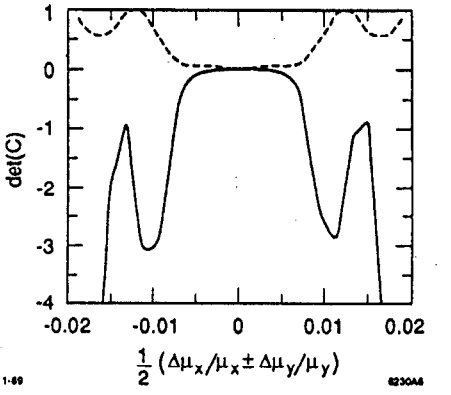

Fig. 6. det C *as a function of systematic phase-advance errors of equal sign (dashed line) and of opposite sign (solid line) in the entire North Arc with original roll transitions.*

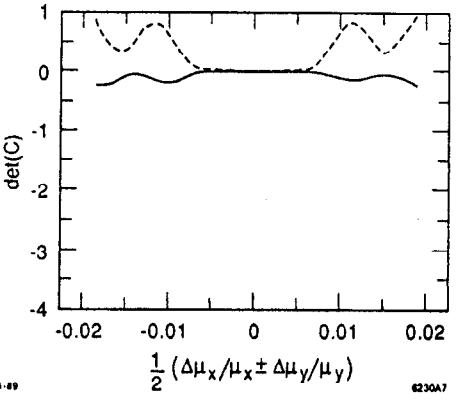

Fig. 7. det C *as a function of systematic phase-advance errors of equal sign (dashed line) and of opposite sign (solid line) in the entire North Arc with tapered roll transitions.*

In the modified North Arc, and in the case of equal emittances in both planes (for which cross-plane coupling with $0 <$ det C < 1 is benign), this particular tolerance is very broad and one expects the sensitivity to errors to be comparable to that of a flat Arc. For unequal x and y emittances, the improvements are, however, not expected to be as great (see Fig. 7 — dashed line).

In practice, the system can be perturbed by both random and systematic errors. Also, the tolerance to errors depends on the requirement put on the phase-space at the Arc exit. As was mentioned in the introduction, the cross-plane coupling distortions of the phase-space are correctable in the Final

Focus, but large distortions of the beam envelope — from any kind of error — can result in unacceptable background in the experiment, and must therefore be avoided. This leads us to define a tolerance in terms of the maximum deviation from the nominal size reached by the beam envelope at the end of the Arcs, as generated through the mixing of the distortions from both random and systematic errors. Extensive computer simulations[15,16,17] were performed to evaluate the sensitivity of the Arcs, with both random and systematic errors. It was found that in the case of equal emittances, the Arcs with modified roll transitions are about as sensitive to errors as a flat Arc without rolls. We illustrate this point with the result from one of these simulations in Figs. 8(a)–(c), where the geometric mean of the maximum growth of the horizontal and vertical monochromatic beam sizes at the end of the Arcs is calculated for the original North Arc, for the tapered North Arc, and for a hypothetical flat Arc.[15] The errors are the same in each case and correspond to systematic errors of 0.01 and to a sample of randomly distributed errors with a standard deviation of 0.005, in both the focusing and the defocusing magnets. As can be seen, the distortions are almost the same for the tapered Arc [case (b)] and for the flat Arc [case (c)]. Similar results were obtained for the South Arc.

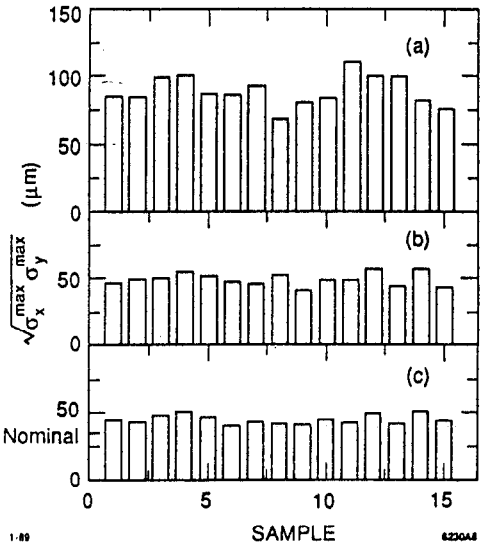

Figs. 8(a), (b) and (c). Maximum growth of the geometric mean of the monochromatic beam sizes in the vertical and horizontal planes at the end of the North Arc perturbed by systematic errors with the same sign in each plane, of 0.01, *and random errors, with a standard deviation of* 0.005. *The same sample of errors are used for comparing the North Arcs with the original roll transitions (a), with the tapered roll transitions (b), and without rolls (c). The nominal value is* 35 μm *in each plane.*

OPTIMIZATION OF TAPERED ROLL TRANSITION

A perfect match of the betatron transfer can be achieved by including at least five cells in the transition, but is not practical because the sign of the rolls must alternate in this case (presumably because the phase-advance across more than two cells becomes larger than π), and because the solution depends in this case very nonlinearly on the total roll of the transition.

The distribution of rolls indicated in Fig. 3(b), however, can be improved. An example of such an optimization is shown in Fig. 9, where the maximum positive and negative values of det C, occuring when the phase-advances between the pairs of roll transitions shown in Fig. 3 are perturbed to satisfy $(1/2)(\Delta\mu_x \pm \Delta\mu_y) = \pm 90^0$, is computed as a function of r. The dependance is fairly flat. The optimum value of $r = 0.28$ results in slight improvements in the overall performance.[14]

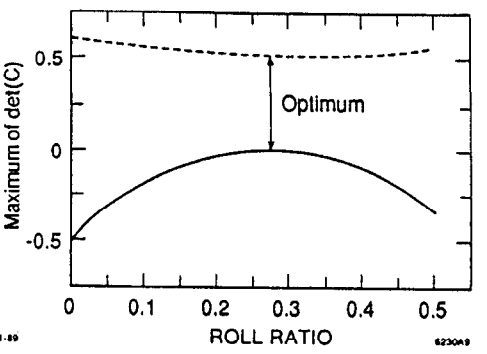

Fig. 9. Maximum value of det C *resulting from systematic errors with opposite sign (dashed line) and with the same sign (solid line) between the tapered transitions of Fig. 3(b), as a function of the roll ratio* r.

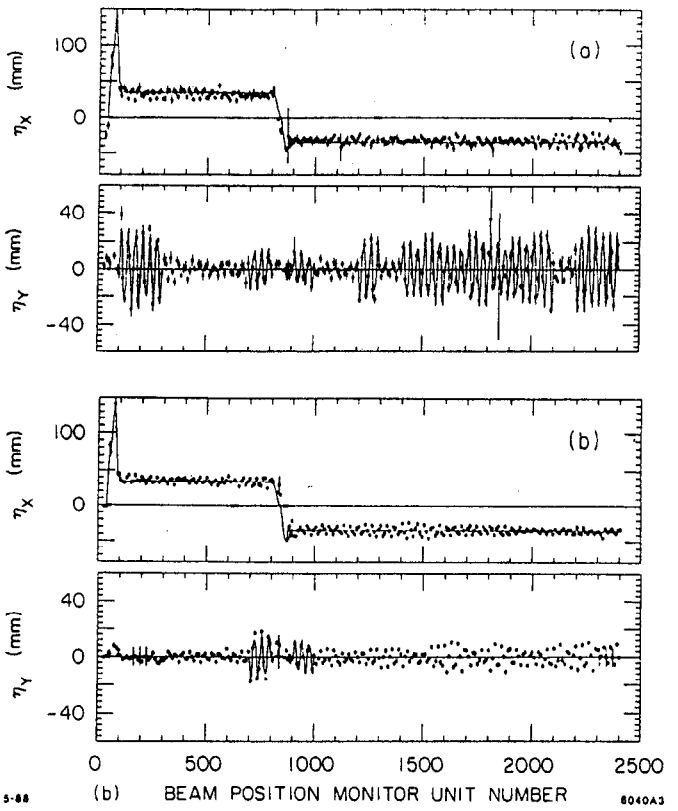

Figs. 10(a) and (b). Horizontal and vertical dispersion measured in the North Arc, before (a) and after (b) the installation of the tapered roll transitions. The vertical dispersion was essentially suppressed by the modification.

PERFORMANCE AND CONCLUDING REMARKS

The performance of the modification was particularly clear for the suppression of vertical lattice dispersion. This can be seen from the measurements in the North Arc, before and after the modification of the roll transitions [see Figs. 10(a) and (b)].

The minimization of the coupling in the betatron transfer which was achieved during the recommissioning of the Arcs after the installation of the modification cannot be attributed solely to this design change. It was also the result of the previous phase-advance adjustments,[8] of several other empirical adjustments and resteering performed at turn-on.

The modification did in addition improve the overall performance of the Arc, by reducing, as expected, the need for

feeding back on the optics to cancel variations from steering or other changes. However, later, expectations on the quality of the phase-space at the exit to the Arcs were also enhanced, in particular from the requirement to minimize beam tail induced backgrounds in the detector.[7] Because of this it became necessary to implement further and more precise corrections.[11]

More recently, it has been possible to determine the transfer matrix along the Arc beam-line, by fitting betatron oscillations launched at several input phases.[18] Such calculations have shown that presently $\det \mathrm{C} \simeq 0.2$ at the exit to the North Arc, leading to small coupling effects in the case of equal emittances.

APPENDIX

It is possible to calculate the projected emittances exactly with the simplifying assumption of upright phase-ellipses and of beams initially uncoupled in both planes, by folding the contributions to each emittance projection from the two planes. Because the phase-ellipses are not in general upright, the derived expression is an upper bound of the cases with phase-ellipses of arbitrary orientation. One obtains:

$$\epsilon_{x,y} = [\epsilon_{x,y}(0)|1 - \det \mathrm{C}| + \epsilon_{y,x}(0)|\det \mathrm{C}|]\sqrt{1+\mathcal{F}} \quad , \quad (4)$$

where $\epsilon_x(0)$ and $\epsilon_y(0)$ are the initial values, and where the factor:

$$\mathcal{F} = \frac{\epsilon_x(0)\epsilon_y(0)|\det \mathrm{C}||1 - \det \mathrm{C}|}{\epsilon_{x,y}(0)|1 - \det \mathrm{C}| + \epsilon_{y,x}(0)|\det \mathrm{C}|}\left(\frac{\lambda_x^2}{\lambda_y^2} + \frac{\lambda_y^2}{\lambda_x^2} - 2\right) \quad (5)$$

describes the mixing which results from folding the phase-ellipses if they are not similar. Such dissimilarity arises from upright quadrupole perturbations to the lattice, both through random and, in the presence of rolls, systematic errors. The parameters $\lambda_{x,y}$ describe the magnitude of the mismatch which result in each plane. These parameters are defined in normalized phase-space as the ratio of the radius of the circle in which a distorted phase-ellipse is inscribed to that of the smaller circle which corresponds to the matched case.[12] If there are no upright quadrupole errors ($\lambda_{x,y} = 1$) or if the two phase-ellipses are similar ($\lambda_x = \lambda_y$), then the mixing term $\mathcal{F} = 0$. For mismatches with $\lambda_{x,y} \lesssim 2$, corresponding to upright quadrupole errors of up to 1%, then $\sqrt{1+\mathcal{F}} \lesssim 2.5$. For such cases, the inequality sign in the expression given in Eq. (2) can be replaced by an equality sign, for approximate calculations.

ACKNOWLEDGEMENTS

The sensitivity of the Arc beam transfer to systematic errors was a central issue in the commissioning of the SLC during the summer of 1987. At that time, a large number of people contributed to understanding and to solving these problems, each one from his or her point of view. In particular, we would like to acknowledge the work and enthusiasm of F. Bulos, D. Burke, J. Haïssinski, J. Murray, N. Phinney, M. Placidi, L. Rivkin, J. Sheppard and R. Stiening.

Last, but not least, we would like to thank the Mechanical Engineering and SLC Alignment Groups for the very rigorous and efficient installation and alignment work related to the initial set-up of the Arcs and to this tapered "rollfix."

REFERENCES

1. S. Kheifets *et al.*, "Beam Optical Design and Studies of the SLC Arcs," SLAC-PUB-4013 (1987).
2. K. L. Brown, "A Second-Order Magnetic Optical Achromat," SLAC-PUB-2257 (1979).
3. T. H. Fieguth *et al.*, "Studies of Anomalous Dispersion in the SLC Second Order Achromats," SLAC-PUB-4096 (1987).
4. M. Sands, "Betatron Oscillations and Rolled Achromat," SLAC-CN-355 (1987).
5. J. J. Murray, private communication (1984).
6. P. S. Bambade, "Beam Dynamics in the SLC Final Focus System," SLAC-PUB-4227 (June 1987).
7. D. L. Burke *et al.*, "Beam Collimation and Detector Backgrounds at e^+e^- Linear Colliders," these proceedings.
8. J. Haïssinski *et al.*, "A Technique for Correcting the Betatron Tunes of the SLC Arcs," these proceedings.
9. E. D. Courant and H. S. Snyder, "Theory of the Alternating Gradient Synchrotron," Ann. of Phys. 3, 1–48 (1958).
10. K. L. Brown and R. V. Servranckx, "Cross-Plane Coupling and its Effects on Projected Emittances," SLAC-PUB-4679 (July 1988).
11. P. S. Bambade and A. Hutton, "Specification of Harmonic Corrections (Wirefix) for the SLC Arcs," in preparation.
12. P. S. Bambade, "Betatron Phase-Space Diagnostic in a FODO Array," SLAC-CN-367 (October 1988).
13. See also: T. H. Fieguth *et al.*, "Tuning the Arcs of the SLAC Linear Collider," SLAC-PUB-4628 (May 1988).
14. This was the result of work by M. Sands and, independently, L. Rivkin.
15. D. M. Ritson, ARCSIM, private program.
16. R. V. Servranckx and K. L. Brown, DIMAD program; SLAC-REP-285 (May 1985).
17. J. J. Murray and T. Fieguth, MURTLE, private program.
18. T. L. Barklow, "A Technique for Measuring the 4X4 Transfer Matrix for Beamline Sections with Cross-Plane Coupling," these proceedings.

VI.3 "Specification of Harmonic Corrections (Wirefix) for the SLC Arcs"

This collider note describes the theory and the design and implementation of harmonic corrections in the arcs. Normally a method which applies to circular accelerators, harmonic corrections can under certain conditions be used efficiently for doing optical corrections in long open FODO arrays. Such corrections were introduced in the last third of the arcs to supplement the optical corrections in the final focus. They are necessary to enable adjusting the beam at the entrance to the final focus, where a nearly matched phase-space is required to minimize backgrounds in the experimental apparatus.

SINGLE PASS COLLIDER MEMO CN-370

AUTHOR: Philip Bambade, Andrew Hutton DATE: February 1, 1989

TITLE: SPECIFICATION OF HARMONIC CORRECTIONS (*WIREFIX*) FOR THE SLC ARCS**

I. INTRODUCTION

In the original SLC commissioning plans, it was thought that accumulated optical mismatch, generated by focusing errors in the whole machine, would be corrected at the very end, in the Final Focus. Dedicated correctors for optical matching and a special adjustment strategy were planned for this purpose, with a large tuning range of up to about a factor four in any dimension of the beam phase-space[1].

For several reasons, this does not appear to be feasible. One major constraint limiting the magnitude of mismatches which can be absorbed in the Final Focus is the background generated in the detector, from electromagnetic debris and from muons produced when beam-tails strike apertures there. The apertures in the Final Focus, normalized to the nominal beam size, are in effect significantly smaller* than in the Arcs, both upstream and downstream of the dedicated optical correctors. Because of this, otherwise correctable optical distortions can result in enhanced backgrounds, as imperfectly collimated beam tails get magnified by the optical distortions, and can get scraped off.

With the present collimation and shielding arrangements, it is necessary to control the beam upstream of the Final Focus in order to inject a nearly matched phase-space there. Following work by Stiening in the Linac[2], and by Fieguth in the Arcs[3], we have developed and installed a new system of harmonic focusing corrections at the end of the SLC Arcs, to provide such control.

⋆ The protection collimator PC18, for example, has a radius of 4 millimeters. After normalizing by the nominal beam size, it is smaller than the Arc 6 millimeter vacuum chamber by a factor 6.7.

** Work supported by the Department of Energy Contract DE-AC03-76SF00515.

The scheme consists of introducing small regular and skew focusing deviations at specific harmonics of the betatron frequency which the phase-space is specially sensitive to. The harmonics in question are the zeroeth harmonic and the second harmonic of the betatron frequency*. The focusing deviations are introduced in the Arc lattice by perturbing the strengths of the combined function magnets with a set of appropriately rewired trim windings at their backleg†. The corrections provide an efficient way for adjusting both for errors in the Arc lattice and for mismatch at the injection to the Arc, generated by the upstream systems.

In this note, we describe the specification of this correction procedure as well as the present installation. Initial operational experience with this new method for adjusting beam-lines is presented elsewhere[4].

We begin with a description of the theoretical work which guided the specification. We then define the harmonics in the case of the Arc lattice, and describe the wiring modification and the strength of the regular and skew quadrupole components which can be generated, as calculated with POISSON[5]. We also describe the intra-magnet wiring arrangement through which the spatial strength modulations are produced.

Finally we present the predicted effects from the present installation, and outline possible improvements.

---

* In a circular accelerator, these harmonics correspond to the half-integer resonance in each plane, and to the sum and difference coupling resonances.

† The backleg windings were introduced in the Arc magnets originally to provide a step-wise adaptation of the strength of the lattice to the energy of the beam, which loses about 1 Gev through the emission of synchrotron radiation in the guide-field.

II. THEORY OF HARMONIC CORRECTIONS

II.1 Concept of Harmonic Correction in a Beam-Line[2,3]

In a beam-line where the focusing lattice consists of a periodic FODO array, the optical mismatch which occurs from focusing errors is conveniently described by an ellipse which rotates in phase-space with the betatron phase-advance[6]. Because ellipses are invariant under rotation of π, the beats in the beam envelope occur at twice the betatron frequency. Therefore, focusing errors which are separated by π, and more generally, which occur at twice the betatron frequency, will build up and enhance the optical mismatch.

Thus it is natural to consider adjusting the lattice and the phase-space in a FODO array by introducing controllable focusing perturbations at twice the betatron frequency. In general, the focusing errors in the lattice are random. Such focusing perturbations will thus add to or subtract from the strength of the Fourier component of the random errors which is at twice the betatron frequency. Controlling the strength of this harmonic thus enables to either make an overall correction of the lattice, or to purposely distort the lattice to minimize optical mismatch in the injected beam. This notion can be applied both to regular focusing errors and to skew focusing errors.

Because the perturbations from the errors are random and contain in general a systematic component, the accumulating optical mismatch will not remain indefinitely in phase with the focusing perturbations which are introduced. The longer the array, the larger the phase-shift between the two will be, and the weaker the effects from the controls become, as the system becomes more narrow-band. Because of this, harmonic corrections cannot be performed over a region that is too long, without losing much of their efficiency.

A second reason why harmonic corrections can in general not be applied over a region that is too long arises if the momentum dependance of the focusing, referred to as the chromaticity of the lattice, is not or is imperfectly corrected. In this case, the finite momentum spread in the beam will cause the optical mismatch from the focusing deviations to filament into a larger effective phase-space. The efficiency of a harmonic correction can in this case be reduced. Because the SLC Arcs are designed to be achromatic, such effects arise only to the extent the chromaticity-correction, because of the errors, is imperfect. For the range of errors which we

consider*, this is a small effect which we will not consider here.

II.2 Scope of Theory

The scope of this theoretical description is not that of full generality or rigor. The goal is rather to show the basic features of betatron oscillations and of transverse phase-space, as they are imaged through a FODO array which has been perturbed by a periodical focusing deviation. We will calculate the effects for each perturbation separately, in an idealized system with no errors, and ignore mixing effects which arise when several perturbations are applied simultaneously. Such mixing effects can change the magnitude of the effects, but do not change the basic features of the solutions which we will derive.

The only case of mixing which we will treat is that of a systematic focusing deviation, from the random errors or applied as an independent perturbation, combined with a periodic focusing perturbation at twice the betatron frequency. Rather than calculating the explicit solution for this case, we will indicate the magnitude of the reduction factor which results.

A practical case of periodic focusing deviation applied to a lattice with random errors will be explored through simulation in section VI.

In order to calculate the effects to be expected from harmonic focusing perturbations in a repetitive lattice, it is convenient to introduce and work with normalized variables.

II.3 Normalized Variables[7]

The transverse motion of a particle in a focusing array is governed by Hill's equation:

$$\ddot{z} + Kz = 0 \tag{1}$$

where $z = x, y$ and $s = ct$ are the transverse and longitudinal coordinates respectively, and where K represents the strength of the varying restoring force from the focusing array.

⋆ We consider focusing perturbations of up to about one percent.

The use of the normalized variables $u_{x,y} = \frac{z}{\sqrt{\beta}}$ and $d\phi = \frac{ds}{\beta}$, where β satisfies:

$$\frac{1}{2}\beta\ddot{\beta} - \frac{1}{4}\dot{\beta}^2 + K\beta^2 - 1 = 0, \tag{2}$$

transforms (1) into the equation of a pure harmonic oscillator:

$$\ddot{u}_{x,y} + u_{x,y} = 0. \tag{3}$$

In (1) and (2), $\dot{f} \equiv \frac{df}{ds}$, where $f = z, \beta$. In (3), $\dot{u} \equiv \frac{du_{x,y}}{d\phi}$. The solution of (1) is thus:

$$z = a\sqrt{\beta}\cos(\phi + b), \tag{4}$$

where a and b are integration constants, and is referred to as a betatron oscillation. By definition the frequency of this oscillation, written as a function of the phase variable ϕ, is one.

Although the form in (4) is general, it is specially suited to periodic arrays consisting of repeated cells. In this case K, β and ϕ are periodic with the cell length and the betatron oscillation is pseudo-harmonic. An equivalent harmonic oscillator can be defined by sampling* (4) at each cell:

$$\begin{cases} z_n = a\sqrt{\beta}\cos(\phi_n + b), \\ \text{with} \quad \phi_n = n\mu. \end{cases} \tag{5}$$

where μ is the phase-shift per cell. In what follows, we consider perturbations of (3). The solutions we will derive coincide with those of (1) at the sampling points, after rescaling by $\sqrt{\beta}$. It is therefore possible to use (1) or (3) interchangeably, as long as one considers the restriction of the solution to the sampling points. We will use this fact to write simplified expressions for the perturbed motion.

II.4 Periodical Focusing Perturbations

II.4.1 Regular Quadrupole Perturbations

* From the sampling theorem, (4) is not undersampled by this procedure as long as the cell phase-shift is less than π, which is always the case[8]. In the SLC Arcs, $\mu = \frac{3\pi}{5}$.

To study the effect from a focusing modulation with regular quadrupoles, we replace K by $K + k\cos(\nu\phi + \psi)$ in the governing equation (1), where $k\cos(\nu\phi + \psi)$ represents a periodic deviation in the restoring force K, of amplitude k and of phase ψ, and with ν cycles per radians of phase-advance along the array. For the horizontal motion ($z = x$), the most important deviations are the ones in the focusing lenses. Conversely, for the vertical motion ($z = y$), the most important deviations are the ones in the defocusing lenses*. We consider small errors so that $k \ll K$.

In the normalized system, the equation of motion in (3) becomes:

$$\ddot{u}_{x,y} + (1 + g^r \cos(\nu\phi + \psi^r))u_{x,y} = 0, \tag{6}$$

with $g^r = \beta^2 k$, and $\psi^r = \psi$. The function β is sampled at the center of each focusing magnet for the horizontal motion, and at the center of each defocusing magnet for the vertical motion. Since only errors in the focusing (respectively defocusing) magnets affect the motion significantly in the horizontal (respectively vertical) planes, the factor g^r can be considered constants in (6).

II.4.2 Skew Quadrupole Perturbations

Similarly, we write the equations which govern the motion when focusing modulations with skew quadrupoles are applied. In this case, the restoring focusing force, proportional to the beam excursion in each transverse plane, acts on the perpendicular plane. This generates cross-plane coupling. The equations of motion are in this case:

$$\begin{cases} \ddot{u}_x + u_x + g^s \cos(\nu\phi + \psi^s)u_y = 0 \\ \ddot{u}_y + u_y + g^s \cos(\nu\phi + \psi^s)u_x = 0, \end{cases} \tag{7}$$

where g^s and ψ^s represent the amplitude and phase of the skew focusing modulation

* This results from the fact that in a FODO array, the beam size is naturally larger in each lens, in the plane in which the lens focuses. Because of this, the set of F and D magnets form close to orthogonal sets, in terms of their effect on the one-dimensional beam motion. A measure of this orthogonality is given by the ratio of the maximum to minimum beam size in the array. In the Arc lattice, this ratio is 2.8. The two sets are orthogonal for all practical purposes.

along the array†.

Defining $u_\pm = u_x \pm u_y$, we can rewrite (7) in a form similar to (6):

$$\ddot{u}_\pm + (1 \pm g^s \cos(\nu\phi + \psi^s))u_\pm = 0. \tag{8}$$

Next, we show that the perturbed motions, solutions of (6) and (7), are affected significantly only for two specific values of the frequency ν of the modulations, namely:

$$\nu \simeq 0 \quad \text{and} \quad \nu \simeq 2, \tag{9}$$

corresponding respectively to the systematic component in the errors and to the second harmonic of the betatron frequency.

II.5 First Order Solution

II.5.1 Method of Variation of Constants

Following Nayfeh, and along with the method of variation of constants, we

---

† The factor g^s can be related to the amplitude of skew quadrupole modulations in the focusing and in the defocusing magnets as follows:

$$g^s_{D,F} = \beta_{x,y}^{\frac{3}{2}} \beta_{y,x}^{\frac{1}{2}} k_{D,F},$$

where $k_{D,F}$ represent deviations to the focusing and defocusing magnet strengths in the regular coordinate system. The largest effect in the first (respectively second) of the two equations in (7) occurs in the defocusing (respectively focusing) magnet, since u_y (respectively u_x) is naturally the largest there. Therefore the term g^s in the first (respectively second) equation in (7) is essentially g^s_D (respectively g^s_F). Since in a FODO array, $\beta^F_{x,y} = \beta^D_{y,x}$, we have $g^s_D = g^s_F$. For this reason, we use the same g^s in the two equations in (7).

Furthermore, it has been shown (through computer simulation) that modulations where the skew quadrupole components have opposite signs in the focusing and in the defocusing lenses produce effects which cancel over one betatron period, except in the case of the systematic component, corresponding to $\nu \simeq 0$. For this reason, we use the same phase ψ^s in the two equations in (7). In the case $\nu \simeq 0$, skew quadrupole focusing perturbations with opposite sign in the focusing and in the defocusing magnets correspond to a rotation of the coordinate system. It can be shown that such a rotation can be expressed in the normalized variables by simply exchanging the sign of g^s in one of the two equations in (7)[9]. In this case, the two equations cannot be decoupled simply as in (8).

solve (6) and (7) by searching for solutions of the form[10]:

$$u = a\cos(\phi + \varphi)). \tag{10}$$

where a and φ are functions of ϕ to be determined. In (10) and in the rest of this paragraph, u represents $u_{x,y,+,-}$. By taking the first derivative of (10), letting a and ϕ vary, and by requiring that the result be what it would be if a and ϕ were constants (i.e. $\dot{u} = -a\sin(\phi + \varphi)$), an equation relating the first order derivatives $\dot{a}$ and $\dot{\varphi}$ is found. By calculating the second derivative of u, and after inserting it in an equation of the form of (6), we find a second equation relating $\dot{a}$ and $\dot{\varphi}$. Thus we have replaced a second order differential equation in u by two coupled first order differential equations in a and in φ. By solving this coupled system, we find that a and φ satisfy:

$$\begin{aligned}\frac{da}{a} &= \frac{g}{4}d\phi\sin[(2-\nu)\phi + 2\varphi - \psi] \\ &\quad + \sin[(2+\nu)\phi + 2\varphi + \psi], \qquad (11a)\\ d\varphi &= \frac{g}{4}d\phi(2\cos[\nu\phi + \psi] \\ &\quad + \cos[(2-\nu)\phi + 2\varphi - \psi] \\ &\quad + \cos[(2+\nu)\phi + 2\varphi + \psi]), \qquad (11b)\end{aligned}$$

where $\psi = \psi^{r,s}$ and $g = g^{r,s}$.

II.5.2 Averaging Method

To find the behavior of the solutions in the limit of small $g\phi$, we solve (11) to first order. To do so, we first note the fact that for values of $\nu \neq 0, 2$, the solutions of (11) are rapidly oscillating functions with amplitudes of order g. We will neglect such contributions, as they are bounded by g. Thus for $\nu \neq 0, 2$, the motion, solution of (6) and (7), is perturbed negligibly.

The amplitudes of the functions a and φ can only become significant if the functions on the right hand side of (11) are slowly varying functions. This occurs for $\nu \simeq 0, 2$.

From now on, we will write g_0 for the magnitude of the systematic focusing deviations, corresponding to $\nu \simeq 0$, and g_2 and ψ_2 for the amplitude and phase of focusing modulations at twice the betatron frequency, corresponding to $\nu \simeq 2$.

We first solve for $\nu \simeq 0$. The solution is obtained by integration of (11b). This gives:

$$u \simeq a_0 \cos[(1 + \frac{g_0}{2})\phi + \varphi_0], \tag{12}$$

where a_0 and φ_0 are integration constants.

Next we solve for $\nu \simeq 2$, integrating this time both (11a) and (11b). From (11b), and including only the slowly varying term $\cos[(2-\nu)\phi + 2\varphi - \psi_2]$, we note that $d\varphi \leq \frac{1}{4} g_2 d\phi$. The total variation of φ over the interval of integration is thus bounded by $\frac{1}{4} g_2 \phi$. Thus the right hand sides of (11) stay about constant if $\frac{1}{4} g_2 \phi \ll \pi$. We can in this case treat the slowly varying terms on the right hand side of (11) as constants in the integration. We obtain in this case:

$$u \simeq a_0 e^{\lambda \phi} \cos[(1 + \kappa)\phi + \varphi_0]. \tag{13}$$

where:

$$\begin{cases} \lambda = \frac{g_2}{4} \sin(2\varphi_0 - \psi_2), \\ \kappa = \frac{g_2}{4} \cos(2\varphi_0 - \psi_2). \end{cases} \tag{14}$$

II.6 Physical Description of Perturbed Motion

II.6.1 One-Dimensional Oscillations

From (14), (15) and (16), we characterize the effect of regular focusing modulations on the one-dimensional motion, in the limit of small perturbation, as follows:

Case $\nu \simeq 0$:

The fundamental frequency of the oscillations is shifted by systematic regular focusing deviations, corresponding to $\nu = 0$. This shift is independent of the initial phase of the betatron oscillation.

Case $\nu \simeq 2$:

The amplitude and frequency of the oscillations are perturbed resonantly by regular focusing modulations at the second harmonic of the fundamental betatron frequency, corresponding to $\nu = 2$. Depending on the phase ψ_2 of this modulation and on the initial phase φ_0 of the betatron oscillation, the amplitude will initially decay or grow exponentially with a growth rate λ, and the frequency will increase

or decrease linearly by the slippage parameter κ. These two effects are out of phase: maximum frequency-slippage coincides with a constant amplitude, and zero frequency-slippage with a maximally perturbed amplitude*.

We will describe the consequences for the phase-space and for the beam envelope in the next section.

II.6.2 Two-Dimensional Oscillations

Case $\nu \simeq 0$: (Systematic Skew Component)

We can use (12) and $u_{\pm} = u_x \pm u_y$ to calculate the effects from systematic skew perturbation. We obtain:

$$u_x \simeq [u_x(0)\cos\phi + \dot{u}_x(0)\sin\phi]\cos g_0^s\phi + [-u_y(0)\sin\phi + \dot{u}_y(0)\cos\phi]\sin g_0^s\phi \qquad (15a)$$

and:

$$u_y \simeq [-u_x(0)\sin\phi + \dot{u}_x(0)\cos\phi]\sin g_0^s\phi + [u_y(0)\cos\phi + \dot{u}_y(0)\sin\phi]\cos g_0^s\phi \qquad (15b)$$

The results in (15a) and (15b) show that in the case of a systematic skew focusing perturbation ($\nu \simeq 0$), oscillations originating in one plane are gradually transferred into the other plane, and that the sum of squares of the oscillation amplitudes in both planes remains constant. Thus there is beating between the two planes. The period of this beating is determined by g. This is true for both the positions $u_{x,y}$ and the angles $\dot{u}_{x,y}$, as can be seen from differentiating (15). Therefore the beating phenomenon which arises is between the two full phase-spaces in both planes.

Case $\nu \simeq 0$: (Coordinate Rotation)

The solutions are in this case simple harmonic oscillators, in the rotated coordinate system. We will not write these solutions explicitly.

Case $\nu \simeq 2$:

* The separation between the two initial phases φ_0, corresponding to maximum growth or decay, and to maximum phase-slippage, depends on the magnitude of the perturbation. It is strictly 45 deg only in the limit of small perturbation. We will describe the behavior for larger perturbation in the next section.

From (8) and (13), the form of the solutions are:

$$u_{\pm} = a_0^{\pm} e^{\lambda_{\pm}\phi} \cos[(1 \pm \kappa_{\pm}\phi + \varphi_0^{\pm}]. \tag{16}$$

For initial conditions contained in one of two $u_x, \dot{u}_x$ or $u_y, \dot{u}_y$ planes, corresponding to the propagation of betatron oscillations launched from one plane at a time (for example: $u_y(0) = \dot{u}_y(0) = 0$), one can show that the solutions can be written as the sum of two functions, one exponentially growing and one exponentially decaying:

$$u_{x,y} = \frac{a_o}{2}[e^{\lambda\phi} \cos[(1+\kappa)\phi + \varphi_0] \pm e^{-\lambda\phi} \cos[(1-\kappa)\phi + \varphi_0]]. \tag{17}$$

In this case, the oscillations will grow exponentially in both planes for arbitrary initial phase.

It is however possible to find initial conditions such that both u_+ and u_- decay simultaneously initially. This has been shown independently by solving (8) numerically[9]. One example of such initial conditions is $u_x(0) = \dot{u}_x(0) = u_y(0) = \dot{u}_y(0)$.

In the next section, we will analyse the consequences from this cross-plane coupling on the areas of the beam phase-space, projected in each plane (projected emittances), and for the beam envelopes, in each of the above cases.

II.7 Physical Description of Perturbed Phase-Space

II.7.1 Matched Phase-Space

In the case of a perfect lattice and when the beam phase-space is matched at the input, it remains matched as it is imaged through the array by the optics.

The equation of the envelope of the matched phase-space is easily constructed from the form of the betatron oscillation in (4). One obtains an ellipse:

$$\gamma z^2 + 2\alpha z\dot{z} + \beta\dot{z}^2 = a^2, \tag{18a}$$

where $\dot{z} = \frac{dz}{ds}$, $\gamma = \frac{1+\dot{\beta}^2}{\beta}$, and $\alpha = \frac{-\dot{\beta}}{2}$. The quantity in (18a) is called the Courant-

Snyder invariant[7]. It can also be written in matrix form:

$$(z, \dot{z})\mathrm{T}^{-1}\begin{pmatrix} z \\ \dot{z} \end{pmatrix} = a^2, \text{where } \mathrm{T} = \begin{pmatrix} \beta & -\alpha \\ -\alpha & \gamma \end{pmatrix} \text{ and } \det(\mathrm{T}) = 1. \qquad (18b)$$

The equations in (18) also define the closed phase-space trajectory of a particle with initial condition a. The parameters α, β and γ are called Twiss parameters. They characterize the lattice. They also describe the beam phase-space if and when it is matched to the lattice. In this case, the beam-matrix[11] $\sigma = \epsilon\mathrm{T}$. The area πa^2 of the ellipse is identified as π times the emittance ϵ.

In the normalized coordinates $u = \frac{z}{\sqrt{\beta}}$ and $\dot{u} = \frac{du}{d\phi} = \sqrt{\beta}(\dot{z} - \frac{\dot{\beta}}{2\beta}z)$ defined in II.3, the matched phase-space is a circle of radius ϵ. This can be verified by direct substitution in (18a).

II.7.2 Perturbed One-Dimensional Phase-Space

Case $\nu \simeq 0$:

In II.6.1, we described the effect of a systematic regular focusing deviation, with magnitude g_0^r, corresponding to $\nu \simeq 0$. The motion is in this case simply frequency-shifted, and the solutions in (12) will satisfy the equation of the matched circle defined in II.7.1. The beam phase-space remains in this case matched*.

Case $\nu \simeq 2$:

When the lattice is perturbed by focusing errors, this matched circle is distorted into an ellipse. We describe this condition of the beam phase-space by mismatch. We characterize this mismatch by the ratio M of the radius of the larger circle in which this ellipse is inscribed to that of the initial circle corresponding to the matched case, and by the angle ϕ_0 between its major axis and the abscissa (see Fig. 1): M and ϕ_0 are the amplitude and the phase of the mismatch.

⋆ This is strictly speaking only approximately true, as the Twiss parameters in (18b), which characterize the FODO array, depend on the phase advance per cell. For example, it can be shown that for a thin lens FODO array[12]:

$$\beta_\pm = L\frac{1 \pm \sin(\mu/2)}{\sin\mu},$$

where $\beta_\pm$ are the maximum and minimum values, occurring in each plane in the lenses which are focusing, and respectively defocusing, in that plane. For small systematic perturbations of up to one percent, the variation of the Twiss parameters is of the order of one percent. We neglect such variations.

In II.6.1, we described the effect of a regular focusing modulation at twice the betatron frequency, with magnitude g_2^r and with phase ψ_2^r, corresponding to $\nu \simeq 2$. We found that the maximum oscillation amplitude which can be reached is: $u_{max} = e^{\frac{g_2^r}{4}\phi}$.

The phase ϕ_0 of the mismatch depends on how far along the array the mismatch has propagated, i.e. on the accumulated phase advance ϕ, and on the phase ψ_2^r of the regular focusing modulation. We can thus write:

$$\phi_0 = \phi + \psi_2^r. \tag{19}$$

Since ϕ_0 can take an arbitrary value, we can identify:

$$M = u_{max} = e^{\frac{g_2^r}{4}\phi}. \tag{20}$$

The equation of the distorted ellipse is calculated in terms of M and ϕ_0, first in the coordinates rotated by ϕ_0 in which it is erect, and then transforming back into the unrotated coordinates. This gives:

$$u^2(M^2\cos^2\phi_0 + \frac{1}{M^2}\sin^2\phi_0) + \dot{u}^2(M^2\sin^2\phi_0 + \frac{1}{M^2}\cos^2\phi_0) + 2u\dot{u}\cos\phi_0\sin\phi_0(M^2 - \frac{1}{M^2}) = \epsilon. \tag{21}$$

The corresponding beam-matrix, written in the normalized system, in terms of the amplitude g_2^r and of the phase ψ_2^r, is:

$$\Sigma_{g_2^r,\psi_2^r}(\phi) = \epsilon \begin{pmatrix} \Sigma_{11} & \Sigma_{12} \\ \Sigma_{12} & \Sigma_{22} \end{pmatrix}, \tag{22}$$

where:

$$\begin{cases} \Sigma_{11} = \cosh(\frac{g_2^r}{2}\phi) + \sinh(\frac{g_2^r}{2}\phi)\cos(2\phi + \psi_2^r) \\ \Sigma_{12} = -\sinh(\frac{g_2^r}{2}\phi)\sin(2\phi + \psi_2^r) \\ \Sigma_{22} = \cosh(\frac{g_2^r}{2}\phi) - \sinh(\frac{g_2^r}{2}\phi)\cos(2\phi + \psi_2^r), \end{cases} \tag{23}$$

and where ϵ is the emittance. Transforming back into real coordinates gives:

$$\begin{cases} \sigma_{11} = \beta\Sigma_{11}, \\ \sigma_{12} = \Sigma_{12} - \alpha\Sigma_{11}, \\ \sigma_{22} = \frac{1}{\beta}(\Sigma_{22} + \alpha^2\Sigma_{11} - 2\alpha\Sigma_{12}). \end{cases} \tag{24}$$

For the ideal lattice, characterized by $g_2^r = 0$, (24) reduces to (18b) as expected.

In summary, when the lattice is perturbed by a regular focusing modulation at twice the betatron frequency, with amplitude g_2^r and phase ψ_2^r, the phase-space gradually becomes elongated into an ellipse with a major axis which grows exponentially with the accumulated phase advance, at a growth rate $\frac{g_2^r}{2}$. This ellipse rotates in phase-space at the betatron frequency. The initial value of the phase of the mismatch is determined by the phase ψ_2^r.

From (23), we see that the beam size beats between minimum and maximum values, of $e^{-\frac{g_2^r}{2}\phi}$ and $e^{\frac{g_2^r}{2}\phi}$ respectively. The beating occurs with a period of π, as illustrated in Fig. 1. Equation (23) (and graphically Fig. 1) also allows us to study the behavior of the solutions, both for large and for small perturbation. For small perturbation ($g_2^r\phi \ll 1$), the first equation in (23) reduces to $\Sigma_{11} \simeq 1 + \frac{g_2^r\phi}{2}\cos(2\phi + \psi_2^r)$. In this case, the separation in the phase ϕ between maximally growing or decaying solutions, and solutions with an unperturbed amplitude (corresponding to $M = 1$), is exactly 45 deg. This is in agreement with the results from the first order calculations described in II.6.1. For larger $g_2^r\phi$, the initial phases corresponding to an unperturbed amplitude move closer and closer to the phase corresponding to a maximally decaying solution. For infinite g_2^r, all solutions become eventually exponentially growing, except for the "single" one for which, strictly, $\cos(2\phi+\psi_2^r) = -1$. This has been shown independently by solving (6) numerically[9].

II.7.3 Coupled Two-Dimensional Phase-Space

In II.6.2, we gave expressions describing the cross-coupling of betatron oscillations which occurs from systematic skew focusing errors, corresponding to $\nu \simeq 0$, and from skew focusing modulations at twice the betatron frequency, corresponding to $\nu \simeq 2$. We use these expressions to infer the evolution of the areas of the phase-space projections in each-plane. The correctness of all forms (except (28)) given in this section has been verified through simulation. Results from these simulations are presented in section IV.

We assume an input phase-space where the horizontal and vertical planes are not coupled, but where the emittances are not necessarily equal. Let $r = \epsilon_y/\epsilon_x$

be the ratio of the initial vertical to the initial horizontal emittances (we assume $r \leq 1$), and let us normalize the results to the initial horizontal emittance, by putting $\epsilon_x(\phi = 0) = 1$.

Case $\nu \simeq 0$: (Systematic Skew Component)

In this case, it is possible to calculate, from (15), the projected emittances, as the beam is imaged through the array. We obtain:

$$\begin{cases} \epsilon_x(\phi) = \frac{1}{2}[(1+r) + (1-r)\cos g_0^s \phi] \\ \epsilon_y(\phi) = \frac{1}{2}[(1+r) - (1-r)\cos g_0^s \phi]. \end{cases} \tag{25}$$

Putting $r = 0$ in (25) shows explicitly the beating phenomenon which we described in II.6.2. One obtains in this case:

$$\begin{cases} \epsilon_x(\phi) = \cos^2(g_0^s \phi) \\ \epsilon_y(\phi) = \sin^2(g_0^s \phi) \end{cases} \tag{26}$$

The sum of the two emittances is in this case constant, and transverse oscillation energy is transferred back and forth between one plane and the other. This condition describes adequately the imaging of betatron oscillations launched from one plane at a time.

In the special case of equal emittances, corresponding to $r = 1$, we have from (25) that:

$$\epsilon_x(\phi) = \epsilon_y(\phi) = 1. \tag{27}$$

The motion remains in this case unperturbed by systematic skew focusing deviations.

For an arbitrary value of r, the two emittances will beat between minimum and maximum values of r and 1. As can be seen, the variations of the two emittances are out of phase.

Case $\nu \simeq 0$: (Coordinate Rotation)

In this case, the projected emittances are calculated by transforming a four-dimensional uncoupled beam-matrix through a rotation of the coordinate system. We obtain:

$$\begin{cases} \epsilon_x(\phi) = \cos^2(2g_0^s) + r\sin^2(2g_0^s) \\ \epsilon_y(\phi) = \sin^2(2g_0^s) + r\cos^2(2g_0^s). \end{cases} \tag{28}$$

The same features apply as for the systematic skew component: for $r = 0$, the

sum of the projected emittances is preserved, and for $r = 1$, the phase-space is not perturbed.

Case $\nu \simeq 2$:

In this case, we write, by analogy with (25):

$$\begin{cases} \epsilon_x(\phi) = \cosh^2 \frac{g_2^s}{4}\phi + r^2 \sinh^2 \frac{g_2^s}{4}\phi \\ \epsilon_y(\phi) = \sinh^2 \frac{g_2^s}{4}\phi + r^2 \cosh^2 \frac{g_2^s}{4}\phi. \end{cases} \tag{29}$$

In the special case of zero initial emittance in the vertical plane ($r = 0$), we obtain:

$$\begin{cases} \epsilon_x(\phi) = \cosh^2(\frac{g_2}{4}\phi) \\ \epsilon_y(\phi) = \sinh^2(\frac{g_2}{4}\phi), \end{cases} \tag{30}$$

in accordance with (17), from which all solutions grow exponentially if the initial conditions are restricted to one plane.

The difference between the two emittance projections is in this case constant, and the projected emittances grow exponentially in both planes. This condition describes adequately the imaging of betatron oscillations launched from one plane at a time

In the special case of equal initial emittances in each plane (r=1), we obtain:

$$\epsilon_x(\phi) = \epsilon_y(\phi) = \cosh \frac{g_2^s}{2}\phi. \tag{31}$$

The two projected emittances remain in this case equal, and grow exponentially*.

II.8 Summary Description - Number of Independent Perturbations

Thus we find that, in total, the transverse motion can be perturbed by ten independent parameters:

⋆ Although the envelope grows, there can exist, as we found in (16), individual solutions which are decaying.

1. The one-dimensional horizontal motion can be perturbed in three ways, namely through a systematic strength deviation in the focusing quadrupoles, and through the amplitude and phase of a periodic focusing deviation at twice the betatron frequency in the focusing quadrupoles.

2. The one-dimensional vertical motion can be perturbed in three ways, namely through a systematic strength deviation in the defocusing quadrupoles, and through the amplitude and phase of a periodic focusing deviation at twice the betatron frequency in the defocusing quadrupoles.

3. The two-dimensional coupled motion can be perturbed in four ways, namely through a systematic skew quadrupole component, through the amplitude and phase of a periodic skew focusing deviation at twice the betatron frequency†, and through an overall coordinate rotation.

These ten perturbations correspond to the number of free parameters in a fully general two-dimensional transfer matrix[13].

To the extent that the errors are small and that only one perturbation is applied at a time, it is possible to simply parametrize the perturbed motion as a function of these ten parameters, as was shown above. In general, however, a full parametrization will be complicated as the mixing between the perturbations, not considered here, will yield higher order dependances.

In the case of the four-dimensional beam phase-space, it would appear from our calculations that it only can be perturbed in seven independent ways, since the two systematic strength deviations, in the focusing and in the defocusing magnets, do not distort the phase-space, and since the coupling effect from the overall coordinate rotation can be reproduced through the systematic skew quadrupole component.

This is however in contradiction with the counting of the number of invariants imposed by Hamiltonian Mechanics. As can be shown, two invariants exist for hamiltonian systems with two degrees of freedom: the volume of the four-dimensional phase-space and the sum of the projections onto each coordinate plane of any two-dimensional surface in the four-dimensional phase-space[14]. From this counting, one expects eight degrees of freedom for the fully coupled four-dimensional phase-space. We have not resolved this discrepancy.

In the special case of equal initial emittances in both planes ($r = 1$), our cal-

† With in both cases the same sign skew quadrupole component in the focusing and in the defocusing quadrupoles.

culations show that the fully coupled four-dimensional phase-space has six degrees of freedom. This is in agreement with an independent proof[15], and has also been verified in extensive computer simulations of optical corrections in the Final Focus System[16].

II.9 Case of the SLC Arcs

Not all perturbations are equally important in the case of the SLC Arcs.

Effects from the systematic coordinate rotation can in the SLC be ignored for all practical purposes, because the magnitude of the rotation angle can never be very large: for skew focusing errors of one percent, the rotation angle is only 1.15 degree.

In addition, effects on the phase-space from both the systematic skew quadrupole perturbation and the overall coordinate rotation are vanishing if the beam has, as is nominally specified, equal emittances in both planes.

In the case of the systematic skew quadrupole perturbation, there can however be significant effects on the betatron oscillations and on the transfer matrix. For beams with unequal emittances, the beats which are produced in each of the two emittances out of phase and are bounded by the larger emittance (see equation (25)). In the case of the SLC, where beams with emittance ratios of about one to three are presently measured at the end of the Linac, this is not a large effect*.

Effects from systematic focusing errors, over the whole length of the Arc, in the focusing and in the defocusing quadrupoles, would be small in entirely flat Arcs, except for mixing effects with the other perturbations. In the original design, the Arcs were rolled around their axis to enable following the terrain of the SLAC site, and this generated a strong sensitivity to systematic focusing errors. With the adiabatic roll transition which was introduced to remedy this problem, such systematic errors will produce coupling effects similar to the ones produced by a systematic skew focusing perturbation[17]. In the case of close to equal emittances, the effects on the phase-space from this are small, as was described above, and the modified Arcs have sensitivities which are similar to those of a flat Arc.

---

* This argument ignores mixing effects between several perturbations. It has in particular been shown that the upper bound described above can be significantly larger if the systematic skew deviation is mixed with a systematic phase difference between the motions in both planes and a one-dimensional mismatch from regular quadrupole errors[13].

II.10 Bandwidth Limits

The effect from the focusing modulation at the second harmonic of the betatron frequency, corresponding to $\nu = 2$, is weakened if a systematic focusing deviation, corresponding to $\nu = 0$, is simultaneously present, from either the errors in the array, or applied externally. This results from the gradual phase-shift which accumulates in this case between the resonantly growing optical mismatch and the induced focusing modulation (see Fig. 2). The mixing between the two perturbations will cause the resonant growth of the oscillations to reach a maximum and to then decay, in a long-range beating effect. The nominal phase-space will be fully restored when the phase-shift between the resonantly growing optical mismatch and the induced focusing modulation reaches π.

We will not derive the explicit form of the perturbed solution. We can however evaluate, at any given point along the array, the reduction in the growth of the oscillation amplitudes, by considering the modulation in frequency domain. The harmonic strength - or spectrum - of the focusing perturbation introduced along the array is given by the modulus of the Fourier transform of the perturbation. Here, we consider periodic perturbations - or modulations - which are applied along an array with finite length, corresponding to a total phase shift of $\phi_{max} = n\mu$, where μ is the phase-shift per cell, and n is the number of cells in the array. The harmonic strength is therefore given by:

$$\begin{aligned} \left| \mathcal{F}[d_{n\mu}(\phi) g e^{i\nu_{pert}\phi}] \right| &= \left| g\delta(\nu - \nu_{pert}) \otimes \frac{\sin[n\mu\pi\nu]}{n\mu\pi\nu} \right| \\ &= \left| g \frac{\sin[n\mu\pi(\nu - \nu_{pert})]}{n\mu\pi(\nu - \nu_{pert})} \right|, \end{aligned} \tag{32}$$

where $\delta(\nu)$ is the Dirac distribution, $\otimes$ symbolizes the convolution product, and $d_{n\mu}(\phi)$ is a function of ϕ which is equal to unity between 0 and $n\mu$, and zero everywhere else*.

This calculation is illustrated in Fig. 3. The range $\Delta\nu$ over which the harmonic strength is still reasonably large is given by about half the separation between the zeros of the function in (32), or $\Delta\nu = \pm 1/2n\mu$ cycles per radians. This corresponds to a maximum phase-shift of $\frac{\pi}{2}$, accumulated between the growing mismatch and

* This function is usually called the "door" function.

the focusing modulation, along the total length of the array, or to a maximum systematic phase-error per cell of:

$$\Delta\mu_{max} = \frac{\pi}{2n}. \tag{33}$$

Equation (33) gives the requirement on systematic errors in the array, as a function of its length, to maintain strong effects from the induced focusing modulation. The system of harmonic focusing corrections installed in the SLC Arcs extends over seven achromats, or $n = 70$ cells. The requirement on systematic phase-errors is in this case $\Delta\mu_{max} = \pm 1.3^0$ per cell.

III. HARMONIC PERTURBATIONS IN THE SLC ARCS

III.1 Definitions

A systematic perturbation in the focusing or in the defocusing magnets means that each focusing or defocusing magnet is perturbed the same way.

The cell phase-shift in the SLC Arc lattice is 108^0 or $\frac{3\pi}{5}$. Thus a perturbation at twice the betatron frequency is a perturbation whose strength is modulated by $\exp(i\frac{6\pi}{5}k)$ along the cells in the array, where k is the cell number.

A total of nine* independent harmonic perturbations can be generated in the SLC Arc lattice. We will represent the strength perturbations in the focusing and defocusing magnets respectively by F and D. We have:

1. Cosine-like in-plane (regular) horizontal second harmonic component:

$$F(k) = g_2^r \cos(\frac{6\pi}{5}k)$$

2. Sine-like in-plane (regular) horizontal second harmonic component:

$$F(k) = g_2^r \sin(\frac{6\pi}{5}k)$$

3. Cosine-like in-plane (regular) vertical second harmonic component:

$$D(k) = g_2^r \cos(\frac{6\pi}{5}k)$$

⋆ Only nine adjustments can be generated, out of the ten which are needed to fully control the optical transfer. The missing one would be a regular focusing perturbation, as in 7. below, but with the same sign in the focusing and in the defocusing magnets. Such a perturbation can be generated electrically through the harmonic correction system described in this note, or through the already installed backleg windings, but has no optical effects because of the achromaticity of the lattice. The only way in which it can be generated in the SLC lattice is physically moving the focusing magnets closer or farther horizontally from the defocusing magnets.

4. Sine-like in-plane (regular) vertical second harmonic component:

$$D(k) = g_2^r \sin(\frac{6\pi}{5}k)$$

5. Cosine-like cross-plane (skew) second harmonic component:

$$F(k) = D(k) = g_2^s \cos(\frac{6\pi}{5}k)$$

6. Sine-like cross-plane (skew) second harmonic component:

$$F(k) = D(k) = g_2^s \sin(\frac{6\pi}{5}k)$$

7. Systematic regular focusing strength difference between focusing and defocusing magnets (*FD-Imbalance*):

$$F(k) = -D(k) = g_0^r$$

8. Systematic skew focusing perturbation in the focusing and defocusing magnets:

$$F(k) = D(k) = g_0^s$$

9. Overall coordinate rotation:

$$F(k) = -D(k) = g_0^s$$

III.2 Strength Perturbations in the Alternating Gradient Magnets

III.2.1 Backleg Wiring Modification

The combined function magnets in the Arc lattice are equipped with backleg windings on each coil. These backleg windings have 29 turns and are connected in series along one achromat. Their purpose is to provide a step-wise adaptation of the lattice to the energy of the beam, which loses about 1 Gev through the emission of synchrotron radiation in the guide-field. The strengths of each magnet in the 7 last achromats are perturbed individually by separately connecting and powering 4 out of 29 backleg winding turns on the upper and lower coils. The remaining 24 turns* are connected as for the original use of the backleg windings. A schematic of the modified wiring arrangement is shown in Fig. 4.

III.2.2 Strength Calculation

The separate four-turn-windings are inter-connected to produce periodic and systematic perturbations along the 7 last achromats in a way which we will describe below. Each circuit is presently powered with bi-polar HCOR12 supplies limited to ± 5 amperes by the voltage requirement. With four turns in each circuit and with the main Arc magnets powered with about 4000 amperes, the maximum strength perturbation of each magnet is of the order of ± 0.005.

More precisely, the magnitudes of the nominal and incremental dipole and quadrupole components† which are generated on the central trajectory have been calculated with POISSON, for Arc-type magnet, nominally powered with 3766 amperes in the main coil, and trimmed with 20 ampere-turns in the backleg windings[5].

When the top and bottom windings are perturbed with the same polarity, mid-plane symmetry is preserved and the strengths of the horizontally deflecting dipole field (vertical magnetic field), and of the regular quadrupole component in the combined function magnets are perturbed.

When the top and bottom windings are perturbed with opposite polarity, a vertically deflecting dipole field (horizontal magnetic field), and a skew quadrupole component are generated. The magnitudes of the components are listed below:

1. Nominally powered magnet: horizontal dipole = 5701.60 Gauss, regular quadrupole = 715.64 Gauss/mm.

2. Trimmed magnet with same polarity for top and bottom coils: incremen-

---

* The bottom windings on each coil have in some magnets been observed to droop and to cause partial shorts. As a preventive measure, the last turn was cut off and disconnected on each of the modified coils.

† We neglect the perturbation to the sextupole component, which is very small (less that 0.005 of the nominal value) and for which the tolerance for sizeable effects on the beam is loose (a few percent).

tal horizontal dipole = 27.87 Gauss, incremental regular quadrupole = 3.49 Gauss/mm. The magnitudes of the perturbations are close to equal in the focusing and defocusing magnets, and correspond to a 0.00488 of the nominal values.

3. Trimmed focusing magnet with opposite polarity for top and bottom coils: incremental vertical dipole = 14.05 Gauss, incremental skew quadrupole = 1.59 Gauss/mm. This corresponds to 0.0022 of the nominal values.

4. Trimmed defocusing magnet with opposite polarity for top and bottom coils: incremental vertical dipole = 16.58 Gauss, incremental skew quadrupole = 2.15 Gauss/mm. This corresponds to 0.0030 of the nominal values.

It can be noted that the skew components have about half the strength of the regular components. In addition, the magnitudes of the effects from trimming the focusing and defocusing magnets with opposite polarity for top and bottom coils are slightly assymetric. This may arise from an assymetry in the pole shape which exists between the two magnets.

III.2.3 Polarities of Components

We use the TRANSPORT polarity convention[11]. We have determined that:

1. A positive trim current in both top and bottom coils, to generate regular quadrupole components, will strengthen both focusing and defocusing magnets. This means that both the total bending angle and quadrupole component become stronger.

2. A positive trim current in the top coil and a negative trim current in the bottom coil, to generate skew quadrupole components, will generate a negative vertical kick in the defocusing magnets, a positive kick in the focusing magnets, and a negative skew quadrupole in both focusing and defocusing magnets.

III.3 Magnet Interconnections - Wiring and Layout

III.3.1 Intermagnet Wiring

Each trim winding, top or bottom, is connected in series with equivalent windings, top or bottom, exactly five cells (corresponding to 3π betatron phase-advance) (or ten magnets) apart, along the 7 last achromats (70 cells or 140 magnets) in the

Arcs. Since focusing and defocusing magnets are wired separately, there are thus 20 independent circuits. The wiring arrangement is illustrated in Fig. 5.

III.3.2 Nomenclature

The database formal names for the 20 supplies are listed below.

SMPS,CA13,1703=Top coil of defocusing magnet.

SMPS,CA13,1704=Bottom coil of defocusing magnet.

SMPS,CA13,1708=Top coil of focusing magnet.

SMPS,CA13,1709=Bottom coil of focusing magnet.

SMPS,CA13,1713=Top coil of defocusing magnet.

SMPS,CA13,1714=Bottom coil of defocusing magnet.

SMPS,CA13,1718=Top coil of focusing magnet.

SMPS,CA13,1719=Bottom coil of focusing magnet.

SMPS,CA13,1723=Top coil of defocusing magnet.

SMPS,CA13,1724=Bottom coil of defocusing magnet.

SMPS,CA13,1728=Top coil of focusing magnet.

SMPS,CA13,1729=Bottom coil of focusing magnet.

SMPS,CA13,1733=Top coil of defocusing magnet.

SMPS,CA13,1734=Bottom coil of defocusing magnet.

SMPS,CA13,1738=Top coil of focusing magnet.

SMPS,CA13,1739=Bottom coil of focusing magnet.

SMPS,CA13,1743=Top coil of defocusing magnet.

SMPS,CA13,1744=Bottom coil of defocusing magnet.

SMPS,CA13,1748=Top coil of focusing magnet.

SMPS,CA13,1749=Bottom coil of focusing magnet.

The last digit of the unit number (3,4,8,9) refers to top or bottom windings and to focusing and defocusing magnets. The next to last digit (0,1,2,3,4) refers

to the cell number of the first coil in the each string. The first two digits (17) refer to the achromat number of the first coil on each string.

III.3.3 Multiknob Definitions

The nine harmonic perturbations defined in III.1 are produced by linearly combining the 20 above supplies according to the coefficients given in the same paragraph, using the software multiknob facility[18]. The table below gives the mapping relating the 20 supplies to the 9 knobs:

	SINXX	COSXX	SINYY	COSYY	SINXY	COSXY	SYSKEW	SYSROT	FDIMB
1703	+0.00	+0.00	-0.59	-0.81	-0.59	-0.81	+1.00	+1.00	+1.00
1704	+0.00	+0.00	-0.59	-0.81	+0.59	+0.81	-1.00	-1.00	+1.00
1708	-0.59	-0.81	+0.00	+0.00	-0.79	-1.09	+1.35	-1.35	-1.00
1709	-0.59	-0.81	+0.00	+0.00	+0.79	+1.09	-1.35	+1.35	-1.00
1713	+0.00	+0.00	+0.95	+0.31	+0.95	+0.31	+1.00	+1.00	+1.00
1714	+0.00	+0.00	+0.95	+0.31	-0.95	-0.31	-1.00	-1.00	+1.00
1718	+0.95	+0.31	+0.00	+0.00	+1.28	+0.42	+1.35	-1.35	-1.00
1719	+0.95	+0.31	+0.00	+0.00	-1.28	-0.42	-1.35	+1.35	-1.00
1723	+0.00	+0.00	-0.95	+0.31	-0.95	+0.31	+1.00	+1.00	+1.00
1724	+0.00	+0.00	-0.95	+0.31	+0.95	-0.31	-1.00	-1.00	+1.00
1728	-0.95	+0.31	+0.00	+0.00	-1.28	+0.42	+1.35	-1.35	-1.00
1729	-0.95	+0.31	+0.00	+0.00	+1.28	-0.42	-1.35	+1.35	-1.00
1733	+0.00	+0.00	+0.59	-0.81	+0.59	-0.81	+1.00	+1.00	+1.00
1734	+0.00	+0.00	+0.59	-0.81	-0.59	+0.81	-1.00	-1.00	+1.00
1738	+0.59	-0.81	+0.00	+0.00	+0.79	-1.09	+1.35	-1.35	-1.00
1739	+0.59	-0.81	+0.00	+0.00	-0.79	+1.09	-1.35	+1.35	-1.00
1743	+0.00	+0.00	+0.00	+1.00	+0.00	+1.00	+1.00	+1.00	+1.00
1744	+0.00	+0.00	+0.00	+1.00	+0.00	-1.00	-1.00	-1.00	+1.00
1748	+0.00	+1.00	+0.00	+0.00	+0.00	+1.35	+1.35	-1.35	-1.00
1749	+0.00	+1.00	+0.00	+0.00	+0.00	-1.35	-1.35	+1.35	-1.00

Only seven of these nine knobs have been connected and used. The two missing ones are the second harmonic skew modulations: SINXY and COSXY. It can be noted that for the skew multiknobs, the focusing magnets have coefficients which are scaled by a factor of 1.35 with respect to those of the defocusing magnets, in order to account for the assymetry between the skew components which was noted in III.2.2

IV. SIMULATION OF EFFECTS

IV.1 Introduction to Simulation

We have used ARCSIM1[19] and TRANSPORT[11] to simulate the effects from focusing perturbations at zero and twice the betatron frequency.

ARCSIM1 is a fast simulation which treats small perturbations of the Arc magnets through a linear expansion around the design optical transfer matrix. The overall perturbed optical transfer is then reconstructed by multiplying each individually perturbed Arc matrix.

ARCSIM1 is ideally suited to study the physics of the harmonic focusing perturbations. However, in its current version, ARCSIM1 does not include steering effects from the combined function magnets. Such steering effects do not modify the physics but do modify the magnitude of the effects. In effect, through the sextupole component in the combined function magnets, horizontal deflections will cause regular quadrupole perturbations and vertical deflections will cause skew quadrupole perturbations. Because the strength perturbations are at zero or twice the betatron frequency, the trajectory excursions from these deflections, and the induced optical effects, will also be at zero or twice the betatron frequency. The optical effects will thus add to or subtract from the optical effect from the perturbations of the quadrupole components themselves. In addition, the perturbations will also cause net trajectory deviations* at the end. As will be seen, the trajectory deviations are large enough to require a correction. To correctly estimate the magnitude of the combined effects, we have used a perturbed TRANSPORT deck of the Arcs, in second order and including steering effects.

We first show the maximum effects of the first order optical distortions from the nine multiknobs defined above, in a perfect planar SLC Arc lattice. We do not consider second order optical distortions which arise from deviations in the achromaticity of the optical transfer caused by the first order distortions. Such effects have not been calculated in detail, but are estimated to be small.

Effects from rolls, which are present in the stretch of Arc lattice where the harmonic correction is introduced, will result in not fully orthogonal controls. The

---

* In theory, trajectory deviations would be resonant if the deflections were at the betatron frequency, and not at zero or twice the betatron frequency. In reality, because of the phase-slippage induced by the second harmonic (see II.6.1), the steering effects will grow slightly as the cancellations of deflections π apart no longer occur perfectly.

magnitude of the effects is however not strongly affected, since the component of the perturbed phase-space which is coupled into the other plane across each roll is not driven in that plane. In addition the component of the perturbed phase-space which is coupled into the other plane is not very large. To illustrate this point, we show the magnitude of one of the optical distortions in a lattice with the actual rolls installed in the present North Arc.

The plots shown are made with ARCSIM1, but the strengths of the knobs have been adjusted so that the maximum effect at the end of the seven achromat long stretch corresponds to the magnitude calculated with TRANSPORT, including the steering effects (this fudging exercise has however not been done for the phasing of the knobs).

We then show one simulated example of empirically correcting a lattice perturbed by errors with the harmonic correctors defined above. In the case of a systematic regular focusing error, we also illustrate the bandwidth limit discussed in II.10.

IV.2 Simulated Effects of Harmonic Correctors

IV.2.1 One-Dimensional Oscillations

Case $\nu \simeq 0$: *FD-Imbalance*

A nominal horizontal oscillation is shown in Fig. 6a. The same oscillation, but with the focusing and defocusing magnets perturbed through systematic regular focusing errors of ± 0.005 respectively is shown in Fig. 6b. As can be seen the amplitude of this oscillation is perturbed negligibly, but its frequency is shifted. It can be calculated that the corresponding shift, including optical effects from the displacement of the trajectory, is[9]:

$$(\Delta\mu_x, \Delta\mu_y) \simeq (\pm 87\,\mathrm{deg}, \mp 115\,\mathrm{deg}).$$

The trajectory displacement can also be calculated: it is 42μm[9]. Both agree well with simulated values.

A plot of the unperturbed and perturbed horizontal beam envelopes is shown in Fig. 7a,b. As can be seen, the beam envelopes are negligibly perturbed.

Case $\nu \simeq 2$: *Regular Second Harmonic*

Two one-dimensional horizontal oscillations with the same initial amplitude, but with two different initial phases separated by 90 deg, and with the focusing

magnets perturbed through regular focusing periodic modulation at twice the betatron frequency, with amplitude ± 0.005, are shown in Fig. 8a,b. The two initial phases have been chosen to obtain a maximally growing and a maximally decaying oscillation. As can be seen, the predicted maximum growth is about a factor four. The beats generated in the horizontal and vertical beam envelopes are shown in Fig. 9a,b. As can be seen, the orthogonality of the focusing and defocusing magnets which was noted in II.4.1 is almost perfect (i.e. there is almost no effect on the vertical beam envelope). This orthogonality is however not fully preserved if rolls are present in the lattice. To illustrate this point, we show in 9c,d the beats produced in the horizontal and vertical beam envelopes, from the same perturbation as in 9a,b applied to the North Arc with the present roll configuration. A reduction of the effect in the horizontal plane and some coupling into the vertical plane can be seen*.

Identical effects can be obtained for vertical oscillations with the defocusing magnets perturbed through regular focusing periodic modulation at the twice the betatron frequency.

The displacement of the trajectory is nearly 300μm from these knobs. This is large and requires a correction at the very end in order to be able to launch into the Final Focus.

IV.2.2 Two-Dimensional Oscillations

Case $\nu \simeq 0$: *Systematic Skew Component*

The coupling of an initially fully horizontal oscillation into the vertical plane, from the systematic skew knob set to its maximum of 5 amperes, is shown in Fig. 10a,b. As can be seen the maximum effect is just under 50%, which is rather weak. The same coupling would be obtained for an initially fully vertical oscillation into the horizontal plane, and for any input phase of the oscillation.

Plots of the corresponding beam envelopes are shown†, for a nominal initial phase-space in the horizontal plane and for zero initial phase-space in the vertical plane (Fig. 11a,b), and for a nominal equal initial phase-space in both planes (Fig. 12a,b). These two cases correspond to the beating effect described in II.7.2 through (26) and (27) respectively. In the case of nominal initial phase-space in

---

* A slightly smaller effect from these rolls would have perhaps been seen if the harmonic correction had been installed in a region where the major rolls are matched. Such a region could have been the region between the beginning of achromat 14 and the end of achromat 20.

† In order to make the effects more visible, we have calculated the perturbations of the envelopes for a systematic skew perturbation with three times the maximum knob strength.

both planes (Fig. 12a,b), the envelopes are not perturbed, as was found in (27).

The displacement of the trajectory from setting this knob at its maximum of 5 amperes is about 30μm. This is a small effect (partly because the knob is weak).

Effects from the systematic coordinate rotation are very small and are not illustrated here.

Case $\nu \simeq 2$: *Skew Second Harmonic*

The coupling of an initially fully horizontal oscillation into the vertical plane resulting from the skew second harmonic knob set to its maximum of 5 amperes is shown in Fig. 13a,b[*]. As can be seen the maximum effect is quite small. The same coupling would be obtained for an initially fully vertical oscillation into the horizontal plane, and for any input phase of the oscillation.

Plots of the corresponding beam envelopes are shown[†], for a nominal initial phase-space in the horizontal plane and zero initial phase-space in the vertical plane (Fig. 14a,b), and for a nominal initial phase-space in both planes (Fig. 15a,b). These two cases correspond to the exponentially growing cross-plane coupling effects which were described in II.7.2 through (30) and (31) respectively.

The displacement of the trajectory from setting this knob has not been calculated in detail but appears to be large enough to require a correction at the very end, to launch properly into the Final Focus System.

IV.3 Systems with Errors

IV.3.1 Bandwidth Limit from Systematic Error

In Fig. 9.a, we showed the beat in the one-dimensional horizontal beam envelope caused by a regular second harmonic focusing perturbation. In Fig. 16, we show the same envelope, but now perturbed also by a systematic focusing perturbation corresponding to 3^0 per cell, or about twice the maximum systematic perturbation which can be caused by the FD-Imbalance. This corresponds to just over twice the maximum cell phase-shift which can be allowed for the harmonic knobs to work properly, as stated in II.10 by (33). As can be seen, the growth

---

$\star$ The two skew second harmonic knobs have not been tried experimentally.

† In order to make the effects more visible, we have calculated the perturbations of the envelopes for a skew second harmonic perturbation with five times the maximum knob strength.

in the beating envelope is in this case reversed half way through, and is nearly cancelled at the end.

IV.3.2 Empirical Correction of Randomly Perturbed Lattice

Fig. 17 shows the horizontal beam envelope imaged through the seven achromat long stretch, perturbed by random regular focusing errors only, with strengths normally distributed with a standard deviation of 0.01. The particular "seed" shown in Fig. 17 was chosen as one which generates significant growth of about a factor two. With this magnitude error, such a large growth represents a rather improbable case*. Fig. 18 shows a correction of the case presented in Fig. 17, by combining the sine-like and cosine-like regular focusing second harmonic correctors. Correction is found empirically rather easily for such one-dimensional cases. In lattices fully perturbed with regular and skew focusing errors, the empirical method is in some cases difficult.

⋆ As per IV.2.2, a factor two growth can be generated with a regular focusing modulation at twice the betatron frequency of amplitude 0.0025 (half the knob strength). For randomly distributed regular focusing errors with a standard deviation of 0.01, the one standard deviation expectation value for the strength of the component at twice the betatron frequency is $\frac{0.01}{\sqrt{n}} = 0.0012$, where $n = 70$ is the number of cells in the seven achromats. Thus a 0.0025 strength would correspond to about two standard deviations of the strength distribution, or about 5% of the seeds.

V. LIMITATIONS AND PROSPECTS

V.1 Strength Limitations

The strength of the controls provided in the installation described above is severely limited in the case of the cross-plane coupling correctors (the "skew knobs"). Stronger "systematic skew knobs" in particular would be important for future operation with assymetric emittances, to fully cancel the coupling between the two emittances. They do however not appear to be essential for the present operation with close to equal emittances, a case for which they have no or little effect on the beam envelope (see II.7.3).

In addition, in the presence of systematic regular focusing errors of more than one degree per cell, the strength of the correctors for one-dimensional mismatches are significantly weakened. More generally, the strengths of all the correctors are weakened by phase errors distributed in the stretch where the harmonic correction is installed.

V.2 Guide-line for Upgrade

The obvious upgrade would consist in raising the maximum current through the rewired backleg windings, from the present value of about 5 amperes, to twice or three times that. There may be an impediment to doing this from the limited elasticity in the copper wires composing the windings: after the controls have been turned on and off a large number of times, the repeated thermal contractions and dilatations may cause the windings to sag. An enhanced support mechanism would perhaps be required. The possibility of this sagging is presently being examined.

Another possible upgrade would consist in repeating the installation in one or two new stretches upstream of the one described above. Because of the observed tendency of the bottom turn of the backleg windings to droop (see the footnote at the bottom of page 22), it may be desirable, as a preventive measure, to implement the wiring modification in the remaining 16 achromats. In this case, two new installations similar to the one in achromats 17-23 could be installed in achromats 9-16 and in achromats 1-7. The existing supplies could in this case be kept, as knobs in adjoining stretches could be combined to enhance the effects. The drawback of this is evidently a much increased complexity, as one would then have to deal with

a theoretical* total of 27 knobs, with their relative phasing "and so on".

In summary, if the possible sag in the wires from heating can be solved with a better clamping mechanism, or otherwise shown not to be a problem, and if it is not essential to implement the wiring modification as a preventive measure for the sagging of the last wire, our recommendation would be to upgrade the power supplies.

V.3 Predictive and Precision Control

The harmonic corrections are presently performed successfully as approximate and empirical adjustments to control the beam shape at particularly sensitive places at the entrance to the Final Focus, where significant backgrounds can be generated by optical mismatches, or to adjust the overall lattice of the Arcs to be close to nominal[4].

More work would be required to design fully predictable model-driven corrections for precision control of phase-space parameters at the end of the Arcs. This may be doable by using empirically determined transfer matrices for the Arcs, together with a perturbation technique similar to the one described in IV.1[20]. Some attempts which were made in this direction have shown that this is not straightforward, and requires a detailed understanding of the propagation of measurement errors involved in the empirical matrix determination. More work in this direction may enable precision controlling the phase-space for future optical optimizations of the SLC Arcs.

* In practice, the coordinate rotations do not matter, so "only" 24 knobs would be used.

ACKNOWLEDGEMENTS

Several people have contributed to this work in a major way, and should be acknowledged. Rae Stiening was the first to propose harmonic corrections as a method for adjusting long open FODO arrays. Ted Fieguth pioneered the method in the case of the SLC Arcs, through a system of harmonic steering bumps.

In addition, we have benefited from discussions with Karl Brown, Fatin Bulos, Dave Burke, Dick Early, Jacques Haïssinski, Thomas Lohse, David Ritson, Matt Sands and Nobu Toge.

Finally, we would like to thank the Mechanical Engineering and Power Supply Groups, and the cable installation crews for their support in the installation of "Wirefix".

REFERENCES

(1) P. Bambade, "Beam Dynamics in the SLC Final Focus", SLAC-PUB-4227 (June 1987), C. Hawkes and P. Bambade, "First Order Optical Matching in the Final Focus Section of the SLAC Linear Collider", Nucl. Instr. and Meth. A274 (1989) 27 and P. Bambade *et al.*, "Operational Experience with Optical Matching in the SLC Final Focus System", SLAC-PUB-4776 January (1989).

(2) R. Stiening, "Focusing Errors in the SLC Linac Quadrupole Lattice", SLAC-CN-161 (February 1982).

(3) T. Fieguth, "Harmonic Orbit Distortions", Minutes of GIAT Group Meeting (October 1985).

(4) P. Bambade *et al.*, "Initial Operational Experience with Harmonic Corrections in the SLC Arcs", To be published at the Particle Accelerator Conference, in Chicago (March 1989).

(5) D. Early, "Steering Effects in the Main E Bend Magnet", SLAC-CN-216 (January 1983).

(6) P. Bambade, "Betatron Phase-space Diagnostic in a FODO Array", SLAC-CN-367 (October 1988).

(7) E. Courant and H. Snyder, "Theory of the Alternating Gradient Synchrotron", Ann. of Phys. 3,1-48 (1958).

(8) E. Brigham, "The Fast Fourier Transform", New Jersey, Prentice-Hall, Inc.

(9) J. Haïssinski, Private Communications (April 1987 through January 1989).

(10) A. Nayfeh, "Introduction to Perturbation Techniques", New York, Wiley (1981).

(11) K. Brown *et al.*, "TRANSPORT", SLAC-91, Rev. 2 (May 1977).

(12) E. Wilson, "Circular Accelerators-Transverse", AIP Conf. Proc. 153, p. 3, (1987).

(13) K. Brown and R. Servranckx, "Cross-Plane Coupling and its Effects on Projected Emittances", SLAC-PUB-4679 (July 1988).

(14) L. Teng, "Concerning N-Dimensional Coupled Motions", FermiLab Report FN-229 (May 1971).

(15) The first of the three references in (1).

(16) At this point, this is common knowledge.

(17) P. Bambade *et al.*, "Rollfix - An Adiabatic Roll Transition for the SLC Arcs", SLAC-PUB-4835 (January 1989). (18) Julian Kupiec, "User Guide to the Multiknob Facility".

(19) D. Ritson, ARCSIM, private program (March 1988). A modified version (ARCSIM1) exists with harmonic focusing corrections using regular quadrupoles. Both versions are installed on the shared SLC 197 disk.

(20) T. Barklow, "A Technique for Measuring the 4X4 Transfer Matrix for Beam-Line Sections with Cross-plane Coupling", To be published at the Particle Accelerator Conference, in Chicago (March 1989).

FIGURE CAPTIONS

(1) Mismatched one-dimensional phase-space. The beam-size beats between maxima and minima of M and 1/M respectively.

(2) If a systematic regular focusing error is present, the focusing modulation being applied and the beat of the beam size become gradually out of phase. This weakens the effect of the harmonic corrector.

(3) Harmonic strength associated to a focusing modulation over a finite length.

(4) Wiring modification of backleg trim windings. Four of the twenty-nine turns are connected to a separate circuit, via the upper right terminal. The twenty-five remaining turns are connected as for the original use of the backleg windings, via the top terminal, except for the bottom, which is removed from the circuit.

(5) There are twenty independent circuits connecting the 280 top and bottom coils of the last seven achromats in the Arcs. In each circuit, top and bottom coils of magnets separated by five cells are connected in series.

(6) Horizontal betatron oscillation in seven achromats of the SLC Arcs, with no errors (a), and with a 1% FD-Imbalance (b).

(7) Horizontal beam size in seven achromats of the SLC Arcs, with no errors (a), and with a 1% FD-Imbalance (b).

(8) Horizontal betatron oscillation in seven achromats of the SLC Arcs, with a cosine-like regular quadrupole modulation at twice the betatron frequency in the focusing magnets, corresponding to COSXX=5 Amperes, and for two initial phases amounting to maximum growth (a) and maximum decay (b).

(9) Horizontal and vertical beam sizes in seven achromats of the SLC Arcs, with a cosine-like regular quadrupole modulation at twice the betatron frequency in the focusing magnets, corresponding to COSXX=5 Amperes. Cases (a) and (b) correspond to respectively the horizontal and vertical beam sizes in entirely flat Arcs. As can be seen, the modulation affects mostly the horizontal motion. Cases (c) and (d) correspond to respectively the horizontal and vertical beam sizes in the last seven achromats of the North Arc, with the present roll distribution. As can be seen, some coupling is generated in the vertical plane, and the beats in the horizontal plane are weakened by about 25%.

(10) Horizontal (a) and vertical (b) betatron oscillation in seven achromats of the SLC Arcs, with a systematic skew focusing perturbation, corresponding to

SYSKEW=5 Amperes.

(11) Horizontal (a) and vertical (b) beam size in seven achromats of the SLC Arcs, with a systematic skew focusing perturbation, corresponding to SYSKEW=15 Amperes. In these plots, the initial emittance is zero in the vertical plane. An exchange of oscillation energy from the horizontal plane to the vertical plane can be seen.

(12) Horizontal (a) and vertical (b) beam size in seven achromats of the SLC Arcs, with a systematic skew focusing perturbation, corresponding to SYSKEW=15 Amperes. In these plots, the initial emittances are equal in the horizontal and vertical planes. In this case, the skew focusing perturbation has no effect on the beam envelopes.

(13) Horizontal (a) and vertical (b) betatron oscillation in seven achromats of the SLC Arcs, with a skew focusing modulation at twice the betatron frequency, corresponding to COSXY=5 Amperes.

(14) Horizontal (a) and vertical (b) beam size in seven achromats of the SLC Arcs, with a skew focusing modulation at twice the betatron frequency, corresponding to SYSKEW=25 Amperes. In these plots, the initial emittance is zero in the vertical plane. Growth of the phase-space in both the horizontal and vertical planes can be seen.

(15) Horizontal (a) and vertical (b) beam size in seven achromats of the SLC Arcs, with a skew focusing modulation at twice the betatron frequency, corresponding to SYSKEW=25 Amperes. In these plots, the initial emittances are equal in the horizontal and vertical planes. Growth of the phase-space in both the horizontal and vertical planes can be seen.

(16) Horizontal beam size in seven achromats of the SLC Arcs, with a cosine-like regular quadrupole modulation at twice the betatron frequency in the focusing magnets, corresponding to COSXX=5 Amperes, and with a systematic focusing perturbation of 1.33% in the focusing magnets. As can be seen, a beat in the beam size is initiated as in Fig. 9a, but is reversed in the middle of the section and vanishes almost at the end.

(17) Horizontal beam size in seven achromats of the SLC Arcs with the focusing magnets perturbed by random quadrupole errors with a 1% standard deviation. The particular "seed" was chosen as one which generates large beats at the end.

(18) Horizontal beam size in seven achromats of the SLC Arcs with the focusing magnets perturbed by the same random quadrupole errors as in (17), and corrected

by superimposing a quadrupole modulation at twice the betatron frequency in the focusing magnets, corresponding to COSXX=3.9 Amperes and to SINXX=0.7 Amperes. As can be seen, the correction is almost perfect at the end.

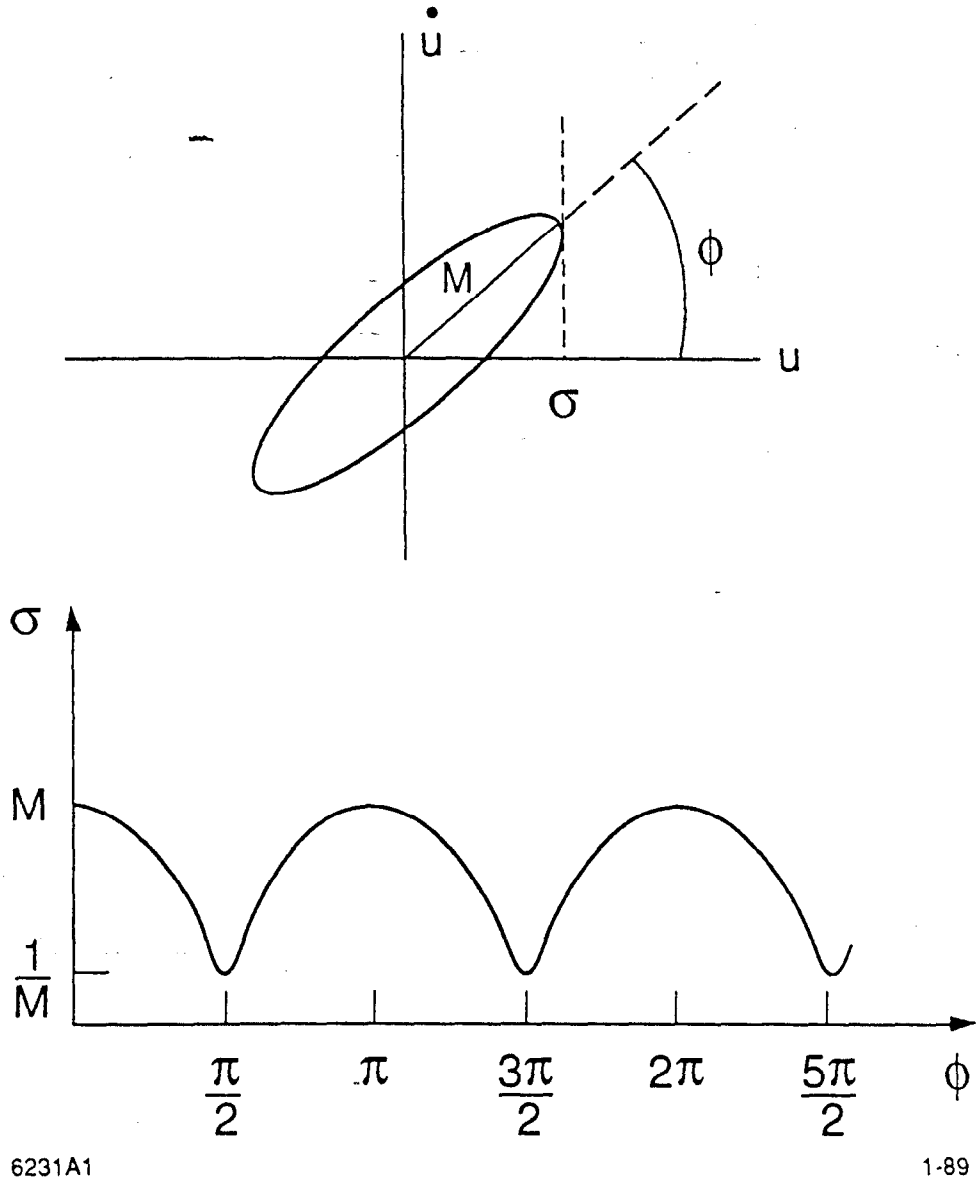

Fig. 1

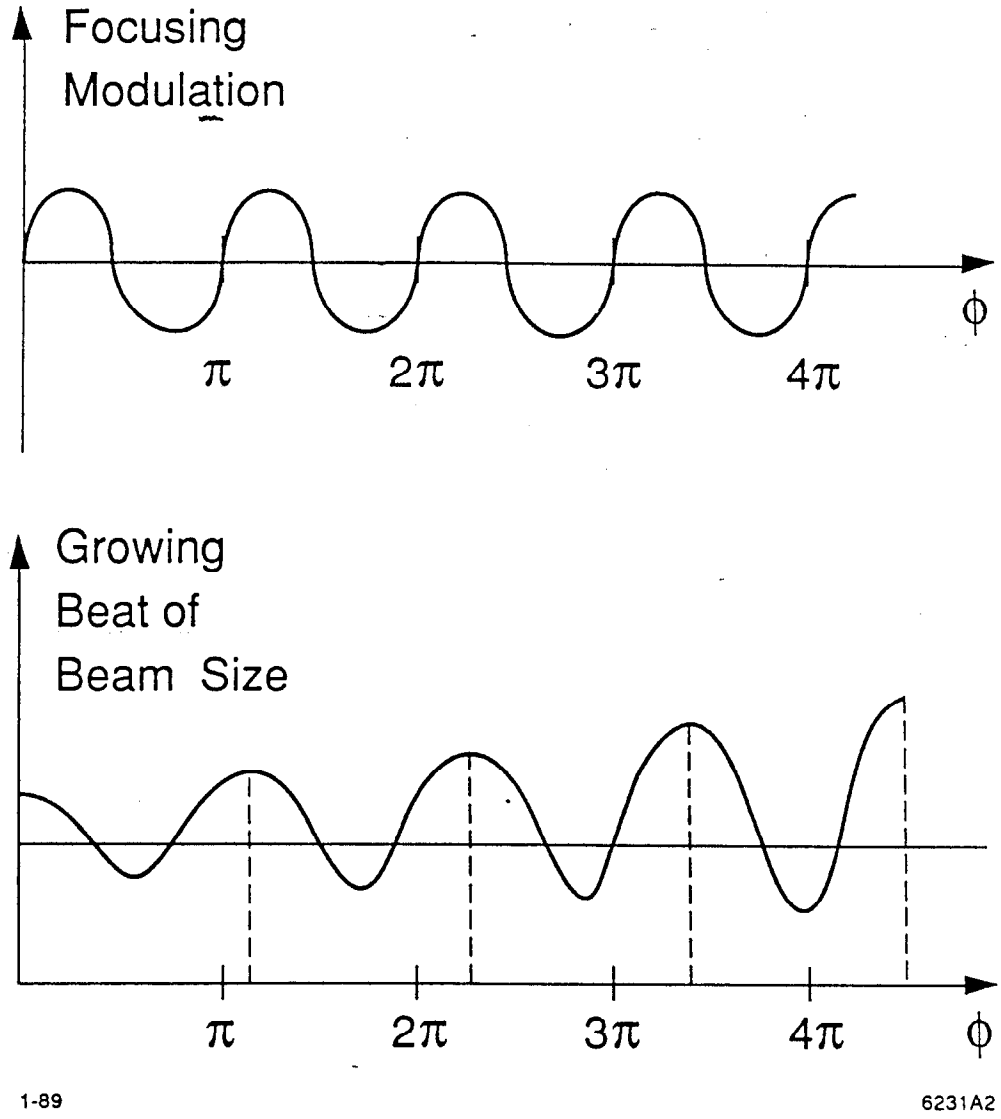
Focusing
Modulation
π
2π
3π
4π
ϕ
Growing
Beat of
Beam Size
π
2π
3π
4π
ϕ
1-89
6231A2

Fig. 2

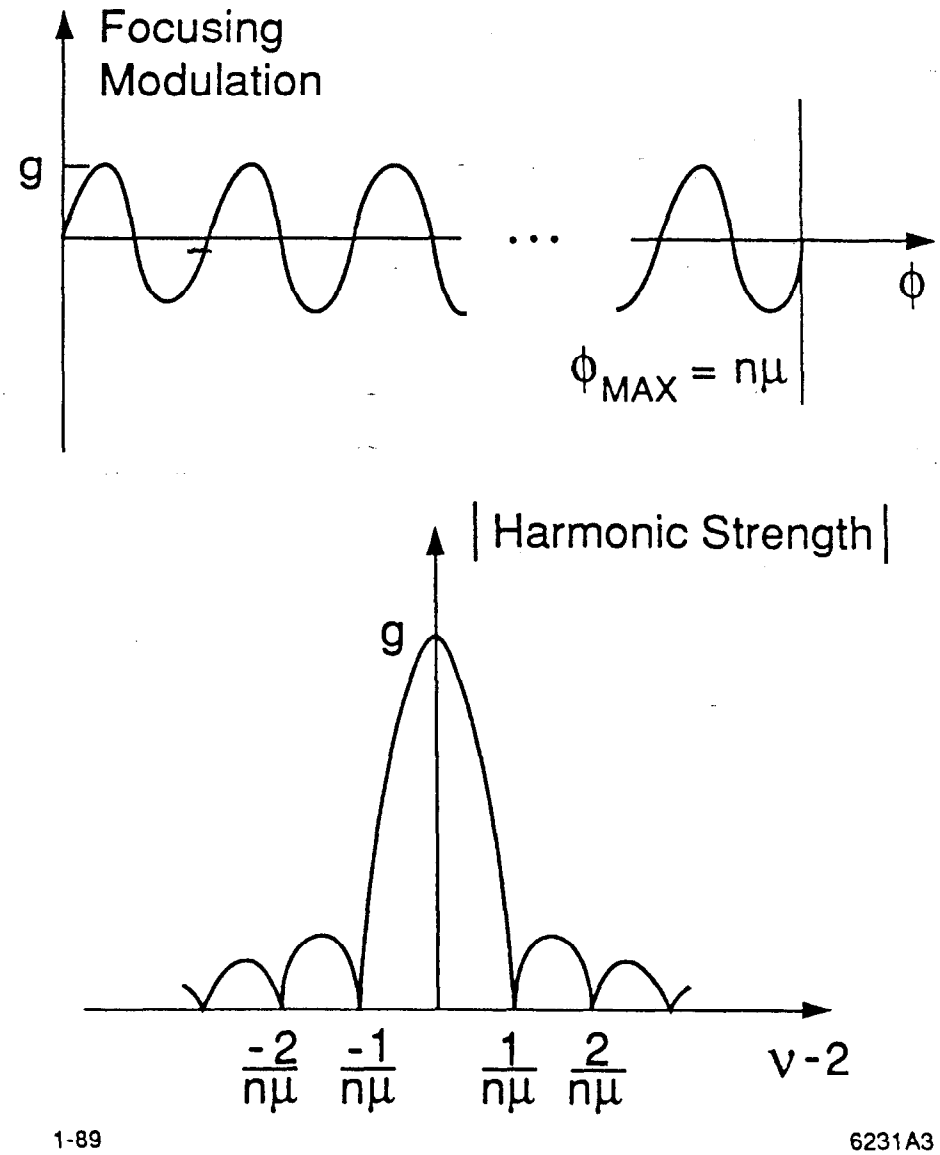
Focusing
Modulation
g
ϕ
$\phi_{MAX} = n\mu$
Harmonic Strength
g
$\frac{-2}{n\mu}$
$\frac{-1}{n\mu}$
$\frac{1}{n\mu}$
$\frac{2}{n\mu}$
ν-2
1-89
6231A3

Fig. 3

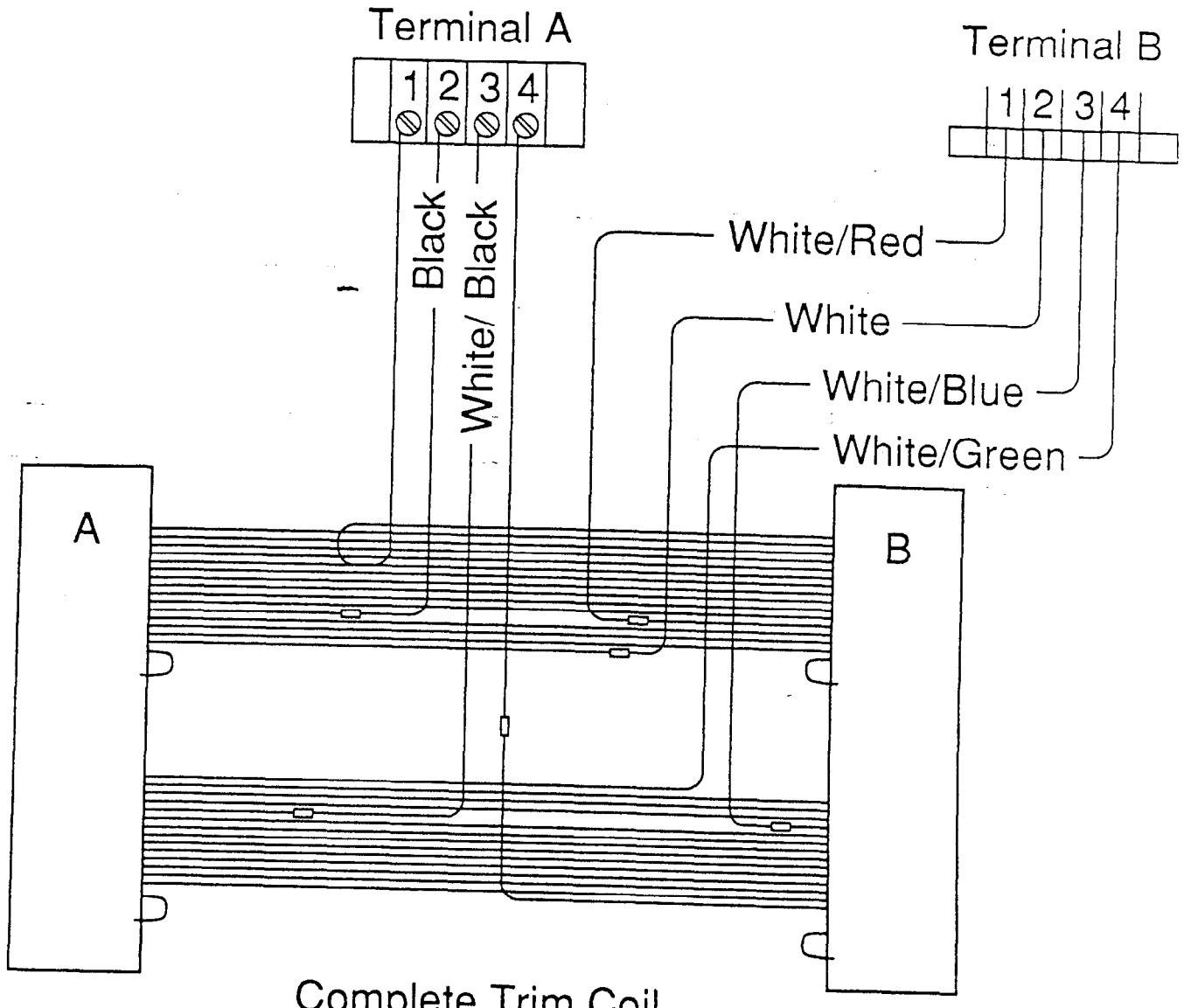
Terminal A
1
2
3
4
Terminal B
1
2
3
4
Black
White/ Black
White/Red
White
White/Blue
White/Green
A
B
Complete Trim Coil
After Wire Fix
1-89
6231A4

Fig. 4

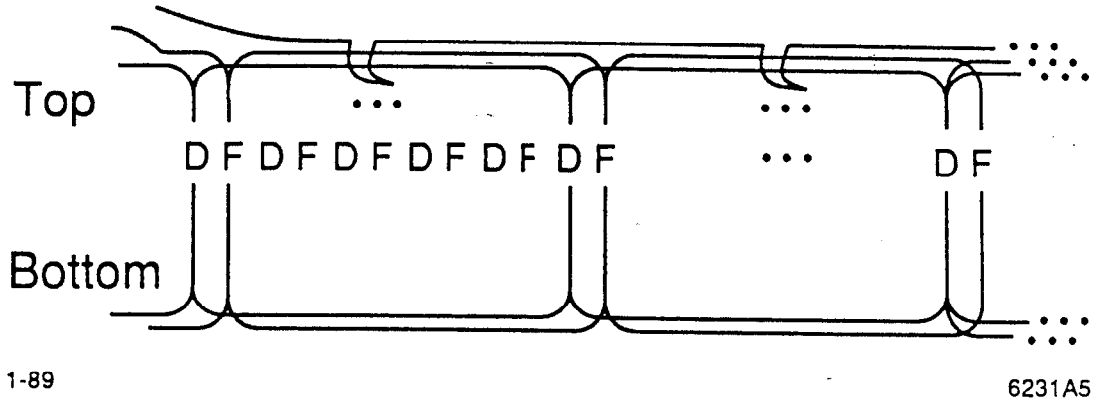

Fig. 5

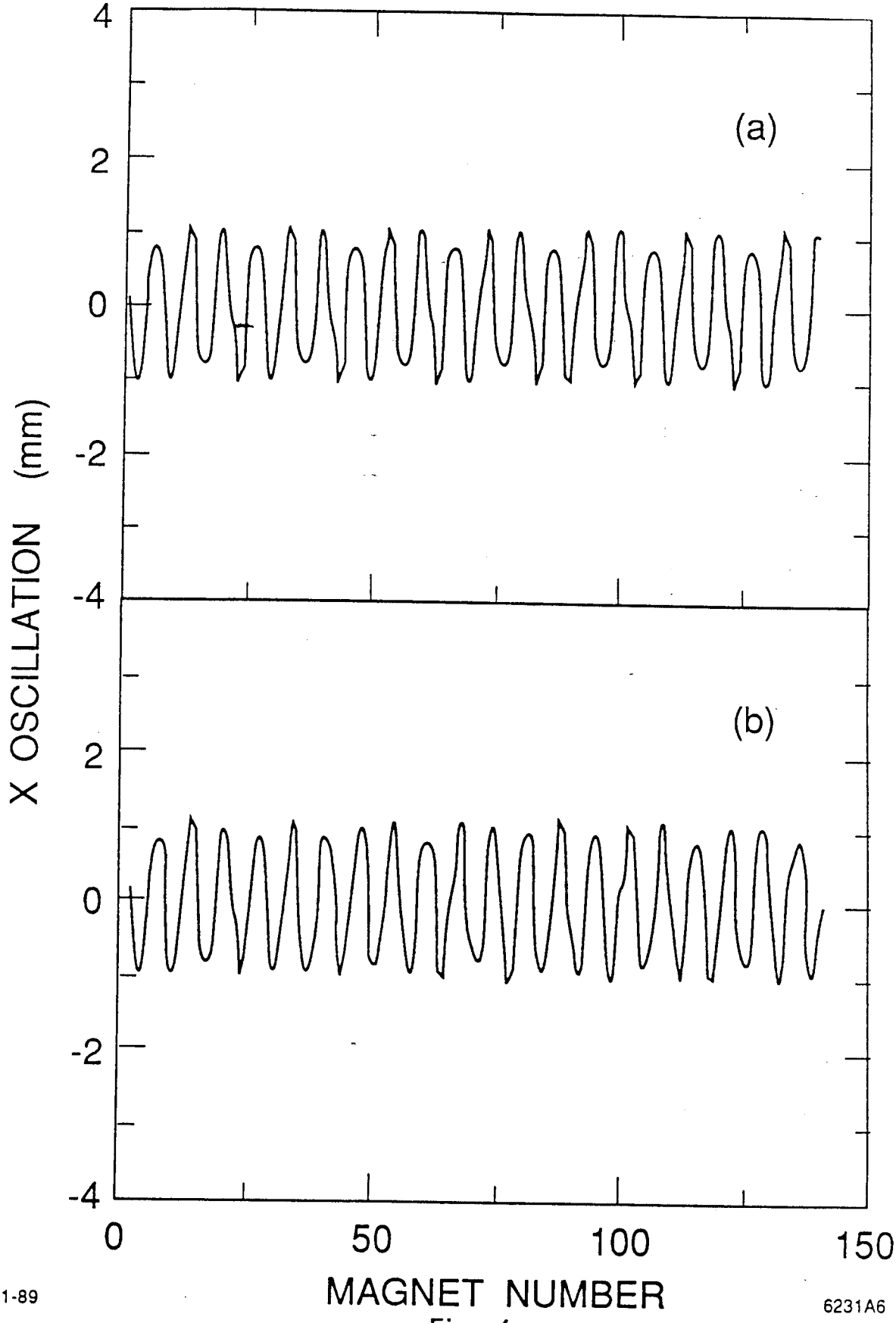
4
2
0
-2
-4
(a)
(b)
X OSCILLATION (mm)
0
50
100
150
MAGNET NUMBER
1-89
6231A6

Fig. 6

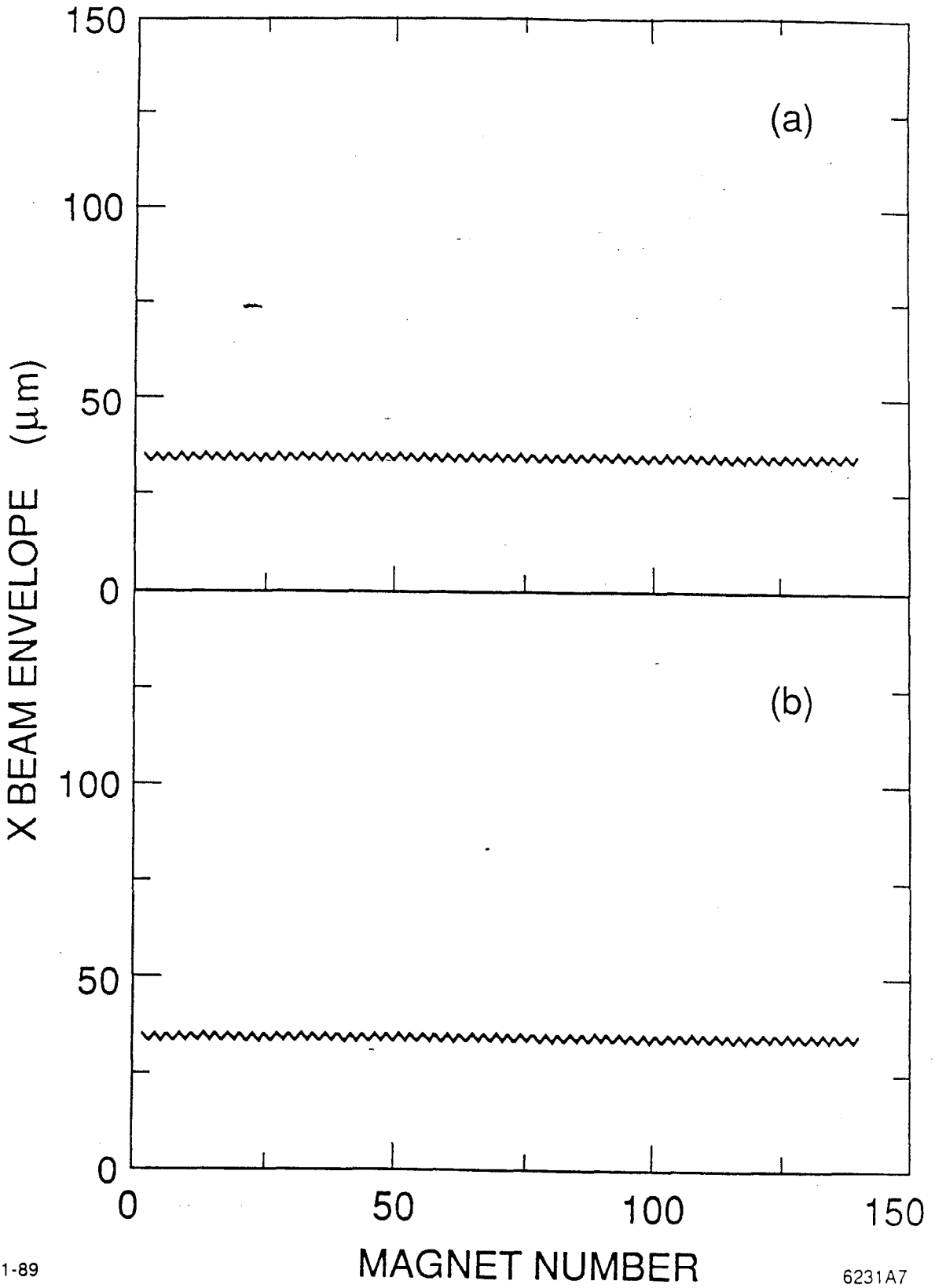
150
100
50
0
(a)
X BEAM ENVELOPE (μm)
100
50
0
(b)
0
50
100
150
MAGNET NUMBER
1-89
6231A7

Fig. 7

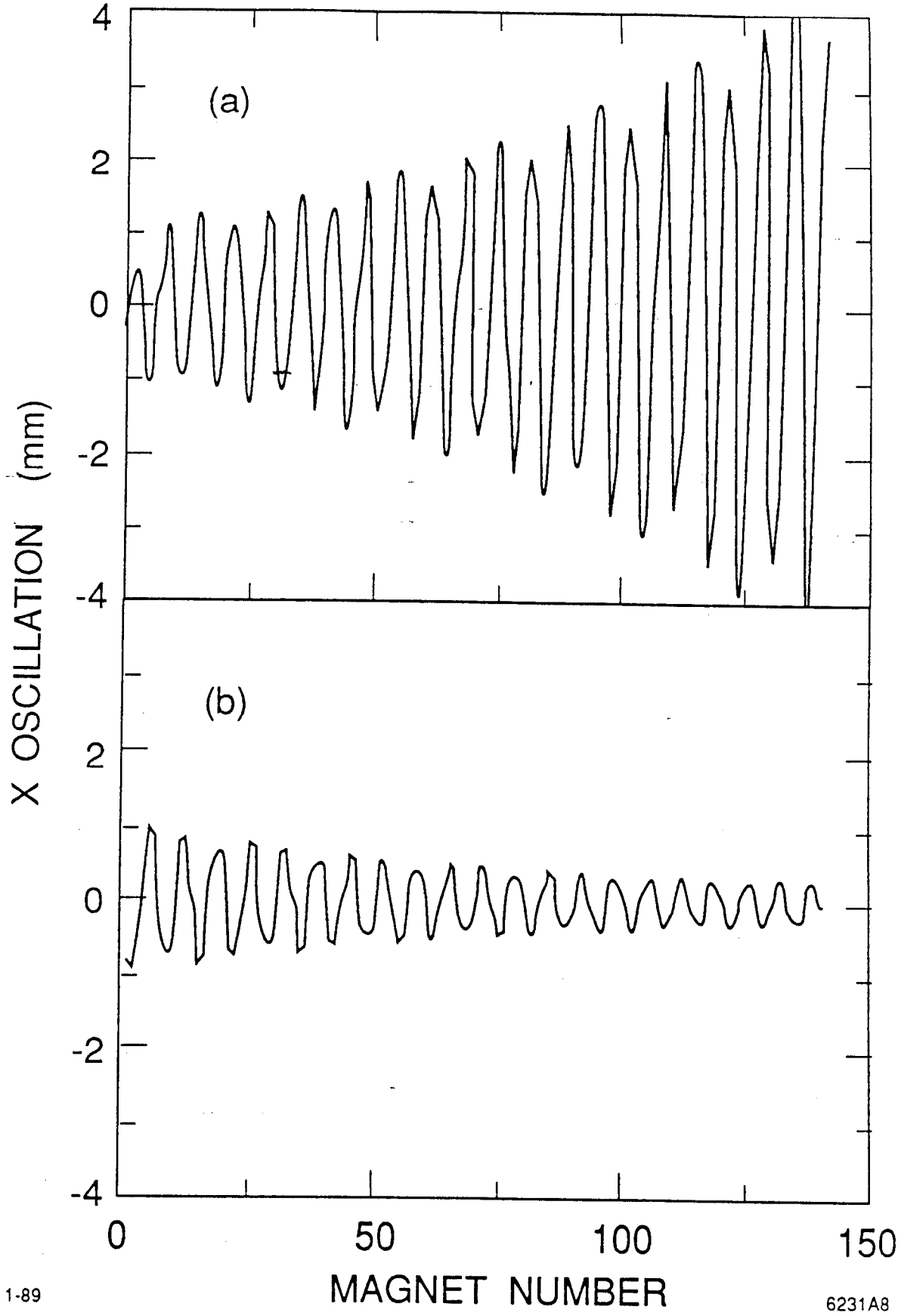
(a)
(b)
4
2
0
-2
-4
X OSCILLATION (mm)
0
50
100
150
MAGNET NUMBER
1-89
6231A8

Fig. 8

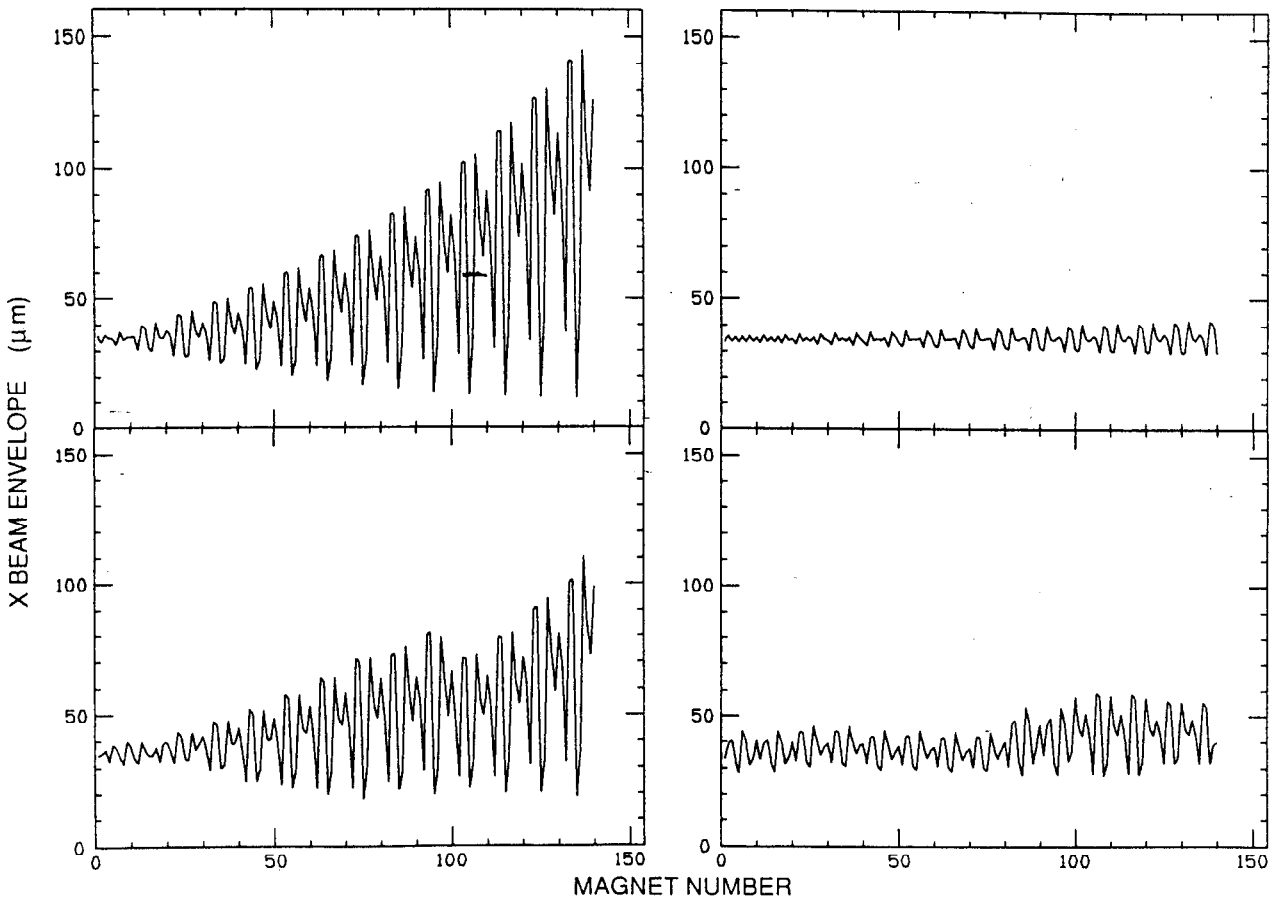

Fig. 9

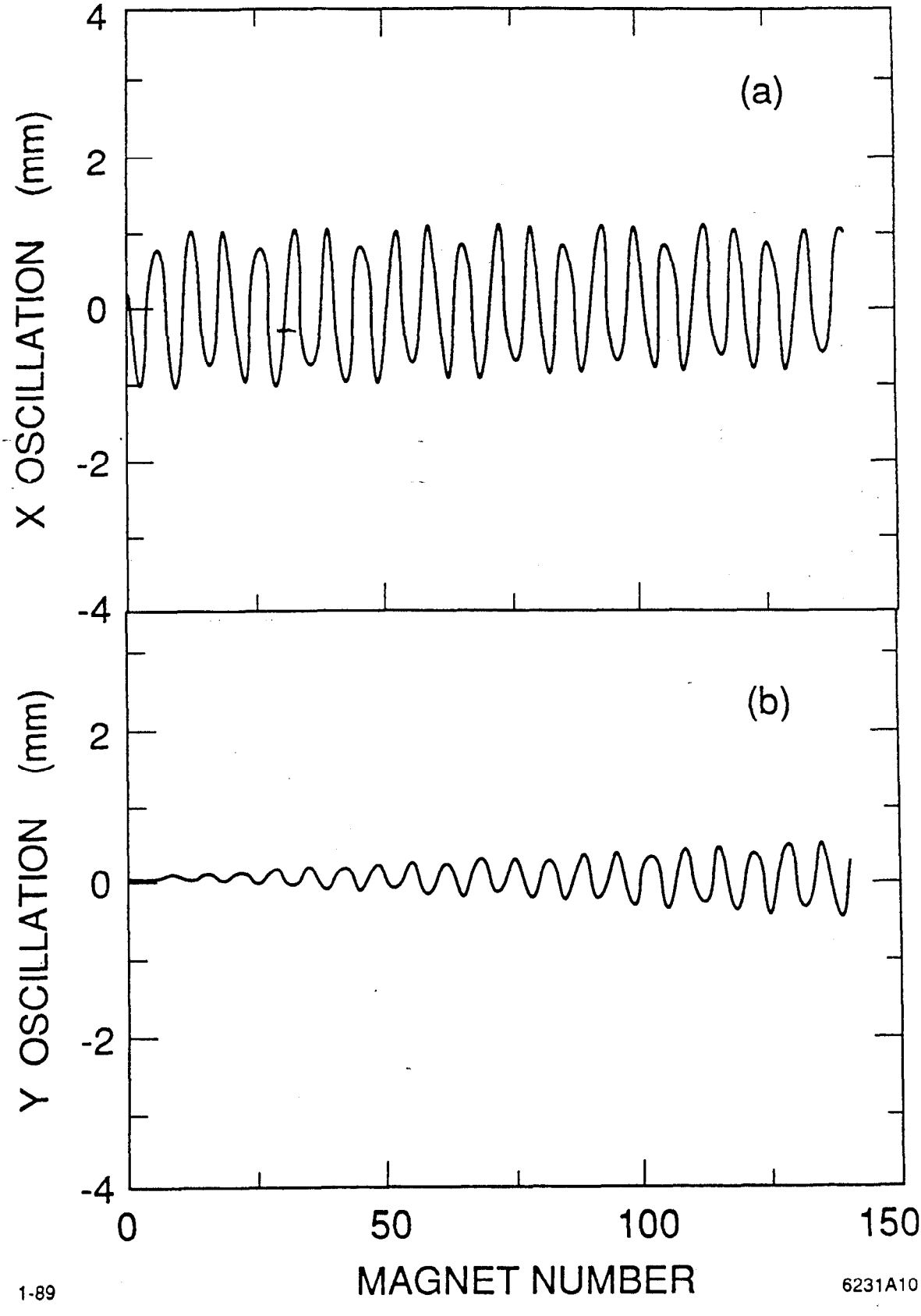
4
2
0
-2
-4
X OSCILLATION (mm)
(a)
(b)
Y OSCILLATION (mm)
0
50
100
150
MAGNET NUMBER
1-89
6231A10

Fig. 10

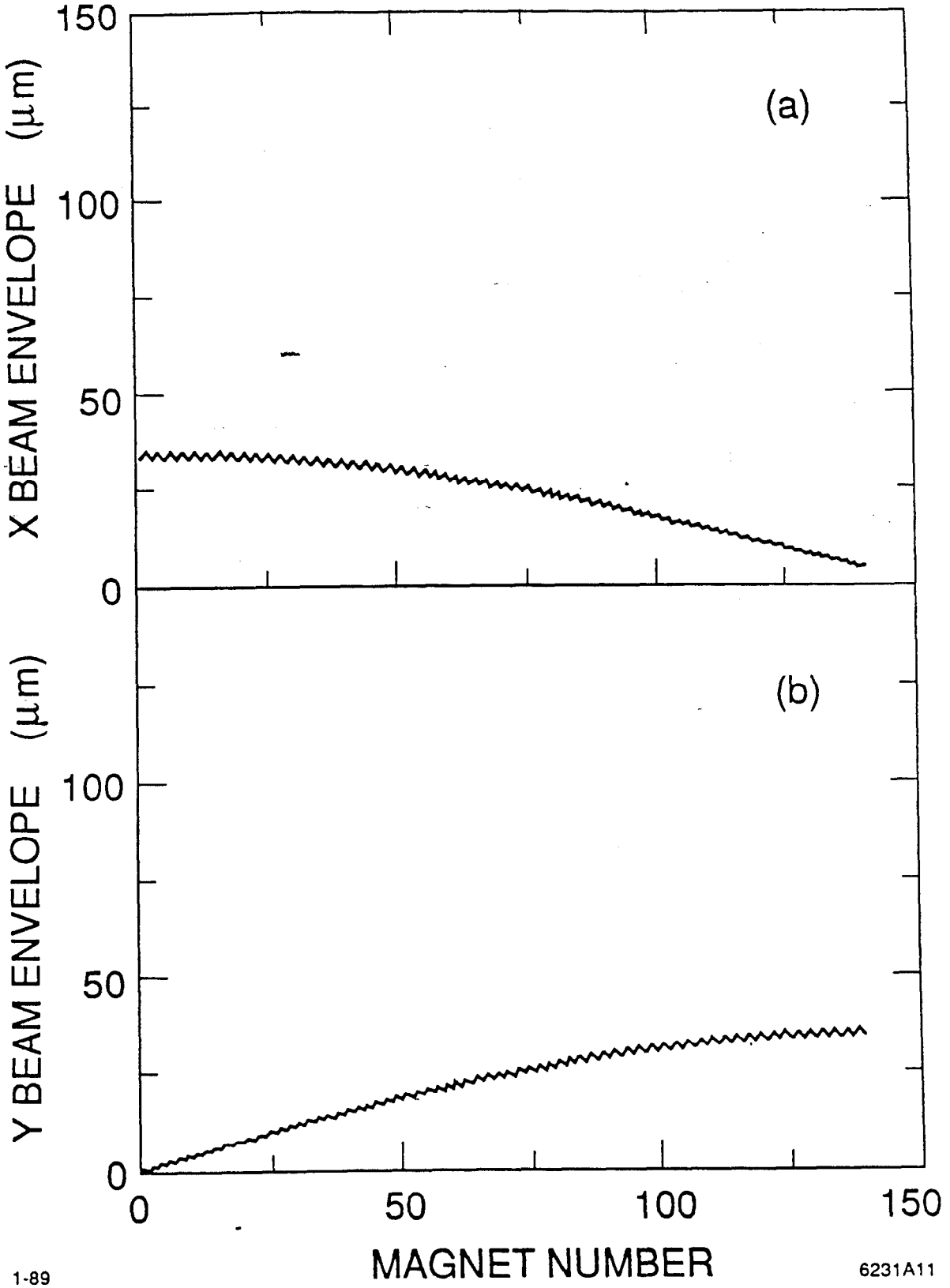
150
100
50
0
X BEAM ENVELOPE (μm)
(a)
(b)
Y BEAM ENVELOPE (μm)
100
50
0
0
50
100
150
MAGNET NUMBER
1-89
6231A11

Fig. 11

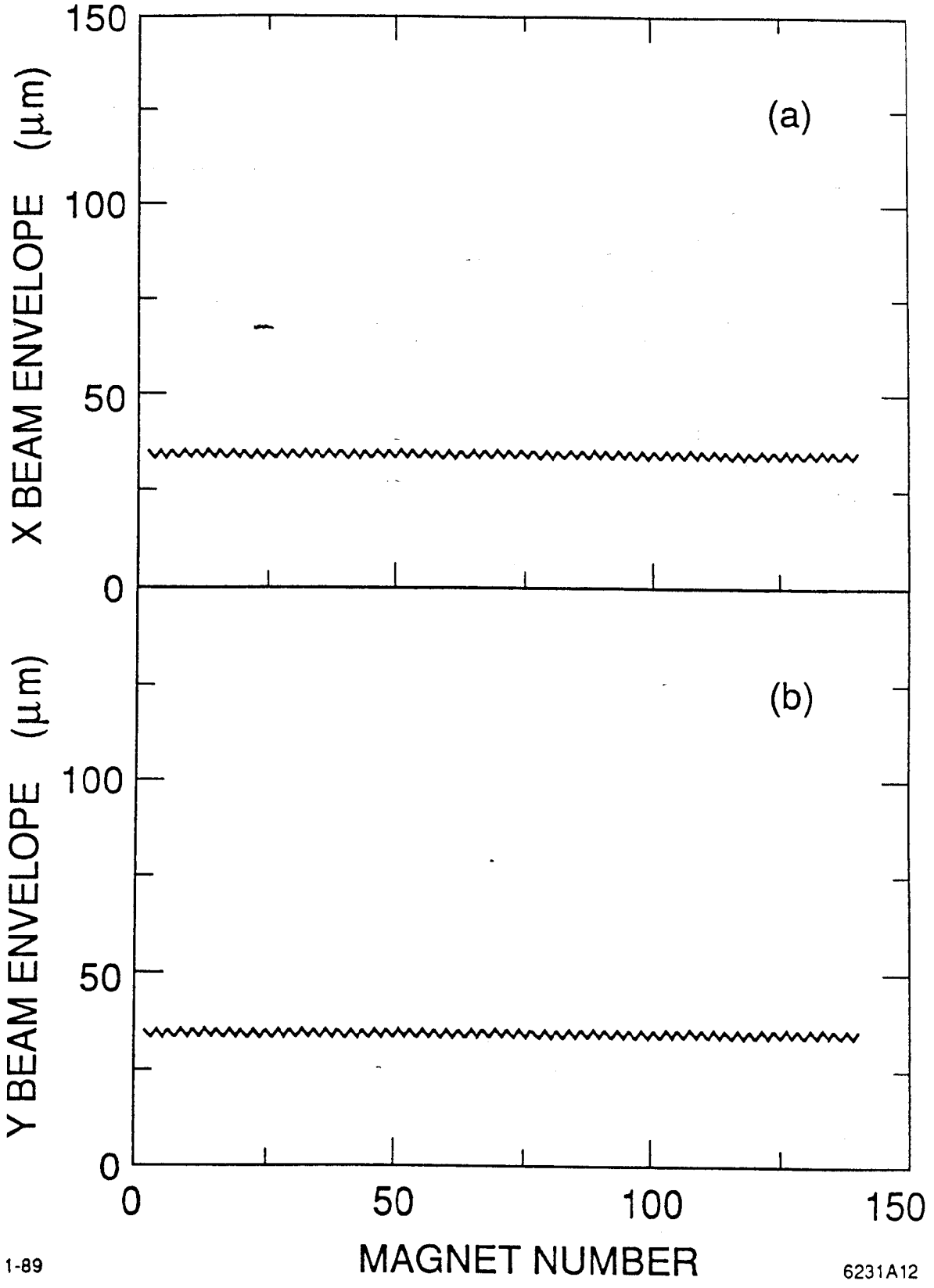
150
100
50
0
X BEAM ENVELOPE (μm)
(a)
100
50
0
Y BEAM ENVELOPE (μm)
(b)
0
50
100
150
MAGNET NUMBER
1-89
6231A12

Fig. 12

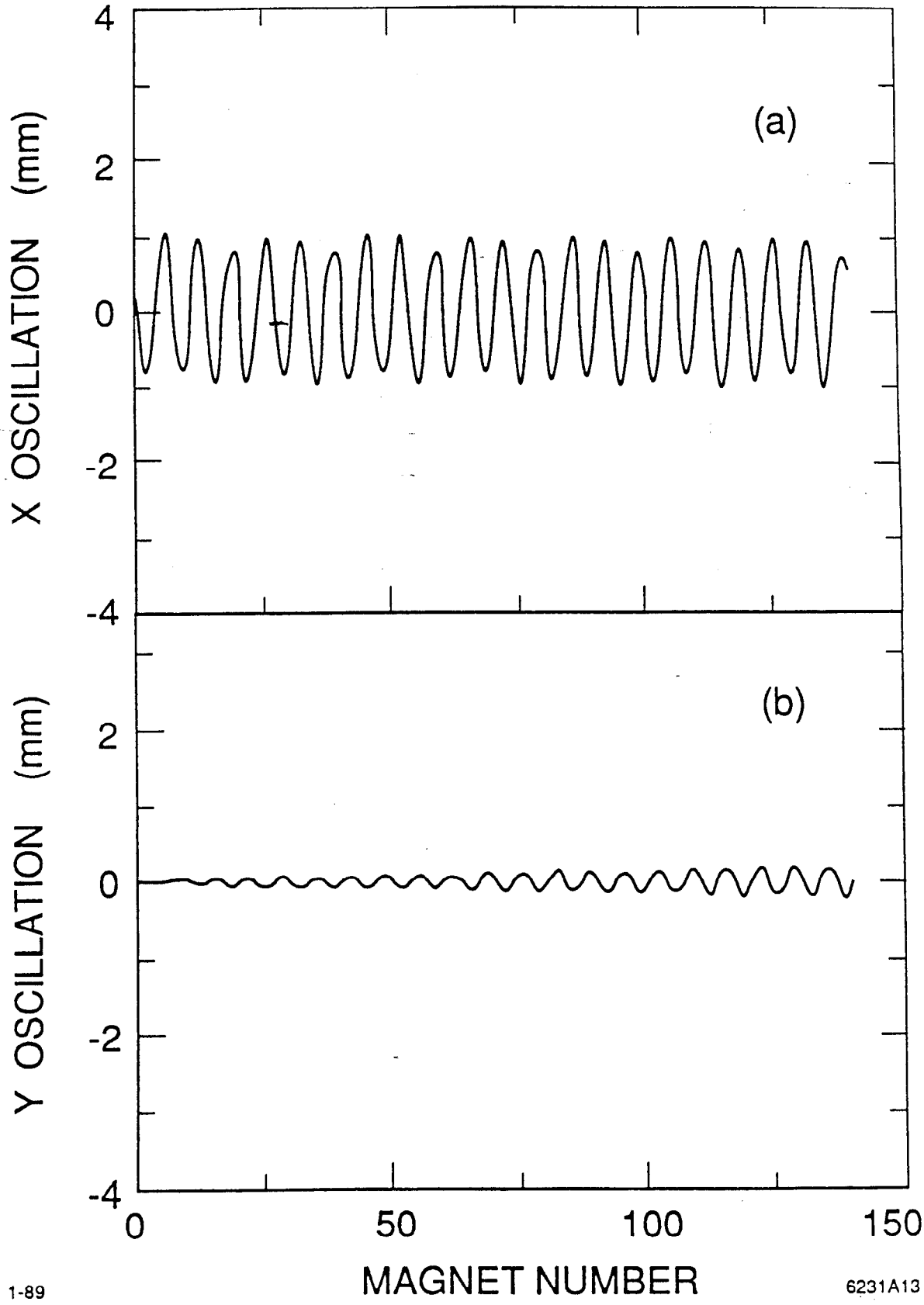
4
2
0
-2
-4
X OSCILLATION (mm)
(a)
4
2
0
-2
-4
Y OSCILLATION (mm)
(b)
0
50
100
150
MAGNET NUMBER
1-89
6231A13

Fig. 13

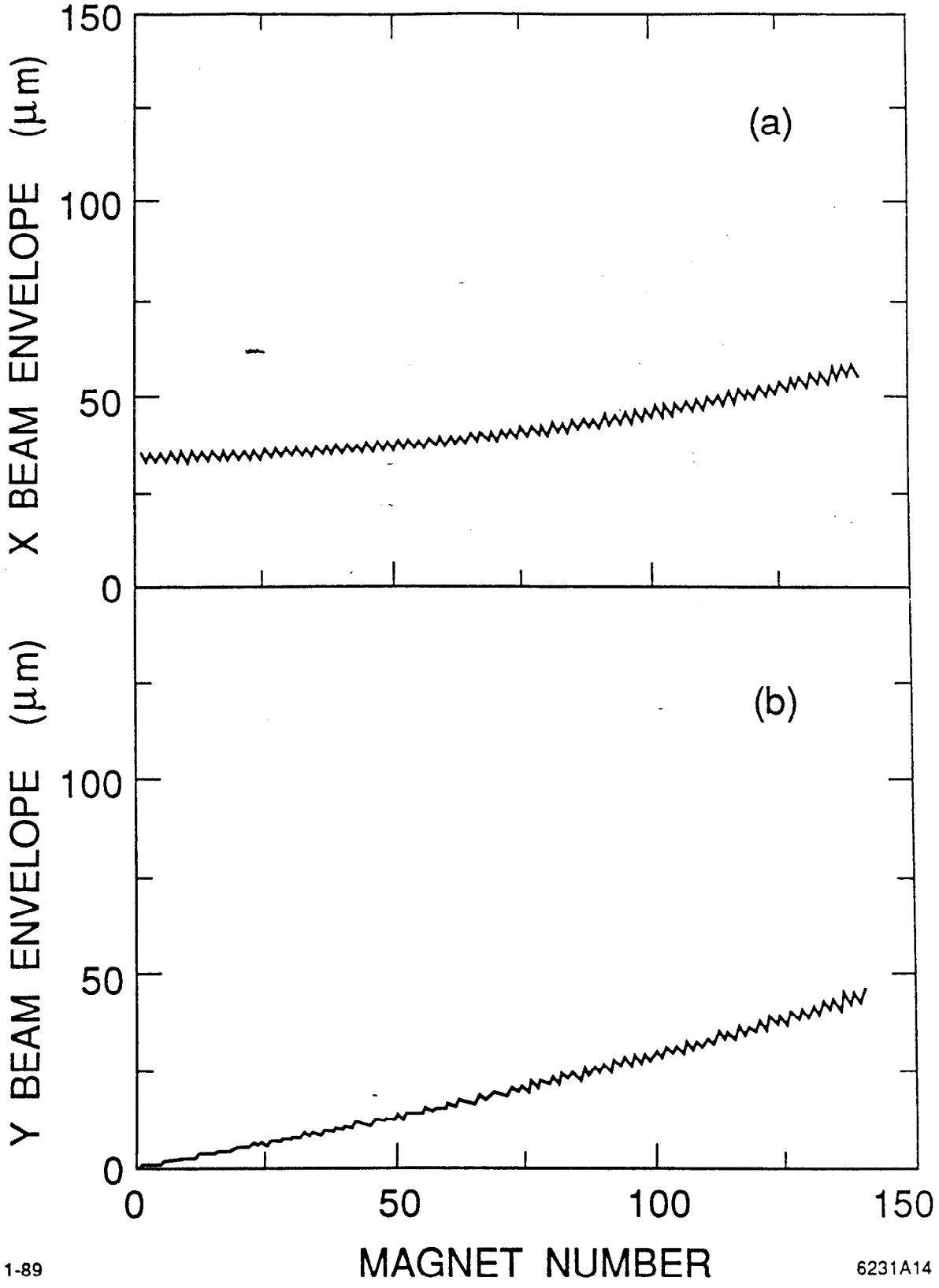
150
100
50
0
X BEAM ENVELOPE (μm)
(a)
100
50
0
Y BEAM ENVELOPE (μm)
(b)
0
50
100
150
MAGNET NUMBER
1-89
6231A14

Fig. 14

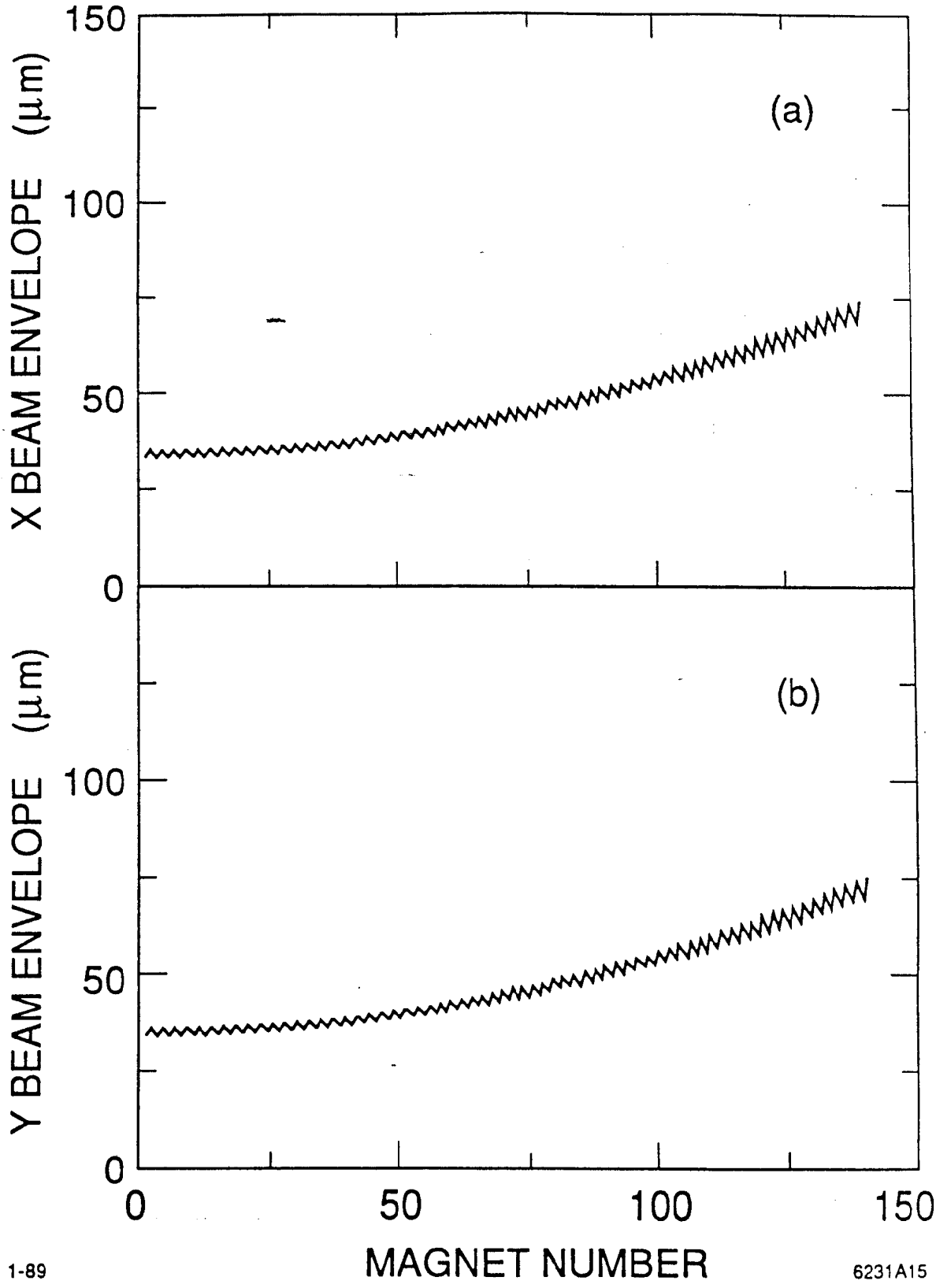
150
100
50
0
X BEAM ENVELOPE (μm)
(a)
100
50
0
Y BEAM ENVELOPE (μm)
(b)
0
50
100
150
MAGNET NUMBER
1-89
6231A15

Fig. 15

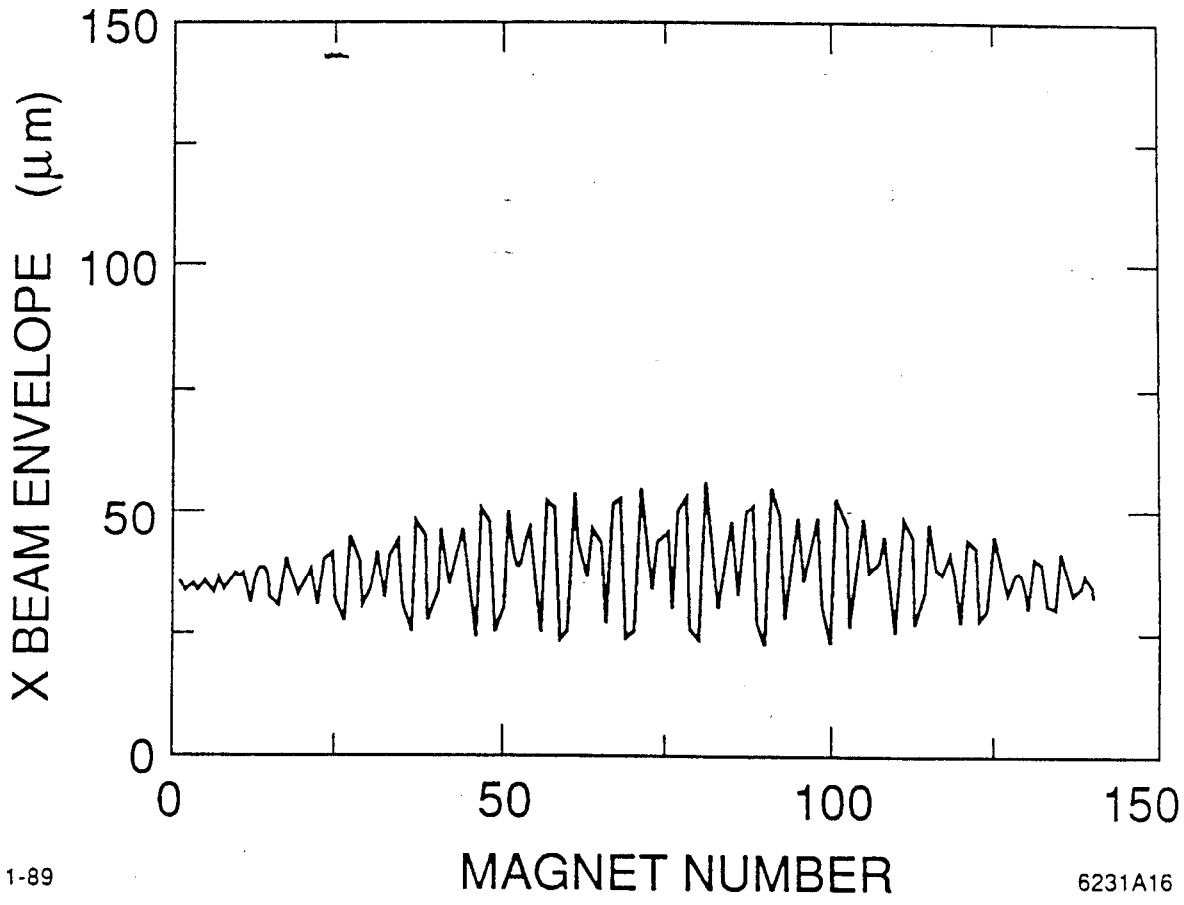
150
100
50
0
X BEAM ENVELOPE (μm)
0
50
100
150
MAGNET NUMBER
1-89
6231A16

Fig. 16

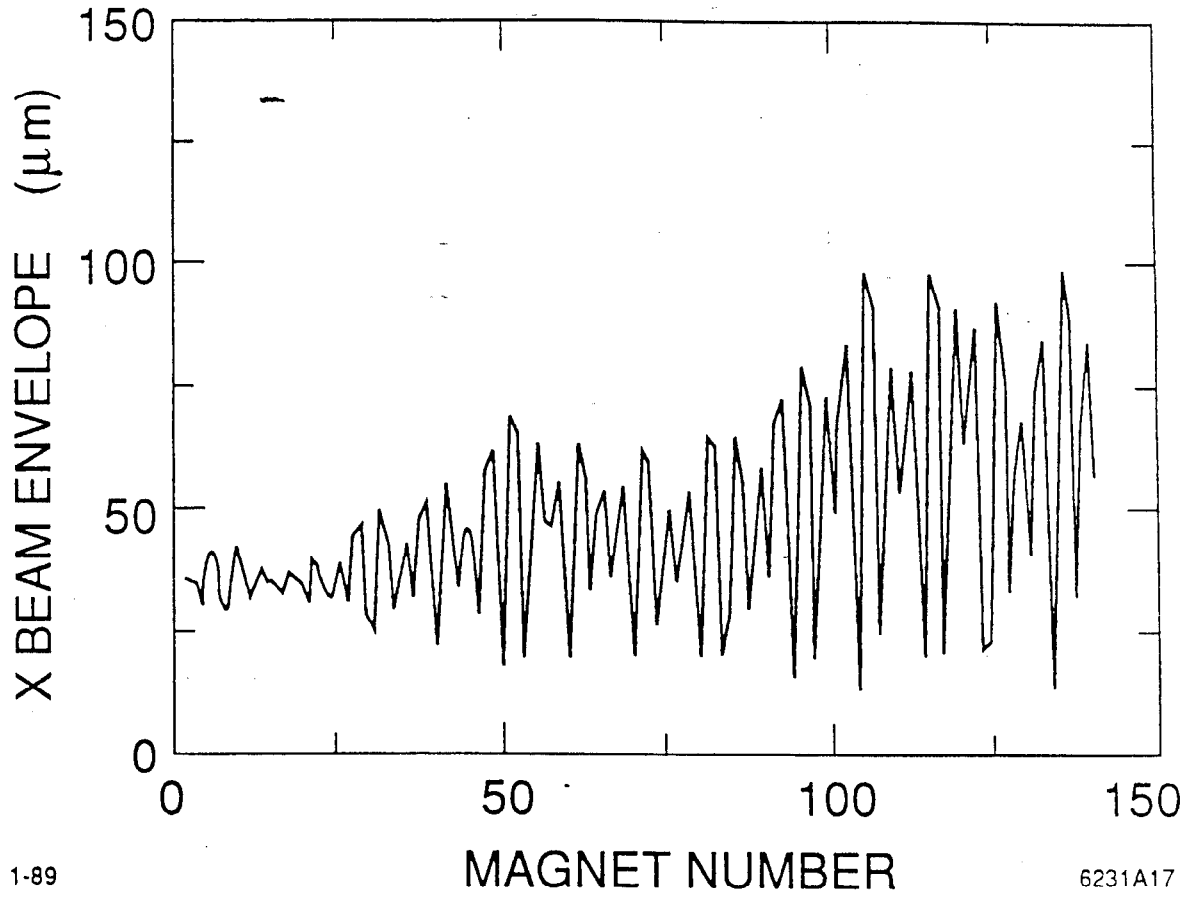
150
100
50
0
X BEAM ENVELOPE (μm)
0
50
100
150
MAGNET NUMBER
1-89
6231A17

Fig. 17

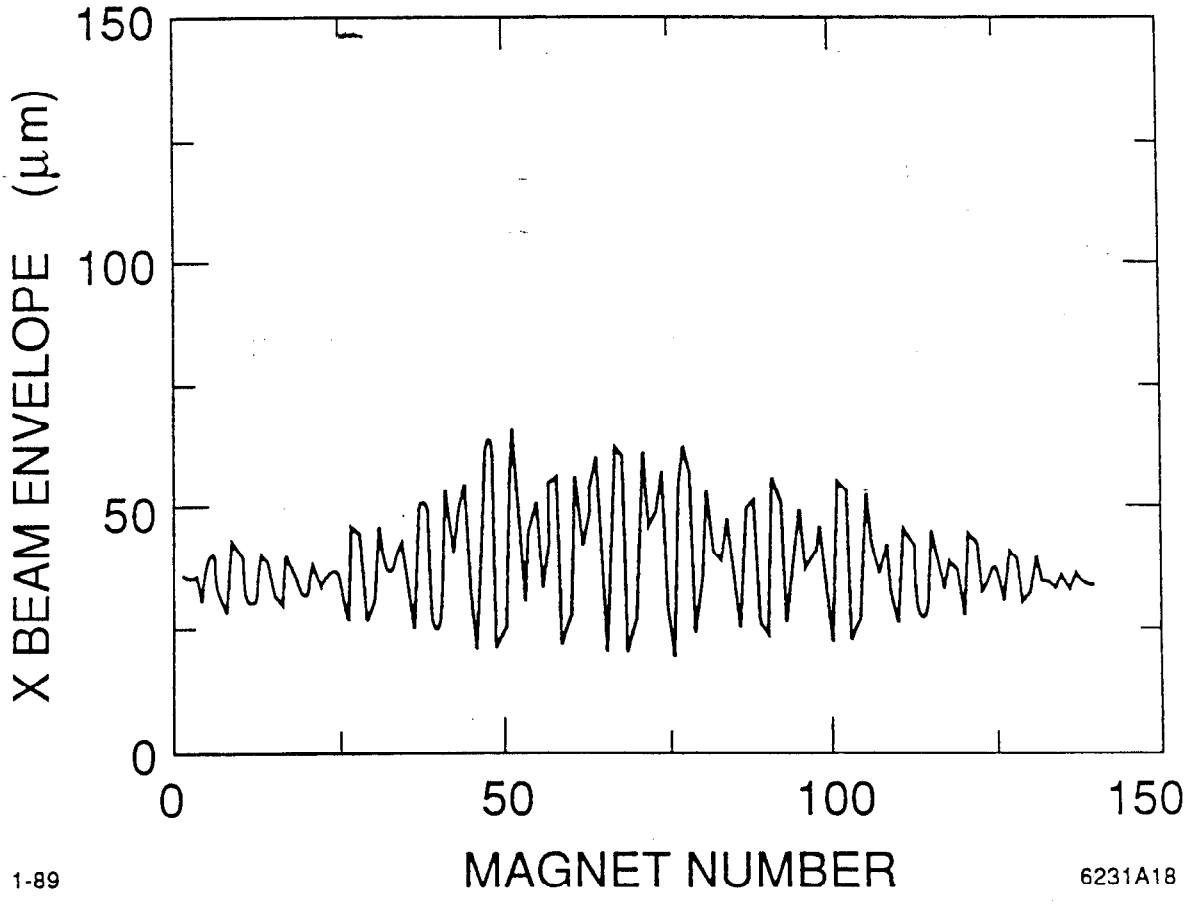
150
100
50
0
X BEAM ENVELOPE (μm)
0
50
100
150
MAGNET NUMBER
1-89
6231A18

Fig. 18

VI.4 FIRST TESTS OF HARMONIC CORRECTION METHOD

In this section, we present the first tests made with the system of harmonic corrections described in VI.3. These tests have shown that it was possible to adjust the phase-space, empirically, at the exit to the arcs, to minimize backgrounds produced by mismatches. Although it has not been possible to study all the cases which were explored in the collider note above, the measurements we have made confirm qualitatively the theoretical results presented in this note, and the validity of this approach towards adjusting open beam-lines.

VI.4.1 Resonant Amplification of One-Dimensional Motion

In Figs. 20a-f and 21a-f, we show a set of betatron oscillations in the north arc and in the first third of the north final focus section*. These oscillations are launched horizontally in the last sector of the linear accelerator. The plots correspond to two different settings of the harmonic correction at twice the betatron frequency, and to two different initial phases for the betatron oscillation. The harmonic correction is applied in the last third of the arc. Figs. 20a-f represent the horizontal transfer of the these oscillations, and Figs. 21a-f the coupling into the vertical plane of these oscillations.

We first concentrate on Figs. 20a-f. Figs. 20a-c and 20d-f correspond to oscillations which are separated by $\pi/4$ at the origin. In Figs. 20a and 20d, no perturbation has been applied. As can be seen, the amplitudes of the oscillations are almost regular in Fig. 20a, while they are slightly damped in Fig. 20d. In 20b and 20e, we have applied, respectively a sine- and a cosine-like regular focusing perturbation at twice the betatron frequency, with an amplitude close to 0.005 of the nominal focusing strength. As can be seen in both cases, the amplitudes of the two oscillations are damped. In 20c and 20f, we have applied the same perturbations to the same oscillations, but with opposite sign. In this case, the oscillation which was slightly damped (Fig. 20d) becomes regular, and the one which was regular (Fig. 20e) becomes rather strongly amplified.

The effects are in good qualitative agreement with the description given in section II.6.1 of the collider note presented in VI.3: solutions with a maximally perturbed amplitude (damped or amplified) correspond to harmonic perturbations which are π out of phase. Furthermore, the effects (damping or amplification) remain unchanged if the phase of the launched betatron oscillation is varied by $\pi/4$ and if the phase of the harmonic perturbation is varied by $\pi/2$. This is in agreement with the phase dependance of the effects, as calculated for small perturbation in section II.5.2 of the collider note mentionned above.

In Figs. 21a-f, we show the coupling into the vertical plane corresponding to the oscillations in Figs. 20a-f. As can be seen, this coupling, already present for the unperturbed oscillations (Figs. 21a,d), is modified rather appreciably by the perturbations we apply. As was explained in section IV.2.1 of the collider note above, this modification results from the rolls introduced in the arcs to follow the terrain of the SLAC site (see section VI.2). This coupling contributes to weaken the perturbation in the horizontal plane. This explains partially the fact that the amplitude of this perturbation is weaker than was predicted, by almost a factor two. The two other reasons for a weaker perturbation than predicted are:

1. The fact that the relative phase of the perturbation and of the betatron oscillation at its origin has not been tuned to better that $\pi/2$ in these first tests. This relative phase

---

* *In the arcs, the data are raw, while in the final focus section, they are scaled with the square root of the ratio of the β-functions in the two respective sections. This enables to make the oscillation comparable in the two sections.*

is a priori arbitrary, because of the large distance between the end of the linear accelerator, where the betatron oscillations are launched, and the part of the arc which we perturb.

2. The focusing errors in the part of the arc which we perturb. Such errors can reduce the effects from the harmonic perturbations, as was shown in section II.10 of the above collider note, especially in the case of systematic errors.

VI.4.2 Separation of Horizontal and Vertical Betatron Frequencies

We show in Figs. 22a,b the vertical phase-shift produced by a systematic regular focusing deviation of 0.0035 of the main field, and of opposite sign for the focusing and defocusing magnets*. In Fig. 22a, a negative perturbation has been induced in the focusing magnets, and in Fig. 22b, a positive perturbation.

As can be seen, the variation of the vertical phase is positive in Fig. 22a, and negative in Fig. 22b, for the part of the arc where the perturbation has been applied (units 1700 to 2400). The cumulative phase-shift is about 80^0, which is close to what is expected for a relative perturbation of 0.0035.

VI.4.3 Other Perturbations and Empirical Adjustments

As shown in chapter IV of the collider note above, the skew focusing perturbation are too weak to have significant effects. We have however used the full set of perturbations to tune, the lattice on the one hand, and the spots at the entrance to the final focus section on the other hand, in an empirical way. We give exemples of this below.

We show in Figs. 23 and 24 a full set of betatron oscillations, horizontal and vertical, with their couplings in the opposite plane, and for four initial phases separated by $\pi/4$. These oscillations were measured after empirical adjustments of the harmonic correctors.

---

* *The phase-shift is calculated in the following way*[24]*: By noting that consecutive measurement points are separated by the phase-shift per cell, which is* $\mu = 108^0$*, and by considering that a weakly perturbed oscillatory mouvement can be represented by letting the phase and the amplitude of the oscillation vary slowly, one can solve, for each couple of consecutive data points* (x_n, x_{n+1})*, the system:*

$$\begin{cases} x_n = a_n \cos(n\mu + \Delta\phi_n), \\ x_{n+1} = a_n \cos((n+1)\mu + \Delta\phi_n), \end{cases} \tag{24}$$

where a_n *and* $\Delta\phi_n$ *represent the variable amplitude and phase in question. An exact calculation would also give terms proportional to the derivatives of* a *and* ϕ*. Since we consider that these functions are slowly varying, we can neglect these terms.*

As can be seen, they are essentially regular.

We show in Figs. 25a,b the beam shape on a phosphor screen, photographed before and after adjusting it empirically. The two sets correspond to two different experiments, where the optical parameters of the beam at the entrance to the arc were different. In both cases, it was possible to adjust the harmonic correctors to cancel the variations.

VI.4.4 Conclusions from the First Tests

These first tests have shown the feasibility of the harmonic correction method which we have proposed, have contributed to improve the optical transfer of the arcs, and given the system an additional "knob", upstream of the final focus section, to adjust the matching of the phase-space there.

These tests have also shown that the effects are weaker the predicted, in most part because of systematic errors and because of the rolls along the part of the arc where the harmonic correction system is installed. To obtain larger effects, the current of the power supplies feeding the correction windings would have to be raised, by a factor of two or three.

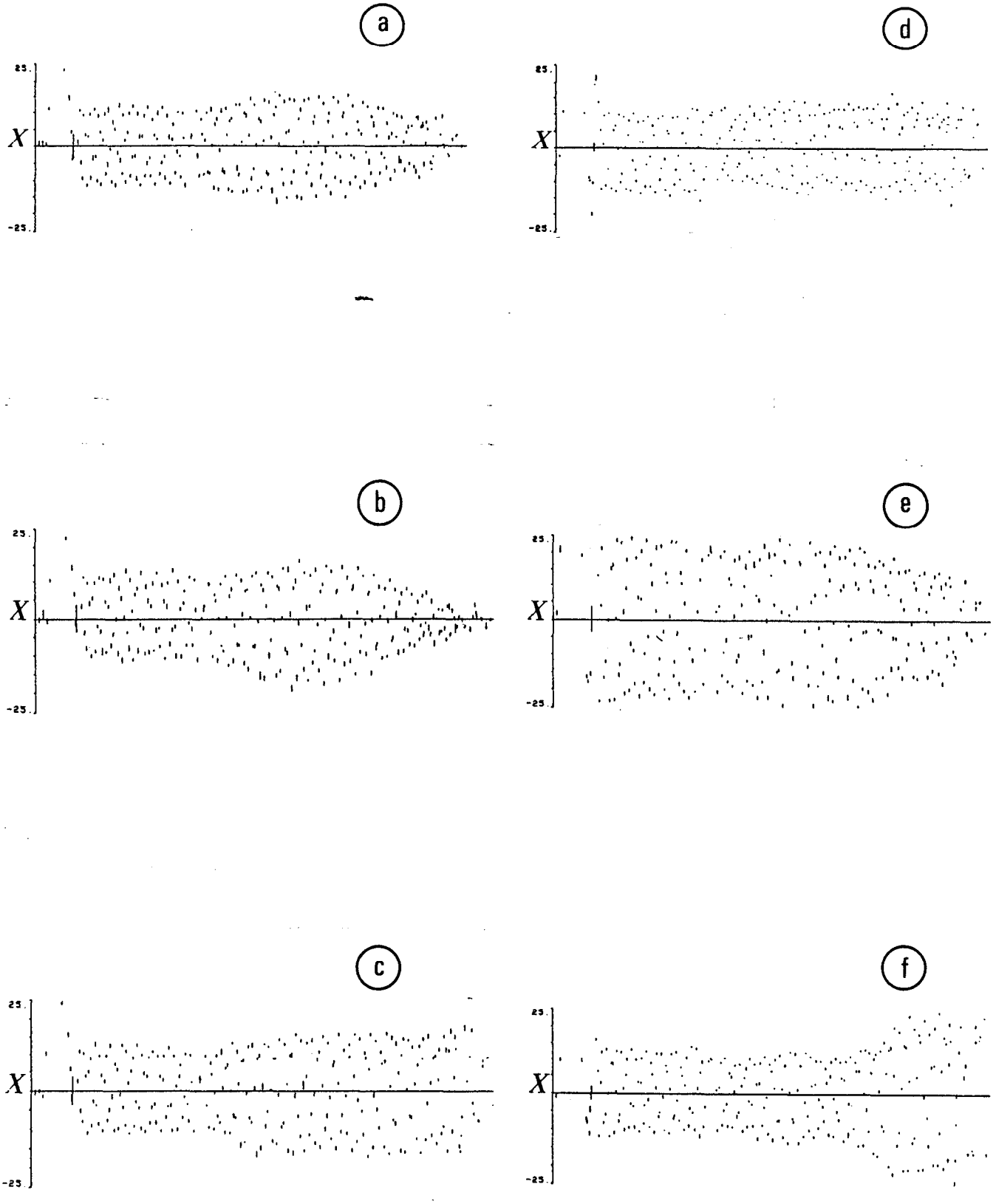

Figure. 20 Resonant growth of the horizontal betatron oscillations, from a focusing perturbation at twice the betatron frequency.

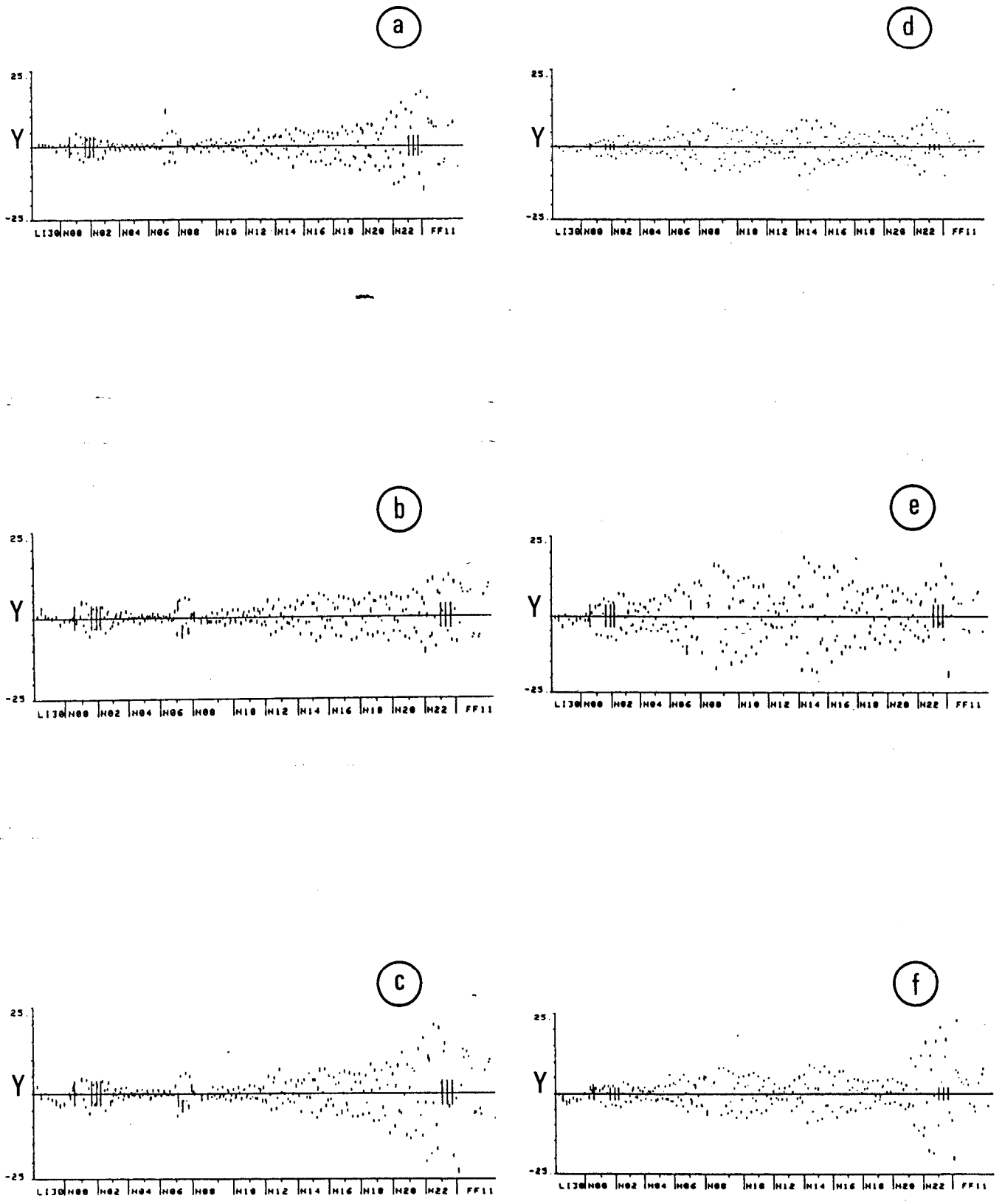

Figure. 21 Coupling into the vertical plane corresponding to the oscillation in figure 20.

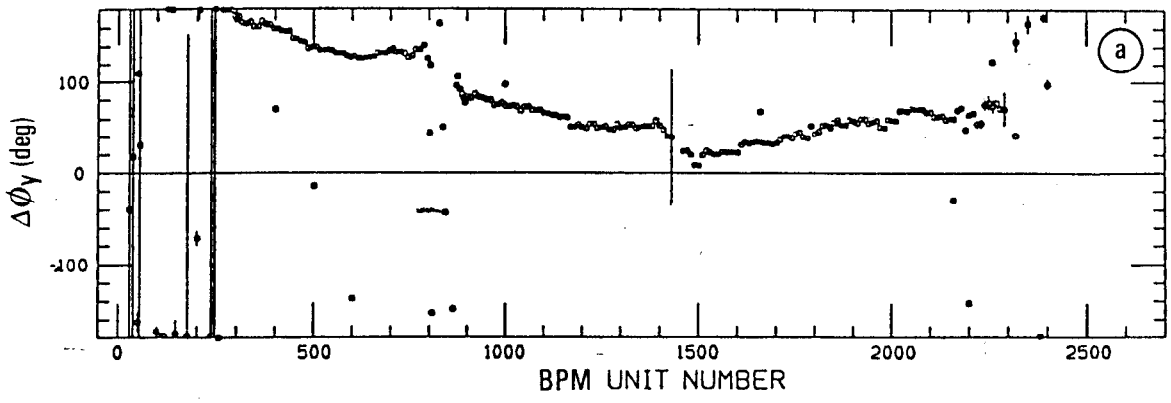

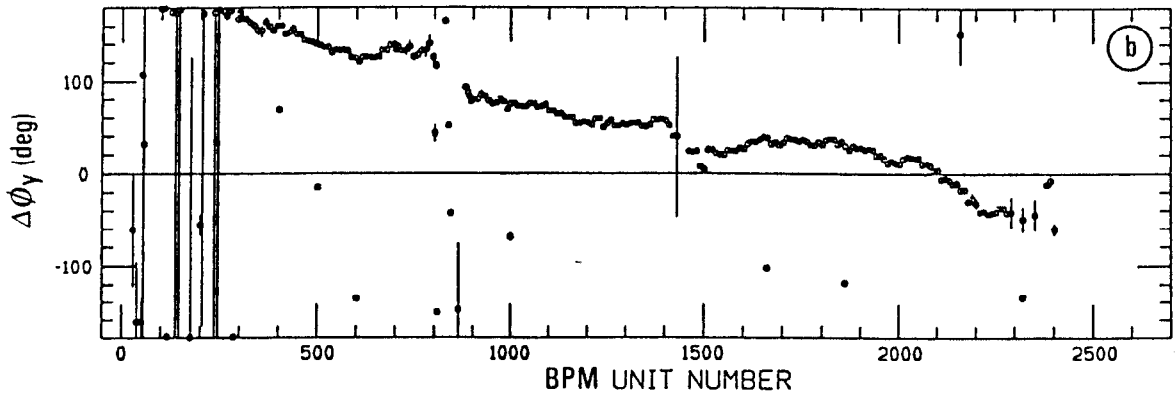

Figure. 22 Shift in vertical betatron frequency from systematic perturbations of focusing and defocusing magnets with opposite signs.

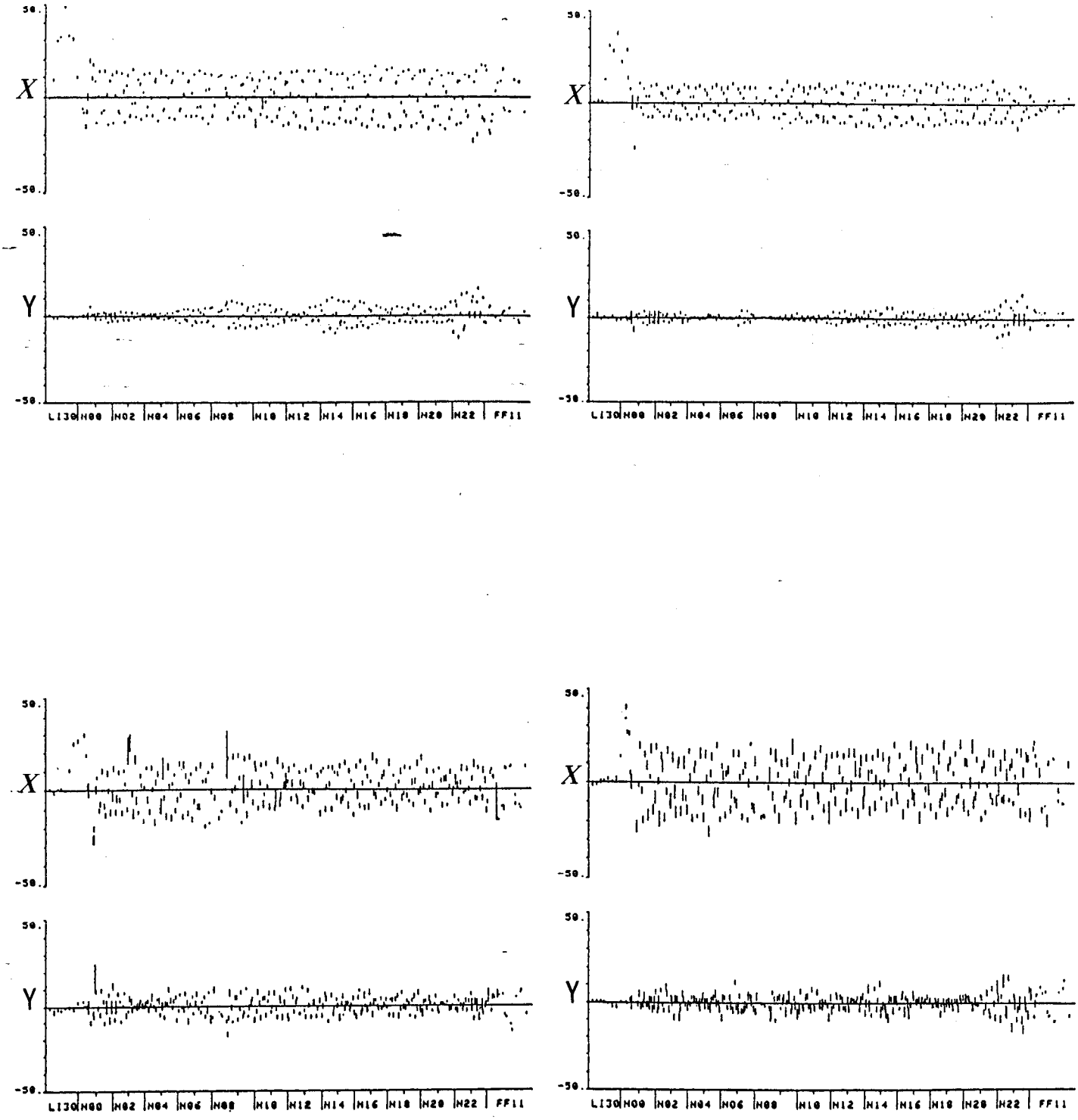

Figure. 23 Transfer of horizontal betatron oscillations, and coupling into the vertical plane, for four initial conditions corresponding to phases separated by 45^0, after optimization of the harmonic correctors.

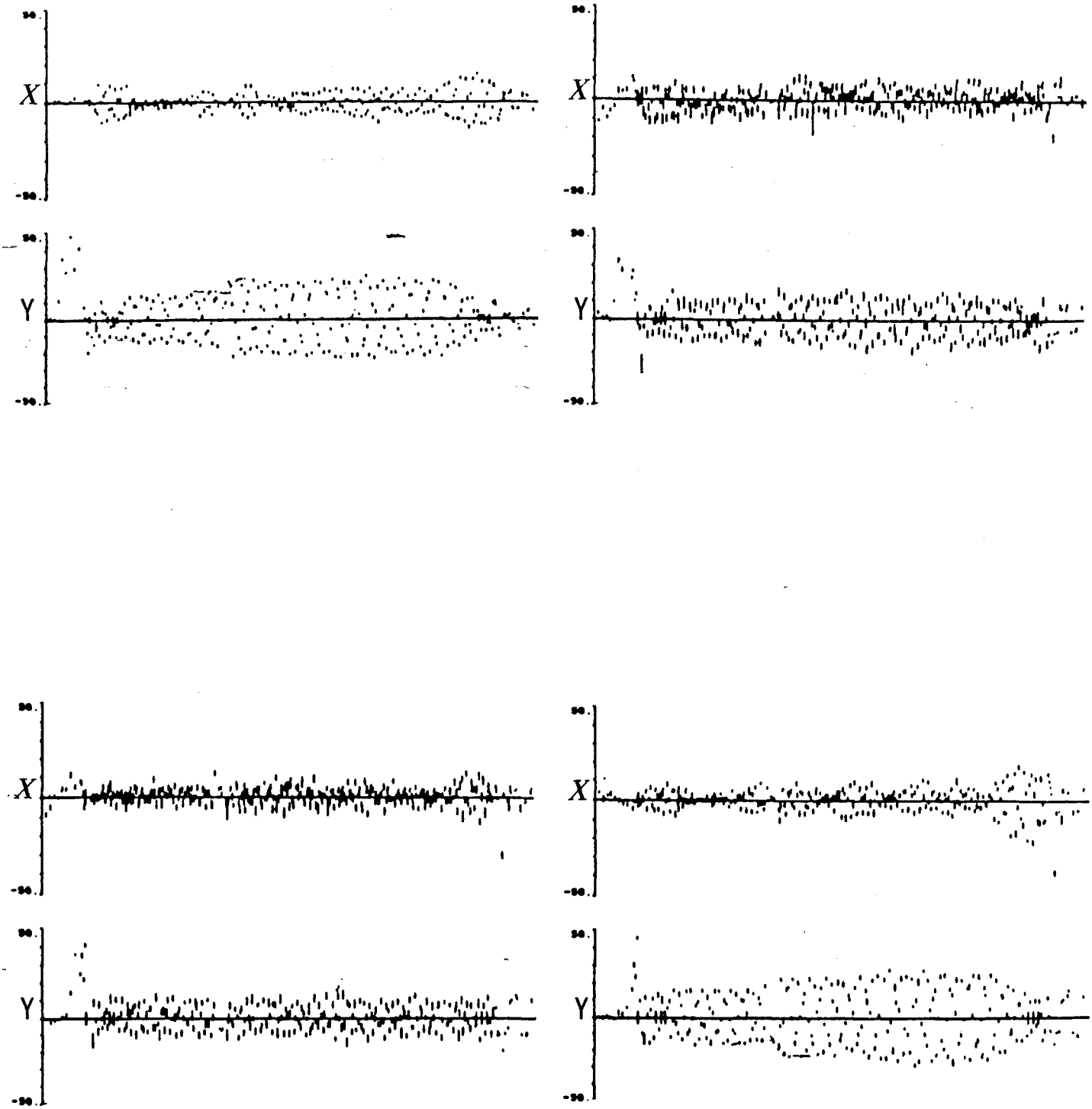

Figure. 24 Transfer of vertical betatron oscillations, and coupling into the horizontal plane, for four initial conditions corresponding to phases separated by 45^0, after optimization of the harmonic correctors.

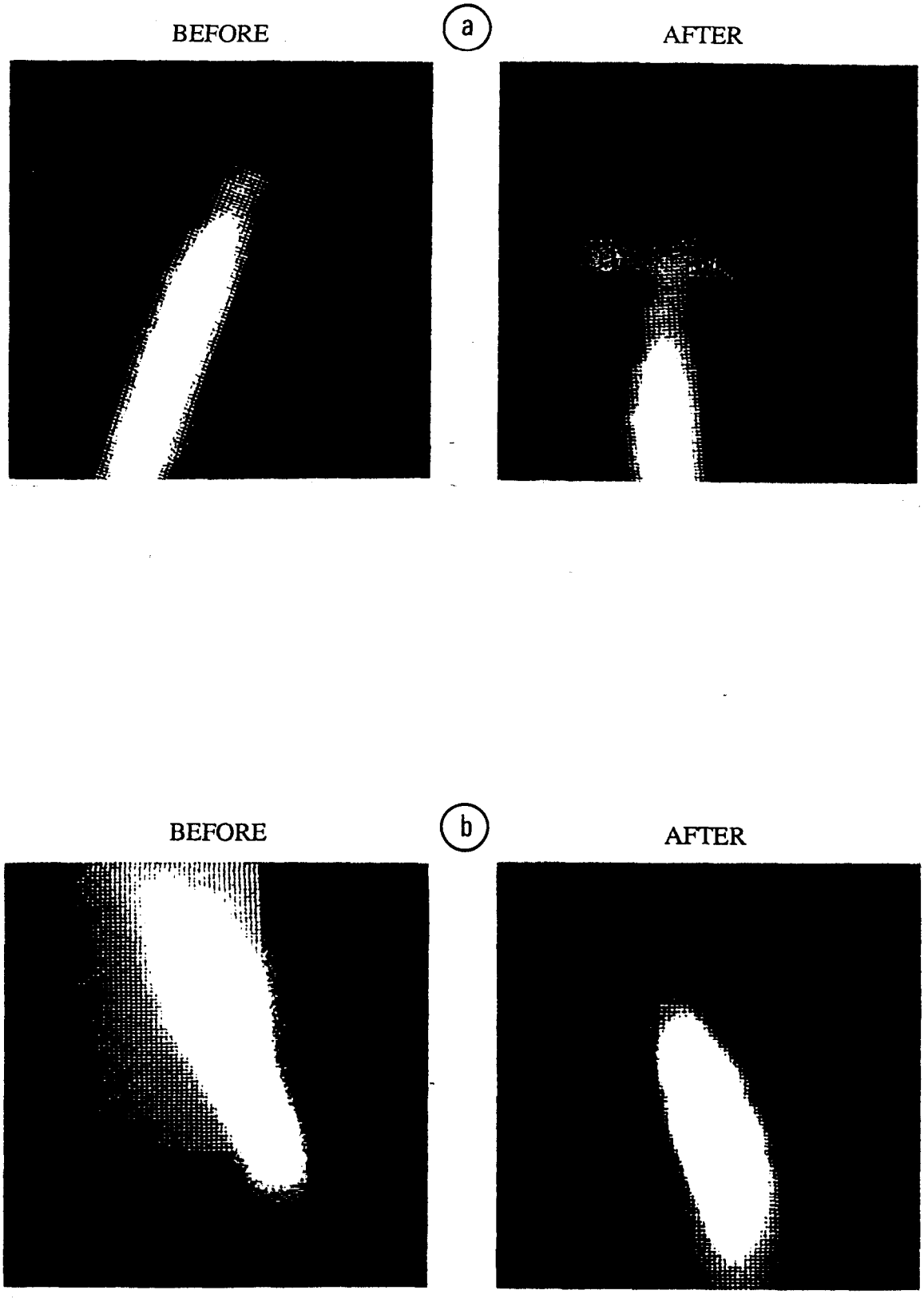

Figure. 25 Empirical adjustments of the beam size at the end of the arc, on two occasions ((a) et (b)). The photographs on the right show the beam before correction, and those on the left the beam after correction.

VII. REPORTS AND PUBLICATIONS ON OPTICAL CORRECTIONS IN THE FINAL FOCUS

VII.1 "Orthogonality of Final Waist Corrections at the IP of the SLC"

The optical corrections in the final focus are all strongly coupled except for the three final adjustments to position the waists at the interaction point, which can be made fully orthogonal. This enable to simultaneously correct and measure phase-space parameters at the interaction point. The orthogonalization is shown in this collider note, together with a summary of the experimental algorithm.

SINGLE PASS COLLIDER MEMO CN-369

AUTHOR: Philip Bambade DATE: October 27, 1988

TITLE: ORTHOGONALITY OF FINAL WAIST CORRECTIONS AT THE IP OF THE SLC*

I. INTRODUCTION

Because the SLC final IP spot is produced by an aberration-dominated optical system[1], all components and couplings between dimensions of transverse phase-space must[2] be controlled in the experimental tuning algorithm. For equal emittances $\epsilon_x = \epsilon_y$, this amounts to *ten* linear optics adjustments[2†] . These adjustments are coupled and depend non-linearly on phase-space parameters. A ten-dimensional non-linear fitting program[3] is therefore used to match the lattice in the Final Focus to the input beam. Local orthogonal "knobs" are also defined for fine-tweaking around the initial solution, although this is not always practical because of steering from the lenses.

The three final waist corrections[4] are however fully orthogonal to the other seven optical adjustments. This means that they do not cause any of the other seven optical distortions. We refer to this as *external orthogonality.*

They can also be made *internally orthogonal.* This means that each one of the three orthogonalized controls can be applied independently of the two others. It also allows one to simultaneously correct and determine the phase-space at the IP.

*Work supported by Department of Energy Contract DE-AC03- 76SF00515.

† In the case of equal emittances these ten adjustments are grouped[2] in three sets:

1. Four corrections to minimize the spatial and angular dispersion in both planes,
2. Three corrections to the betatron angular spread at the IP, by controlling the magnitude of $< x'^2 >$ and of $< y'^2 >$, and by minimizing the $< x'y' >$ correlation, and
3. Three adjustments to position the waists in both planes at the IP, by minimizing the correlations between the positions x,y, and the angles x',y' in both planes.

The ten variable quadrupoles used for these corrections are shown in Fig. 1. Because each correction is coupled to the ones downstream, they must be applied sequentially. A flow diagram illustrating this sequential application is shown in Fig. 2.

Both have been demonstrated to work experimentally[5,6], and form the basis for the on-line tuning algorithm[7]. In this note, we show the orthogonality of the corrections and outline the experimental procedure and its limits.

II. EXTERNAL ORTHOGONALITY OF WAIST CORRECTIONS

The three final waist corrections are designed to cancel the correlations between the positions x, y, and the angles x', y' in both planes at the IP. The $< xx' >$ and $< yy' >$ correlations* are minimized by combining trim windings in two regular quadrupoles of the Final Triplet, one defocusing (QD2B), and one focusing (QF3). We refer to them as the *in-plane* waist adjustments. The $< xy' >$ correlation, which at the waist and for $\epsilon_x = \epsilon_y$ is equal[8] to $< yx' >$, is minimized with a single skew quadrupole (SQ3) just upstream of the Final Triplet. This one is referred to as the *out of plane* waist adjustment. The correction elements are indicated in Fig. 1.

These final adjustments are normally decoupled from *dispersion* corrections because the dispersion is nominally zero in the Final Triplet.

They are also close to decoupled from the *angular spread* corrections. To see this, we consider for simplicity an uncorrelated ($< xx' >=0$) beam focused to a waist by a thin lens in the horizontal plane. From linear optics, we compute (to first order) the variation of the spatial beam size σ_x and of the angular beam size $\sigma_{x'}$ as a result of varying the strength of the lens:

$$\begin{cases} \sigma_x^2(\delta_Q) = \sigma_x^2(0) + \delta_Q^2 \sigma_Q^2, \\ \frac{\Delta\sigma_{x'}}{\sigma_{x'}} \simeq \frac{-\delta_Q}{1+(\frac{\sigma_x}{\sigma_Q})^2}. \end{cases} \tag{1}$$

In (1), σ_Q is the beam size at the lens and δ_Q is the fractional strength variation of the lens.

For σ_Q large compared to the minimum beam size $\sigma_x(0)$, small adjustments are sufficient to change the size at the waist significantly, with only a small perturbation to the angular spread. At the Final Triplet, σ_Q is typically a thousand times larger than $\sigma_x(0)$. The quadrupole adjustments need therefore be only a few percent. Over that range, the change in angular spread is negligible.

Thus the three final waist adjustments are essentially orthogonal to the other seven optical corrections. The opposite is not true: the other seven corrections

* In Transport[9] notation, $< xx' >= \sigma_{21}$, $< yy' >= \sigma_{43}$, and so on...

are strongly coupled to the three final waist adjustments. The experimental tuning algorithm is therefore *sequential.* It is summarized in the flow diagram in Fig. 2.

III. INTERNAL ORTHOGONALITY OF WAIST CORRECTIONS

We begin by considering the *in-plane* waist adjustments (i.e. the minimization of the $< xx' >$ and $< yy' >$ correlations). A regular lens perturbs each plane proportionally to the beam size at the lens in that plane. Since this beam size is naturally larger in each lens in the plane in which it is focusing, QF3 and QD2B can be combined to control the horizontal and vertical waists independently. The coupling coefficients, found using TRANSPORT[9], are:

$$\begin{pmatrix} \Delta f_x \\ \Delta f_y \end{pmatrix} = \mathrm{C} \begin{pmatrix} \delta_{Q3} \\ \delta_{Q2B} \end{pmatrix}, \quad \text{with} \quad \mathrm{C} = \begin{pmatrix} -1.89 & 0.70 \\ 0.80 & -1.37 \end{pmatrix} \tag{2}$$

In (2), the fractional quadrupole strengths δ_{Q3} and δ_{Q2B} are in parts per thousand, and the longitudinal waist motions $\Delta f_{x,y}$ are in centimeters.

The couplings in C are close to independent of input mismatch. This is evident for a mismatch of the IP angular spreads from the form of (2). It is also true in the case of a largely correlated input phase-space into the Final Triplet (*in-plane* correlations), which the waist corrections are designed to cancel. This can be seen by considering the nominal IP phase-space obtained after the correction, and by back-tracking the beam into the lenses: since the changes in the strengths of QF3 and QD2B required by the correction are small, the beam sizes are perturbed negligibly in the lenses. Since their effect is proportional to this beam size, the couplings in C do not change significantly. The linear combinations defined in (2) can thus be used for orthogonal control *independent* of the mismatch of the input beam phase-space* .

In the case of the *out of plane* waist-adjustment, (the $< xy' >$ and $< yx' >$ correlations) using the skew lens SQ3, orthogonality to the *in-plane* corrections is obtained by requiring an upright beam shape near the Final Triplet (i.e. $<$

* This is not the case for the other optical adjustments in the Final Focus, where the relative settings must be calculated through a non-linear fitting program[3] and depend thus on the initial condition. Since this initial condition must be obtained from measurements with possibly large errors, the calculated solution can be significantly off as a result. The correction can in this case require several iterations. This is especially the case for the angular spread corrections. Operationally, some improvement is obtained by basing the calculations on time-averaged quantities.

$xy >= 0$). Operationally, this condition is obtained by observing the beam on a profile monitor (ST4) near the Final Triplet, and by adjusting a second skew lens, SQ17.5, located in the First Telescope, which is part of the angular spread corrections.

We show this by the following thin lens argument[10]. Consider two lenses, one regular and one skew, of strengths K and S respectively, with parallel to point focusing to the waist. The change in angular spread at the waist is in this case strictly zero. The combined effect of the two lenses on the beam is:

$$\sigma^{out} = R\sigma^{in}R^t, \text{with } R = \begin{pmatrix} -K & 1 & -S & 0 \\ -1 & 0 & 0 & 0 \\ -S & 0 & K & 1 \\ 0 & 0 & -1 & 0 \end{pmatrix}, \quad (3)$$

where $\sigma_{out,in}$ are the beam matrices[9] describing the four-dimensional phase-space at the waist and in the lenses. From (3), the beam-size at the waist is, in the horizontal plane:

$$(\sigma_x^{out})^2 = \sigma_{x'}^2 + \sigma_x^2 K^2 + \sigma_y^2 S^2 - 2 < xx' > K - 2 < yx' > S + 2 < xy > KS, \quad (4)$$

where the subscript *in* has been omitted on the right hand side. The coupling between the two corrections cancels if the correlation $< xy >= 0$. This has been verified independently in two simulations[11,12] of the optical corrections for the Final Focus System.

IV. EXPERIMENTAL PROCEDURE AND PHASE-SPACE DETERMINATION AT THE IP

After the $< xy >$ correlation has been minimized at ST4, by adjusting the skew lens SQ3, the *out of plane* waist adjustment SQ3 and *in plane* controls $\Delta f_{x,y}$ defined in (2) form an orthogonal set of correctors. For minimization of the IP spot, they can therefore be applied independently and in any order.

From (4) or from (1), we see that the beam sizes depend parabolically on the controls. This enables one to find the optimal corrections by symmetry *even* if the minimum of the parabola is not resolved instrumentally. This minimum is not resolved for beam sizes smaller than the carbon filament target[12] used for diagnostic purposes (there are three wires, with diameters of 4,7, and 20 microns).

In order to simultaneously measure the phase-space parameters at the IP, we first apply the SQ3 correction, to minimize the *out of plane* correlations. After this, the beam sizes at the IP can be written as a function of the *in-plane* Final Triplet orthogonal controls $\Delta f_{x,y}$ as:

$$\sigma_{x,y}^2 = \epsilon_{x,y}\beta_{x,y} + \frac{\epsilon_{x,y}}{\beta_{x,y}}\Delta f_{x,y}^2. \tag{5}$$

where $\epsilon_{x,y}$ and $\beta_{x,y}$ are the emittances and the β-functions in each plane respectively. Fitting a parabola to each measurement gives $\epsilon_{x,y}$ and $\beta_{x,y}$. Although the angular spreads $\sigma_{x,'y'} = \sqrt{\frac{\epsilon_{x,y}}{\beta_{x,y}}}$ are well determined from the branches of the parabolas, the minimum linear beam sizes $\sigma_{x,y} = \sqrt{\epsilon_{x,y}\beta_{x,y}}$ are not if the minimum of the parabola is not resolved. This lack of resolution can occur because of the finite wire-target size mentioned above, and because of the following optical reasons:

1. For unequal emittances, because the correlations $< xy' >$ and $< x'y >$ are not[8] necessarily equal, there may be residual uncorrected cross-plane coupling terms in the spot.

2. Before full implementation[3] of the seven other optical corrections, the size of the third order chromatic aberrations can dominate[5] the linear component of the beam size at the IP* .

In both cases, the linear variables $\beta_{x,y}$ and $\epsilon_{x,y}$ will be over-estimated. In order to relieve the effects from 2., a detuned optical configuration, with purposely small angular spreads, can be used, such that the third order aberrations are negligible compared to the linear beam size. For the reason, such a configuration, with $\beta_{x,y} = 3$ centimeters, instead of the nominal $\beta = 0.75$ centimeters, was used in the initial commissioning phase.

Effects from 1. cannot be handled in the Final Focus with the present correction scheme, which is designed for equal emittances in both planes. Operationally, it is therefore desirable to maintain equal emittances throughout the upstream parts of the SLC.

---

* The second order aberrations must also be cancelled by fitting the chromatic correction sextupoles after each significant optical adjustment, to take into account the deviations in the lattice caused by the optical matching. This results from the fact that the six quadrupoles used to correct the betatron phase-space straddle the chromatic correction.

ACKNOWLEDGEMENTS

I wish to thank K. Brown, A. Hutton, J. Haïssinski and W. Kozanecki for useful comments on this note. In addition, I would like to acknowledge the contribution of D. Ritson, with whom I collaborated on these problems.

REFERENCES

(1) "SLC Design Handbook" (December 1984).

(2) P. Bambade, "Beam Dynamics in the SLC Final Focus", SLAC-PUB-4227 (June 1987),

(3) C. Hawkes and P. Bambade, "First Order Optical Matching in the Final Focus Section of the SLAC Linear Collider", SLAC-PUB-4621 (May 1988)

(4) J. Murray *et al.*, "The Completed Design of the SLC Final Focus System", SLAC-PUB-4219 (February 1988)

(5) P. Bambade, "Recent Progress at the SLAC Linear Collider", SLAC-PUB-4610 (April 1988)

(6) P. Bambade *et al.*, "Operational Experience with Optical Matching in the SLC Final Focus System", To be published at the Particle Accelerator Conference, in Chicago (March 1989).

(7) N. Phinney *et al.*, "An Automated Focal Point Positioning and emittance Measurement Procedure for the Interaction point of the SLC", To be published at the Particle Accelerator Conference, in Chicago (March 1989).

(8) P. Bambade, "Number of Dimensions of Optical Correction Space in the SLC Final Focus System", Collider Note in preparation.

(9) K. Brown *et al.*, "TRANSPORT", SLAC-91, Rev. 2 (May 1977).

(10) This argument was suggested by D. Ritson.

(11) D. Ritson and P. Bambade, private simulation.

(12) R. Servranckx and K. Brown, private simulation.

(13) C. Field *et al.*, "High Resolution Wire-Scanner for Micron Size Profile Measurements at the SLC", SLAC-PUB-4605.

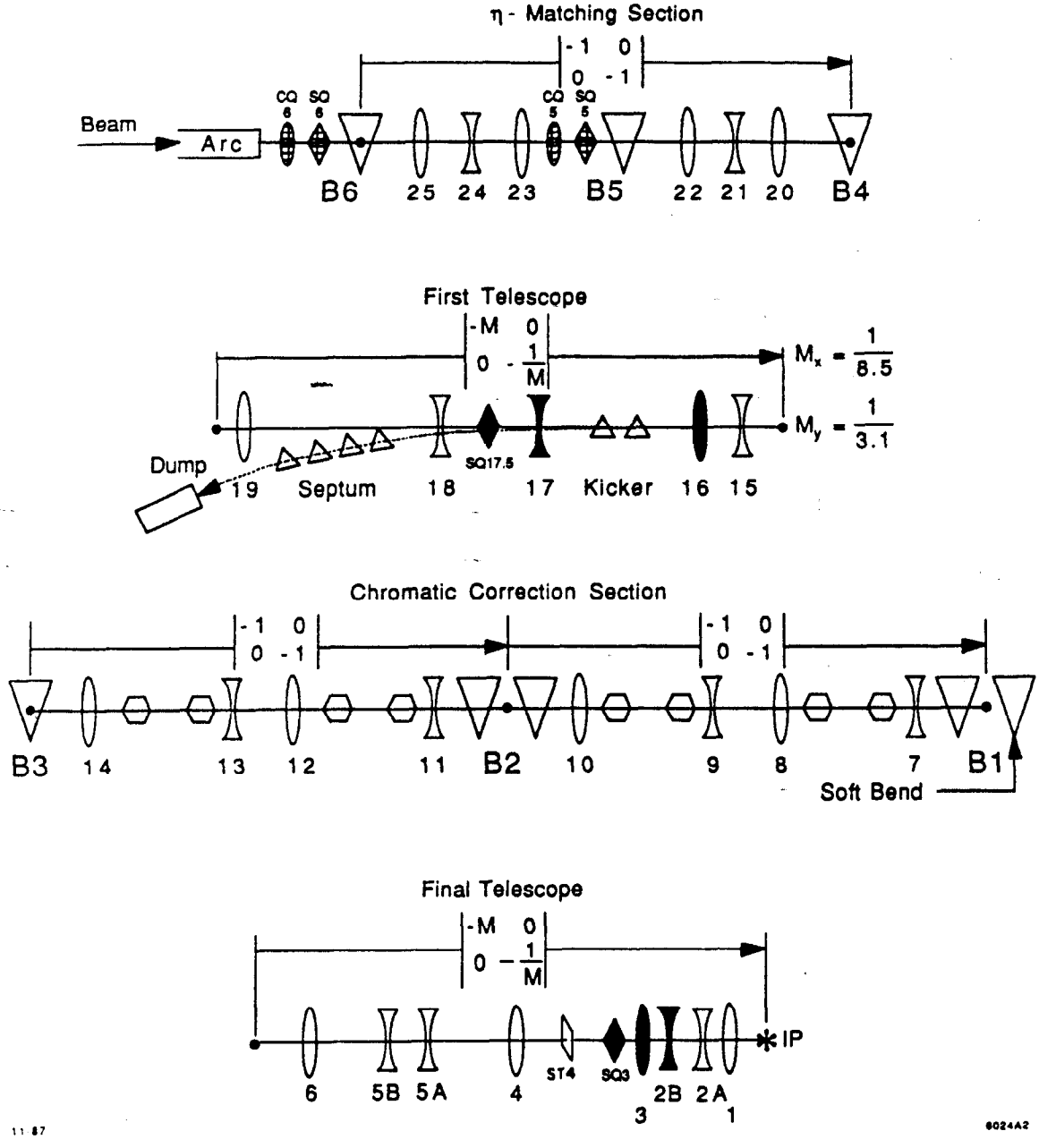

Fig. 1: Schematic of the SLC Final Focus System optics. The *six* variable quadrupoles used for adjusting the betatron phase-space are shown shaded. The *four* quadrupoles used to correct the dispersion function are shown cross-hatched. The profile monitor ST4 is located immediately upstream of the skew quadrupole SQ3. The sequential application of these *ten* adjustments is summarized in the flow-diagram in Fig. 2.

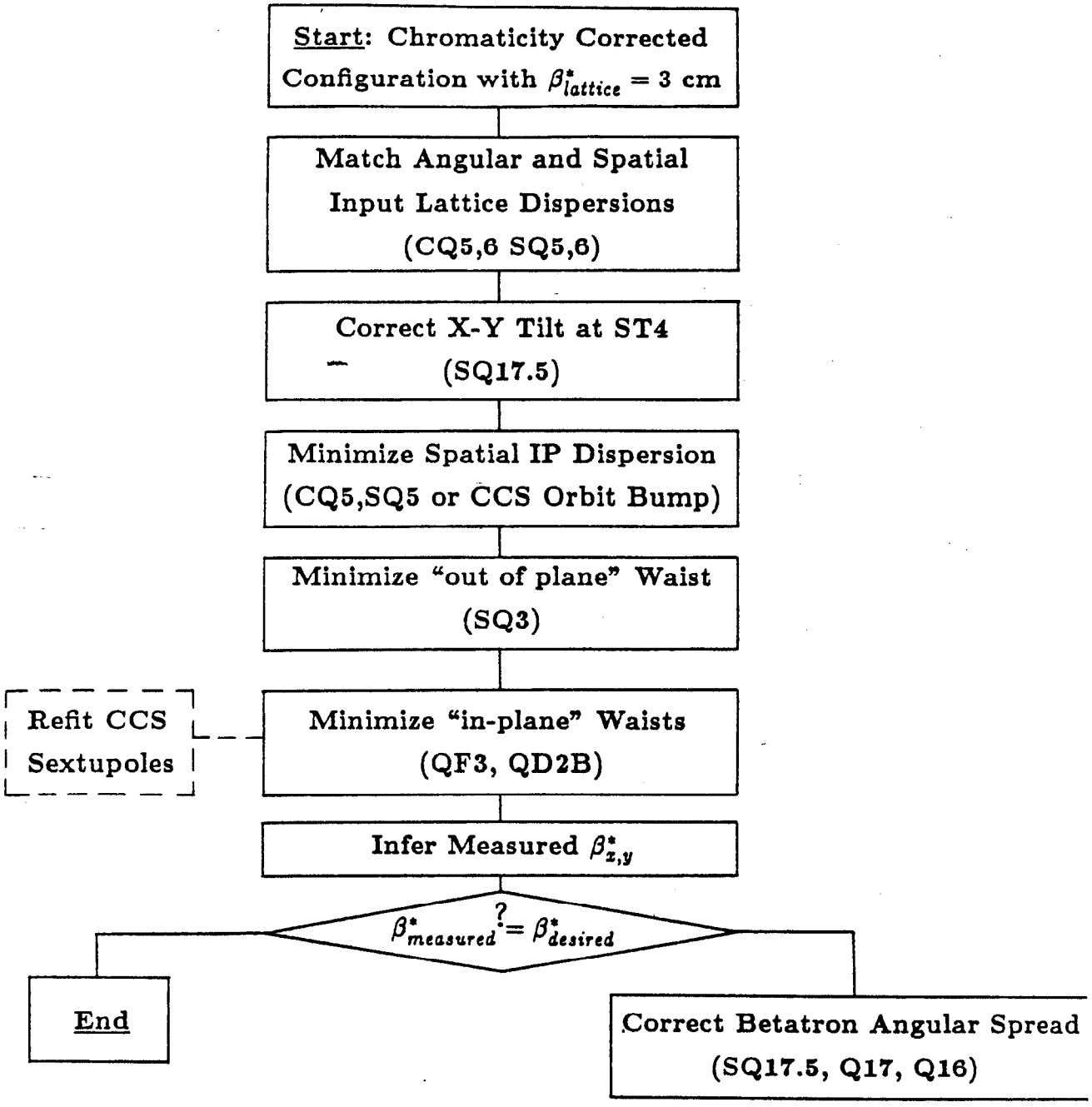

Fig. 2: Flow-diagram summarizing the *ten* linear optics adjustments required to minimize the beam size at the IP of the SLC. These adjustments are grouped and applied sequentially as shown in the boxes. Some iteration of the waist and IP dispersion minimization is usually performed. In addition, the sextupoles are refitted after each significant waist correction. The main correctors used at each step are indicated in parenthesis. The full system is shown in Fig. 1.

VII.2 "Beam Dynamics in the SLC Final Focus System"

This conference article describes the initial development of the experimental tuning algorithm, enabling to adjust the final focus for maximum luminosity, given a perturbed input phase-space. The correction algorithm had to be designed pragmatically and given the already built final focus beam-line. It is based on the general framework of the optical design of the system. The paper gives an overview of the general commissioning strategy for the final focus. It also provided the basic groundwork for the specification of the on-line computer control and modeling of the final focus, and served as a building block towards further work on this subject.

SLAC – PUB – 4227
June 1987
(A)

BEAM DYNAMICS IN THE SLC FINAL FOCUS SYSTEM*

P. S. BAMBADE
Stanford Linear Accelerator Center
Stanford University, Stanford, California 94305

Abstract

The SLC luminosity[1] is reached by colliding beams focussed to about 2 μm transverse sizes. The Final Focus System (FFS) must enable, beyond its basic optical design,[1,2] the detection and correction of errors accumulated in the system. In this paper, after summarizing the design, we review the sensitivity to such errors and the ability to correct them. The overall tuning strategy involves three phases: single beam spot minimization, steering the beams in collision and luminosity optimization with beam-beam effects.

Summary of Optical Design[1,2]

Focussing the beam to a small transverse size would be easy if the input phase space (transverse emittance and energy spread) were small enough. A *monoenergetic* beam with horizontal emittance $\epsilon_x = \sigma_x^{in}\sigma_\theta^{in}$ would, for example, be focussed to $\sigma_x^* = \sigma_x^{in} l^*/L$ a distance l^* from a lens with focal length $1/f = 1/l^* + 1/L$ (see Fig. 1). In a more realistic beam with finite energy spread σ_E, rays on the edge of the energy distribution are focussed at an axial position displaced by $l^*\sigma_E$, thus adding $2l^*\sigma_E\sigma_\theta^*$ to the overall size (a factor 2 is put in since at least two lenses are used to focus both planes). This *chromatic aberration* is negligible if $\epsilon\sigma_E \leq \sigma_x^{*2}/2l^*$. In the SLC where $\sigma_x^* \simeq 1.5\mu m$, $\epsilon \simeq 3\ 10^{-10}$ mrad, $\sigma_E \simeq 0.002$ and $l^* \approx 5m$ (computed to the principle plane of the final lenses), it amounts to $\sigma^*_{chrom} \simeq 4\mu m$, and thus dominates the spot.

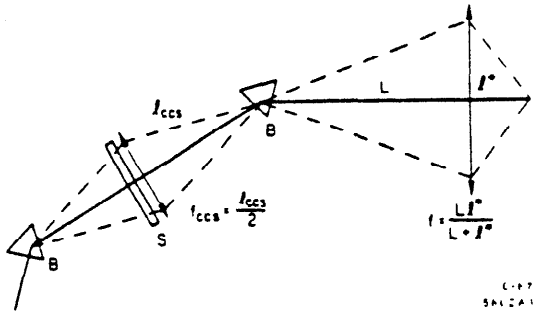

Fig. 1. A simplified Final Focus.

The resulting luminosity, computed by averaging the usual expression over the two beams' energy distributions (assumed square with half-width σ_E), is given by:

$$\mathcal{L}(\beta^*,\sigma_E) = \frac{fN^2}{2\pi\sigma_E^2}\int_0^{\sigma_E}\int_0^{\sigma_E}\frac{d\delta_E^+ d\delta_E^-}{2\epsilon\beta^* + \frac{\epsilon}{\beta^*}F^2(\delta_E^{+2}+\delta_E^{-2})} \quad (1)$$

where $F=\sigma_x^*(\delta_E)/\sigma_\theta^*\delta_E$ is a measure of the aberration. It is shown versus β^* in Fig. 2, normalized to $\mathcal{L}(\beta^*_{nom},\sigma_E=0)$, for an as-built FFS with no chromatic compensation ($F \approx 15m$). Independent of ϵ, it gives the optimum β^* for such an FFS. For $\sigma_E = 0.002$ and $\beta^*_{opt} \simeq 1.5$ cm, $\mathcal{L}$ is down by a factor 3.5. This is not as low as what we get directly with the size estimate because the aberration spreads the edges of the bunch out more than its core, and because the luminosity is a sum of squares.

* Work supported by the Department of Energy, contract DE-AC03-76SF00515.

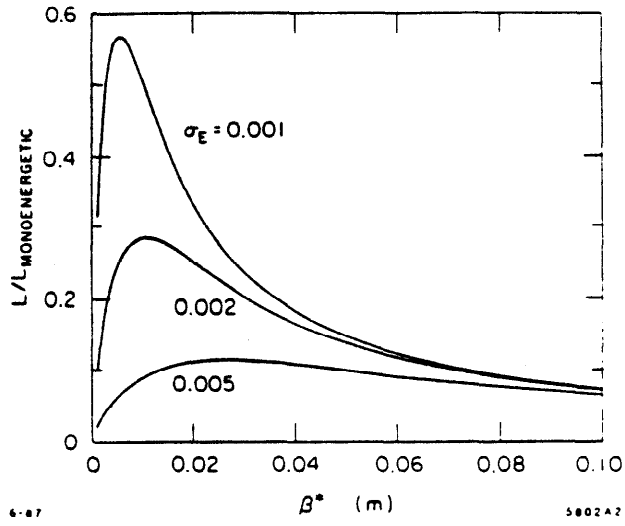

Fig. 2. Relative luminosity loss versus β^* and σ_E for a Final Focus without chromatic correction.

Compensation requires a special Chromatic Correction Section (CCS) upstream of the final lens. In a simplified CCS, two dipoles of strength B separated by $2l_{ccs}$, are imaged by a quad with focal length $l_{ccs}/2$, resulting in a 1^{st} order achromat (see Fig. 1). Near the quad is a sextupole of strength S, in which the field varies quadratically with excursion, and in which rays with energy deviation δ_E are transported off-axis. This produces a stronger overall quad for rays both off-angle and off-energy ($\theta\delta_E$ term), which offsets the weaker focussing in the final lens. Equating the contributions to σ^*_{chrom} from the final lens and from the sextupole (neglecting the CCS quad), we find that $M = l^*/L$, $R_l = l^*/l^2_{ccs}$, B and S scale like $S \propto R_l/MB$.

Unfortunately, the sextupole also deflects rays solely off-energy or off-angle, thus giving terms in θ^2 and δ_E^2. Cancelling these two new aberrations requires that the CCS be made of two consecutive and identical sections, with sextupoles in pairs π phase shift apart and sequential symmetry for the η-function. The real system,[2] designed to focus achromatically in both planes, uses telescopes, each consisting of two triplets, instead of the lenses. This minimizes[1,3] the dominant $\theta\delta_E, \phi\delta_E$ terms and suppresses the other 2^{nd} order term in $x\delta_E, y\delta_E$ while demagnifying in both planes. The chromatic correction, also done in both planes, requires two sextupole families. Coupling effects between them can significantly enhance 3^{rd} order chromatic and geometric contributions and must be minimized. The three dominant terms are $\theta\delta_E^2$, $\theta^2\delta_E$ and θ^3. Neglecting the final lenses, these terms scale like $S^2B^2\sigma_E^2\sigma_\theta^* M$, $S^2B\sigma_E\sigma_\theta^{*2}M^2$ and $S^2\sigma_\theta^{*3}M^3$. Substituting for the sextupole strength needed to correct, we get $\frac{R_l^2\sigma_E^2(\epsilon/\beta^*)^{1/2}}{M}$, $\frac{R_l^2\sigma_E(\epsilon/\beta^*)}{B}$ and $\frac{R_l^2M(\epsilon/\beta^*)^{3/2}}{B^2}$. For given phase-space volume, space constraints and desired β^* the overall effect of these aberrations is minimized adjusting M,B and S to balance them out. An approximate criterion[1,2] is obtained equating the two 1^{st} terms giving $\sigma_\theta^{in}=\sigma_E B$. Physically this means that monochromatic and chromatic sizes should be about equal in the sextupoles.

Invited paper presented at the 1987 Particle Accelerator Conference, Washington, D. C., March 16–19, 1987

These considerations are relevant not only to the design, but as we shall see, to the *experimental tuning strategy:* We must in effect insure proper optical matching into the CCS to maintain the optimization. The whole system is shown in Fig. 3. It includes two more sections to match the Arc lattice.

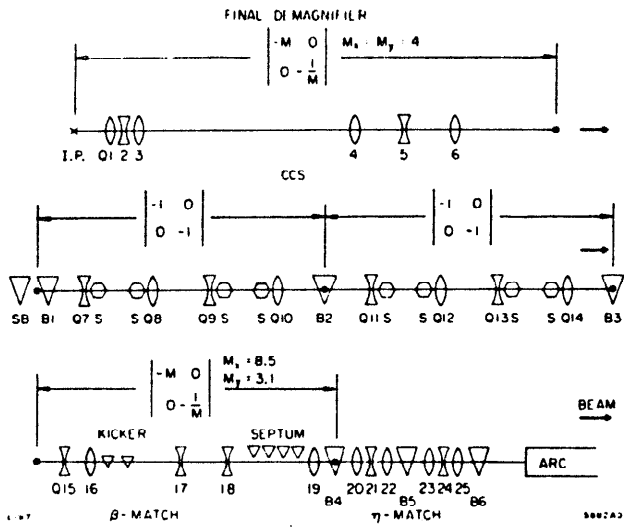

Fig. 3. Schematic of FFS.

Sensitivity to Optical Mismatch

In real operation, both the volume and shape of the injected phase space differ from specification because of errors, thereby increasing σ^*.

Enhancements in ϵ, from wakefields in the Linac or synchrotron radiation in the Arc, as well as an imperfectly minimized σ_E, are uncorrectable in the FFS. The damage can, however, be reduced somewhat by retuning the betatron match into the CCS. For larger ϵ, σ^* is first dominated by the 3^{rd} order $\theta^2\delta_E$ term. Varying β^* to minimize the overall $(\epsilon\beta^* + (\sigma_E\epsilon/\beta^*)^2)^{\frac{1}{2}}$ size gives $L \propto \epsilon^{-\frac{4}{3}}$ for $\beta^*_{opt} \propto \epsilon^{\frac{1}{3}}$. Similarly for σ_E (now with $\delta_E^2\theta$) we would get $L \propto \sigma_E^{-2}$ for $\beta^*_{opt} \propto \sigma_E^2$ if the bunch remained gaussian. Actual simulation (MURTLE[4]) shows close to linear loss with weak dependance on β^* (see Fig. 4).

Optical distortions from gradient errors upstream are mostly linear[5] and can be corrected within some bounds. The primary effect results from a 1^{st} set enhancing σ^* directly by correlating positions with angles or with δ_E at the IP. This amounts to axial offsets in the waists, x-y coupling ($x\phi$ or $y\theta$ terms) and anomalous $\eta_{x,y}$. The axial waist offset Δ_{waist} must be corrected to better than β^*=0.75 cm, since $\beta^*_{eff} = \beta^* + \Delta_{waist}{}^2/\beta^*$, and $\eta_{x,y}$ to better than 1 mm. A 2^{nd} set affects luminosity indirectly by perturbing the IP angular spread, through the magnitude of $<\theta^2>$ and $<\phi^2>$, and through anomalous $\eta_{\theta,\phi}$ and $\theta\phi$ coupling terms. Smaller spread increases β^* linearly. Inversely, a larger spread reduces it but also enhances the 3^{rd} order $\theta\delta_E^2$, $\theta^2\delta_E$ and θ^3 aberrations, as the criterion for optimal balancing is no longer satisfied. The relative luminosity loss versus β^* is shown from simulation in Fig. 4 for different σ_E. The shape is the same as in the chromatically uncorrected case in Fig. 2. Here, although the CCS has left 3^{rd} aberrations, it has removed the dominant 2^{nd} order terms, thereby raising $\mathcal{L}^{max}$ and shifting β^*_{opt} towards smaller values. The tolerance on β^* is about $\pm 20\%$. Outside this range, the spot will not have the design size even if the 1^{st} set of distortions are corrected. For β^* too large, $\mathcal{L} \propto 1/\beta^*$ from

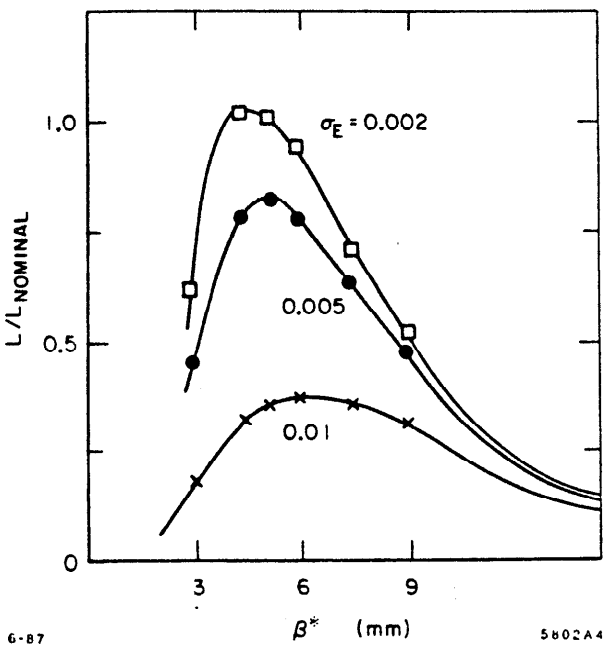

Fig. 4. Relative luminosity loss versus β^* and σ_E for a Final Focus chromatically corrected to 2^{nd} order.

linear optics. For β^* too small, $\mathcal{L}$ falls off, first linearly, than parabolically, as it becomes dominated by 3^{rd} aberration.

Optical Corrections

The FFS could in principle be designed to fully match optical distortions generated upstream. Accumulated errors of any size would then be left for correction there. This is not feasible in the SLC because of the Arc, where minimizing synchrotron radiation induced emittance growth requires a reasonable optical match throughout. The 1^{st} step to specify the matching solution is to set tolerances for the Arc and its input match to avoid large growth. Investigating such tolerances is beyond the scope of this paper. Let us simply mention that the blowup is small[6] for random imperfections three times the specified tolerance.[7] Input mismatch and systematic errors are more damaging.

The distortion's size then determine the range over which the FFS must be tunable, and the above sensitivities how well one must match. Not all parameters are important. With no pinch effect initially and with σ_E basically set by the Linac, we consider distortions only in the four betatron dimensions and in their couplings to energy. Betatron space is described by the usual σ-matrix,[8] with ten terms $\sigma_{ij}=<x_i x_j>$. The R-matrix describing the lattice has 16 terms. Output phase space is related to input by $\sigma_{out} = R\sigma_{in}R^t$ where R^t is the transpose of R. For linear optics and neglecting synchrotron radiation, Poincarré invariance requires[9,10] that R be symplectic:

$$R^tSR = S, \quad \text{with} \quad S = \begin{pmatrix} 0 & -1 & 0 & 0 \\ 1 & 0 & 0 & 0 \\ 0 & 0 & 0 & -1 \\ 0 & 0 & 1 & 0 \end{pmatrix} \qquad (2)$$

thereby restricting the number of free terms in R to ten. Applying the same algebra to the σ-matrix, we find that the betatron space can only be perturbed by the optics in six independent ways. With the four dispersions $\eta_{x,\theta,y,\phi}$, we thus have a total of *ten independent distortions* to correct.

We choose to represent them by those for which tolerances were given above: the five IP angular sizes $< \theta^2 >$, $< \phi^2 >$, $< \theta\phi >$ and $\eta_{\theta,\phi}$, and the five correlations of IP positions to angles and energy $< x\theta >$,$< y\phi >$,$< y\theta >$ (or $< x\phi >$) and $\eta_{x,y}$. Ideally correction would be done upstream of the CCS, to avoid perturbing its optimization relative to the Final Demagnifier. This is possible for η, but only partially possible for betatron space.

Dispersion is corrected perturbing the η-match with four quads,[2] installed in pairs $\pi/2$ and π phase shift from the IP, to control spatial and angular η, respectively. Each pair consists of an erect and a skew quad for control in both planes. Naturally orthogonal for small input $\eta_{y,\phi}$ (the two erect ones perturbing the match of the horizontal lattice dispersion, and the two skew ones coupling it into vertical), they are coupled if it is large. Correction range is limited by quad strengths but also by the particular orientation of input η. Some specific values make them ineffective. This happens, for example, when $\eta_{x,\theta}^{anomalous}$ exactly cancels $\eta_{x,\theta}^{lattice}$. The domain of correctable $\eta_{x,\theta}$ therefore has a *dead zone* (see Fig. 5). With $\eta_{ARC}^{lattice}$ modulating around 35 mm with maximum slopes of ± 18 mrad, uncorrectable cases appear if, for instance, the horizontal betatron phase in the back of the Arc is off by a quarter of a modulation cycle with the appropriate sign. Gross control is thus required upstream to bring η within *capture range*.

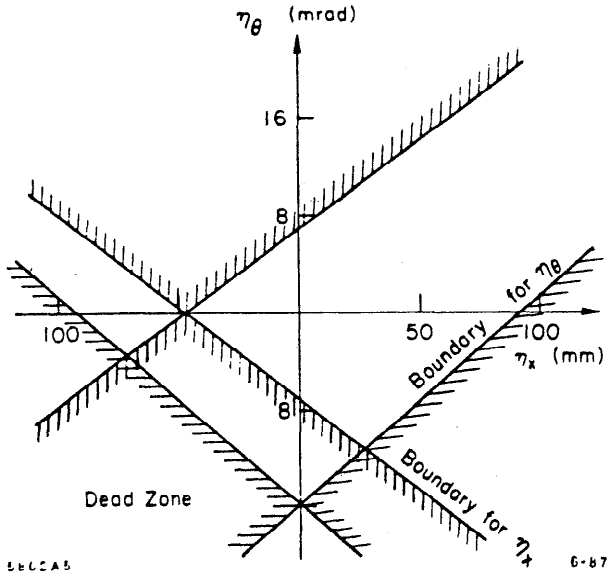

Fig. 5. Domain of correctable horizontal dispersion.

Betatron matching is split across the CCS, in the β-match and Final Demagnifier. The three angular terms $< \theta^2 >$, $< \phi^2 >$ and $< \theta\phi >$ are adjusted upstream of the CCS with two of the β-match quads and a skew quad, allowing to control the ratio of betatron to chromatic sizes in the sextupoles. The three waist offsets $< x\theta >$,$< y\phi >$ and $< y\theta >$ cannot be adjusted within the β-match independently of the angular terms. The are taken out at the very end, with two of the final lenses and a 2^{nd} skew quad. This strategy does not maintain exactly the relative optimization of the Final Demagnifier and CCS, as the last lenses are tweaked. The luminosity, somewhat derated as some 2^{nd} order aberration reappears, can be restored readjusting the sextupoles. Except for some cases of large errors, this is a small effect. With present hardware, the correction range is about $\pm 40 \times \beta^*$ for waist control (or 30 cm for $\beta^* \simeq 0.75$ cm) and a factor 3 in either direction for angular spread. Simulations and calculations show that random errors three times those expected in the Arc can be handled.

Overview of Tuning Strategy

Turning 12 coupled knobs guided only by the IP spot—let alone optimizing two colliding beams—would be very difficult without an ordered procedure. Since measuring μm-size beams is not straightforward, we must minimize the number of tuning experiments requiring IP information by diagnosing as many aspects of phase space as possible before demagnification or wherever conventional instruments are adequate.

Our tuning strategy begins with optical matching of a single beam using strip-line Beam Position Monitors (BPMs) with about 20 μm resolution and phosphor screens with about 35 μm resolution. At the IP, crude measurements are done using thin carbon wires, about 5 μm in diameter, from which spot sizes and centroids are inferred by scanning. Such wire targets and BPMs near the IP have been designed for initial commissioning, but are also part of the early detector configuration.

After both beams are minimized, they are brought and kept in collision, first with BPMs near the IP, and then exploiting the electromagnetic fields from the bunches, which for small enough size and large enough population cause them to be deflected if they miss each other.[11] The ability to detect this effect determines the size and intensity to be reached in the single beam phase. We shall see that about 5 μm and a few 10^{10} particles is adequate.

Finally we maximize luminosity looking at beam-beam effects in three ways: magnitude of deflection, synchrotron radiation from the collisions (Beamstrahlung)[12] and disruption imaged in the extraction-lines.[13] Detector background[14] minimization is not covered here.

Single Beam Spot Minimization

We first correct anomalous input η. BPMs at the end of the Arc and in the FFS are used to measure beam motion versus energy. This does not give the position-energy correlation within the bunch if anomalous η exists where the energy is varied, but gives a good estimate if the Arc is (as expected) the dominant contributor. As more accuracy is needed, one must constrain η in the Linac or measure spot sizes directly. With 1% energy scans, we determine η to a few mm, or about 5% of the Arc average. Using a model, we determine $\eta_{x,\theta,y,\phi}^{anomalous}$ from a least-square fit to the measurements and calculate the matching solution. Locally orthogonal "knobs" are derived for fine-tweaking. We first correct the β-match, to enable measuring betatron phase space there. Final settings for IP correction will differ if the CCS and Final Demagnifier generate η, for example, through orbit errors. The resulting η_{IP} is mostly spatial as the lenses there are $\pi/2$ phase shift from the IP. Final IP correction is inferred from BPM measurements and from measuring σ^* versus the derived orthogonal knobs, using the wire targets.

Betatron phase space is then diagnosed measuring spot size on a screen versus the strength of an upstream quad, and fitting a parabola.[15] Special emphasis is put on emittance, to help guide tuning in the Arc. Since ϵ enters as a overall scale, we must resolve the parabola's minimum. For a quad and a screen separated by l, this requires $\epsilon l^2/\beta \gg r^2$, where r is the screen resolution. This condition is met before demagnification, in the β-match. A setup with about 100 μm minima in both planes is installed. Twiss parameters, found from the parabola's axis and branches, serve to diagnose gross betatron mismatch. x-y coupling obscuring the ϵ-measurement is diagnosed looking at the tilt of the spot versus quad strength, giving another parabola and three more terms. With nine terms in total, we can in principle fully determine betatron space. In practice, being mostly interested in ϵ, while betatron mismatch is better

measured elsewhere, we simply correct for the measured x-y coupling.

Betatron mismatch is best diagnosed in the Final Demagnifier, where angular and spatial sizes are naturally separated. Using the three β-match knobs, we first set the three angular terms $< \theta^2 >$, $< \phi^2 >$ and $< \theta\phi >$, looking at a nominally round spot on a high-β screen upstream of the Final Triplet. We begin, first ignoring $\epsilon_{x,y}$, by standing the beam upright using the skew quad. Then, taking $\epsilon_{x,y}$ into account, we perturb the two sizes with the erect quads, so as to best satisfy the $\beta^*_{opt} \propto \epsilon^{\frac{1}{3}}$ scaling law (minimizing 3^{rd} order aberration). After this, the beam will have the predicted size at the axial position where it comes to a waist, although that place may be offset from the IP. Correction, amounting to cancel $< x\theta >$, $< y\phi >$ and $< x\phi >$ terms, is calculated sweeping the three Final Triplet knobs and measuring $\sigma^*_{x,y}$ versus strength. As in the phase-space measurement, only the parabola's axis and branches are needed. The axis give the offsets and the branches the derivatives of size versus strength. In principle, resolving the minima is not essential. With all lenses $\pi/2$ from the IP, it can be shown that the skew quad is fully orthogonal to the two other waist controls, provided the $< \theta\phi >$ coupling term is properly nulled; however, the latter two are coupled. The algorithm first orthogonalizes them using the derivatives and then sets them based on the measured axis. The skew quad is adjusted equivalently before or after. η_{IP} can also be cancelled with such parabolic sweeps. Final minimization is achieved iterating all the corrections.

Steering the Beams in Collision

The average mutual deflection of two gaussian beams colliding at an offset Δ is[11]

$$\Theta(\Delta) = \frac{-2r_e N_T}{\gamma} \frac{1 - exp(\Delta^2/2\sigma_T^2)}{\Delta} F(\sigma_P/\sigma_T) \qquad (3)$$

where r_e is the classical electron radius, γ the relativistic factor, N_T the number of particles in the target and $\sigma_{T,P}$ the target and probe sizes. $F(r)=\frac{Ln(1+r^2)}{r^2}$ is a form factor computed for small Δ by folding in the probe distribution. It reduces the average for $\Delta \simeq \sigma$, whereas it should be dropped for $\Delta \gg \sigma$, as the beams then see each other as point charges. Deflection versus offset is shown in Fig. 6 for 50 GeV beams with 5×10^{10} particles and 2, 5 and 10 μm sizes. Detection is best done at the system's high-β points, near the Final Triplet, where it translates into the largest possible shift. Special BPMs are designed[16] for this purpose.

The tuning method proceeds in three steps:

1. *Initial beam finding:* After bringing the beams close with BPMs near the IP, one of them (the most intense) is toggled *on* and *off* while the other is measured at the outgoing high-β point. This gives the shift induced by the collision, the sign telling in which direction to steer. For large Δ and with numerical factors, we get $\delta X_{out}(\mu m) \approx \frac{70 N_T/5\times10^{10}}{\Delta/100\mu m}$.

2. *Beam centering:* Scanning one beam across the other enables optimal centering on the zero-deflection symmetry point (see Fig. 6). The largest shift occurs for $\Delta \simeq 1.5\sigma_T$ giving $\delta X^{max}_{out}(\mu m) \approx \frac{1000 N_T/5\times10^{10}}{\sigma_T/2.5\mu m}$. With 20 μm measurements and about 2×10^{10} particles initially, we expect good signals for $\sigma \leq 5\mu m$. This sets the goal for single beam optimization.

3. *Feedback:* The mutual deflections are also used to keep the two beams in collision. In simple versions of such feedback, we sample position deviations from an initial reference at reciprocal high-β points on ingoing and outgoing paths. Drifts in the offset are approximated by $\Delta(t) \propto (\delta X_{out}(t) - \delta X_{in}(t))$. A slow

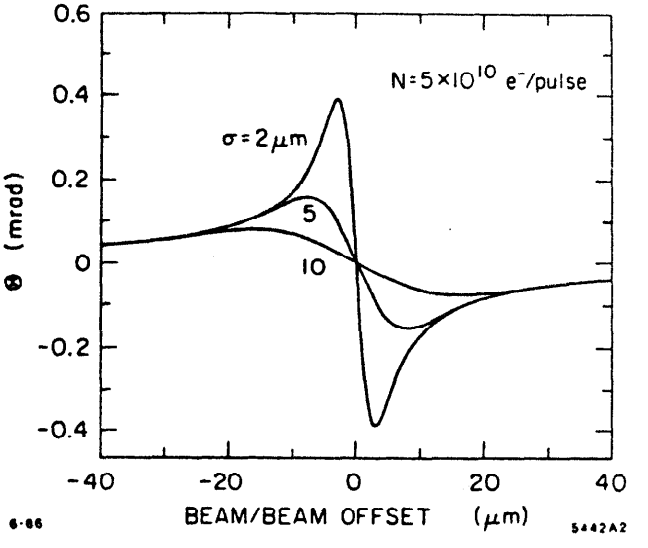

Fig. 6. Beam-beam deflection versus offset for three spot sizes.

version of such a system, with a time constant of about 20 seconds, is available as an extension of existing software.[17] More sophisticated pulse to pulse schemes with optimal filtering[18] of specific frequencies are in progress.

Luminosity Optimization with Beam-Beam Effects

Algorithms based on three beam-beam signals are in progress.

1. *Magnitude of deflection:* The maximum deflection produced in the centering scan is a strong function of beam sizes and can be used for tuning. For centered beams, this signal allows separating improvements in the two planes, but unfortunately not in the two beams. This can be seen noticing that after normalizing by $N_{T,P}$, conservation of the total transverse momentum implies equal average deflections for each beam. The maximum must thus be symmetric in the two beam sizes, making it hard to know which one needs to be optimized (except by sensing derivatives).

2. *Beamstrahlung:*[12] The total photon flux emitted in the collisions is a strong function of beam sizes. For each particle, $N_\gamma \propto \sigma_z/\rho^2 = \theta^2/\sigma_z$, where σ_z, θ and ρ are the bunch-length, deflection angle and radius of curvature. For centered beams of equal size σ_R and populations $N_{1,2}$, Beam 1 radiates $N^{total}_\gamma \propto N_1 N_2^2/\sigma_z\sigma_R^2$. Without the shape of the photon beams it is hard to separate the two planes. One *can* however distinguish the larger from the smaller by scanning one across the other. This is the reversed situation from the deflection signal, making the two methods complementary. The reason is the θ^2-dependence of N_γ, leading to a sum of squares for N^{total}_γ. The dependence of N^{total}_γ from the probe versus Δ is indicated in Fig. 7 for a target with equal, larger or smaller size.

3. *Disruption:* When beams have been made small and intense enough, they act as lenses for each other, thereby increasing their angular spread after collision. In the linear approximation, σ^*_θ grows by about 50% for beams with 2×10^{10} particles and 2 μm transverse sizes. Monitoring of this effect will be possible in the extraction lines, by imaging IP angles on screens through optics designed for the planned energy spectrometers.[13] Tuning for the largest possible spot on these screens will then maximize luminosity.

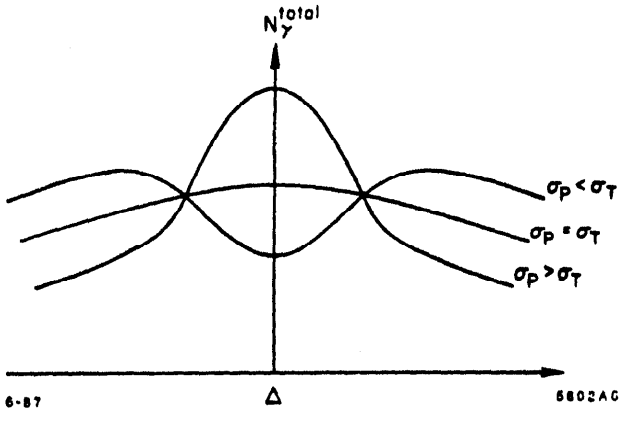

Fig. 7. Total beamstrahlung flux versus offset for unequal transverse beam sizes.

Acknowledgements

I am indebted to several SLC and Mark II colleagues for fruitful discussions. Special credit should be given to K. Brown, T. Fieguth and J. Murray for designing the optics, to W. Kozanecki and R. Erickson for leading our group, and D. Ritson for reviewing many of our algorithms.

References

1. *SLC Design Handbook* (December 1984).
2. J. J. Murray *et al.*, *The Completed Design of the SLC Final Focus System*, these Proceedings.
3. K. L. Brown, private communication (June 1987).
4. J. J. Murray and T. Fieguth, MURTLE, Private Program.
5. K. L. Brown *et al.*, GIAT Committee Report (February 1986).
6. R. V. Servranckx, private communication (June 1987).
7. S. Kheifets *et al.*, *Beam Optical Design and Studies of the SLC Arcs*, SLAC-PUB-4013 (June 1986).
8. K. L. Brown *et al.*, SLAC-91, Rev. 2 (May 1977).
9. E. D. Courant *et al.*, *Theory of the Alternating-Gradient Synchrotron*, Ann. of Phys. 3, 1–48 (1958).
10. L. C. Teng, *Concerning n-Dimensional Coupled Motion*, Fermilab Internal Report FN-229 (May 1971).
11. P. S. Bambade *et al.*, *Beam-Beam Deflection as an Interaction Point Diagnostic for the SLC*, SLAC-PUB-3979 (May 1986).
12. G. Bonvicini *et al.*, *Beamstrahlung Monitor for SLC Final Focus Using Gamma Ray Energies*, SLAC-PUB-3980 (May 1986).
13. Mark II Coll. and SLC Final Focus Group, *Extraction-Line Spectrometers for SLC Energy Measurements*, SLAC-SLC-PROP(2) (1986).
14. W. Kozanecki, GIAT Committee Report (January 1986).
15. M. C. Ross *et al.*, *High Resolution Beam Profile Monitors in the SLC*, SLAC-PUB-3640 (April 1985).
16. J. C. Denard *et al.*, *Monitoring the Beam Position in the SLC Interaction Region*, these Proceedings.
17. K. A. Thompson *et al.*, *Feedback Systems in the SLC*, these Proceedings.
18. R. Stiening, *Sampled Feedback in the Linear Collider*, SLAC CN-14 (November 1980).

VII.3 "First Order Optical Matching in the Final Focus Section of the SLAC Linear Collider"

This publication describes the modeling and fitting algorithms that were developed to perform on-line model-driven optical corrections. The tuning algorithm is summarized, and some initial experimental results presented.

SLAC – PUB – 4621
CALT – 68 – 1495
May 1988
(A)

FIRST ORDER OPTICAL MATCHING IN THE FINAL FOCUS SECTION OF THE SLAC LINEAR COLLIDER*

C.M. HAWKES

California Institute of Technology,
Pasadena, California 91125

and

P.S. BAMBADE

Stanford Linear Accelerator Center,
Stanford University, Stanford, California 94309

ABSTRACT

The procedures used for dispersion and betatron matching in the first order optical tuning of the SLC Final Focus are described. Associated modelling and fitting algorithms are presented.

A straightforward method for extending uncoupled optical models to incorporate cross-plane coupling is explained.

Submitted to *Nuclear Instruments and Methods* A

* Work supported by Department of Energy, contracts DE-AC03-81-ER40050 (Caltech) and DE-AC03-76SF00515 (SLAC)

1. INTRODUCTION

The SLAC Linear Collider[1] (SLC) is designed to collide electron and positron bunches each with a round beam spot and with a transverse size of about 2 microns at the interaction point (IP). The Final Focus[2,3] sections of the beam lines, on each side of the IP, are responsible for focusing the beams to this small size.

The Final Focus optical system, shown in Fig. 1, consists of five telescopic modules. Demagnification is achieved in two stages, in the First and Final Telescopes. The chromaticity of the quadrupole array is compensated through sextupoles in the Chromatic Correction Section. Matching of the dispersion and the betatron motion to the Arc lattice is provided in the η-Matching Section and the First Telescope respectively. Extraction of the spent beam, moving in the opposite direction, is achieved in the First Telescope, through a pulsed magnet and a septum.

The Final Focus must also provide variable optical matching for the correction of distortions in the lattice arising through gradient errors in the beam line upstream and within the Final Focus Section itself. This note describes two parts of the optical tuning procedure used during the commissioning and running of the SLC Final Focus: the dispersion and betatron matching.

To attain the desired beam spot size, any contribution from the finite energy spread of the beam must be eliminated by making the beam dispersion zero at the IP. The method for doing this is described in Section 2.

The SLC design has equal emittances in the horizontal and vertical planes. In this case, six adjustments are involved to match the Final Focus monochromatic beam envelope to that coming out of the Arc. The procedure for doing this, referred to as betatron matching, is discussed in Section 3.

In order to perform these matching operations routinely it is necessary to have detailed optical modelling and fitting included as part of the online control program for the Final Focus. The existing online SLC optical model was not adequate since it assumes that the beam dynamics in the horizontal and vertical planes are independent and hence cannot accommodate cross-plane coupling. A straightforward and general method for extending the model to incorporate cross-plane coupling was devised and is explained in Appendix A.

2. DISPERSION CORRECTION

2.1 DEFINITIONS

Dispersion refers to the correlation between the transverse position or angle of a particle in a bunch and its energy relative to the mean energy of the bunch; e.g. horizontal spatial dispersion:

$$\eta_x = \frac{\Delta x}{\delta} \tag{2.1}$$

where x is displacement in the local horizontal plane and δ is the energy spread, $\delta = \Delta E/E$. More precisely this can be termed the "beam dispersion". It corresponds to the sixth column of the beam σ-matrix* and contributes to the first-order transverse beam size according to the formula:

$$\sigma = \sqrt{\epsilon\beta + (\delta\eta)^2} \tag{2.2}$$

where ϵ is the emittance and $\sqrt{\epsilon\beta}$ is the monochromatic ($\delta = 0$) beam size.

The term "lattice dispersion" will be used to describe a slightly different quantity. It is a property of the optical lattice of the beam line, independent of the beam, and corresponds to the sixth column of the transfer matrix, or R-matrix,* describing a section of beam line. The lattice dispersion adds on to the beam dispersion of a beam passing through the section; e.g. for horizontal spatial dispersion from point A to point B:

$$\eta_x^B = R_{11}\eta_x^A + R_{12}\eta_x'^A + R_{13}\eta_y^A + R_{14}\eta_y'^A + R_{16} \tag{2.3}$$

where η^A is the beam dispersion at the start of the section, η^B is the beam dispersion at the end of the section and R is the transfer matrix across the section. The horizontal spatial lattice dispersion from A to B is R_{16}.

* The σ-matrix and R-matrix are defined in the manual for the program TRANSPORT.[4]

2.2 DESIGN DISPERSION

The SLC requires zero spatial and angular beam dispersion (η and η') in x and y at the interaction point in order to optimise the luminosity. With an energy spread of 0.5% a residual spatial beam dispersion of only 1 mm will more than double the spot size from 2 to 5 microns.

Fig. 2 shows the design value for η_x as a function of distance along the beam line (z) in the Final Focus from the end of the Arc to the IP. Whereas η_y is designed to be zero everywhere in the Final Focus, this is not true of η_x. The condition $\eta_x^{IP} = 0$ is achieved by having non-zero beam dispersion at the end of the Arc, $\eta_x^{ARC} = 47.5\,\text{mm}$. This is cancelled by an equal and opposite lattice dispersion in the η-Matching Section at the beginning of the Final Focus, leading to $\eta_x^{FT} = 0$ at the end of the First Telescope (FT). The Chromatic Correction Section (CCS) temporarily generates large values of η_x as part of its function, but the design value of η_x returns to zero at the end of the CCS and through the Final Telescope to the IP.

2.3 Anomalous Dispersion

In practice the dispersion functions sometimes show anomalous deviations from the design. Possible errors contributing to a non-zero beam dispersion at the IP can be grouped into two classes.

(a) Beam dispersion coming from the Arc which is different from its design value.

(b) Anomalous dispersion arising from errors in elements of the Final Focus beam line itself. These are most likely to come from the CCS (due to misalignment of a sextupole or quadrupole, for example) since η_x is locally large there, and so small errors lead to big effects at the IP.

It is desirable to deal with errors of type (a) first by correcting the dispersion at the end of the First Telescope to give $\underline{\eta}^{FT} = \underline{0}$.* If this anomalous dispersion is left uncorrected at the end of the FT it will propagate through to the IP. The Final Focus optics cause demagnification of the spatial dispersion component and magnification of the angular component. The resulting anomalous η'^{IP} is likely to be of much greater magnitude than η^{IP}, making it difficult to measure η^{IP} accurately enough for it to be corrected at the IP.

Errors of type (b), combined with residual errors of type (a), must then be handled separately by correcting the dispersion at the IP to give $\underline{\eta}^{IP} = \underline{0}$.

In both cases the tools available to make the dispersion correction are the same: two pairs of small quadrupoles in the η-Matching Section of the Final Focus with one upright and one skew quadrupole in each pair. These are shown cross-hatched in Fig. 1.† The skew quadrupoles, which are tilted at 45° to the standard axes, are needed to couple the non-zero x beam dispersion into the y plane and hence give some control over η_y. The pair CQ6 and SQ6 are approximately in phase with the end of the FT whereas the pair CQ5 and SQ5 are approximately $\frac{\pi}{2}$ out of phase. The IP is in antiphase with the end of the FT. Hence, for a beam with design specifications coming from the Arc and with the correctors initially set to zero, the first pair controls η'_x and η'_y whereas the second pair controls η_x and η_y. This orthogonality is lost in moving away from the design parameters for the beam and lattice. However, it is always possible to find a combination of four quadrupole settings to correct the four $\underline{\eta}$ components at the end of the FT or at the IP. The only limitation is the maximum current available from the magnet power supplies.*

* The vector notation $\underline{\eta}$ will be used to represent all four components of η and η'.

† In Fig. 1 upright quadrupoles are represented by lens shapes and skew quadrupoles are represented by diamond shapes.

2.4 Measuring Dispersion

The spatial dispersion (η_x and η_y) at a point along the beam line can be measured by stepping the beam energy through, say, ±0.3% about its nominal value and finding the slope of a plot of displacement versus energy.[6] This can be done only at points where there is a device for measuring the transverse beam position, such as a beam position monitor (BPM) or, at the IP, a secondary emission wire target called the wire scanner.[6] This technique is illustrated in Fig. 3.

To infer the spatial and angular dispersion at any point a fit must be made to the η measurements. The details of this fitting procedure are given in Appendix B.

It should be noted that this technique in fact measures the *lattice* dispersion of the beam line between the point where the beam energy is varied (the Linac) and the location of the BPM. Any beam dispersion already in the Linac cannot be measured in this way. The design dispersion in the Linac is zero and any anomalous Linac dispersion is expected to be small. However, it will not be measured and hence will not be corrected by the First Telescope Dispersion Correction scheme to be described in Section 2.5. It will propagate through to the IP and must be corrected there as described in Section 2.6.

* There are some values of $\underline{\eta}^{ARC}$ for which the effective range of the correctors becomes so small that the dispersion cannot be corrected using this scheme.[6] These "dead zones" can be avoided by adjusting the dispersion upstream.

2.5 First Telescope Dispersion Correction

To correct the dispersion at the end of the First Telescope it is first necessary to determine the spatial and angular dispersion at the end of the Arc, $\underline{\eta}^{ARC}$. This is done by measuring the spatial dispersion at BPMs near the end of the Arc, as described in Section 2.4, and then using the fitting technique described in Appendix B.

The model is used to transport $\underline{\eta}^{ARC}$ through the η-Matching and FT Sections of the Final Focus to give $\underline{\eta}^{FT}$ at the end of the FT:

$$\underline{\eta}^{FT} = R^{ARC\to FT}(k_1, k_2, k_3, k_4)\,\underline{\eta}^{ARC} \tag{2.4}$$

where, now,

$$\underline{\eta}^{ARC} = \left(\eta_x^{ARC}, \eta_x'^{ARC}, \eta_y^{ARC}, \eta_y'^{ARC}, 0, 1\right) \tag{2.5}$$

$$\underline{\eta}^{FT} = \left(\eta_x^{FT}, \eta_x'^{FT}, \eta_y^{FT}, \eta_y'^{FT}, 0, 1\right) \tag{2.6}$$

and $R^{ARC\to FT}$ is the transfer matrix from the end of the Arc to the end of the FT calculated from the model. The sixth element of the $\underline{\eta}$ vectors, which is always unity, ensures that the lattice dispersion elements contained in the final column of R are correctly incorporated according to equation (2.3).

The matrix, $R^{ARC\to FT}$, is a function of k_1, k_2, k_3 and k_4, the magnetic strengths of the four dispersion corrector quadrupoles described above. In order to make $\underline{\eta}^{FT} = \underline{0}$, the values of k_1, k_2, k_3, k_4 must be found which minimise $\underline{\eta}^{FT}$. This is done using the least squares fitting program, NPSLAC.[7] The corrector strengths are varied and $R^{ARC\to FT}$ and $\underline{\eta}^{FT}$ evaluated for each new set of strengths. The minimisation program exits when the sum

$$\sum_{i=1}^{4} \left\{\eta_i^{FT}\right\}^2 \tag{2.7}$$

is sufficiently small. The corresponding values of k_1, k_2, k_3, k_4 are returned and can be used to set the strengths of the physical magnets.

This algorithm was used regularly during the 1987 period of the SLC Final Focus commissioning[6] and has now become routine and highly reliable. Correction usually yields a dispersion function within a few per cent of the design. One example is shown in Fig. 4. Up to now, the ultimate limit to the precision of this correction has been small alignment errors on the dispersion correction quadrupoles themselves. As their strengths are varied to perform the correction, the misalignment causes the beam to be steered as well as focused downstream and hence the result is not exactly as predicted by the online model.

2.6 Interaction Point Dispersion Correction

Even after a successful $\underline{\eta}^{FT}$ correction there might still be beam dispersion at the IP which must be corrected. This can be due to residual anomalous dispersion propagating from the FT or due to alignment or magnetic errors in the Final Focus beam line itself.

One possible technique is to determine $\underline{\eta}^{IP}$ using the wire scanner and the BPMs near to the IP and the measurement and fitting schemes described in Section 2.4 and Appendix B. Corrector settings can then be calculated which will generate an equal and opposite $-\underline{\eta}^{IP}$. On iteration the IP dispersion should tend towards zero. There are two disadvantages to this method. Firstly it requires an accurate measurement of $\underline{\eta}^{IP}$. As explained in Section 2.4 this is difficult because of the spatial demagnification produced by the Final Focus. Secondly, the measurement technique of Section 2.4 is insensitive to anomalous dispersion

generated in the Linac or further upstream, since it actually measures the lattice dispersion between the point where the beam energy is varied and the measurement device. Hence this contribution to the beam dispersion at the IP would not be corrected.

Another technique involves minimising the true beam dispersion at the IP by using the transverse beam spot size as measured by the wire scanner.[6] The spot size is directly related to the beam dispersion according to equation (2.2). For each of the four components of $\underline{\eta}^{IP}$, four coefficients are found corresponding to the changes in each of the four corrector quadrupole settings needed to produce a unit change in that component of $\underline{\eta}^{IP}$ while leaving the other three components of $\underline{\eta}^{IP}$ unchanged. These represent orthogonal "η-knobs" for controlling the dispersion at the IP.* A scan can then be made over a suitable range of each component of $\underline{\eta}^{IP}$ and the size of the spot at the IP measured at each point in the scan. To first order, the minimum spot size corresponds to the optimum corrector settings.

3. BETATRON MATCHING

3.1 Betatron Phase-Space Distortions

The six distortions of the betatron phase-space which are possible[6] in the case of equal horizontal and vertical emittances are the two waist offsets ($< x\theta >$ and $< y\phi >$ correlations), the two IP angular spreads and two cross-plane correlations of IP angles ($< \theta\phi >$) and of IP positions to angles ($< x\phi >$).

* In fact the problem is nonlinear. Adjustments to upstream corrector quadrupoles change the dispersion of the beam passing through downstream correctors, and hence they cannot be decoupled completely. However, over a limited range of $\underline{\eta}^{IP}$ a linear approximation is valid.

If the Final Focus optics has been changed from the design configuration of $\beta^* = 7.5\,mm$ (see Section 3.2) then these "η-knobs" will also move the positions of the beam waists along z away from the IP ($\alpha \neq 0$). Additional corrections must be made to compensate for this effect.

The angular spread terms are controlled upstream of the CCS by cancelling the $< \theta\phi >$ cross term with a skew quadrupole (SQ17.5) and by varying β^* in each plane with two quadrupoles (16 and 17). This amounts to detuning the overall demagnification factor in the Final Focus beam line. Waist terms are corrected at the very end, with trim windings on the last quadrupoles (2B and 3) and another skew quadrupole (SQ3) immediately upstream. Two additional terms ($< xy >$ and $< y\theta >$) would require additional correction elements in the case of unequal emittances, but are redundant otherwise. All six quadrupoles which must be controlled to achieve this are shaded in Fig. 1.

The waists must be positioned at the collision point to within the depth of field $\beta^* \simeq 1\,cm$ and the $< x\phi >$ correlation removed.

After cancelling the $< \theta\phi >$ cross-term, β^*, which for fixed emittance determines the angular spread, must[6] be adjusted close to the design optimum. This optimum occurs when linear optics and higher order effects contribute about equally to the spot size at the waist. For β^* too small, the IP spot is dominated by chromatic aberrations (third order if the second order chromatic correction is properly tuned, second and third order otherwise). Conversely for β^* too large, it is dominated by a larger linear size. The tolerance[6] on β^* is about 50%.

3.2 Correction Procedure

Waist controls can be made orthogonal, linear and independent of input phase-space distortions, allowing position to angle correlations in the IP spot to be cancelled by empirically minimising its size. This is done using the wire scanner.[6] Spots are measured as functions of the orthogonal waist controls, and a parabola, $\epsilon\beta^* + \epsilon/\beta^*\Delta f^2$, is fitted to the square of the spot size (where Δf is the distance to the waist) to determine both ϵ and β^*.

Actual angular spreads are well determined from the branches of the parabola, but both ϵ and β^* estimates suffer if the linear spot is not resolved. This can arise through residual cross-plane coupling, only partially corrected in cases of unequal emittances, and through third order chromatic aberration which can dominate before the betatron matching is fully implemented. Sextupoles must also be fitted in the perturbed lattice at each iteration of the betatron matching procedure described here, to preserve good second order correction.

Measured values of β^* are used to determine angular corrections needed for matching. The adjustments are nonlinear functions of the three quadrupoles used for control. In addition, the correctors also affect the waists. The solution must therefore be the result of an overall fit of the six correctors towards the desired IP phase-space. The fitting procedure is outlined in Section 3.3. Because of the uncertainty in the measurement noted above, some amount of guessing is also necessary to determine the matching correction required. The procedure must in general be iterated in an empirical search for the optimal angular correction.

The online modelling and fitting package developed allows full flexibility in the generation of detuned optical configurations needed to match distorted beam envelopes, based on measured or on estimated optical parameters. The fitting procedure can also be adjusted conveniently by user intervention, to suit specific situations. This is explained in more detail in Appendix C. An example of such a detuned solution is shown in Fig. 2. The solid β_x and β_y curves show the design lattice of $\beta^* = 7.5\,mm$. The dash-dotted curves show a detuned configuration calculated to give $\beta^* = 30\,mm$. This lattice is presently installed as the default configuration for commissioning of the SLC. It corresponds to a first guess of the most probable angular correction needed to match possibly varying optical mismatch at the Final Focus input, generated by errors and tuning in the upstream systems. In this configuration, residual angular errors are small enough to reproduce small IP spots at the five micron level by sweeping *only* the three waist controls. It is anticipated that additional iterations of this matching will be required to optimise the spot size further.

3.3 Fitting Procedure

Before starting the last stage of betatron matching it is assumed that, to a first approximation, the dispersion has been corrected as described in Section 2, and the waist and cross-plane coupling corrections have been completed as outlined in Section 3.2. Hence α_x, α_y and all the cross-plane terms in the beam σ-matrix* at the IP are approximately zero. The assumed initial σ-matrix ("0^{th} iteration") is:

$$\sigma^{IP}(0) = \begin{pmatrix} \beta_x^*(0)\epsilon_x & 0 & 0 & 0 \\ 0 & \epsilon_x/\beta_x^*(0) & 0 & 0 \\ 0 & 0 & \beta_y^*(0)\epsilon_y & 0 \\ 0 & 0 & 0 & \epsilon_y/\beta_y^*(0) \end{pmatrix} \qquad (3.1)$$

It is diagonal and can be specified by four independent parameters. Any two out of σ_x^* (spatial size at IP $= \sqrt{\sigma_{11}}$), $\sigma_x'^*$ (angular size at IP $= \sqrt{\sigma_{22}}$), ϵ_x (emittance) and β_x^* (betatron function at IP) can be measured to determine the initial σ_x^{IP} matrix, and similarly for y.

The σ matrix of the beam at the end of the Arc is then:

$$\sigma^{ARC} = R^{-1}(\underline{k}(0)) \,.\, \sigma^{IP}(0) \,.\, \left[R^{-1}(\underline{k}(0))\right]^T \qquad (3.2)$$

where $R(\underline{k}(0))$ is the initial transfer matrix from the end of the Arc to the IP and

$$\underline{k}(0) = k_1(0), k_2(0), \ldots, k_n(0) \qquad (3.3)$$

are the initial strengths of the n quadrupoles and skew quadrupoles in the Final Focus beam line which are used for the betatron matching.

* The notation used for σ-matrix elements is the same as that described on pages 33-35 of the TRANSPORT manual.[4] For simplicity, only the first four columns and rows of the σ-matrix are shown.

The goal after the 1st iteration of betatron matching is to find a new set of strengths, $\underline{k}(1)$, such that:

$$\sigma^{\mathrm{IP}}(1) = R(\underline{k}(1)) \cdot \sigma^{\mathrm{ARC}} \cdot [R(\underline{k}(1))]^{\mathrm{T}} = \begin{pmatrix} \beta_x^*(1)\epsilon_x & 0 & 0 & 0 \\ 0 & \epsilon_x/\beta_x^*(1) & 0 & 0 \\ 0 & 0 & \beta_y^*(1)\epsilon_y & 0 \\ 0 & 0 & 0 & \epsilon_y/\beta_y^*(1) \end{pmatrix} \tag{3.4}$$

is the desired σ-matrix at the IP. To go from equation (3.1) to (3.4) the spatial magnification is changed by a factor of $\sqrt{\beta^*(1)/\beta^*(0)}$ (which may be different in x and y), while the off-diagonal terms (α_x, α_y and cross-plane coupling) are kept at zero. The details of the fitting algorithm used are presented in Appendix C. The quadrupole strengths, $\underline{k}(1)$, returned by the fitter after the first iteration can be used to set the physical magnets on the beam line.

The beam spot is then remeasured and further iterations of the matching procedure are implemented to optimise the luminosity.

One example of a small spot measured during the 1987 SLC commissioning is shown in Fig. 5. At the time of writing the smallest electron spot sizes which have so far been obtained were measured at 3-4 microns. Simultaneous electron and positron spot sizes of 5-7 microns can be reproduced without difficulty. Commissioning work is continuing to bring the SLC parameters up to the level necessary for the production of Z^0 events.

APPENDIX A

MODELLING CROSS-PLANE COUPLING

A1 TWISS PARAMETERS

In the SLC control program[9] the standard online optical model of the machine[10] is stored in the form of so-called Twiss parameters at each significant point along the beam line:

ψ_x = the horizontal betatron phase or tune (sometimes denoted by ν_x)
β_x = the horizontal betatron function
α_x = the horizontal alpha function
η_x = the horizontal spatial dispersion
η'_x = the horizontal angular dispersion

and similarly in the vertical (y) direction. The Twiss parameters are generated by running the program COMFORT (Version 3),[11] using as input either design parameters or values taken from the SLC online database.[10,9]

In order to model a section of the beam line between points A and B it is necessary to know the 6×6 first order beam transfer matrix,* R, from A to B. If the optics in x and y planes are independent then it can be written in the form:

$$R = \begin{pmatrix} R_{11} & R_{12} & 0 & 0 & 0 & R_{16} \\ R_{21} & R_{22} & 0 & 0 & 0 & R_{26} \\ 0 & 0 & R_{33} & R_{34} & 0 & R_{36} \\ 0 & 0 & R_{43} & R_{44} & 0 & R_{46} \\ 0 & 0 & 0 & 0 & 1 & 0 \\ 0 & 0 & 0 & 0 & 0 & 1 \end{pmatrix} \tag{A1}$$

with all cross-plane coupling elements at zero.

* The notation used for transfer matrix elements is that described on pages 4 and 5 of the TRANSPORT manual.[4]

In this case the elements of R can be evaluated from the Twiss parameters at points A and B using standard formulae. For x:

$$\begin{aligned} R_{11} &= \sqrt{\beta_B/\beta_A}(\cos\Delta\psi + \alpha_A \sin\Delta\psi) \\ R_{12} &= \sqrt{\beta_A\beta_B}\sin\Delta\psi \\ R_{16} &= \eta_B - R_{11}\eta_A - R_{12}\eta'_A \\ R_{21} &= -\{(1+\alpha_A\alpha_B)\sin\Delta\psi + (\alpha_B - \alpha_A)\cos\Delta\psi\}/\sqrt{\beta_A\beta_B} \\ R_{22} &= \sqrt{\beta_A/\beta_B}(\cos\Delta\psi - \alpha_B\sin\Delta\psi) \\ R_{26} &= \eta'_B - R_{21}\eta_A - R_{22}\eta'_A \end{aligned} \tag{A2}$$

where $\Delta\psi = \psi_B - \psi_A$

For y, these formulae give R_{33}, R_{34}, R_{36}, R_{43}, R_{44} and R_{46} respectively. To obtain the transfer matrix elements only the change in the Twiss parameters between points A and B is needed. Their absolute values at each point are not important for this purpose.

A2 CROSS-PLANE COUPLING

The procedure outlined in Section A1 is valid only if there is no coupling between x and y planes since the x and y Twiss parameters are assumed to be independent. That is, it works only if the transfer matrix can be written in the form of equation (A1).

This is a valid representation for most standard beam line elements, but it is invalid for skew quadrupoles and rotations of the coordinate system (rolls). Since skew quadrupoles play a vital part in the SLC Final Focus optics it was necessary to modify the online modelling.

One solution would be to abandon the present model and replace it with one where the full two-dimensional transfer matrix to each beam line point is stored. Since COMFORT (Version 3)[11] does not include cross-plane coupling this would also need to be upgraded.†

Instead it was decided to keep the Twiss parameters and to add a relatively small amount of extra dedicated Final Focus modelling and fitting code to handle cross-plane coupling where this was necessary. To do this the model beam line is divided into a series of discrete, sequential sections of two sorts:

(a) those for which cross-plane coupling is unimportant, i.e. there are no skew quadrupoles, rolls or similar beam line elements;

(b) those for which cross-plane coupling is important.

For category (a) the online Twiss parameters for the points at the beginning and end of the section are sufficient. The full two-dimensional transfer matrix can be found using equations (A2) and (A1).

For category (b) the Twiss parameters cannot be used. However, these sections can be reduced so that they consist of just a single beam line element – a single skew quadrupole or a roll, for example. In these cases the full two-dimensional transfer matrix can be determined separately using a small number of input parameters taken from the online database. In the case of a skew quadrupole the data required are the integrated magnetic field gradient (strength), the effective length of the magnet, the skew angle and the energy and charge of the beam.

Thus a set of consecutive transfer matrices is produced, running between each of the points along the whole beam line. By multiplying this string of matrices together in the correct sequence the cumulative transfer matrix between any two of the points can be obtained. This is all that is needed for a model incorporating cross-plane coupling.

It is sometimes useful to enlarge category (b) above. For example, to perform a fit in which the magnetic strengths of certain quadrupoles are allowed to vary

† When COMFORT is used to generate Twiss parameters for the present online model rolls are ignored and skew quadrupoles are treated as drift spaces.

in the model, each of these quadrupoles is treated as a separate beam line section. After each iteration of the fit, their transfer matrices are recalculated using the new magnetic strengths and hence the cumulative transfer matrix for the whole beam line is updated. This technique is used in the programs for the dispersion and betatron matching which are described in the main text.

APPENDIX B

DETERMINATION OF SPATIAL AND ANGULAR DISPERSION

This Appendix describes the fitting technique used to determine the spatial and angular dispersion at any point P from spatial dispersion measurements made by beam position monitors.

Measure η_x^i and η_y^i, i = 1,N, the spatial dispersions in x and y at N points. Using a model of the beam line, as explained in Appendix A, evaluate the transfer matrices, R^i, between P and each of the measurement points. From the first and third rows of each transfer matrix a new matrix, A, of dimensions $4 \times 2N$, can be formed, which relates the spatial and angular dispersions at the point P to the spatial dispersion measurements:-

$$\Delta\underline{\eta} = A\,\underline{\eta}^P \tag{B1}$$

where

$$\Delta\underline{\eta} = \left(\eta_x^1 - R_{16}^1, \eta_y^1 - R_{36}^1, \eta_x^2 - R_{16}^2, \ldots, \eta_x^N - R_{16}^N, \eta_y^N - R_{36}^N\right) \tag{B2}$$

$$\underline{\eta}^P = \left(\eta_x^P, \eta_x'^P, \eta_y^P, \eta_y'^P\right) \tag{B3}$$

and the rows of A are formed from the rows of R^i by (j=1,4):

$$\begin{aligned} A_{1j} &= R_{1j}^1 \\ A_{2j} &= R_{3j}^1 \\ A_{3j} &= R_{1j}^2 \\ &\vdots \\ A_{(2N-1)j} &= R_{1j}^N \\ A_{2Nj} &= R_{3j}^N \end{aligned} \tag{B4}$$

The R_{16} (R_{36}) elements are subtracted from the η_x (η_y) measurements in order to eliminate the lattice dispersion component which the model associates with the beam line between P and the measurement points. The remainder, $\Delta\underline{\eta}$, is the spatial dispersion at the points associated solely with the dispersion at P.

In order to solve for $\underline{\eta}^P$ the matrix equation (B1) must be inverted. Since A is not a square matrix the solution is not unique. The estimated uncertainties, σ_i, on the η_i measurements can be used as weighting factors to obtain a unique inversion. The χ^2 sum:-

$$\sum_{i=1}^{2N} \left\{ \frac{\left(\sum_{j=1}^{4} A_{ij}\eta_j^P\right) - \Delta\eta_i}{\sigma_i} \right\}^2 \tag{B5}$$

is minimised by taking

$$\underline{\eta}^P = (BA)^{-1} B\,\Delta\underline{\eta} \tag{B6}$$

where the elements of the $2N \times 4$ dimensional matrix B are formed from those of A by

$$B_{ji} = \frac{A_{ij}}{\sigma_i^2} \tag{B7}$$

Hence the spatial and angular dispersions at P can be inferred from the measurements.

APPENDIX C

FITTING ALGORITHM FOR BETATRON MATCHING

The details of the fitting algorithm used for the betatron matching scheme described in Section 3.3 are presented in this Appendix.

The least squares fitting program NPSLAC[7] is used. The strengths, $\underline{k}$, of all the quadrupoles to be used for the betatron matching are varied and $R(\underline{k})$, the transfer matrix from the end of the Arc to the IP, and σ^{IP}, the beam σ-matrix at the IP, are evaluated for each new set. The program minimises a sum of squares composed from the elements of σ^{IP}:

$$(\beta_x \text{ term})^2 + (\beta_y \text{ term})^2 + \left(\frac{\sigma_{12}}{\sqrt{\sigma_{11}\sigma_{22}}}\right)^2 + \left(\frac{\sigma_{34}}{\sqrt{\sigma_{33}\sigma_{44}}}\right)^2$$

$$+\left(\frac{\sigma_{13}}{\sqrt{\sigma_{11}\sigma_{33}}}\right)^2 + \left(\frac{\sigma_{24}}{\sqrt{\sigma_{22}\sigma_{44}}}\right)^2 + \left(\frac{\sigma_{23}}{\sqrt{\sigma_{22}\sigma_{33}}}\right)^2 + \left(\frac{\sigma_{14}}{\sqrt{\sigma_{11}\sigma_{44}}}\right)^2 \tag{C1}$$

Depending on the input beam parameters some of these terms may be omitted from the sum so that those σ-elements remain free.

The third and fourth terms of this sum constrain α_x and α_y to remain at zero and hence keep the beam waists at the IP. The last four terms keep all cross-plane coupling terms at zero. The denominators make each term a dimensionless and reasonably scaled number.

Studies using offline simulations[12,8] have shown that different expressions are needed for the "β_x term" and "β_y term" depending on the initial input, in order to ensure that the fit converges rapidly and reliably. For many input conditions, using:

$$\beta_x \text{ term} = \frac{\sigma_{22} - \epsilon_x/\beta_x^*(1)}{\epsilon_x/\beta_x^*(1)} \tag{C2}$$

(similarly for β_y) is found to give satisfactory results. This is equivalent to fitting the angular beam size. Sometimes it is better to fit the spatial beam size:

$$\beta_x \text{ term} = \frac{\sigma_{11} - \beta_x^*(1)\epsilon_x}{\beta_x^*(1)\epsilon_x} \tag{C3}$$

or sometimes spatial and angular sizes together.

For both cases (C2) and (C3) it is necessary to constrain the R_{22} and R_{44} elements of the transfer matrix between the end of the Arc and the IP to remain less than zero. This ensures that the fit converges to the correct minimum.* For difficult situations, such as having unequal emittances in x and y, it is sometimes better to fit these elements directly:

$$\beta_x \text{ term} = \frac{R_{22} - R_{22}(\text{fit})}{R_{22}(\text{fit})} \tag{C4}$$

where $R_{22}(\text{fit}) = R_{22}(\underline{k}(0))\sqrt{\beta_x^*(0)/\beta_x^*(1)}$.

The efficiency and resilience of the fitting program can also be improved by splitting the minimisation up into several steps. The output from step number n is used as the input to step number n+1. The steps are chosen to guide the fitter along a path which is known to lead towards the desired minimum, taking into account the properties of the optics of the Final Focus beam line. For a range of input conditions the following two-step fit is found to be suitable:

(a) Fit β_x, β_y and minimise σ_{13}, leaving other σ-elements free. Only two upright quadrupoles (17 and 16) and the nearby skew quadrupole (SQ17.5) are allowed to vary in the fit, all others having their strengths fixed. These quadrupoles are in the First Telescope and are the ones most sensitive to β_x, β_y and σ_{13}. Quadrupoles 17 and 16 control the overall demagnification factor of the Final Focus and are the ones whose strengths are changed most during the betatron matching.

* A solution with R_{22} or R_{44} greater than zero corresponds to having an extra beam waist, in x or y, upstream from the IP.

(b) Minimise α_x, α_y and σ_{23} while keeping β_x, β_y and σ_{13} at the values they have after step (a). In addition to the three quadrupoles varied during step (a), two more upright quadrupoles (3 and 2B) and the nearby skew quadrupole (SQ3) are also allowed to vary. These are in the Final Telescope. Step (b) amounts to a minor retuning of the optics to reposition the horizontal and vertical beam waists at the IP ($\alpha = 0$) and eliminate remaining cross-plane coupling.

This two-step fit is the default used in the SLC control program, but great flexibility is available for changing the fitting algorithm when necessary.

ACKNOWLEDGEMENTS

We wish to thank all the people who have helped in the design and commissioning of the Final Focus and the rest of the SLC.

Karl Brown, Ted Fieguth and Joe Murray designed the optics of the Final Focus. Ted, Joe and Dave Ritson contributed in several major ways to the tuning algorithms and correction procedures that were evolved and that are now used.

Len Sweeney wrote all the code that was necessary for communication between the modelling and fitting programs described in this paper and the rest of the SLC control system. He also produced the control panels and displays. Witold Kozanecki, Nan Phinney and Martin Lee have provided much helpful advice.

We also thank Margaret Wright and Philip Gill of the Systems Optimization Laboratory of Stanford University for creating a modified version (NPSLAC) of their NPSOL[7] fitting package for use in SLC optical modelling.

REFERENCES

1. SLC Design Handbook, SLAC (December 1984)

2. Roger A. Erickson: Final Focus Systems for Linear Colliders, U.S. Summer School on High Energy Particle Accelerators (Batavia, Illinois; August 1984). SLAC-PUB-4479 (November 1987)
   J.J. Murray, K.L. Brown, T. Fieguth: The Completed Design of the SLC Final Focus System, Particle Accelerator Conference (Washington, DC; March 1987). SLAC-PUB-4219 (February 1987)
   Karl L. Brown: A Conceptual Design of Final Focus Systems for Linear Colliders, Joint US-CERN School on Particle Accelerators (South Padre, Texas; October 1986). SLAC-PUB-4159 (June 1987)

3. P.S. Bambade: Beam Dynamics in the SLC Final Focus System, Particle Accelerator Conference (Washington, DC; March 1987). SLAC-PUB-4227 (June 1987)

4. K.L. Brown, F. Rothacker, D.C. Carey, Ch. Iselin: TRANSPORT – A Computer Program for Designing Charged Particle Beam Transport Systems, SLAC-91, Rev. 2 (May 1977)

5. Miguel Flores: Correlation Plots Dispersion Function Measurement Utility (February 1987), unpublished

6. C. Field et al: A High Resolution Wire Scanner for Micron-Size Profile Measurements at the SLC, to be published. SLAC-PUB-4605 (April 1988)

7. NPSLAC is a modified version of the fitting package, NPSOL: Philip E. Gill, Walter Murray, Michael A. Saunders, Margaret H. Wright: User's Guide for NPSOL (Version 4.0): A Fortran Package for Nonlinear Programming, Technical Report SOL 86-2, Systems Optimization Laboratory, Stanford, CA 94305 (January 1986)
   Differences between NPSOL and NPSLAC are discussed in an internal SLAC Single Pass Collider Memo: Chris Hawkes, Martin Lee: Recent Upgrading of the Modelling Program COMFORT, CN-342 (September 1986)

8. W. Kozanecki: Progress Report on the SLAC Linear Collider, International Europhysics Conference on High Energy Physics (Uppsala, Sweden; June-July 1987). SLAC-PUB-4465 (November 1987)

9. N. Phinney, H. Shoaee: The SLC Control System – Status and Development, Particle Accelerator Conference (Washington, DC; March 1987). SLAC-PUB-4215 (March 1987)
   N. Phinney: Report on the SLC Control System, IEEE Trans. Nucl. Sci., NS-32 no. 5, 2117 (1985). SLAC-PUB-3668 (May 1985)
   R.E. Melen: Design and Performance of the Stanford Linear Collider Control System, IEEE Trans. Nucl. Sci., NS-32 no. 1, 230 (1985). SLAC-PUB-3467 (October 1984)

10. M.D. Woodley, L. Sanchez-Chopitea, H. Shoaee: Application of Online Modeling to the Operation of SLC, Particle Accelerator Conference (Washington, DC; March 1987). SLAC-PUB-4249 (February 1987)
    J.C. Sheppard, R.H. Helm, M.J. Lee, M.D. Woodley: On-Line Control Models for the Stanford Linear Collider, IEEE Trans. Nucl. Sci., NS-30 no. 4, 2320 (1983). SLAC-PUB-3072 (March 1983)

11. L. Sanchez, H. Shoaee, M. Woodley: COMFORT – Control of Machine Functions, Orbits, and Trajectories, Version 3.0, SLAC (March 1986), unpublished
    M.D. Woodley, M.J. Lee, J. Jäger, A.S. King: Control of Machine Functions or Transport Systems, IEEE Trans. Nucl. Sci., NS-30 no. 4, 2367 (1983). SLAC-PUB-3086 (March 1983)
    See also Ref. 10.

12. W. Kozanecki: private communication

FIGURE CAPTIONS

1. The optical design of the SLC Final Focus. The four quadrupoles used for the dispersion correction are shown cross-hatched and the six quadrupoles used for betatron matching are shown shaded.

2. Betatron and dispersion functions of the SLC Final Focus. The η_y function (not shown) is zero everywhere. The solid curves show the SLC design whereas the dash-dotted curves show β_x and β_y in the detuned $\beta^* = 30\,\text{mm}$ configuration described in Section 3.2 of the main text.

3. Dispersion Measurement Technique. To measure the lattice dispersion of a section of beam line from A to B (here represented as a single bend magnet) the beam energy is increased from E to $E + \Delta E$ and the beam deflection at point B, Δx, is measured using a BPM. The dispersion is $\Delta x/(\Delta E/E)$. If the beam dispersion at A is zero then this is a measure of η_x^B, the beam dispersion at B. In practice the dispersion is obtained by averaging over a scan of several different beam energies, and at each energy point Δx is measured by taking the average of several BPM readings on successive beam pulses.

4. The First Telescope Dispersion Correction. The horizontal (upper figures) and vertical (lower figures) dispersion is shown before (left) and after (right) correction, using an example of data taken during the 1987 SLC commissioning. Note the changes in scale. In each figure the error bars on the solid curve show the results of simultaneous dispersion measurements on the electron beam using BPMs in the SLC North Arc and the η-Matching, First Telescope and Chromatic Correction Sections of the North Final Focus. The solid curve is a series of straight lines joining these measurement points. The dotted curve is a series of straight lines joining points showing the corresponding value of the design dispersion at the location of each of the BPMs. After correction the measured dispersion in the η-Matching and First Telescope Sections is very close to the design values.

5. An example of a transverse scan of the electron beam at the Interaction Point, using wire scanner data from the 1987 SLC commissioning. Unfolding the 3.5 micron size of the wire target gives a corrected beam size of 4.6 microns.

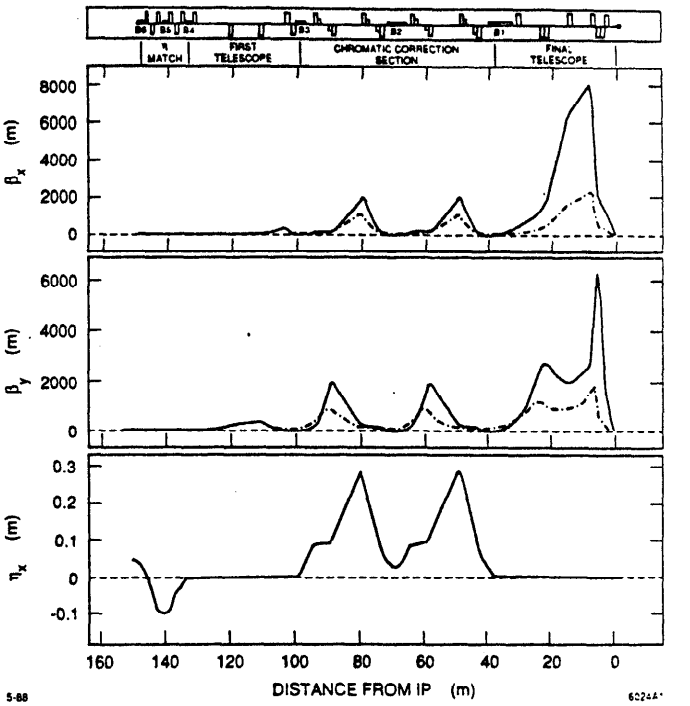

Fig. 2

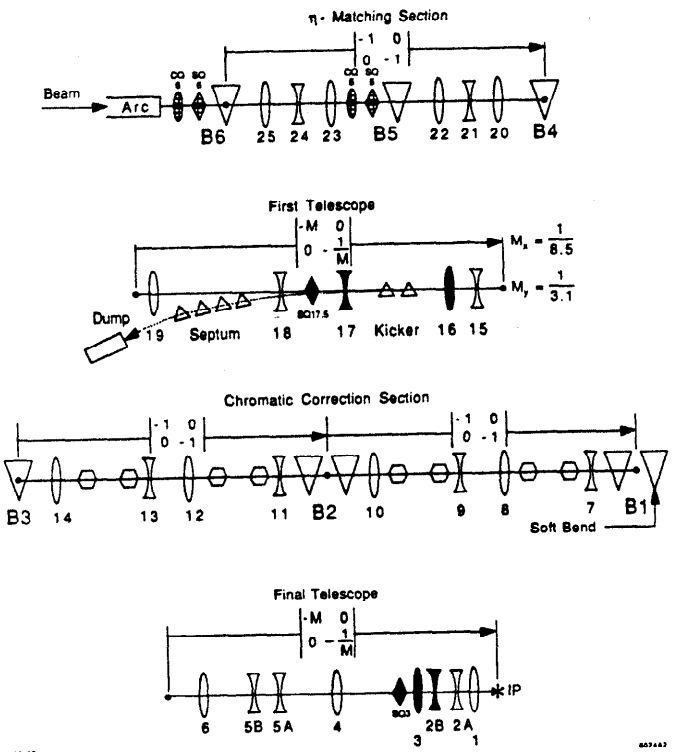

Fig. 1

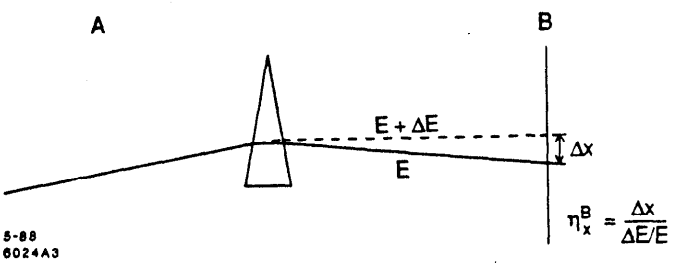

Fig. 3

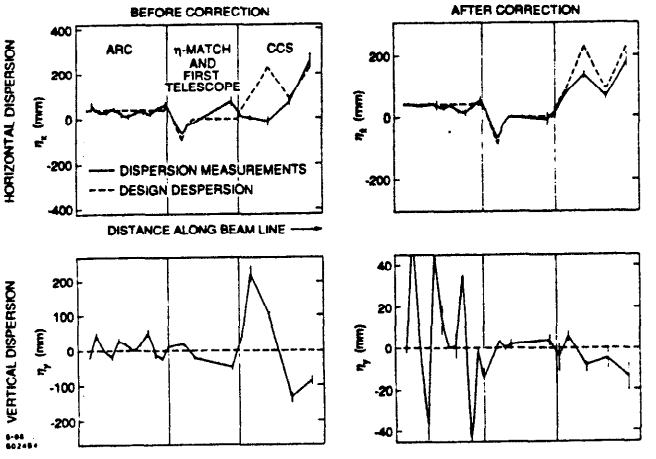
BEFORE CORRECTION
AFTER CORRECTION
HORIZONTAL DISPERSION
ARC
η-MATCH AND FIRST TELESCOPE
CCS
DISPERSION MEASUREMENTS
DESIGN DESPERSION
DISTANCE ALONG BEAM LINE
VERTICAL DISPERSION

Fig. 4

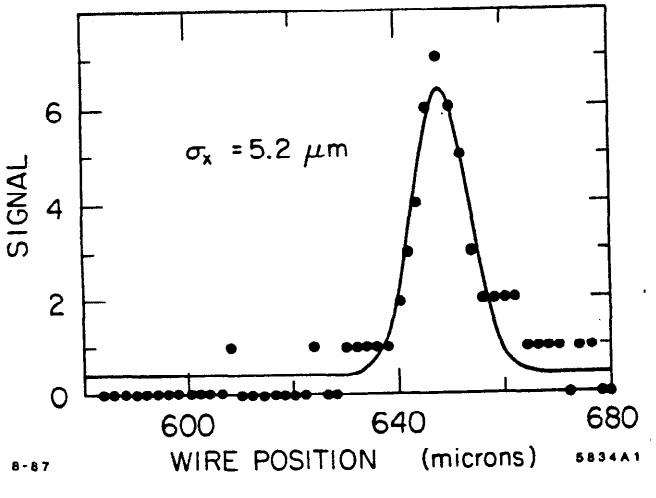
SIGNAL
σx = 5.2 μm
WIRE POSITION (microns)
8-87
5834A1

Fig. 5

VII.4 "Operational Experience with Optical Matching in the SLC Final Focus System"

This conference article summarizes the experience acquired with the optical tuning algorithm developed for the final focus. The algorithm and some of the control software are reviewed, and a comprehensive set of measurements are presented. The algorithm has allowed to focus spots at the collision point with transverse sizes of 3 to 5μm, and to diagnose its various components. The residual beam size at the collision point is limited by a somewhat larger than nominal emittance delivered by the linear accelerator, and by the requirement to minimize backgrounds in the detector, from which a larger than nominal β^* parameter must be used.

SLAC-PUB-4776
January 1989
(A)

OPERATIONAL EXPERIENCE WITH OPTICAL MATCHING IN THE SLC FINAL FOCUS SYSTEM*

P. BAMBADE,* P. BURCHAT,† D. BURKE, W. FORD,‡ C. HAWKES,§ W. KOSKA,¶
W. KOZANECKI, T. LOHSE, T. MATTISON, N. PHINNEY, M. PLACIDI,* D. RITSON, S. WAGNER‡

Stanford Linear Accelerator Center, Stanford, University, Stanford, CA 94309

ABSTRACT

In the SLC Final Focus System, all components of transverse phase-space and the couplings between them must be controlled to minimize the beam size at the interaction point. After summarizing the experimental algorithm and the on-line tuning programs, we present a consistent set of measurements and describe our present understanding of the various contributions to this beam size.

INTRODUCTION

The Final Focus System[1] (FFS) is the last section of beam-line in the Stanford Linear Collider (SLC) before the interaction point (IP). Its main function is to maximize the luminosity by focusing the beam to the smallest possible size. Because the beam has a finite emittance and energy spread, a nominal beam size of 2 μm at the IP can only be achieved with elaborate optics where higher order aberrations are carefully minimized.[2] In operation the FFS must also be *tunable* to absorb focusing errors accumulated in the transport lines upstream and in the FFS itself.[3] Effects from such errors manifest themselves primarily as linear mismatches between the transverse phase-space of the injected beam and the FFS optics, and must be corrected before the final focusing works properly. An experimental tuning algorithm has been developed[3] to achieve these corrections, and extensive operational experience has been acquired.[4]

Initially it was thought that this tuning would be used as an overall correction for mismatches accumulated in the entire SLC, or at least in the Arcs: except for a few special cases, it is possible in principle to absorb optical distortions of up to a factor of four.[3] It was also thought that variations would be tuned continuously in the FFS. Neither appears to be feasible. Elimination of backgrounds[5] in the detector from electromagnetic debris and muons produced when beam-tails strike aperture limits upstream of the matching elements requires a nearly matched phase-space at injection. Thus, major mismatches must be corrected upstream, and in practice only small adjustments are made in the FFS. The main limitations to continuous optical feedback are lack of orthogonality in the corrections and the fact that the only place available to diagnose all the distortions is the higher order corrected focal point at the IP. As a result of non-orthogonality, even modest variations in the incoming phase-space can require extensive re-tuning. These weaknesses result from *adding-on* the optical and background tuning strategies to a design where the basic architecture was already fixed, and suffered from severe space limitations.

Operationally, the optical tuning has evolved towards determining a stable set-up. Partly because the Linac emittance presently exceeds the design value by a factor of about three in the horizontal plane,[6] the optics must be configured with a larger than optimal β-function at the IP (β^*), in order to reduce backgrounds generated in the last quadrupoles by the beam tails. The larger β^* and Linac emittance limit the attainable luminosity. Phase-space parameters are monitored routinely to distinguish stable changes from spurious ones, and to base corrections on time-averaged quantities. After reviewing the optics, the tuning strategy and the on-line programs used, we describe measurements made with the electron beam in the last run (September 1988). Similar results have been obtained with the positron beam.

SUMMARY OF OPTICS

The FFS consists of four telescopic modules (Fig. 1). Optical demagnification is achieved in the first and final telescopes, which straddle a chromatic correction section where the intrinsic first-order chromaticity of the beam-line is compensated. The Arc lattice η- and β-functions are matched in the η-match section and in the first telescope, respectively.

The optimization of the chromatic correction is the central point of the design.[2] The Chromatic Correction Section (CCS) consists of two $-I$ telescopes, combined with dipoles at the foci, to generate significant energy dispersion at the quadrupoles. Sextupoles, where the focusing strength varies linearly with excursion, are put near the quadrupoles to provide additional focusing proportional to energy. This allows cancellation of the intrinsic first-order chromaticity. Additional first-order perturbations to the imaging produced by each sextupole are made to cancel over the length of the CCS by appropriate symmetries. In this way, all residual perturbations are pushed to second-order. The effective β^* can thus be written:

$$\beta^*_{eff} \simeq \beta^* + \kappa_1^2 \frac{\delta_E^4}{\beta^*} + \kappa_2^2 \frac{\epsilon\delta_E^2}{\beta^{*2}} + \kappa_3^2 \frac{\epsilon^2}{\beta^{*3}} \quad , \qquad (1)$$

where $\kappa_{1,2,3}$ measure the magnitudes of the residual second-order chromatic and geometric perturbations, ϵ is the emittance, and δ_E is the fractional energy spread.

The effect of the chromatic correction is to broaden the energy band-pass over which rays are imaged to the same IP focal point. The width of this band-pass scales roughly as $\sqrt{\beta^*}$ (if

* Work supported by the Department of Energy, contracts DE-AC03-76SF00515, DE-AC02-76ER01112, DE-AC02-86ER40253, DE-AC03-81ER40050 and DE-AM03-76SF00010.

⋆ PRESENT ADDRESS: LABORATOIRE DE L'ACCÉLÉRATEUR LINÉAIRE, BÂT. 200, ORSAY, FRANCE 91405
† UNIVERSITY OF CALIFORNIA, SANTA CRUZ, CA 95064.
‡ UNIVERSITY OF COLORADO, BOULDER, CO 80309.
§ CALIFORNIA INSTITUTE OF TECHNOLOGY, PASADENA, CA 91125.
¶ UNIVERSITY OF MICHIGAN, ANN ARBOR, MI 48109.
* CERN, CH-1211, GENEVA, 23, SWITZERLAND

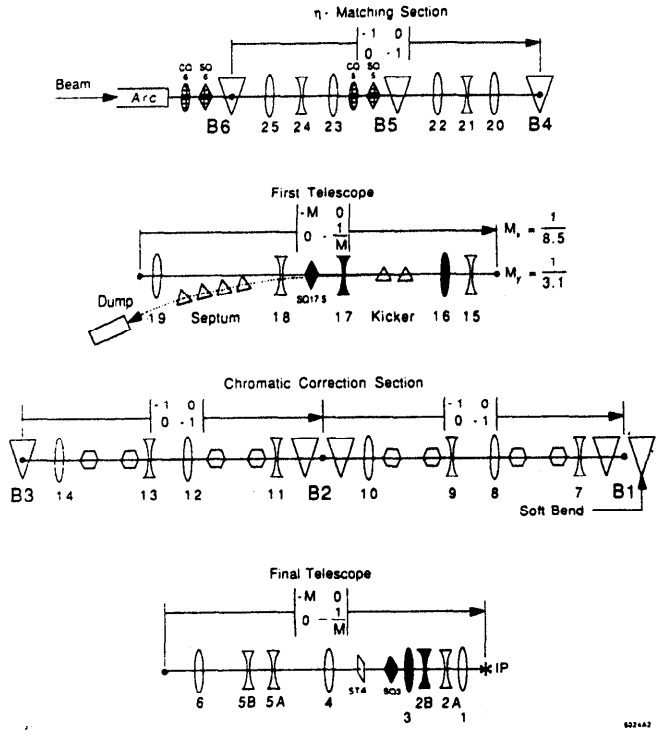

Fig. 1. Schematic of the Final Focus. The four quadrupoles used for dispersion corrections are shown cross-hatched, and the six quadrupoles used for betatron corrections are shown shaded.

only the term in κ_1 from (1) is used).[2] Defining it quantitatively as the band of energy deviations for which $\beta^*_{eff} \leq 1.25\beta^*$, it is $\pm 0.5\%$ for $\beta^* = 16$ mm, and $\pm 0.22\%$ for $\beta^* = 4$ mm. Without chromatic correction, it is less than $\pm 0.05\%$ in both cases (Fig. 2).

emittances from correcting only these ten distortions. is close to $4r/(1+r)^2$, where r is the ratio of the smaller to the larger emittance.[8] The reduction can become severe for $r < 1/4$.

The distortions are best characterized by what matters physically at the IP:

1. Five correlations of positions to angles and energy: σ_{21}, σ_{43}, $\sigma_{32} = -\sigma_{41}$, η_x and η_y, corresponding respectively to longitudinal offsets of the waists in both planes at the IP (we refer to these as offsets of the *in-plane* waists), cross-plane coupling (by analogy we refer to this as an offset of the *out-of-plane* waist), and residual spatial dispersion. The waists must be positioned to within some fraction of the depth of focus β^* of the demagnifying optics, and the dispersion η must be tuned to less than $\sqrt{\epsilon\beta^*}/\delta_E$ to avoid dominating the final spot size.
2. Five terms affecting the angular spread at the IP: σ_{22}, σ_{44}, $\sigma_{31} = \sigma_{42}$, $\eta_{x'}$ and $\eta_{y'}$, determine the band-pass of the optics. This is illustrated in Fig. 3, which shows the luminosity L versus β^* for an energy spread of 0.002 ($1/\beta^*$ is taken as a measure of the overall angular spread)[3]. If the band-pass is larger than the energy spread, linear optics dominates and L drops as $1/\beta^*$. If it is smaller, L is dominated by second order chromatic and geometric perturbations and drops rapidly with decreasing β^* [see Eq. (1)]. The optimum occurs when the band-pass and energy spread are matched. For energy spreads of 0.002 now achieved[10], $\beta^*_{opt} \simeq 4$ mm. This defines the optical limit to the luminosity.

Correction elements for the above ten distortions are shown in Fig. 1. The waists are corrected with trim windings on two of the last quadrupoles just before the IP, and with a skew quadrupole just upstream. The betatron angular spread is controlled with one skew and two upright quadrupoles in the first telescope. These, combined with the waist controls, form an effective zoom-lens. Spatial and angular dispersions are corrected by perturbing the η-match with two pairs of upright and skew quadrupoles.[11]

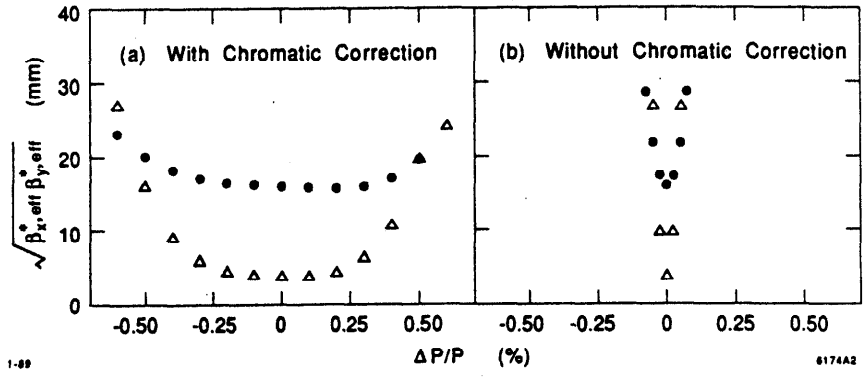

CORRECTION SCHEME

We describe the four-dimensional transverse phase-space with the usual[7] beam-matrix σ, where $\sigma_{ij} = < x_i x_j >$. The matrix σ has eight free terms if the emittances ϵ_x and ϵ_y are set. With the four dispersion functions η_x, $\eta_{x'}$, η_y and $\eta_{y'}$, we thus need twelve parameters to describe an arbitrary optical mismatch. For the SLC, equal emittances $\epsilon_x = \epsilon_y$ are specified. In this case, two of the four cross-plane coupling correlations — $\sigma_{31}, \sigma_{41}, \sigma_{32}, \sigma_{42}$ — are redundant.[8] With the condition $\sigma_{21} = \sigma_{43} = 0$ at the IP, this redundancy takes the form $\sigma_{31} = \sigma_{42}$ and $\sigma_{32} = -\sigma_{41}$.

The tuning strategy is designed for this case and thus involves ten corrections. It can be shown that the maximum luminosity reduction factor, which results in the case of unequal

TUNING STRATEGY

The flow diagram in Fig. 4 summarizes the experimental algorithm. Because each correction is coupled to the ones downstream, they must be applied sequentially.

After matching the input dispersion, the core of the program is to bring the beam to a focus at the IP in a condition such that the phase-space parameters can be correctly measured at that point. Therefore, the initial set-up has a purposely enlarged β^* of 30 mm, with the sextupoles tuned to suppress the first-order chromaticity. In addition to reducing backgrounds, this helps to avoid having the beam size at the IP dominated by the second order chromatic and geometric perturbations. It is also a guess of the most probable direction for the angular spread correction.

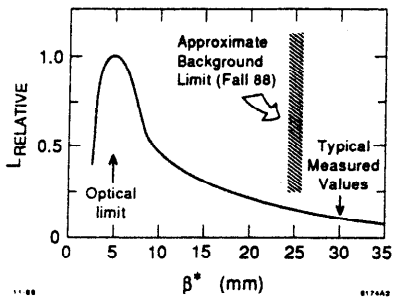

Fig. 3. Optical luminosity versus β^* in the chromaticity-corrected Final Focus, for an energy spread $\delta_E = 0.002$. The curve is obtained through a simulation.[9] The approximate background limit depends on the efficacy of the collimation and shielding, and on the beam intensity.

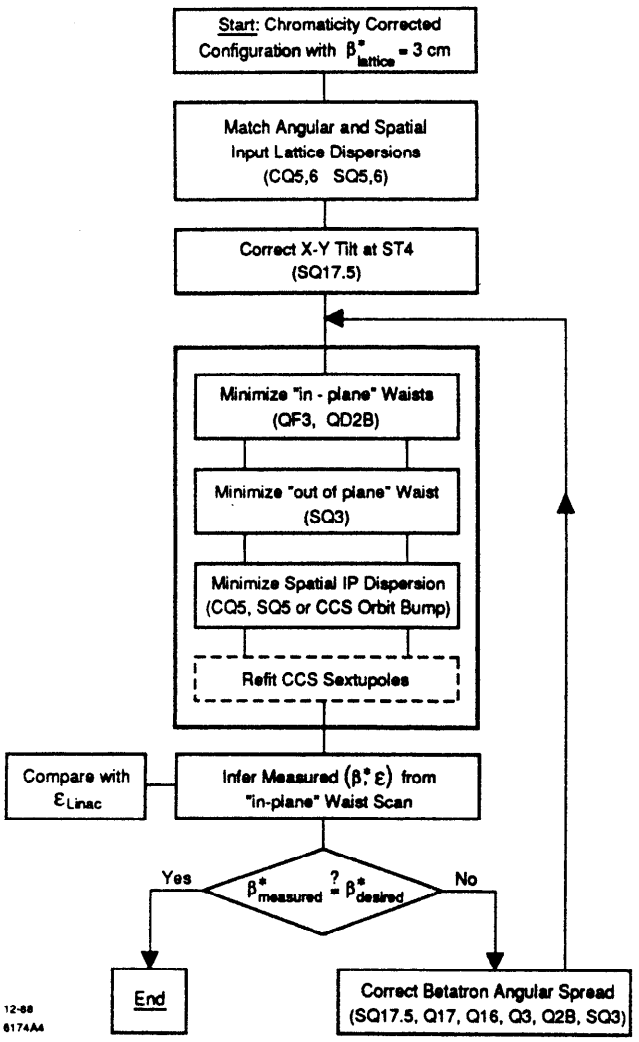

Fig. 4. Flow-diagram summarizing the application of the 10 linear optics adjustments required to minimize the IP spot.

In order to decouple the final *in-* and *out-of-plane* waist adjustments (one of the angular spread corrections) the minimization of the cross-plane σ_{42} correlation is applied first.[12] Then the beam is brought to an initial focus by correcting the *in-plane* waists. This, if residual angular dispersion is present, and if the σ_{42} correlation has been imperfectly minimized, helps to diagnose residual spatial dispersion and cross-plane σ_{32} and σ_{41} correlations in the IP beam size. It thus reduces the number of iterations of waist and dispersion corrections needed to minimize the beam size. In the case of unequal emittances, the two cross-plane correlations cannot in general be simultaneously made zero. In this case, it is advantageous to set the *out-of-plane* waist correction to minimize the beam size in the plane with the smaller emittance (typically the vertical plane). Finally, to maintain the minimization of the first-order chromaticity, the sextupoles are refitted after each major optical adjustment.

After this, and unless the angular spread at the IP is too large in spite of the $\beta^* = 3$ cm configuration, scans of the *in-plane* waists can be used to measure phase-space parameters at the IP. Inferred values of β^* are used to calculate angular spread corrections, and of ϵ to compare with measurements in the rest of the machine.

ON-LINE MATCHING PACKAGES

An on-line modeling and fitting package is required for dispersion and betatron angular spread corrections.[13]

For *dispersion matching*, the input consists of η_x and η_y measured at chosen strip-line beam position monitors, and, optionally, at the wire targets[14] which are used to diagnose the beam at the IP. The data are obtained by recording beam motion correlated with varying the energy in the Linac. The η_x and η_y values consistent with the model are determined from a fit to the measurements and give η_x, $\eta_{x'}$, η_y and $\eta_{y'}$ at the entrance to the FFS. The strengths of the four correction quadrupoles in the η-match section are then varied to minimize the four dispersion terms at the end of the first telescope or at the IP.

For corrections to the *betatron angular spread*, the waist measurements at $\beta^* = 3$ cm are used to specify an initial diagonal beam σ-matrix at the IP. The σ-matrix at the entrance to the FFS is calculated from the model. The six quadrupole strengths of the zoom-lens are then varied in a fit to give a new diagonalized σ-matrix with the desired β^* at the IP. To help convergence, considerable flexibility is incorporated, including multistep fitting and choice of which σ- and R-matrix elements to include in the χ^2 function to be minimized.

The waists are also adjusted through automated procedures, which record beam profiles measured with the wire-targets at the IP, while stepping orthogonal combinations of the two trim windings on the last quadrupoles, or the nearby skew quadrupole.[15] Estimates of β^* and ϵ are obtained by fitting

$$\sigma^2 = \epsilon\beta^* + \frac{\epsilon}{\beta^*}\Delta f^2 \qquad (2)$$

to the *in-plane* waist data, where Δf is the displacement of the waist at the IP along the beam direction. Because the squares of the beam sizes vary parabolically, the optimal correction is found, by symmetry, even if the minimum beam size is less than the wire size.

INPUT DISPERSION MATCH

Figure 5 shows measurements of the lattice dispersion, measured in the η-match, First Telescope and chromatic correction sections, before and after correction. Variations serve to diagnose changes in the set-up of the Arc and are usually correctable.[16] In this Figure the horizontal (upper figures) and vertical (lower figures) dispersion is shown before (left) and after (right) correction, using an example of data taken during the 1987 SLC commissioning. Note the changes in scale. In each figure the error bars on the solid curve show the results of simultaneous dispersion measurements on the electron beam using BPMs in the SLC North Arc and the η-Matching, First

Telescope and Chromatic Correction Sections of the North Final Focus. The solid curve is a series of straight lines joining these measurement points. The dotted curve is a series of straight lines joining points showing the corresponding value of the design dispersion at the location of each of the BPMs. After correction the measured dispersion in the η-Matching and First Telescope sections is very close to the design values. Such measurements are performed routinely to monitor the match. They are usually repeated to average out trajectory fluctuations during the measurement which can mimic dispersion mismatch. The match has been observed to be stable over periods of days to weeks.

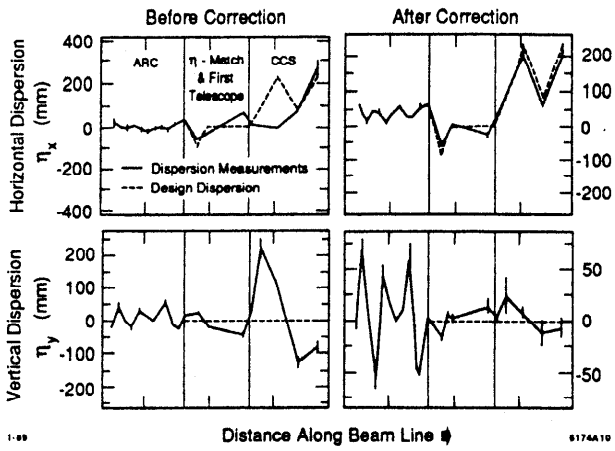

Fig. 5. The First Telescope dispersion correction.

CROSS-PLANE COUPLING CORRECTION

Figure 6 shows the correction for the tilt in the spot on a phosphor screen near the Final Triplet (ST4 in Fig. 1). A tilted spot at that point corresponds to a finite σ_{42} correlation at the IP. This is done manually by adjusting the skew quadrupole in the first telescope. The correction is difficult to set accurately and reproducibly because of changing beam tails and saturation effects on the screen. A fit of the σ_{13} correlation coefficient using the digitized profile may improve this. The available correction range is large, but the practical range is severely limited by perturbations caused to the trajectory of the opposing outgoing beam, which must pass off-axis through the skew quadrupole before reaching the final beam dump. A procedure for controlling cross-plane coupling within the Arc has been developed, which mitigates this problem substantially.[17] Such control has reduced coupling in the lattice to about 50% and has brought the FFS skew corrections to acceptable values, although this is not fully stable and depends on the ratio of emittances at the Linac exit, as described above.

WAIST ADJUSTMENTS AT THE IP

Figure 7 shows an example of a waist scan (in the vertical plane). Such scans are done routinely, allowing minimum beam sizes of 3 to 5 μm to be attained.

DISPERSON CORRECTIONS AT THE IP

There can be significant residual dispersion in the IP beam size, even after the input dispersion has been matched, due to imperfections in the FFS lattice or in the beam trajectory, or from energy-position correlations in the phase-space at the end of the Linac. Dispersion from the FFS can be measured by the online package described earlier. Corrections with the four quadrupoles in the η-match section are practical for moderate dispersions ($\eta_{IP} \leq 2$ mm). Larger dispersions, however, can require extreme corrector strengths which, in turn, also distort the betatron phase-space.

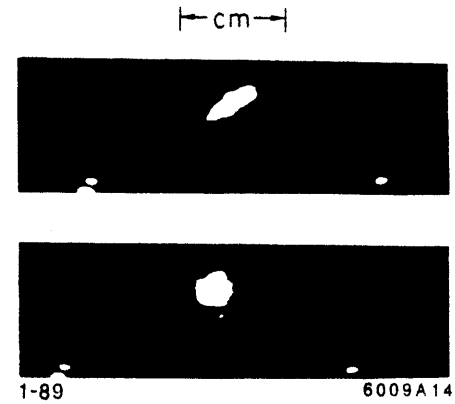

Fig. 6. Approximate correction of cross-plane coupling in the IP angular spreads, looking at the tilt in the beam shape on a screen at the high-β point in the system.

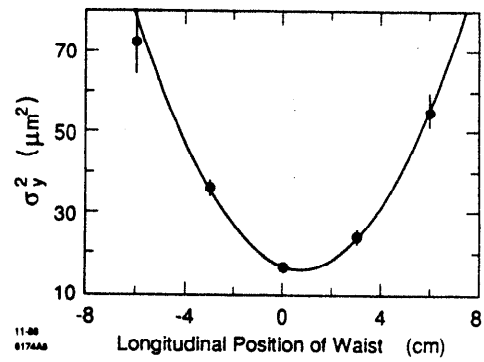

Fig. 7. Minimization of the vertical IP beam size by displacing the vertical waist with an orthogonal combination of trim windings in the last quadrupoles.

A complementary scheme for empirically minimizing residual spatial dispersion at the IP makes use of closed steering bumps in the chromatic correction section. Such orbit distortions generate spatial dispersion at the IP, through the first-order chromaticity of this section. For the range of interest, second-order chromatic and geometric perturbations remain small. An example of successfully applying this method to minimize the spot at the IP is shown in Fig. 8. In combination with the lattice dispersions measured in the first telescope and at the IP, this method has allowed separation of lattice dispersion generated in the Arcs and in the FFS. Since the spatial dispersion introduced by this bump to minimize the spot size has coincided with the previously measured lattice dispersion at the IP, it has been possible to put an upper limit on beam dispersion at the end of the Linac.

BETATRON PHASE-SPACE DIAGNOSTICS AND ADJUSTMENTS AT THE IP

History plots of ϵ and β^*, estimated from *in-plane* waist scans performed after iterating the waist and dispersion corrections to minimize the spot at the IP, are shown in Fig. 9.

The emittances ϵ_x and ϵ_y were mostly larger than nominal and reflected, in most cases, larger than nominal values in the Linac. The β^* values were larger than the expected optimum of $\beta^*_{opt} \simeq 4$ mm needed to optimize the luminosity, and resulted from requiring a small enough angular spread to minimize beam

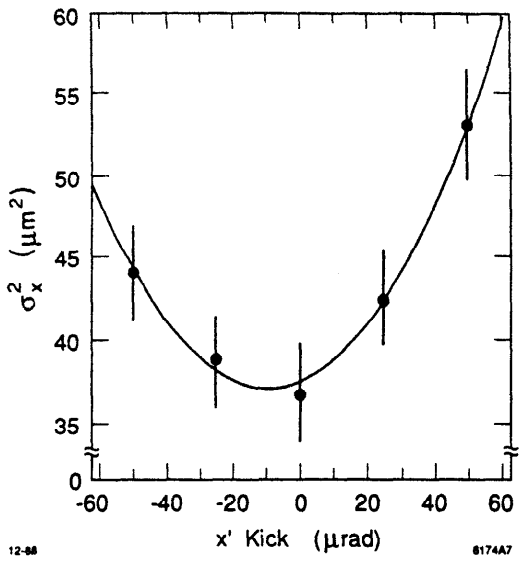

Fig. 8. Correction of residual dispersion at the IP, by minimizing the spot size with a closed dispersion-generating trajectory bump in the CCS. The parameter x'KICK is the magnitude of the kick applied by a steering dipole located at the upstream end of the CCS. A corresponding dipole at the downstream end is used to close the bump.

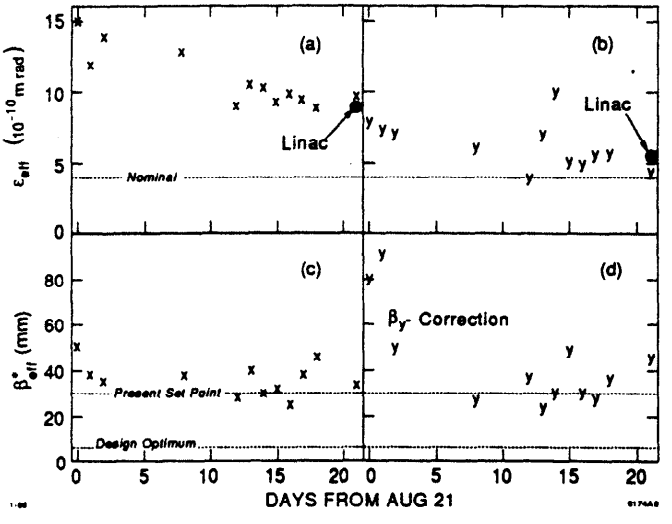

Fig. 9. History plots of the emittances and β-functions inferred from in-plane waist-scans at the IP. The effect of an initial attempt towards reducing the vertical β-function is indicated. As can be seen, at the end of the run, emittance measurements performed simultaneously at the end of the Linac and at the IP gave consistent results.

tail-induced backgrounds in the last quadrupoles. In some cases, larger than nominal *effective* ϵ and β^* values were also obtained because of an imperfectly corrected phase-space at the IP. The data in Fig. 9 are therefore generally upper limits of actual values.

A first attempt to enlarge the (vertical) betatron angular spread is indicated by an arrow in Fig. 9(d). The effect from this was clear but smaller than expected, and may have been partially offset by an upstream variation. Such adjustments will have to be iterated in order to reach the expected optimum value of $\beta^*_{opt} \simeq 4$ mm.

The last values in the plot were obtained in the final run before the September 1988 shutdown. Dispersion at the IP generated by trajectory errors and misalignments was measured and minimized with the bump technique described above. This, and several iterations of the waist corrections, resulted in emittances close to the design value in the vertical plane and too large in the horizontal by a factor of three. This was consistent with measurements performed simultaneously at the end of the Linac,[6] showing that the final beam sizes at the IP were not dominated by chromatic effects, and that the residual cross-plane coupling from the Arc did not significantly enlarge projected emittances. At that time, the linear phase-space at the IP was thus correctly estimated from these measurements.

CONCLUSION AND PROSPECTS

The experimental algorithm developed for the FFS has enabled beams focused at the IP with 3 to 5 μm transverse sizes to be attained, and the various contributions to the residual beam size to be diagnosed.

The residual beam size is presently limited by the larger than optimal β^* (dictated by detector backgrounds) and by the somewhat larger than nominal Linac emittance. The reduction in luminosity from this is about an order of magnitude. In addition, a small loss in attainable luminosity arises from not fully correcting the cross-plane coupling in the case of asymmetric emittances. This loss can be up to about 25%, with the current emittance ratio of one to three.

In the next run, a new collimation system will be available at the end of the Linac which, combined with the existing slits and with additional muon shielding that has been installed in the FFS tunnel, will enable beam tails to be cut more efficiently. This, coupled with progress in maintaining a nominal phase-space at the injection to the Arcs, and in reducing the β-function at the IP, should enable the *optical limit* to the luminosity to be reached.

ACKNOWLEDGEMENTS

We wish to thank the very large number of people, from SLAC and elsewhere, who have helped to make all this possible. In particular, we wish to acknowledge the contributions of K. Brown, R. Erickson, T. Fieguth and J. Murray, who initiated and finalized the design of the Final Focus optics, and of L. Sweeney, who contributed to much of the control software. Fieguth and Murray also initiated the work on the experimental tuning algorithm.

We also wish to acknowledge the support and enthusiasm of our colleagues from the SLC, MarkII and Operations Groups, who helped carry through many of the measurements described here.

In addition, two of us (W. F. and T. L.) were supported respectively by a Faculty Fellowship from the University of Colorado and by a grant from the Max Kade Foundation.

REFERENCES

(1) *SLC Design Handbook*, December 1984, Stanford Linear Accelerator Center.

(2) K. L. Brown, *A Conceptual Design of Final Focus Systems for Linear Colliders*, SLAC-PUB-4159 (June 1987).

(3) P. S. Bambade, *Beam Dynamics in the SLC Final Focus System*, SLAC-PUB-4227 (June 1987).

(4) P. S. Bambade, *Recent Progress at the Stanford Linear Collider*, SLAC-PUB-4610 (April 1988).

(5) D. L. Burke *et al.*, *Beam Collimation and Detector Backgrounds at e^+e^- Linear Colliders*, these proceedings.

(6) W. B. Atwood *et al.*, *Observation and Control of Emittance Growth in the SLC Linac*, these proceedings.

(7) K. L. Brown *et al.*, SLAC-91, Rev. 2, May 1977.

(8) P. S. Bambade, *Number of Dimensions of Optical Correction Space in the SLC Final Focus System,* collider note in preparation.

(9) J. J. Murray and T. Fieguth, MURTLE, private program.

(10) E. J. Soderstrom *et al.*, *Fast Energy Spectrum and Transverse Beam Profile Monitoring and Feedback Systems for the SLC Linac,* these proceedings.

(11) J. J. Murray *et al.*, *The completed design of the SLC Final Focus System,* SLAC-PUB-4219 (February 1987).

(12) P. S. Bambade, *Orthogonality of Final Waist Corrections at the IP of the SLC,* CN-369 (October 1988).

(13) C. M. Hawkes and P. S. Bambade, *First Order Optical Matching in the Final Focus Section of the SLAC Linear Collider,* SLAC-PUB-4621 (May 1988).

(14) D. L. Burke *et al.*, *Measurements of Cross Sectional Intensity Profiles of Beams at the e^+e^- Interaction Point of the SLC,* these proceedings, and submitted to Nuclear Instruments and Methods.

(15) N. Phinney *et al.*, *An Automated Focal Point Positioning and Emittance Measurement Procedure for the Interaction Point of the SLC,* these proceedings.

(16) T. H. Fieguth *et al.*, *Dispersion in the Arcs and Special Sections of the SLAC Linear Collider,* these proceedings.

(17) P. S. Bambade *et al.*, *Wirefix — Or Harmonic Corrections in the SLC Arcs,* these proceedings.

VIII. REPORT ON GENERAL STATUS

VIII.1 "Recent Progress at the Stanford Linear Collider"

This article describes the main advances in the commissioning of the SLC, during the spring, summer, and winter 1988. The seminar concentrates on the start-up of the arcs and final focus, which were the main activities in those periods.

SLAC – PUB – 4610
April 1988
(A)

RECENT PROGRESS AT THE STANFORD LINEAR COLLIDER*

P. S. BAMBADE
Stanford Linear Accelerator Center, Stanford University, Stanford, California 94309, USA

ABSTRACT

A status report on SLC commissioning is given, with special emphasis on recent progress in the Arcs and Final Focus.

INTRODUCTION

The Stanford Linear Collider (SLC) has two main goals [1]. The first is the production of high luminosity electron-positron collisions for studying the physics of the Z^0. The second is to test linear colliders as a new approach towards future high-energy machines.

Circular colliders, where counter-rotating electrons and positrons are stored, are not easily extrapolated to very high energy because of copious synchrotron radiation emitted in the bends. Both size and cost scale [2] as E^2 for an optimized design. Linear colliders avoid this by accelerating beams in linacs to the desired energy and by aiming them at each other on each pulse. More favorable scaling is predicted, but not fully established, and new problems exist. Besides the acceleration mechanism, a special challenge is the small collision point beam size needed to make up in the luminosity for low crossing rate. At the SLC, it is about 2 μm in radius. Both elaborate optics and emittance reductions via radiation damping are required. Considerable effort is also needed to preserve and control phase-space through the system. The SLC, serving to explore such problems, is an important learning experience.

PROJECT OVERVIEW

Table 1 shows the basic parameter specifications [3,4]. The design luminosity is ambitious and will take several years to reach. Initial parameters are projections based on recent progress. Fortunately, even a thousandth of the design luminosity allows to do some interesting physics.

Table 1. Basic parameters for the SLC.

	Design Goal	Initial Goal	Achieved	Units
Beam energy at IP	50	46	46	GeV
Beam energy at end of linac	51	47	53	GeV
Electrons at entrance of arcs	7×10^{10}	10^{10}	3.5×10^{10}	
Positrons at entrance of arcs	7×10^{10}	10^{10}	0.9×10^{10}	
Repetition rate	180	120 Hz	10 Hz	Hz
Normalized transverse emittance at end of linac (electrons)	3×10^{-5}	10×10^{-5}	$3\text{–}10 \times 10^{-5}$	rad-m
Spot radius at IP	1.6	4 μ	~ 4 μ	μm
Luminosity	6×10^{30}	6×10^{27}	–	$cm^{-2}sec^{-1}$

*Work supported by the Department of Energy, contract DE–AC03–76SF00515.

Invited talk presented at the 19eme Ecole de Physique des Particules, Marseille–Luminy, France, September 7–11, 1987 and at the CERN Accelerator School, Berlin, Germany, September 14–25, 1987

Figure 1 shows the entire SLC complex. Two electron bunches are generated and co-accelerated to 1.2 GeV in the Injector [5]. At 200 MeV, they are joined by a positron bunch. The three are then injected for cooling into two Damping Rings [6], from which they are extracted before the next linac pulse. The existing SLAC Linac has been upgraded [7] and co-accelerates them to 50 GeV. The 6 mm equilibrium ring bunch length is compressed to 1.5 mm before injecting into the Linac in order to minimize wakefield effects there. The last electron bunch is ejected onto a target at 33 GeV, to produce [8,9] positrons. These are returned along the length of the Linac to the 200 MeV point in the Injector. At the end of the Linac, electrons and positrons are brought into collision through two Arcs [1,10]. The Final Focus System [11-13], straddling the interaction area, demagnifies and steers the beams into collision.

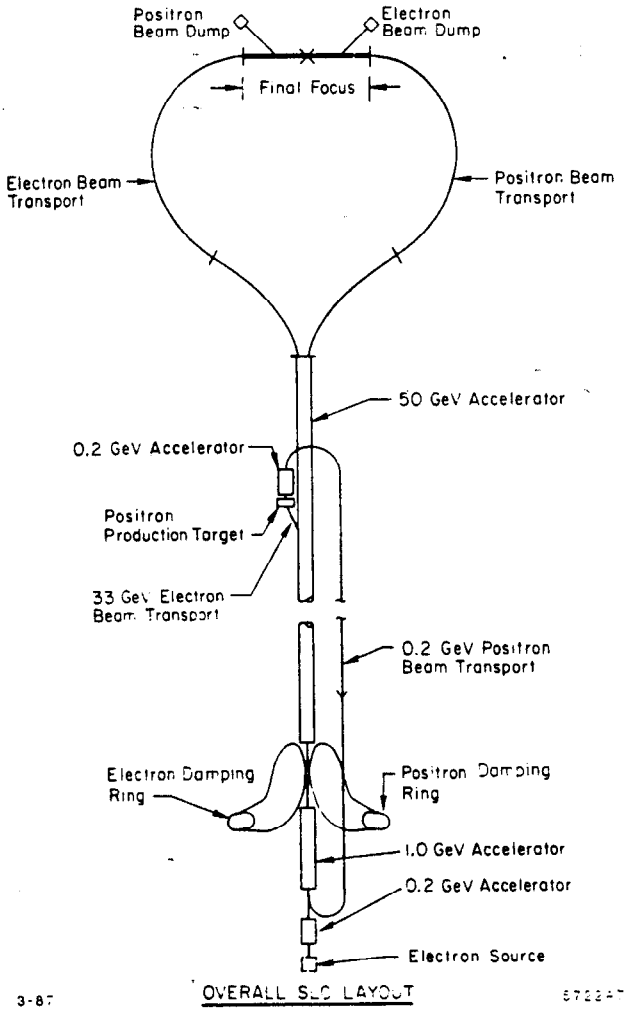

Fig. 1. The Stanford Linear Collider (SLC).

Commissioning and tests of successive stages have been ongoing since the Fall of 1981 and throughout the construction period (Fall 1984 to Spring 1987). Subsequently, much work has been devoted to the newly installed Arcs and Final Focus Systems, with continuing improvements upstream in the Linac, the Electron and Positron Sources, and in the Damping Rings. In this paper, we review the Arcs and Final

Focus activities in detail. The general status of the project, reported on numerous occasions [3,14-18], is briefly summarized.

LINAC AND SOURCES

Injector [5]

The Electron Source and Injector are specified to provide two bunches of 7×10^{10} particles with a momentum spread within the Damping Ring acceptance of $\pm 1\%$. Invariant emittances must be smaller than 180×10^{-5} mrad at 120 Hz operation. These goals are met easily for 5×10^{10} particles per bunch and the system is stabilized through computer controlled feedback.

Damping Rings [6]

The Damping Rings have provided the design invariant emittance of 3×10^{-5} mrad at 1.2 GeV. Both rings are operational but useful current extracted is limited to about 2×10^{10} particles per bunch because of bunch lengthening. The origin of this effect is excessive longitudinal impedance from discontinuities in the vacuum chamber. It is possible to extract larger currents, but the bunches can then not be compressed in the ring to linac transport because of limited aperture. Short-term fixes have included opening up this aperture, and inducing quadrupole oscillations to precompress the bunch within the ring just before extraction.

Some reduction of the impedance can be achieved by installing sleeves inside the bellows, to smooth out the transitions there.

Such fixes are expected to help bring the current up towards the design value. In the short term, the system is adequate for operation at 10^{10} particles per pulse.

Positron Source [8,9]

At 33 GeV in the Linac, the second electron bunch is ejected onto a W-Re target to produce positrons. These are captured in a high gradient acceleration section and confined through solenoidal focusing. They are then transported at 200 MeV back to the beginning of the Linac for reinjection. The biggest issue is to increase the yield of damped positrons reinjected into the Linac per electron incident on the target. Prior to the Fall 1987 shutdown, this yield was down about a factor two due to combined failure of the capture section, which could not be operated at the design 40 MeV/m gradient, and the DC solenoid, which had developed turn-to-turn shorts. This hardware has now been replaced. The solenoid is working properly but the capture section still works more reliably at a reduced gradient. The yield has improved slightly but has not yet been pushed to the design value. 1×10^{10} positron bunches have been obtained at the end of the Linac.

Linac [7]

The Linac has been upgraded with about 200 new 67 MW klystrons [19]. Energies up to 53 GeV have been measured, but running-in is at 47 GeV to produce collisions at the Z^0. Co-acceleration of 10^{10} electrons and positrons is fairly easy and common automated beam guidance is operational. The energy spread can be minimized to .2 to .3%, and work is ongoing to improve launch and energy feedback

stabilization into the Arcs. Optical matching, important to preserve emittances, is underway both at the injection and throughout the lattice. A klystron management program, enabling automatic scaling of the lattice to match to a varying klystron population, is being tested. Invariant emittances between 3 and 10×10^{-5} mrad are at present obtained at the end of the Linac for both beams.

ARCS

Summary of Optics Goals [1,20]

The Arcs are designed to bend the beams without significant dilution of transverse phase-space. Two mechanisms must be counteracted.

The first effect results from *synchrotron radiation*. The photons, emitted at random, cause energy fluctuations. Lower energy particles are bent more and follow curves with shorter average radius. This disperses their trajectories incoherently which enhances horizontal phase-space. Such trajectories execute betatron oscillations in the quadrupole lattice. To minimize the growth, both photon emission rates and oscillation amplitudes must be small [21,22]. This is achieved by making the bending radius large and the betatron period short, through tight focusing. As can be shown [1], the growth is proportional to T_β^3/ρ^4, where T_β is the betatron period and ρ the average radius. Alternating gradient transport modules with the lowest possible field compatible with the SLAC site are therefore used. The packing factor is maximized using combined function magnets, and the lattice chosen to minimize the average invariant amplitude of the dispersed oscillations. For a FODO array, the optimum [23] cell phase-shift to minimize emittance growth is near 135°. For reasons explained below, the adopted design uses 108°. At 50 GeV, the emittance added in one passage is [1] 1.5×10^{-10} rad-m, or one-half of the design value.

The second mechanism for phase-space dilution arises through residual energy spread resulting from the bunch length and the accelerating Linac RF [24]. Because of energy dependance in the focusing, or *chromaticity*, optical distortions from gradient errors are not imaged coherently. For example, an off-energy slice of a mismatched phase-space transmits with a phase-shift $\Delta\psi \approx 2\pi N_\beta \delta_E$ where δ_E is the relative energy error and N_β the number of betatron periods. For a large phase-shift, the overall mismatch averaged over all energies looses its phase relation to the input. The effective volume occupied by the observable phase-space is thereby enlarged. Such *chromatic filamentation* is illustrated in fig. 2, where a normalized phase-space with area one but amplitude two distortion gradually fills up an area of two. With $N_\beta \simeq 70$ in the Arc and for $\sigma_E \simeq 0.5\%$, the spread in betatron phases at the output is about $\sigma_\psi \simeq 0.7\ \pi$.

This effect can be controlled in two ways. In an *active* approach, it is reduced with careful energy spread minimization [7] and good trajectory and optics matching into and through the Arc. In the adopted *passive* approach, sextupoles are used to cancel the chromaticity. Accumulated errors are thus imaged coherently and the final correction can be concentrated in the Final Focus. From a purely optical standpoint, this eases requirements on upstream control. In practice and as we shall explain, much upstream control is still necessary to maintain detectable luminosity.

Sextupoles were introduced by shaping the combined function magnet poles [10]. For the horizontal optics, the vertical component of the magnetic field may be expressed as:

$$B_y(x) = B_o(1 - Qx + Sx^2) \ ,$$

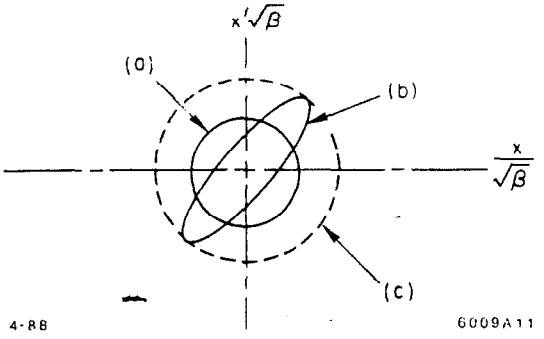

Fig. 2. Nominal phase-space (a), distorted by optical mismatch (b), *filaments* (c) into a larger area when not correcting the chromaticity of the lattice.

where Q and S are the quadrupole and sextupole strengths. The sextupole provides additional focusing for off-energy and off-axis rays with $x = \delta x + \delta_E \eta$, where η is the dispersion function, which suppresses the chromaticity if $2\ S\eta = Q$. Since sine and cosine-like components are equivalent modulo $\pi/2$ in a repetitive lattice, only one family per plane is needed. Additional terms in x^2 and δ^2 for rays solely off-axis or off-energy are suppressed by grouping cells into reasonably local cancellations. *Second-order achromats* [25] achieve this by pairing sextupoles π phase-shift apart into superperiods with the smallest possible multiple of 2π compatible with the cell phase-shift. In the SLC Arcs, each superperiod is 6π, consisting of ten 108° cells. This is a compromise between achromat compactness, best with 90°, and quantum growth, smallest near 135°.

The price to pay for using sextupoles is a lattice sensitive to misalignments. A poorly controlled trajectory generates erect and skew gradient errors through the sextupole which add to magnet imperfections [26] and enhance optical distortions. This lead to stringent magnet to magnet alignment tolerances [20] of about 100 μm.

The efficacy of the chromatic correction was tested by comparing a set of betatron oscillations at two energies. An example of this is shown in fig. 3, where the input beam was deflected horizontally on-energy and 400 MeV off-energy. Overlaying the plots shows no phase difference.

Nonplanar Geometry

Commissioning revealed another problem. Although the beam [10] was steered through the North Arc early on with little loss, spots measured at several stages neither reproduced nor agreed with the design, and the beam injected in the Final Focus for hardware tests would not fit in the aperture easily. At times, loss also appeared in the Arc, pointing to suspected mechanical problems with the vacuum chamber or the magnet movers used for steering. In attempts to probe available aperture with beam, it was found that launched oscillations coupled strongly from one plane to the other with growing amplitude (see fig. 4). Measured η also showed coupling and amplification. The origin of this was the nonplanar geometry dictated by strongly varying site elevation, and large installation errors in magnet positioning. Achromats were rolled at their interface to follow the terrain, and big couplings correlated with the largest rolls.

In the original design, rolls were matched in pairs one or more achromats apart for long-range suppression of the coupling, and this was sensitive to deviations in the 6 $n\pi$ phase-advance, from systematic

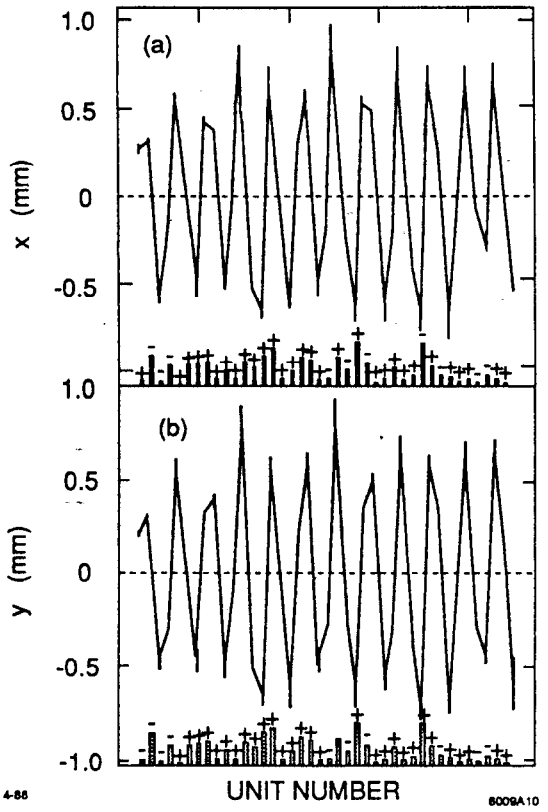

Fig. 3. Betatron oscillation at the end of the Arc, on-energy and 400 MeV off-energy. The chromatic correction suppresses any phase-shift.

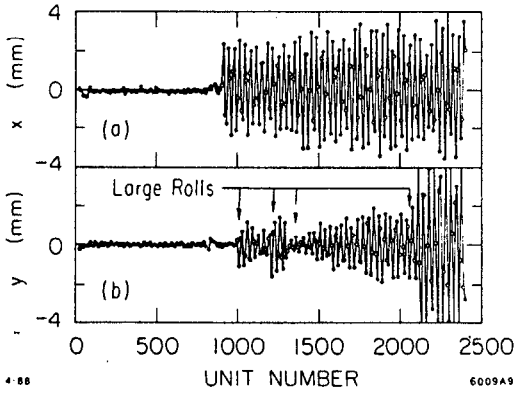

Fig. 4. Cross-coupling of betatron oscillation in the North Arc. Large coupling occurs at the largest rolls.

gradient errors. Such errors initially exceeded the specified design tolerances [1]. Effects can be large as cross-coupling oscillations each time see out of phase optics in the other plane. At a 10° roll, the coupling [27] can be 100%. Overall sensitivity of the betatron size is shown in fig. 5 from TRANSPORT [28], for systematic errors of 3° per cell in each plane. Measured errors were smaller and accounted for a factor three to four overall growth. This was not sufficient to explain the large spots observed in the Final Focus, indicating that the Linac phase-space was not fully controlled.

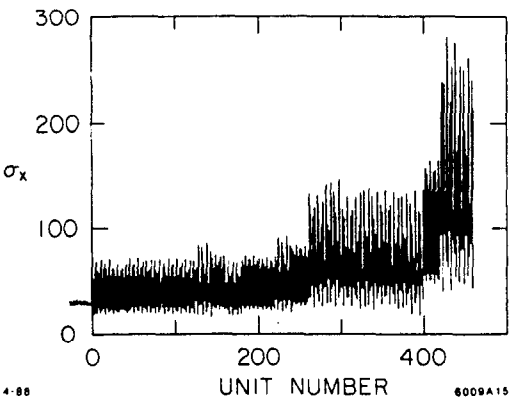

Fig. 5. Growth of betatron spot size in the North Arc, for systematic errors of 3° per cell in each plane.

Phase–Fix and Roll–Fix

Average achromat phase-advances were measured fitting sinusoids to betatron oscillations, and corrected by physically moving magnets, and by combining trim windings in each achromat and a global imbalance between F and D magnets set up in a separate circuit. This *phase-fix*, which was limited by measurement errors, brought errors in the North Arc to within about 0.5° per cell. Overall betatron growth was reduced to a factor 2 and η was essentially matched. The South Arc, only partially corrected, still had large growth. Phase-space injected in the North Final Focus was also reduced, enabling an initial optics program for small IP spots to proceed, but remaining growth, still amplifying variations, would often result in uncorrectable cases.

Splitting up major rolls into smoother transitions was proposed to reduce the sensitivity to systematic gradient errors. It was first found [29] empirically that rolling D lenses near roll transitions by half the total amount suppressed cross-coupling of lattice η. For the betatron motion, an approximate correction scheme was found by splitting rolls in three parts, each a cell apart and with magnitudes satisfying:

$$\theta_{-1}e^{-i2\pi/3} + \theta_0 + \theta_{+1}e^{i2\pi/3} = 0 \ ,$$

as for a matched trajectory bump. Figure 6 illustrates the combined *roll-fix* transition and relative roll ratios. Simulated [30] improvements are shown in fig. 7, for a sample of random and systematic errors, in the as-built and roll-fixed Arcs. Reduction of the growth of spot sizes at the end of the Arc from roll-fix is a factor 1.5 to 2.

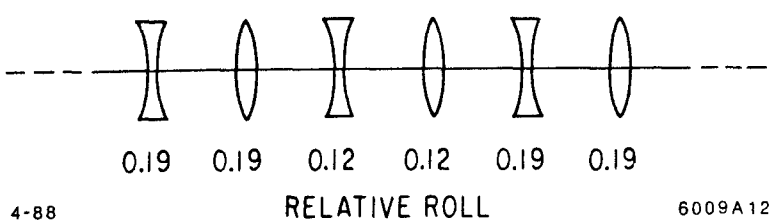

Fig. 6. *Roll-fix* transition.

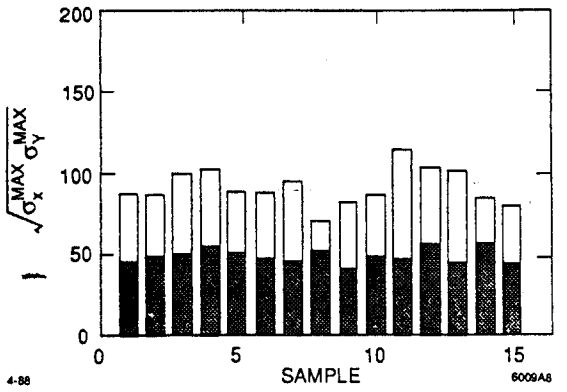

Fig. 7. Growth of betatron size at the end of the Arc, for as-built (white area) and roll-fixed (shaded area) lattice.

Present Status and Plans

Both Arcs have been roll-fixed and recommissioned. In the South, a slightly smoother transition [31] is installed. With proper launch, η is matched throughout. The sensitivity of the betatron motion from systematic gradient errors is reduced, but random erect and skew quadrupole errors still cause some blowup and cross-coupling, although more gradual in nature [see fig. 8 (a)]. Cures involve empirically varying phases in troubled areas to reduce the coherence in the buildup, much as tunes are adjusted away from resonances in circular machines. Such a *detune-fix* [32] is shown in fig. 8(b) where blowup was reduced by disconnecting the FD-imbalance, thus causing about a 1° per cell difference between X and Y phases.

Another planned [33] cure consists of exciting harmonic [34,35] gradient perturbations with a pattern of trim windings, to suppress damaging Fourier components in the errors at twice the betatron frequency. Although this will be required for the final optimization, beams are now routinely transported to the Final Focus with distortions which can be absorbed by optical matching there.

FINAL FOCUS

Summary of Optics Goals [11-13]

The primary goal is to focus both beams to a small transverse size of about 2 μm. This would be easy for small enough transverse emittances and energy spreads. The limiting effect is the *chromaticity* of the focusing system needed to demagnify the beams, which as was described in the Arc causes both sine and cosine-like trajectories to be shifted for different energies. For a simplified Final Focus (see fig. 9), the contribution to the betatron spot size from *chromatic aberration* is $\sigma_{chrom} \simeq 2l^*\sigma_E\sigma_\theta^*$, where σ_θ^* is the IP angular size and l^* the distance from the principal plane of the final lens system to the IP (a factor two is put in since at least two lenses are used to focus both planes). The effect would be tolerable if $\epsilon\sigma_E \leq \sigma_z^{*2}/2l^*$. This is not the case in the SLC Final Focus, where $\sigma_z^* \simeq 1.5$ μm, $\epsilon \simeq 3\ 10^{-10}$ mrad, $\sigma_E \simeq 0.002$ and $l^* \approx 5$ m, amounting to $\sigma_{chrom}^* \simeq 4$ μm.

The reduction in luminosity, computed [36] by averaging the usual expression over the two beam's energy distributions, is shown in fig. 10 (dotted lines) versus β^*, for the as-built Final Focus. With $\sigma_E = 0.002$ and $\beta_{opt}^* \simeq 1.5$ cm, the luminosity is reduced by a factor 3.5.

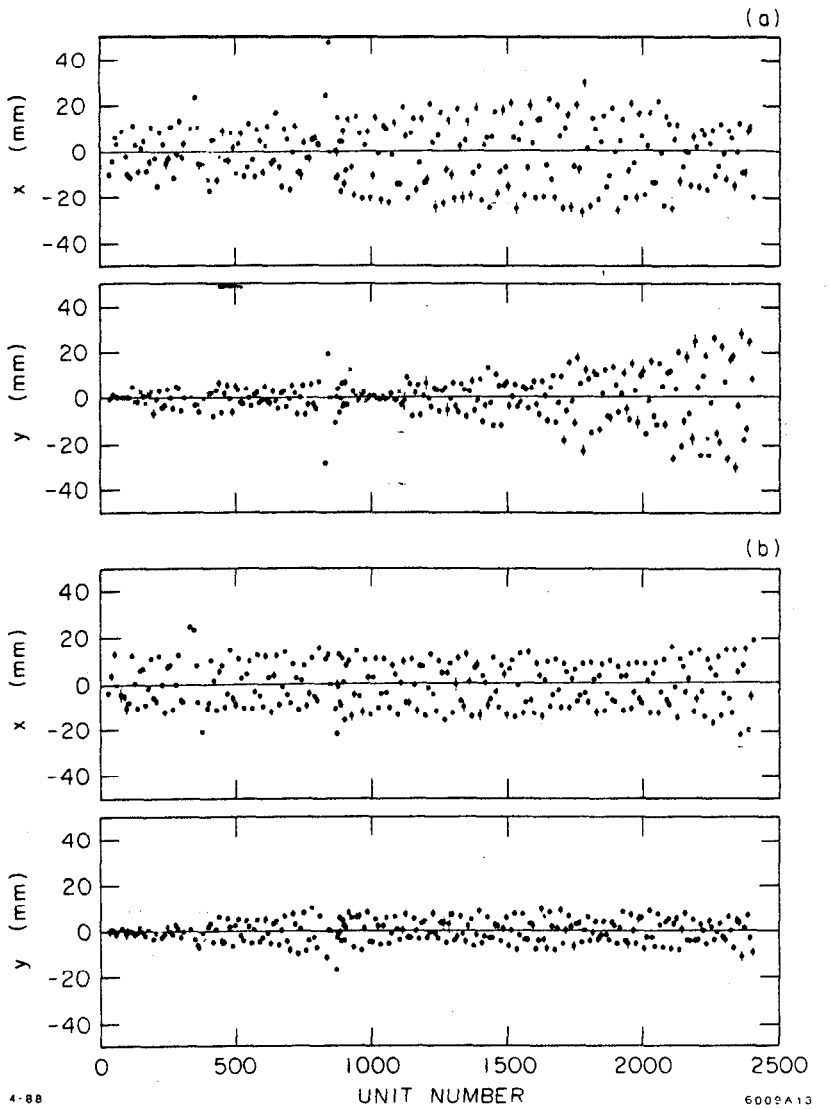

Fig. 8. Growth of a betatron oscillation in the South Arc, before (a) and after (b) *detune-fix*.

A Chromatic Correction Section (CCS) is introduced upstream of the final lens to cancel this effect. In a simplified CCS, two dipoles of strength B, separated by $2l_{ccs}$, are imaged by a quad with focal length $l_{ccs}/2$ (see fig. 9). Near the quad is a sextupole of strength S, through which rays with energy deviation δ_E travel off-axis. This produces a stronger overall quad for $\delta_E > 0$, which must here offset the weaker focusing in *both* final and CCS quads. The largest contribution to the chromaticity is from the final lens. Equating it to the effect from the sextupole, we find that $S \propto R_l/MB$, where $M = l^*/L$ and $R_l = l^*/l_{ccs}^2$.

Additional aberrations in θ^2 and δ_E^2, as in the Arc, are suppressed by pairing the sextupoles π phase-shift apart and by assuring sequential symmetry for η. The section departs, however, from a pure second-order achromat through the bends, placed where angular spreads are large to minimize synchrotron radiation emittance growth. The real system [11-13], designed to focus achromatically in both planes, is

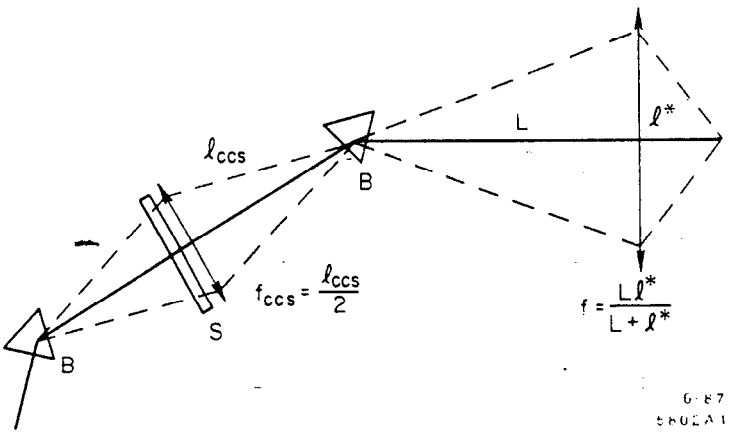

Fig. 9. A simplified Final Focus System.

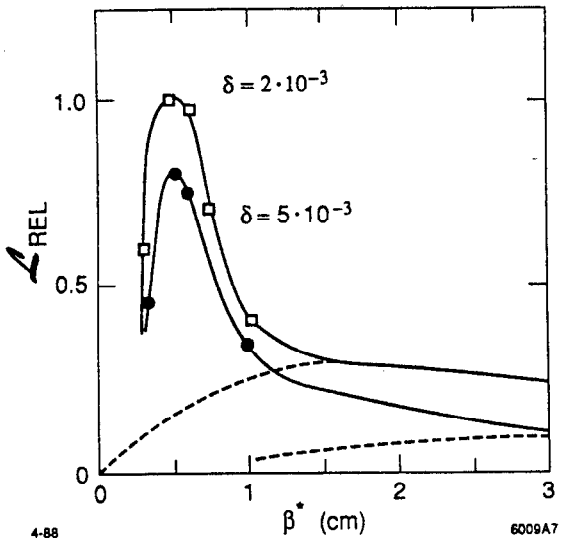

Fig. 10. Luminosity loss versus β^*, with second-order chromatic correction (solid line) and without (dotted line).

telescopic and uses triplets instead of lenses. This suppresses [12,37] the cosine-like terms in $x\delta_E$,$y\delta_E$ and minimizes [13] the sine-like chromaticities in $\theta\delta_E$,$\phi\delta_E$, while demagnifying in both planes. Two interleaved sextupole families are used to correct both planes. Coupling effects between these can enhance third-order aberrations and must be minimized. If we neglect the final lens system, the three dominant terms in $\theta\delta_E^2$, $\theta^2\delta_E$ and θ^3 scale like $S^2B^2\sigma_E^2\sigma_\theta^* M$, $S^2B\sigma_E\sigma_\theta^{*2}M^2$ and $S^2\sigma_\theta^{*3}M^3$. Substituting for the sextupole, we get $\frac{R_1^2\sigma_E^2(\epsilon/\beta^*)^{1/2}}{M}$, $\frac{R_1^2\sigma_E(\epsilon/\beta^*)}{B}$ and $\frac{R_1^2M(\epsilon/\beta^*)^{3/2}}{B^2}$. For given phase-space volume, space constraints and desired β^*, the overall effect from these aberrations can be minimized by adjusting [1] M,B and S to balance them out.

The overall effect of the chromatic correction is shown in fig. 10 (solid line), from MURTLE [38]). As expected, removing all second-order aberrations raises L^{max} and reduces β^*_{opt}. The optimum is now limited by leftover third-order terms. As it is more peaked, it is also more sensitive to proper matching.

The entire system is shown in fig. 11. Two additional sections are included to match the Arc η and β-functions. Extraction of the opposing beam is also provided, in the β-match section, through a pulsed magnet and septum.

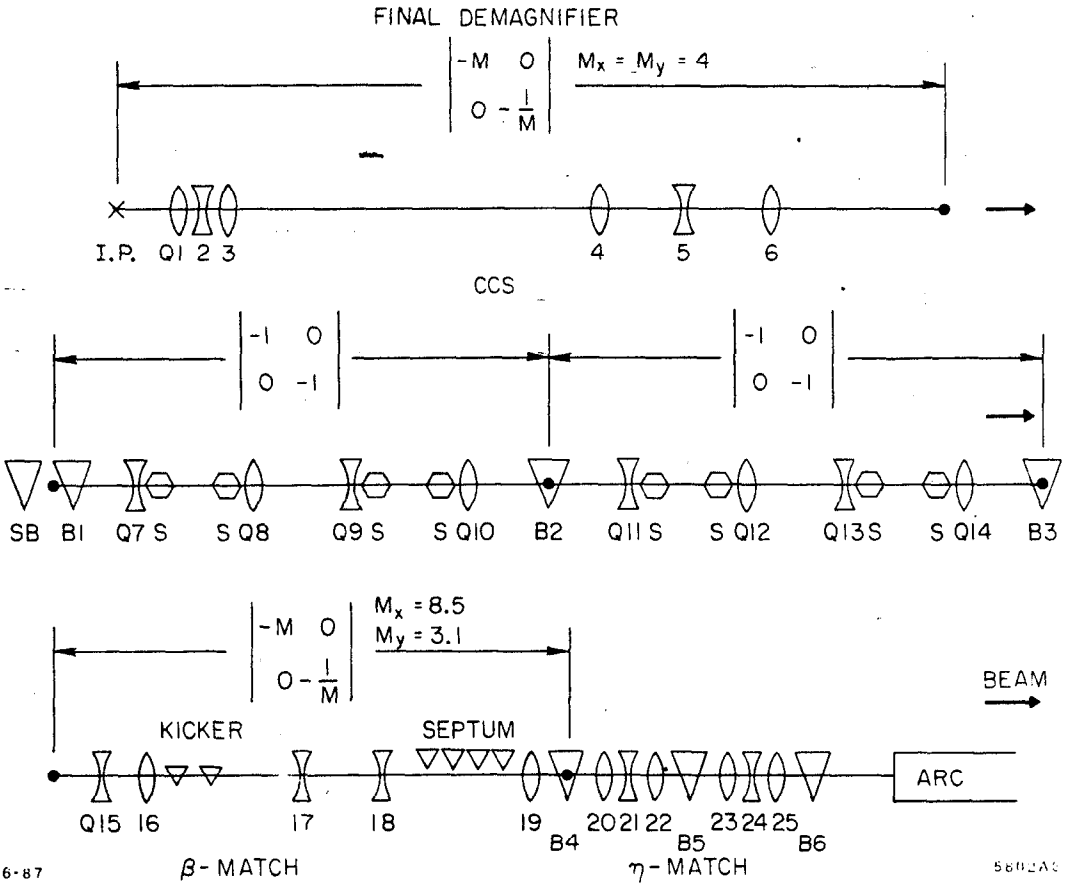

Fig. 11. Schematic of the Final Focus System.

Variable Matching [36]

Both the volume and shape of the input phase-space can be perturbed by imperfections. Errors generated within the Arc are in principle stable, but the linac is more variable as the energy profile depends on the set of klystrons used to accelerate. This set can change as faulty ones are exchanged for spares, and the phase-space then varies unless the focusing is rescaled. Also, mismatch at the Linac input *filaments* through the chromaticity of the Linac lattice, if and when the energy spread is minimized at the end but not locally. Good matching in the Linac is especially important at high current, when large local energy spreads are used to stabilize [39] transverse wakefields. Ongoing efforts have improved controls in the Linac, but some variations still exist. These are then further amplified by distortions in the Arcs.

The Final Focus includes adjustable matching mainly for *static* errors accumulated upstream. In establishing a proper setup and while work on stability proceeds, this matching is also used to some extent as an overall variable feedback. This is not optimal for several reasons, as will be explained.

Enhanced emittances or energy spread are uncorrectable. Larger $\epsilon_{x,y}$ are a major concern for both luminosity and detector backgrounds. The purely optical damage is slightly worse than linear because of third-order aberration, giving [36] $L \propto \epsilon^{-\frac{2}{3}}$ for $\beta^*_{opt} \propto \epsilon^{\frac{1}{3}}$. Third-order effects from a larger σ_E are apparent in fig. 10, showing close to linear loss with σ_E and weak dependance on β^*. The tolerance on σ_E is about 0.005.

Optical distortions in the Arcs are mostly linear [40] and are correctable within some bounds. The primary set enhances σ^* by correlating positions with angles or with δ_E, amounting to axially offsetting the waists, x-y coupling ($x\phi$ or $y\theta$ terms) or anomalous $\eta_{x,y}$. The waist must be corrected to within the depth of field $\beta^* \simeq 0.5$ cm; $\eta_{x,y}$ must be smaller than 1 mm. A second set enlarges σ^* by perturbing IP angular spreads ($< \theta^2 >$,$< \phi^2 >$, anomalous $\eta_{\theta,\phi}$ and $\theta\phi$ coupling terms). Smaller spread increases β^*, leading to $\mathcal{L} \propto 1/\beta^*$ from linear optics. Larger spread reduces β^*, but also enhances higher order contributions, leading to rapid loss. From fig. 10, β^* must be within $\pm 50\%$.

Optical corrections: In the design $\epsilon_x = \epsilon_y$ case, the betatron phase-space can [36] be perturbed in only six independent ways. With the four dispersions, $\eta_{x,\theta,y,\phi}$, there are thus *ten independent distortions* in total. We represent them by those for which tolerances were given: the five IP angular sizes $< \theta^2 >$,$< \phi^2 >$,$< \theta\phi >$ and $\eta_{\theta,\phi}$, and the five correlations of IP positions to angles and energy $< x\theta >$, $< y\phi >$, $< y\theta >$ (or $< x\phi >$) and $\eta_{x,y}$. The Final Focus is equipped to correct these ten distortions. If $\epsilon_x \neq \epsilon_y$, the six betatron variables chosen do not fully describe [41] the phase-space and more correction elements are needed.

Dispersion is corrected in the η-match with four quads [13], installed in pairs $\pi/2$ apart, to control spatial and angular terms, respectively. Each pair consists of an erect and a skew quad to correct both planes. Naturally orthogonal for small input error, these correctors are coupled if it is large. Correction range is mainly limited by quad strengths, but some values of the input make the correction singular; for example, when $\eta^{anomalous}_{x,\theta}$ exactly cancels $\eta^{lattice}_{x,\theta}$. In this case, control is required upstream.

Correctors for betatron mismatch straddle the CCS. The three angular terms are adjusted upstream of the CCS with two erect and one skew quad. The three waist terms cannot be adjusted there independently of the angular terms. They are taken out with trims on two of the final quads and a second skew quad. Correction range is about $\pm 50 \times \beta^*$ for waists and a factor four in either direction for angle spreads. The scheme is shown in fig. 12.

Optically, the system can correct as large as factor three mismatches. In practice, large distortions are not handled well for two reasons.

The first is lack of orthogonality in the corrections resulting from severe space limitations. The three waist corrections can internally be made orthogonal [42], but all the others are coupled. This is the case for the two skew quadrupoles, for the sextupoles, which must be refitted after betatron matching as the correctors straddle them, and for the extraction, which straddles two of the variable lenses and must be reoptimized after betatron matching. The η-correction is also non-orthogonal to the β-match, particularly [43] for magnified or demagnified optical configurations. Operationally, modest variations are amplified by distortions remaining in the Arcs, and can require extensive reoptimization. Effort is therefore directed both towards improving the Arc lattice and towards correcting variations in the Linac, to avoid feeding back on them in the Final Focus.

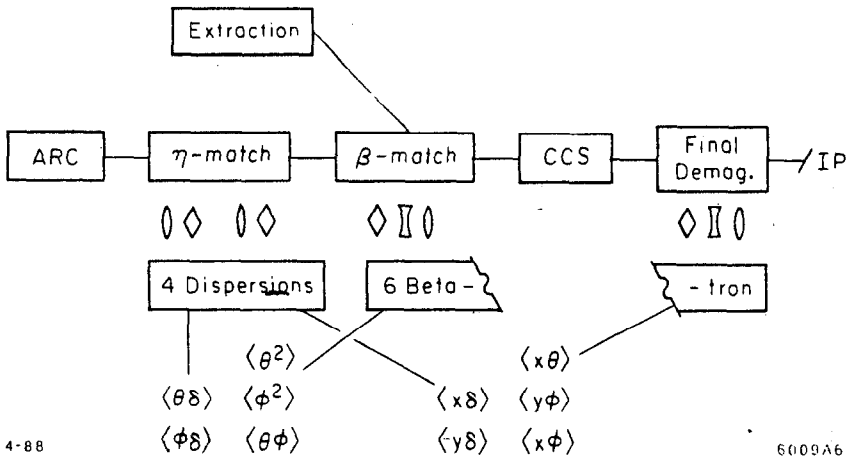

Fig. 12. Optical matching in the Final Focus System.

The second reason is the background induced in the detector by beam-tails impinging on tight apertures at the injection to the Final Focus. These apertures as well as some adjustable collimators are upstream of the main matching elements. Harmful background from hits on these apertures can result from otherwise correctable distortions. Recent experimental work [44] indicates more stringent tolerances on input errors from this viewpoint. This may require introducing further optical corrections in the Arcs, and redeployment of some collimators upstream.

Tuning Strategy and Initial Results

In this section, we describe single-beam optical adjustments in the Final Focus. Combined adjustments of several SLC systems to produce and maintain luminosity with tolerable background are ongoing and not described here. Similarly, two-beam tuning and steering methods are described elsewhere [45,46]. Some initial beam tests are reported.

We first match [47] η from the Arc. Strip-line beam position monitors are used to measure beam motion versus energy. This does not give position-energy correlations in the bunch if anomalous η exists where the energy is varied, but gives a good estimate if the Arc is (as expected) the dominant contributor. Using a model, we determine $\eta^{anomalous}_{x,\theta,y,\phi}$ from a least-square fit to the measurements and calculate the correction. An example of this is shown in fig. 13.

Trajectory errors within the Final Focus can also generate η at the IP. Correction is achieved by undoing some of the upstream match, although this also affects [43] waist-corrections and must be the result of a combined fit.

Betatron mismatch is best diagnosed near the IP, where angular and spatial sizes are naturally separated. The three angular terms, $< \theta^2 >$, $< \phi^2 >$ and $< \theta\phi >$, are first adjusted crudely looking at a nominally round spot on a high-β screen upstream of the Final Triplet. An example of this is shown in fig. 14, where the action of the upper skew quad is seen and where the beam has close to the design size.

This does not give β^* if ϵ is unknown. Also, if waist offsets are large, design size at the high-β screen does not correlate well with IP angular size. For better determination, spot sizes are measured at the IP, by scanning the beam across a thin 5 μm secondary emission wire target [48], as functions of the three waist

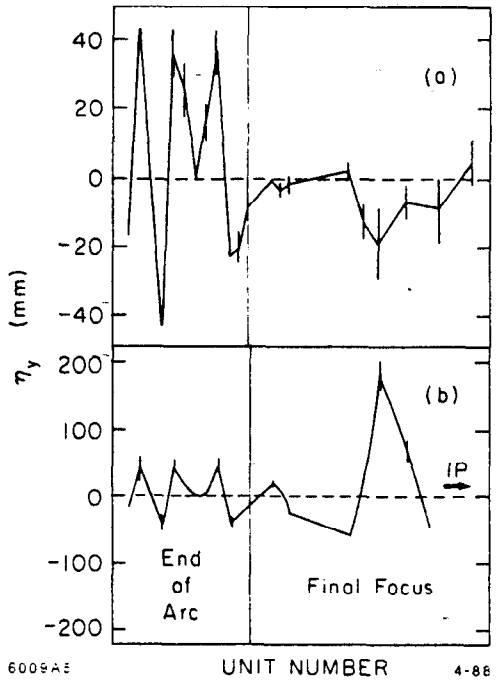

Fig. 13. On-line matching of the vertical dispersion function at the injection to the Final Focus. (b) shows mismatch before correction. (a) shows the effect of the correction. Please note the change of scale.

controls, starting with the second skew quad. Neglecting changes in IP angular spread, β^* and ϵ are found fitting $\epsilon\beta^* + \frac{\epsilon}{\beta^*}$ to the square of the beam size. Angular spreads are well determined from the parabolas branches, but both ϵ and β^* estimates suffer if the linear spot is not resolved. This arises through residual cross-coupling, only partially correctable for $\epsilon_x \neq \epsilon_y$, and through third-order aberration present before fully matching the β-function. Sextupoles must also be fitted in the perturbed lattice before scanning the waists, to maintain good second-order correction. Measured ϵ and β^* values serve as input for fitting the six β-matching quads towards design phase-space parameters. Both on-line and off-line models [47,49,50] are used. An empirical search around the calculated β^* is also planned for optimization.

Relatively small spots were sometimes obtained originally by only scanning the waists. An example of this is shown in fig. 15, where a 5 μm spot was obtained, with sextupoles turned off all together. The phase-space had to be rather close to nominal for this to be possible. As input parameters changed, small spots did not always reproduce.

More recently, the tolerance to input variations has been widened by running with a $\beta^* = 3$ cm lattice, as a starting guess of the most probable angular spread correction needed. Also, improvements have been made on stability and matching upstream. Beams with smaller than 5 μm sizes are now relatively easy to reproduce for both electrons and positrons with only the three waist-scans.

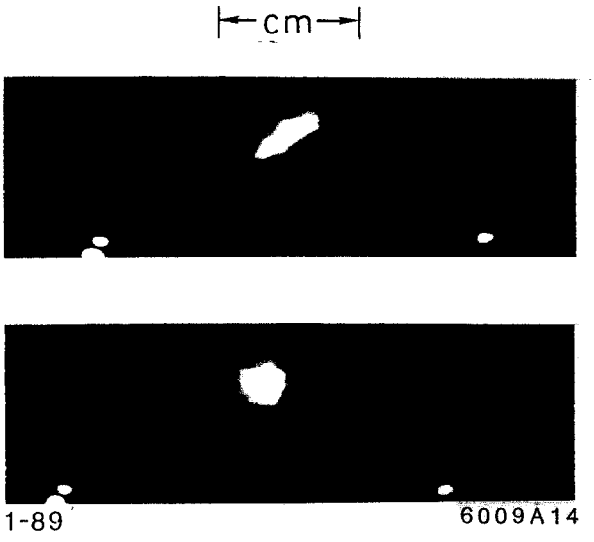

Fig. 14. Crude correction of cross-coupling in the IP angular spreads, looking at the tilt on a screen at the high-β point: (a) before correction; (b) after correction.

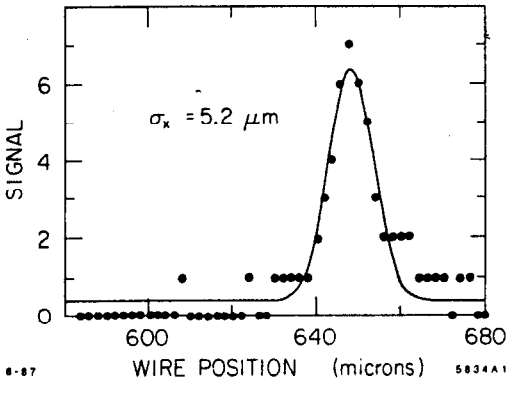

Fig. 15. First measurement of "small spot" at the IP.

SUMMARY STATUS AND NEAR FUTURE

Commissioning is now proceeding rapidly towards an initial low luminosity physics run. Both beams are routinely extracted onto their dumps, and reasonably small beam sizes are usually reproduced at the IP. Main priorities are phase-space controls and stability in the whole machine needed to maintain small spots, background reductions and general system reliability and operability. A shift towards operation has been made to assure more continuity in the commissioning and a more global approach towards stability and tuning issues. The Mark II detector, installed on the beamline during last year's shutdown, has been turned on a few times to help look at backgrounds. Studies indicate that collimators may have to be redeployed from the Final Focus to upstream places where beams can be comfortably trimmed without generating excessive muons in the detector. Also, enhanced optical matching in the Arcs through harmonic corrections is being considered for early installation, to help reduce distortions in the Final Focus. Extrapolating our recent rate of progress, and with some well-deserved luck, we hope to produce and detect a hundred Z^0 before Summer 1988.

ACKNOWLEDGEMENTS

I have profited interacting with numerous SLC and Mark II colleagues on several topics described here. New insight and progress have often resulted. Discussions with Karl Brown, Dave Burke, Roger Erickson, Ted Fieguth, Bill Ford, Andrew Hutton, Witold Kozanecki, Joe Murray, Nan Phinney, Dave Ritson, Lenny Rivkin, Marc Ross, Matt Sands, John Seeman, John Sheppard, Rae Stiening, Nobu Toge and many others, were both stimulating and interesting. I have in particular enjoyed working with Karl Brown and David Ritson on optics problems in the Arcs and Final Focus. Dave and I collaborated on the tuning strategy for the Final Focus. I especially wish to acknowledge his contribution. At last, I wish to thank Karl for reading this paper and for suggesting several improvements.

REFERENCES

[1] *SLC Conceptual Design Report,* SLAC–Report–229, June 1980; *SLC Design Handbook,* December 1984; *Proceedings of the SLC Workshop,* SLAC–Report–247.

[2] B. Richter, Nucl. Inst. Meth. **136**, 47 (1976).

[3] B. Richter and R. Stiening, The SLAC Linear Collider—A Status Report, *Proceedings of the International Symposium on Lepton and Photon Interactions at High Energy* (Hamburg, Germany, July 1987).

[4] R. Stiening, *Proposed Parameter Specification for FY88,* April 1988.

[5] J. C. Shepphard et al., Commissioning the SLC Injector, *Proceedings of the Particle Accelerator Conference* (Washington, D. C., March 1987).

[6] G. E. Fischer et al., A 1.2 GeV Damping Ring Complex for the Stanford Linear Collider, *Proceedings of the Twelfth International Conference on High Energy Accelerators,* FNAL, 37 (1983).

[7] J. T. Seeman et al., Experimental Beam Dynamics in the SLC Linac, *Proceedings of the Particle Accelerator Conference* (Washington, D. C., March 1987).

[8] F. Bulos et al., Design of a High Yield Positron Source, IEEE Trans. Nucl. Sci. **NS–32**, 1832 (1985).

[9] S. Ecklund, The Stanford Linear Collider Positron Source, *Proceedings of the Workshop on Intense Positron Beams* (Idaho Falls, Idaho, June 1987).

[10] G. E. Fischer et al., Some Experiences from the Commissioning Program of the SLC Arc Transport System, *Proceedings of the Particle Accelerator Conference* (Washington, D. C., March 1987).

[11] R. Erickson, Final Focus Systems for Linear Colliders, *Proceedings of the U. S. Summer School on High Energy Particle Accelerators* (Batavia, Illinois, August 1984).

[12] K. Brown, A Conceptual Design of Final Focus Systems for Linear Colliders, *Proceedings of the U. S.–CERN Joint Topical Course: Frontiers of Particle Beams* (South Padre Island, Texas, October 1986).

[13] J. J. Murray et al., The Completed Design of the SLC Final Focus System, *Proceedings of the Particle Accelerator Conference* (Washington, D. C., March 1987).

[14] R. Stiening, Status of the SLAC Linear Collider, *Proceedings of the Particle Accelerator Conference* (Washington, D. C., March 1987).

[15] J. T. Seeman and J. C. Shepphard, Status of the SLC, *Proceedings of the Workshop on New Developments in Particle Accelerator Techniques,* (Orsay, France, June 1987).

[16] A. J. Lankford, The Status of the SLAC Linear Collider and of the Mark II Detector, *Proceedings of the Seventh International Conference on Physics in Collision* (Tsukuba, Japan, August 1987).

[17] W. Kozanecki, Progress Report on the SLAC Linear Collider, *Proceedings of the International Europhysics Conference on High Energy Physics* (Uppsala, Sweden, June 1987).

[18] R. D. Ruth, The Status of the SLC, *Proceedings of the ICFA Seminar on Future Perspectives in High Energy Physics* (Upton, New York, October 1987).

[19] M. A. Allen et al., Performance of the SLAC Linear Collider Klystrons, *Proceedings of the Particle Accelerator Conference* (Washington, D. C., March 1987).

[20] S. Kheifets et al., Beam Optical Design and Studies of the SLC Arcs, *Proceedings of the Particle Accelerator Conference* (Washington, D. C., March 1987).

[21] M. Sands, *The Physics of Electron Storage Rings—An Introduction,* SLAC–121 Addendum (1979).

[22] M. Sands, *Emittance Growth from Radiation Fluctuations,* SLAC–AP–47 (1985).

[23] R. H. Helm and H. Wiedemann, *Emittance in FODO–Cell Lattice,* PEP–Note–303 (1979).

[24] R. Stiening, *Dynamic Beam Loading Compensation and Energy Spread in the SLC,* SLAC–CN–110 (1981).

[25] K. L. Brown, *A Second–Order Magnetic Optical Achromat,* SLAC–PUB–2257 (1979).

[26] B. Weng et al., SLC Arc Transport System–AG–Magnet Measurement and Performance, *Proceedings of the Particle Accelerator Conference* (Vancouver, B. C., Canada, May 1987).

[27] M. Sands, *Betatron Oscillations and Rolled Achromats,* SLAC–CN–355 (1987).

[28] K. L. Brown et al., SLAC–91, Rev. 2, May 1977.

[29] D. Ritson, private communication, June 1987.

[30] D. Ritson, BEAMSIM, private program.

[31] L. Rivkin and M. Sands, private communication, November 1987.

[32] N. Toge, private communication, March 1988.

[33] P. Bambade, *Harmonic Corrections in the Arcs*, in preparation.

[34] R. Stiening, *Focussing Errors in the SLC Linac Quadrupole Lattice*, SLAC-CN-161 (1982).

[35] T. H. Fieguth, *GIAT Committee Report*, October 1985.

[36] P. S. Bambade, Beam Dynamics in the SLC Final Focus System, *Proceedings of the Particle Accelerator Conference* (Washington, D. C., March 1987).

[37] K. L. Brown, private communication, June 1987.

[38] J. J. Murray and T. Fieguth, MURTLE, private program.

[39] K. Bane, Wake-Field Effects in a Linear Collider, IEEE Trans. Nucl. Sci. **NS-32**, 1662 (1985).

[40] K. L. Brown and R. V. Servranckx, *GIAT Committee Report*, February 1986.

[41] L. Rivkin, private communication, October 1987.

[42] P. S. Bambade, *GIAT Committee Report*, March 1987.

[43] B. Ford, private communication, April 1988.

[44] D. Burke, private communication, April 1988.

[45] P. S. Bambade and R. Erickson, Beam-Beam Deflections as an Interaction Point Diagnostic for the SLC, *Proceedings of the Linear Accelerator Conference* (Stanford, California, June 1986).

[46] G. Bonvicini et al., Beamstrahlung Monitor for SLC Final Focus Using Gamma Ray Energies, *Proceedings of the Linear Accelerator Conference* (Stanford, California, June 1986).

[47] C. Hawkes and P. S. Bambade, *First-Order Optical Matching in the Final Focus System of the SLAC Linear Collider*, in preparation.

[48] C. Field et al., *High Resolution Wire-Scanner for Micron Size Profile Measurements at the SLC*, SLAC-PUB-4605, to be published.

[49] W. Kozanecki, BETAMAT, private program.

[50] R. Servranckx and B. Ford, Flight Simulator for the Final Focus, private program.

IX. CONCLUSION

In this thesis, we have developed, tested and analysed the methods for optical tuning in two sections of the Stanford linear collider: the arcs and the final focus. These methods have enabled to reach a quasi-optimal set-up.

In the arcs, we have proposed and studied a design modification reducing harmful effects from the rolls, introduced in the lattice to enable following the terrain of the SLAC site. This modification has made the system much more tolerant to systematic errors.

We have also proposed and studied a new optical tuning method for the arcs, consisting of introducing focusing perturbations at the most efficient harmonics of the betatron frequency. This method has allowed, on the one hand, to make the optical transfer close to perfect, and on the other hand, to adjust the beam empirically at the entrance to the final focus section, to minimize backgrounds produced by mismatches in the phase-space.

In the final focus section, we have designed the optical correction and optimization algorithm. This algorithm has enabled beams focused at the interaction point with three to five micron transverse sizes to be attained, and the optical factors limiting the luminosity to be identified. These factors are mainly the requirement to operate with a β^*-parameter larger than the theoretical optimum, by a factor of five to ten, resulting from the background generated by beam-tails in the last quadrupoles.

APPENDIX: REPORTS AND PUBLICATIONS ON THE BEAM-BEAM DEFLECTION DIAGNOSTIC METHOD

A.1 "Beam-Beam Deflections to Measure Spot Size and Offset at the SLC IP"

This collider note contains the original proposal and description of the beam-beam deflection method. This method allows to detect the interaction of the beams when they interact at the collision point. It is presently the primary method used to optimize the beams in collision.

SINGLE PASS COLLIDER MEMO CN-303

AUTHOR: P. Bambade DATE: June 10, 1985

TITLE: BEAM-BEAM DEFLECTIONS TO MEASURE SIZE SPOT AND OFFSET AT SLC IP

PART 1 : CALCULATIONS

As soon as two SLC beams make it to the IR, both transverse offsets, spot sizes and shapes can be extracted from the pattern of angular deflections produced by the electromagnetic interaction of the two beams, as one is scanned across the other. These deflections, measured in two high resolution Beam Position Monitors (BPM) mounted symmetrically on both sides of the IP (Fig.1), will produce detectable signals allowing spot sizes to be tuned, even with the very low luminosities expected at turn on. They will also furnish a good signal to monitor beam centering and will therefore become an important part of the FFS feedback system.

This note summarizes the formulae which will allow us to correlate BPM offset readings with the properties of the two beams, and describes the range and limitations of the technique in the case of SLC.

Further work needed includes simulations, specifications for the feedback system, such as its algorithm, veto conditions and so on, aswell as integration of the beamstrahlung signal into the diagnostic scheme.

I Basic Principle

The angular deflection produced by the interaction of a SLC beam with the electromagnetic field of its colliding partner (see fig. 1) is easily expressed in the simplified case of a round target beam and a point size probe

$$\theta(\Delta) = \frac{-2r_e N_T}{\gamma} \quad \frac{1-\exp\left[\frac{-\Delta^2}{2\sigma_T^2}\right]}{\Delta} \tag{1}$$

where r_e is the classical radius of the electron, γ the relativistic factor, N_T the number of particles in the target, σ_T its RMS transverse size, and Δ the impact parameter of the probing charge.

Deflection versus impact parameter is shown in fig. 2 for targets with 2.5 and 10 μm

transverse spot sizes respectively.

The basic principle of the method is three-fold:

1. Initial beam finding: One beam — the probe in this case — is temporarily suppressed and BPM readings are compared before and after. In the case of initially large impact parameters, the magnitude of the difference is inversely proportional to the transverse offset at collision point and its sign tells in which direction to steer.
2. Beam centering: Scanning the probe across the target and recording a plot similar to fig. 2 will allow optimal centering of the two, by looking for the zero deflection symmetry point.
3. Spot size tuning: Since the slope of the deflection at the above mentionned symmetry point is inversely proportional to the transverse cross-section of the target, the same measured plot will allow spot sizes to be infered and thus minimized.

In all three cases, the sensitivity of the method is based on the fact that relative rather than absolute position information is used.

Of course, the simplifying assumption of round target and point size probe is not likely to be satisfied, and the problem therefore needs to be parametrized in two dimensions.

II Formulae

The following results are valid for collisions between gaussian, un- pinched beams.

a. Deflection of point charge

The deflection of a point charge colliding with a target consisting of a two dimensional gaussian charge distribution can be written (1,2)

$$\theta_{x,y} = \frac{-2r_e N_T}{\gamma} \Delta_{x,y} \int_0^\infty \frac{\exp\left[-\left(\frac{\Delta_x^2}{2\sigma_{T_x}^2+t} + \frac{\Delta_y^2}{2\sigma_{T_x}^2+t}\right)\right]}{\left(2\sigma_{T_{x,y}}^2 + t\right)^{3/2}\left(2\sigma_{T_{y,x}}^2 + t\right)^{1/2}} dt \qquad (2)$$

The aspect ratio is defined by $f = \sigma_{T_y}/\sigma_{T_x}$. For $f = 1$, (2) reduces to (1).

The two deflection angles are shown in fig. 3 – 5 as a function of impact parameters in both planes, for $N_T = 5 \cdot 10^{10}$ particles. Figures 3.a,b and 4.a,b correspond to round beams ($f = 1$) with $\sigma_{T_{x,y}} = 2.5$ and $7.5\,\mu$m respectively, whereas fig. 5.a,b correspond to a flat target with $\sigma_{Tx} = 25.0\,\mu$m and $\sigma_{T_y} = 2.5\,\mu$m ($f = 0.1$). Note the change in vertical scale going from fig. 3 and 4 to 5.

In the limit of large impact parameters, both target and probe are well approximated by point charges and (2) reduces to

$$\theta_{x,y} \simeq \frac{-4r_e N_T}{\gamma} \quad \frac{\Delta_{x,y}}{\Delta_x^2 + \Delta_y^2} \tag{3}$$

Turning off one of the two beams and comparing BPM readings before and after then allows, via (3), to measure initial offsets.

Taking the limit for small impact parameters gives the linear dependance

$$\theta_{x,y} \simeq \frac{-2r_e N_T}{\gamma} \quad \frac{\Delta_{x,y}}{\sigma_{T_{x,y}}(\sigma_{T_x} + \sigma_{T_y})} \tag{4}$$

Measurement of the slopes of the deflections as a function of impact parameters will then allow, via (4), to infer the two transverse sizes of the target beam to be tuned.

b. Form factor accounting for finite probe beam size

When the two beams are close, the average deflection measured in the BPM is reduced due to the finite size of the probe. This can be accounted for via the convolution of the probe density distribution with (2). The result of the calculation is summarized in two-dimensional form factors, by which the slopes in (4) are reduced, and given by

$$F_x(f, R_x, R_y) = F_y(1/f, R_y, R_x) =$$

$$\frac{1+f}{2} \int_0^\infty \frac{dt}{(1+t)[1+R_x^2+t]^{1/2}[f^2(1+R_y^2)+t]^{1/2}} \tag{5}$$

where R_x and R_y are the ratios of probe to target transverse sizes in both planes ($R_{x,y} = \sigma_{P_{x,y}}/\sigma_{T_{x,y}}$). As is consistent, the form factors become one for small $R_{x,y}$ and zero for large $R_{x,y}$. The functions are shown in fig. 6 and 7 for target aspect ratios $f = .1$ and $f = 1$.

In the special and initially unlikely case of round target and probe beams ($R_x = R_y = R, f = 1$), (5) reduces to

$$F_{Round}(R) = \frac{\mathrm{Log}\,(1+R^2)}{R^2} \tag{6}$$

The corresponding plot is shown in fig. 8.

III. Application to SLC : Numbers and Ranges of Utilization

a. Limitations

Three types of limitations are anticipated. The main and most obvious one is the performance of the measuring BPMs. The better their resolution, the smaller the measurable offsets and the more effective the method. We hope for 20 μm or better on a single pulse. Particular attention has to be payed to their directivity, since beams will be measured from both directions. Harmful synchrotron radiation present in the environment will furthermore have to be masked.

The second limitation, the stability of the beams, is a fundamental limitation of SLC and is common to all colliding beam diagnostic and tuning procedures.

A third difficuly arises from the non-gaussian, assymmetric distributions expected as a result of Linac wakefields and Arc non-linearities. Beam finding at large impact parameters is not affected, but the pattern of deflections shown in fig. 2 and 3 will be distorted to the extent that a lot of charge is carried by the tail. This and uncorrelated tilted $x-y$ distributions of the two beams, due to errors, will make the patterns hard to interpret. Fortunately, tuning for maximum slopes will always lead us in the right direction in the same way as beamstrahlung can be tuned for maximum emission power.

b. Scaling laws and relation to luminosity

The scaling laws are more favorable at low luminosities for this technique than for other beam-beam related signals.

The deflection at large impact parameters, which will be used for initial beam finding, scales as N_T/Δ, as can be seen from (3).

The maximum deflection produced as we scan the beams across each other to minimize spot sizes scales as N_T/σ_T, or as the root of luminosity.

c. Beam finding and centering

Initially, a first SLC beam will be threaded, at low repetition rate and intensity, through Arc and FFS, and to its dump. After best possible optimization of transmission and optical parameters, the above operation will be repeated with the other beam. BPMs on both sides will then be used to match the two orbit as well as possible. After this is done, the two beams will miss each other at the IP by offsets of a few hundred microns, which accounts for limited absolute BPM accuracy and alignment errors.

Bringing the two beams into collision, in preparation for spot size measurements,

will have to be done at full intensity since upstream wakefields, which affect the parameters to be tuned, are intensity dependant. Turning one of the two beams off momentarily will then produce an offset of

$$\Delta R^{BPM} \simeq \frac{-2N_T, r_e}{\gamma} \frac{1}{\Delta} d_{IP \rightarrow \mathrm{BPM}} \tag{7}$$

in the BPM located 2.5 meters away. When this offset is large enough to be resolved, so that we know that the beams feel each other, they can be centered by mapping out two dimensional surfaces similar to those shown in fig. 3 to 5, in order to find the symmetry points.

Assuming $20\,\mu$m resolution, the range of utilization can be written

$$\frac{N_T[5 \cdot 10^{10}]}{\Delta[100\,\mu\mathrm{m}]} \gtrsim \quad 2.8 \tag{8}$$

This means that at $N_T = 5 \cdot 10^{10}$, signals will be measurable when the beams pass within $350\,\mu$m of each other.

c. Spot size minimization

The maximum offset produced in the BPMs, during the above described mapping can be approximated by

$$\left|\Delta R^{BPM}\right|_{\max} \simeq \frac{2N_T\, r_e}{\gamma \sigma_T} \cdot F_{Round}(1) \cdot d_{IP} \rightarrow \mathrm{BPM} \tag{9}$$

or

$$\left|\Delta R^{BPM}\right|_{\max}[\mu\mathrm{m}] \simeq 2000 \frac{N_T[5 \cdot \mathbf{10}^{10}]}{\sigma_T[2.5\,\mu\mathrm{m}]} \tag{10}$$

Also here assuming $20\,\mu$m resolution, the range covered is

$$\frac{N_T[5 \cdot 10^{10}]}{\sigma_T[2.5\,\mu\mathrm{m}]} \gtrsim \quad 10^{-2} \tag{11}$$

which corresponds to a luminosity of $4 \cdot 10^{25}\,\mathrm{cm}^{-2}s^{-1}$.

References

(1) P. Bambade, These de Doctorat 3eme Cycle, Centre d'Orsay (1984)

(2) For example : S. Kheifets , Petra-Note 119 (1976)

Acknowledgements

Many useful discussions with G. Bonvicini, G. Bowden, R. Erickson, H. DeStaebler and A. Minten are eagerly acknowledged. K. Bane suggested useful tricks for calculating some of the integrals.

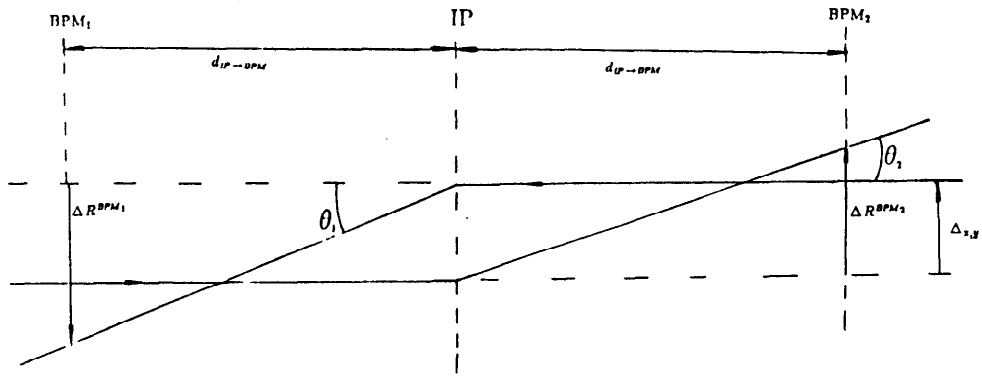

fig. 1

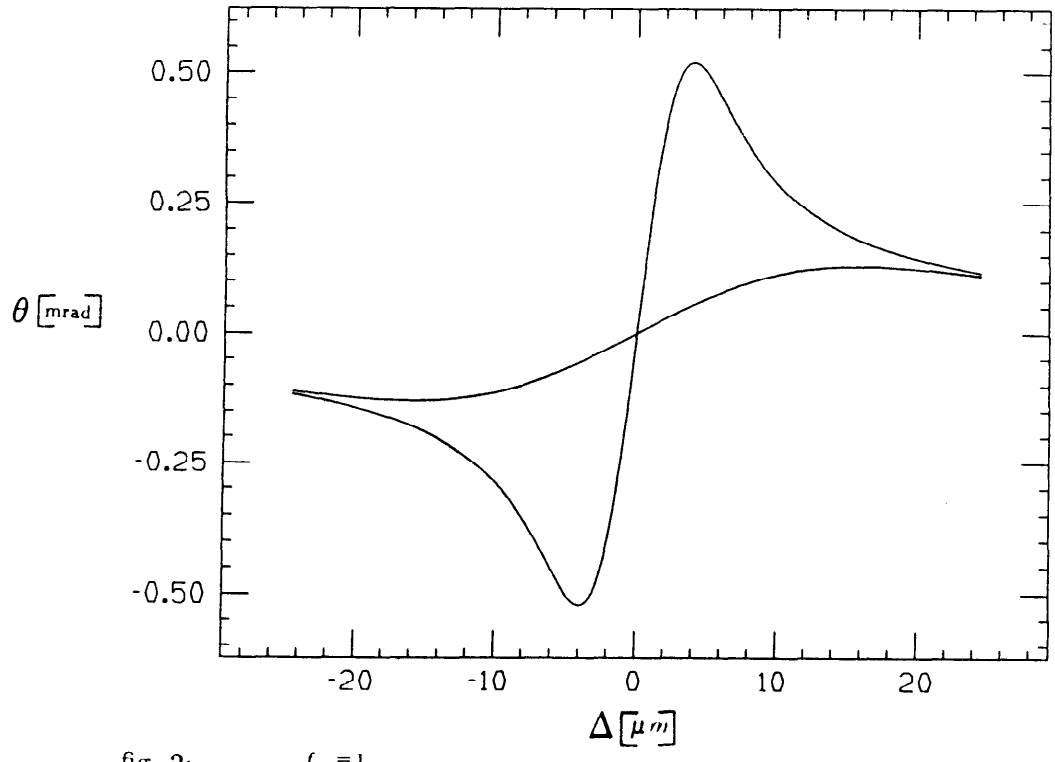

fig. 2: $f = 1$
$N_T = 5 \cdot 10^{10}$

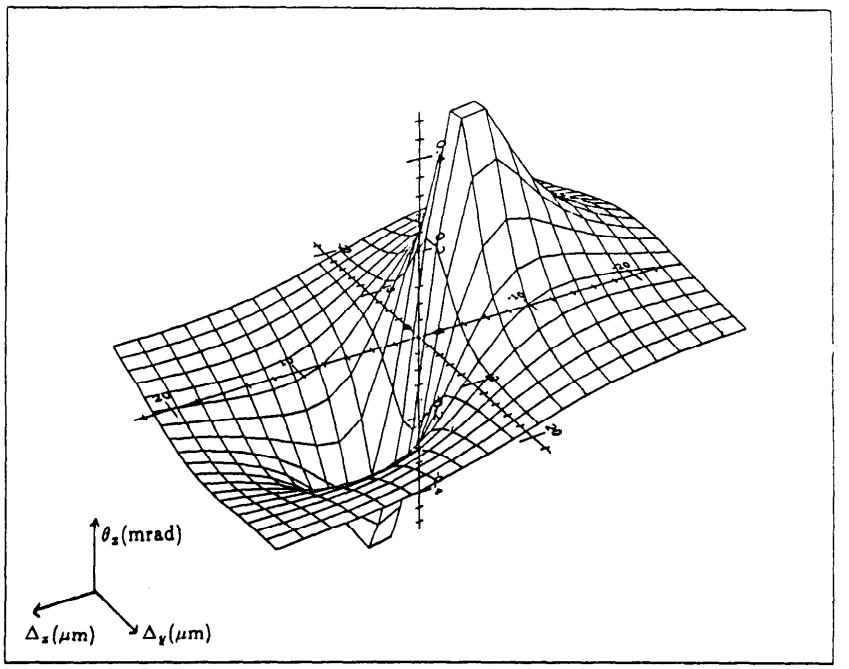

fig. 3.a:

$\sigma_{T_z} = 2.5\,\mu m$
$N_T = 5 \cdot 10^{10}$
$f = 1$

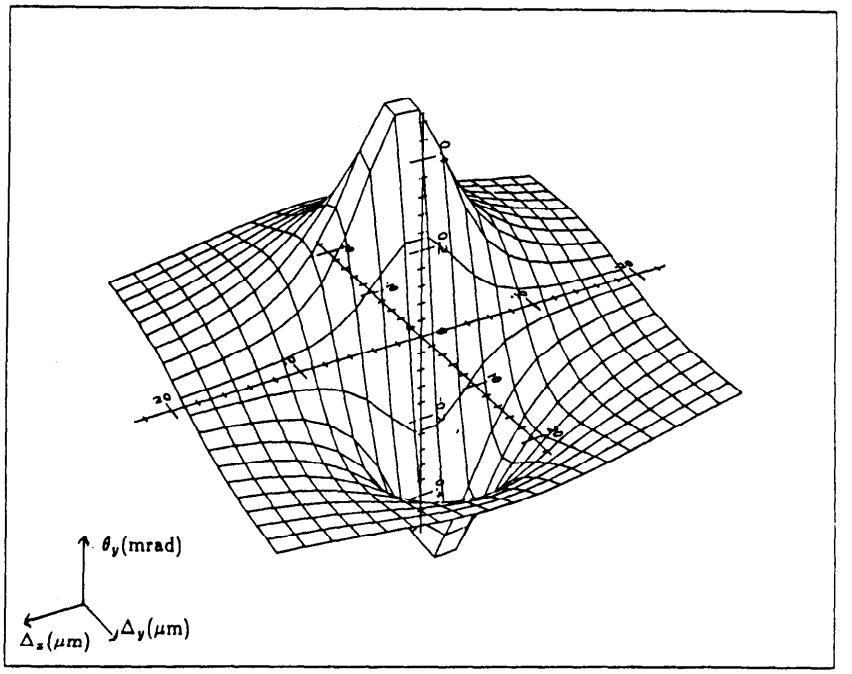

fig. 3.b.:

$\sigma_{T_z} = 2.5\,\mu m$
$N_T = 5 \cdot 10^{10}$
$f = 1$

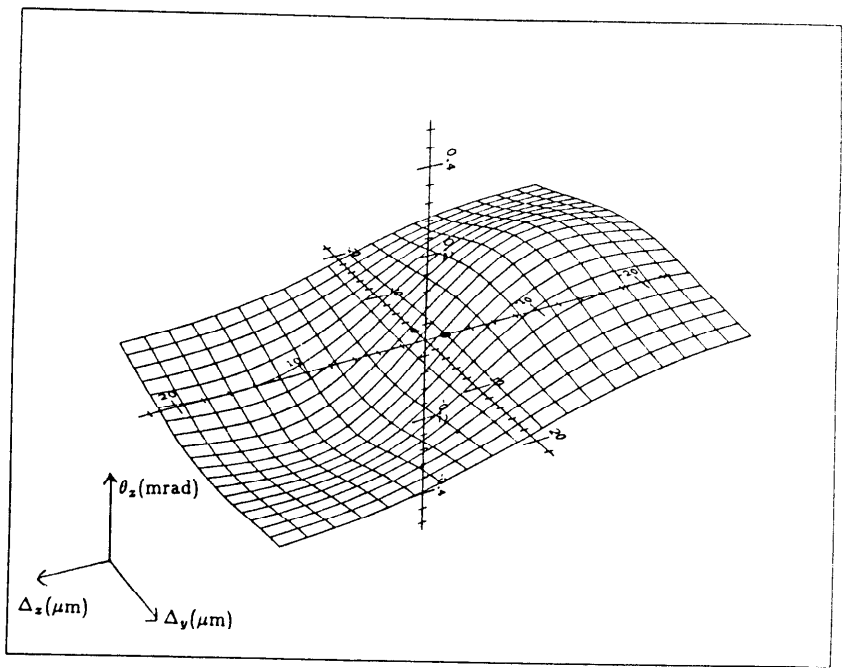

fig. 4.a: $\sigma_{T_z} = 7.5\,\mu m$

$N_T = 5 \cdot 10^{10}$

$f = 1$

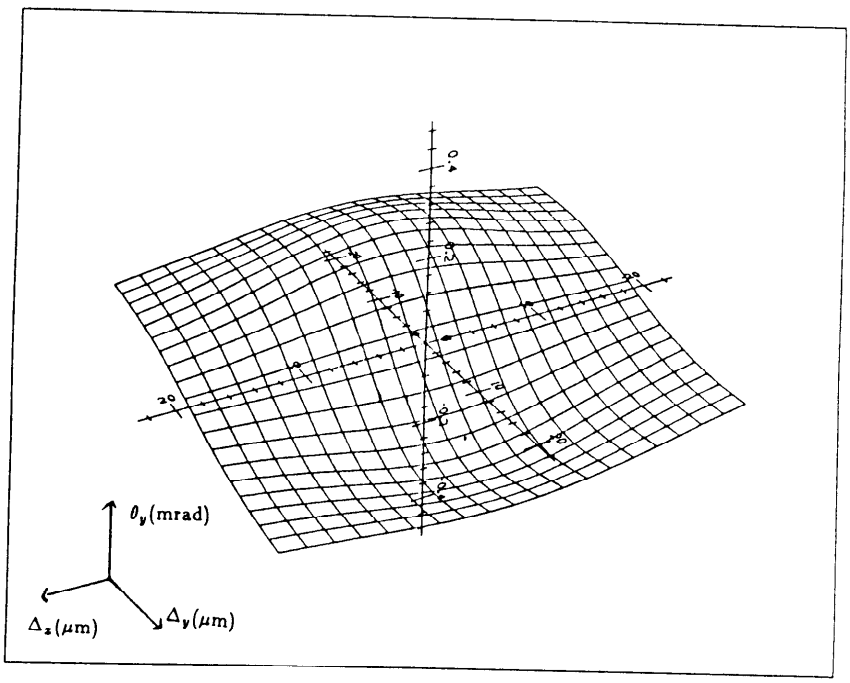

fig. 4.b: $\sigma_{T_z} = 7.5\,\mu m$

$N_T = 5 \cdot 10^{10}$

$f = 1$

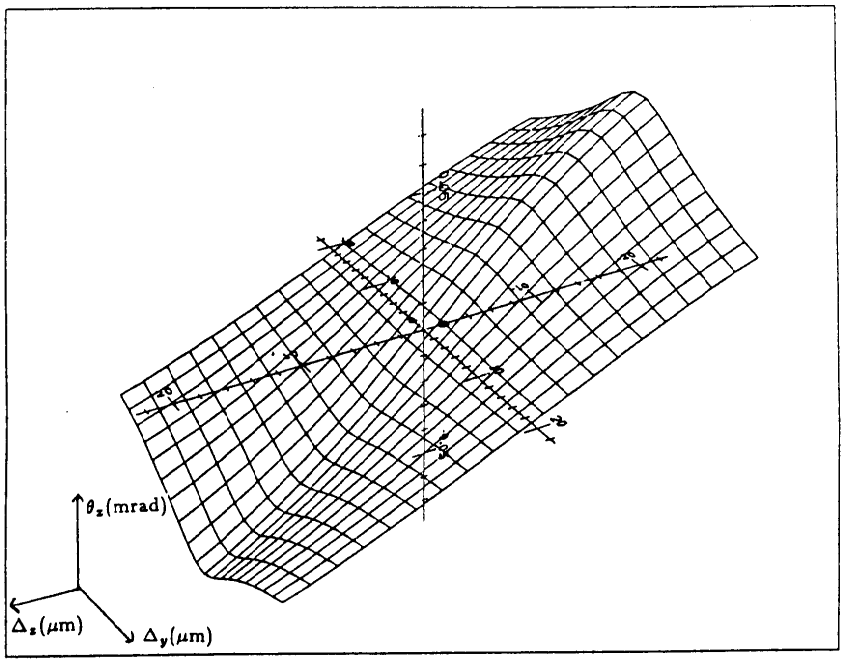

fig. 5.a: $\sigma_{T_z} = 2.5\,\mu m$

$N_T = 5 \cdot 10^{10}$

$f = 1/10$

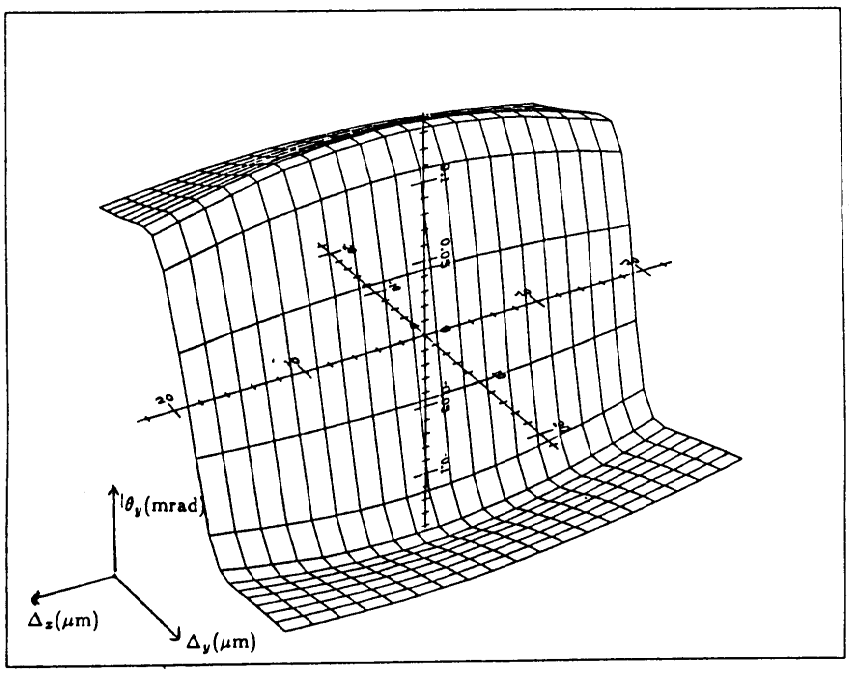

fig. 5.b: $\sigma_{T_z} = 25\,\mu m$

$N_T = 5 \cdot 10^{10}$

$F = 1/10$

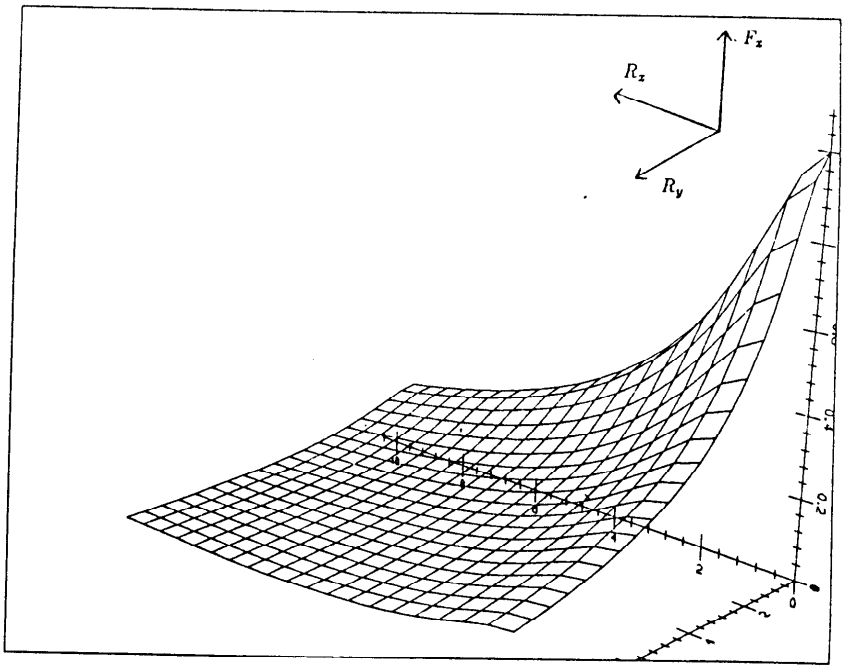

fig. 6: $f = 1$

$R_{x,y} = \frac{\sigma_{P_{x,y}}}{\sigma_{T_{x,y}}}$

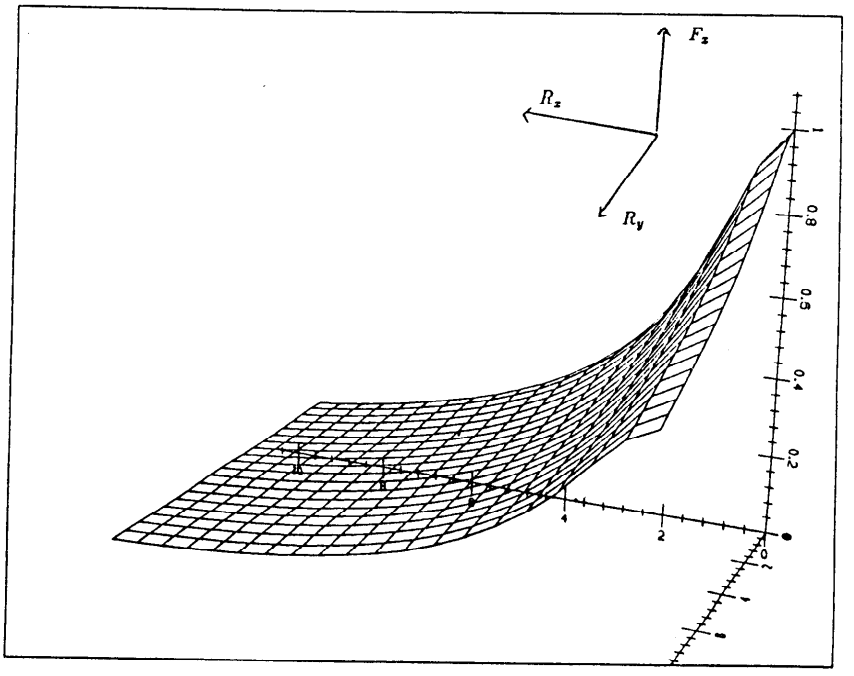

fig. 7: $f = 1/10$

$R_{x,y} = \frac{\sigma_{P_{x,y}}}{\sigma_{T_{x,y}}}$

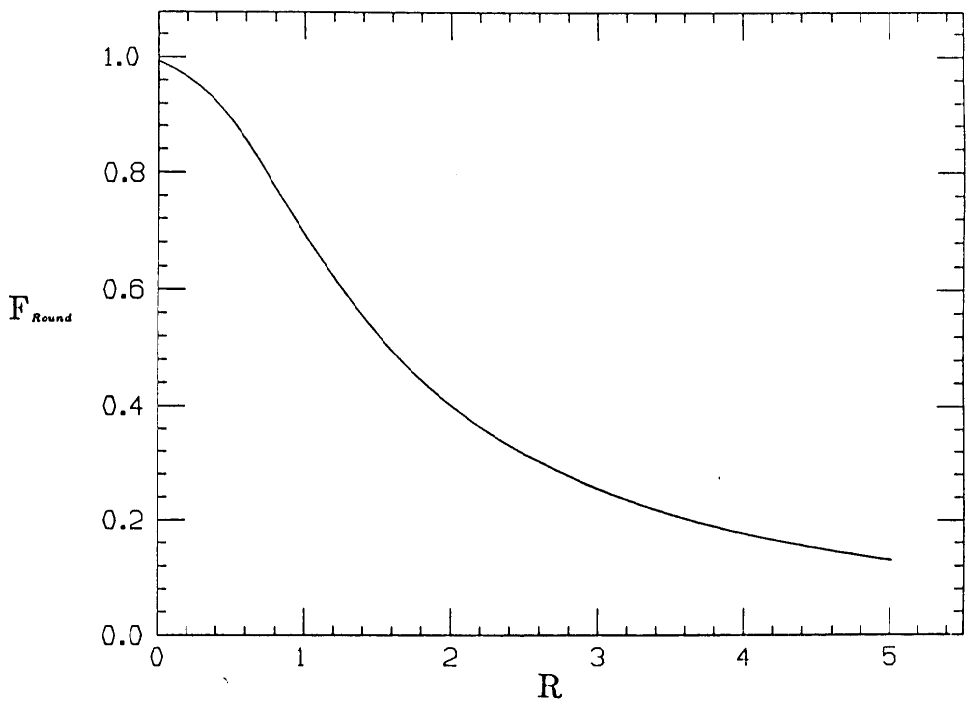

fig. 8: $f = 1$

$R_x = R + y + R$

A.2 "Beam-Beam Deflections as an Interaction Point Diagnostic for the SLC"

This conference article gives a more detailed description of the experimental method and an outline of the diagnostic hardware used.

SLAC – PUB – 3979
May 1986
(A)

BEAM-BEAM DEFLECTIONS AS AN INTERACTION POINT DIAGNOSTIC FOR THE SLC*

P. BAMBADE AND R. ERICKSON

Stanford Linear Accelerator Center
Stanford University, Stanford, California, 94305

Abstract

A technique is described for non-destructive measurement and monitoring of the steering offset of the electron and positron beams at the interaction point of the SLC, based on using stripline beam-position monitors to measure the centroid of one beam as it is deflected by the opposing beam. This technique is also expected to provide diagnostic information related to the spot size of the micron-size beams.

1. Introduction

The electromagnetic force acting between two intense colliding beams of oppositely charged particles will cause them to be deflected in passing by an angle that depends on the offset between the bunches, and the distribution of charge within the bunches. This deflection, measurable with nondestructive techniques, is expected to be the key to the final steering of the e^+e^- beams in the SLC. More generally, the beam-beam deflection phenomenon is a measurable manifestation of the collision of micron-size beams and is applicable to any large future linear collider.

In an e^+ e^- storage ring with a purely magnetic guide field, the counter-rotating beams follow exactly the same central trajectory and thus head-on collisions are unavoidable. There is no a priori reason why this should be true in linear colliders, however. In any linear collider, including the SLC, the opposing beams must be actively steered into collision guided by some observable that is sensitive to the impact parameter. Using state-of-the-art strip-line beam position monitors (BPMs), it may be possible to direct the two beams independently to the intended interaction point with an accuracy of perhaps 100 μm. In order to achieve acceptable luminosity with the SLC, the beams must be steered to within about one beam radius (about 2 μm) of each other. It is in this regime, far below the resolution limits of single-beam diagnostic devices, that the beam-beam deflection is strongest.

2. Basic Formulae

The angular deflection produced by the interaction of an SLC beam with the electromagnetic field of its colliding partner can be estimated analytically in the simplified case of two round Gaussian beams (see Fig. 1). Realistically, the beams are not expected to be round and gaussian until the final focus optical tuning is completed, a procedure that requires that the beams be colliding. A two-dimensional parametrization for the collision of two beams with transverse distributions of arbitrary flatness and orientation is given in Ref. 1.

The deflection of a single particle of charge e, passing at an offset Δ from the centroid of an oppositely charged Gaussian distribution, is given by:

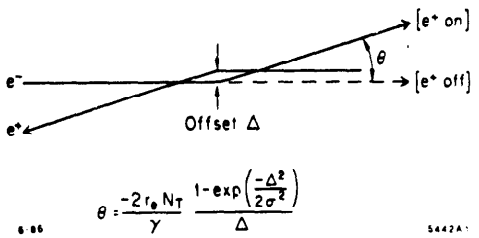

Fig. 1. The trajectory of each beam is deflected by the opposing beam passing at an offset Δ.

$$\theta(\Delta) = \frac{-2r_e N_T}{\gamma} \frac{1-\exp[-\Delta^2/2\sigma^2]}{\Delta}, \qquad (1)$$

where r_e is the classical radius of the electron, γ the relativistic E/m factor, N_T the number of particles and σ the RMS transverse size of the Gaussian distribution.

When the beams pass with offsets large compared to their transverse sizes, they see each other as point charges and (1) is a good approximation for their mutual deflection. When colliding with a small offset, the finite sizes of the beam distributions must be taken into account. This can be done by convoluting (1) with the distribution of the opposing beam. The result of such a calculation, carried out in the limit of small Δ, is expressed in terms of a form factor which reduces the average deflection:

$$F(R) = \frac{Ln(1+R^2)}{R^2} \qquad (2)$$

Here R is the ratio of the transverse sizes of the two beams.

Deflection versus offset is plotted in Fig. 2 for 50 GeV beams consisting of 5×10^{10} particles, with transverse spot sizes σ of 2, 5, and 10 μm. 10 μm is the estimated size of the beams at the SLC interaction point before optical corrections are made. Magnet setting errors and misalignments contribute to this estimate. By adjusting the final focus corrector magnets, σ can be reduced to about 2 μm. The above form factor has been incorporated in the curves as a multiplying reduction factor, assuming in each case $R = 1$.

3. Deflection Detection

Several methods have been studied for detecting and measuring the beam-beam deflections. The most obvious is to use a pair of BPMs straddling the interaction point. If the drift length "lever arm" is long enough, a deflection at the I.P. will result in a measurable position shift at the BPM. The power of this method can be greatly enhanced by suppressing the opposing beam on some pulses and watching the measured beam jump back to its undeflected position. To make this possible, a pair of special pulsed magnets, the "single-beam dumpers",

* Work supported by the Department of Energy, contract DE-AC03-76SF00515.

Contributed to the Stanford Linear Accelerator Conference, Stanford, California, June 2-6, 1986

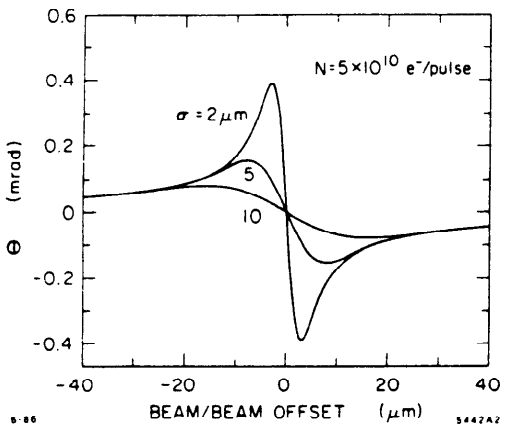

Fig. 2. The deflection angle Θ as a function of offset Δ, plotted for three spot sizes.

will be provided upstream of the final focus to kick either beam out of the transport system on command.

In principle, the beam-beam deflection can also be observed with conventional screen profile monitors located in the paths of the outgoing extracted beams as they are transported to the dumps. In the SLC, such measurements will be possible in the vertical dimension only. Deflections in the horizontal plane will be obscured by the momentum dispersion introduced by the extraction septum magnets. As part of a planned upgrade for the north extraction line,[2] it will be possible to cancel the dispersion with additional magnets to enable deflection measurements in both the horizontal and vertical dimensions. In any case, position measurements in the extraction lines provide essentially no information about the absolute position of either beam near the I.P., because of the large number of magnets, traversed by the outgoing beam before reaching the extraction line. However, relative position shifts can be measured using devices in the extraction lines in conjunction with the single-beam-dumpers mentioned above to give a useful measure of the deflection at the I.P.

Another approach is based on detecting beamstrahlung radiation. This is the name given to the synchrotron radiation emitted by each beam as it is deflected by the other. The angular distribution of this radiation, strongly peaked forward in the direction of the outgoing beam, can be measured with a suitable detector along a line of sight but quite distant from the interaction point.[3]

4. Application to Steering and Tuning Procedures

A three-step tuning procedure is envisioned:

1. Initial beam finding: One beam – designated the "target" in this case – is momentarily suppressed with a single-beam dumper while position measurements are made on the "probe" beam. In this way, the shift induced by the target beam can be determined. When the offset between the beams is large, the magnitude of the shift is inversely proportional to the offset and its sign tells in which direction to steer. This can be seen by taking the limit of (1) for large Δ:

$$\theta(\Delta) \simeq \frac{-2r_e N_T}{\gamma} \frac{1}{\Delta} . \qquad (3)$$

2. Beam centering: Scanning the target across the probe and recording a plot similar to Fig. 2 for the probe will facilitate optimal steering of the two beams. The zero-deflection symmetry point in Fig. 2 is reached when the beams are perfectly centered.

3. Spot size tuning: Taking the limit of (1) for small Δ and multiplying by the form factor (2) gives:

$$\theta(\Delta) \simeq \frac{-r_e N_T}{\gamma} \frac{\Delta}{\sigma^2} F(R) . \qquad (4)$$

The slope of the deflection of the probe beam near the zero-deflection symmetry point is inversely proportional to the cross-sectional area of the target. By differentiating (1), it can be seen that the deflection is maximum for offsets of about 1.6 standard deviations of the target distribution, and that the maximum deflection scales as the inverse of the transverse spot size:

$$\theta_{max} = 0.451 \frac{2r_e N_T}{\gamma} \frac{1}{\sigma} . \qquad (5)$$

A relative measure of spot size can thus be obtained by scanning one beam across the other as in Step 2 above. Guided by these measurements, an operator can adjust optical elements of the transport system to minimize this final spot size.

The procedures described here are based on relative measurements of the outgoing beam position at locations where the angular deflection produced in the collision leads to a transverse position shift. Many of the BPMs in the outgoing transport system have suitable phase shifts from the IP to be used for this purpose. The best locations, however, are in the final optical transformer quadrupoles, where the β-functions reach their largest values, thereby magnifying the deflections the most, and where dispersion is negligible, (which minimizes confusion with energy variations). Three BPMs, near quadrupoles Q1, 3 and 4, are planned for this purpose[3] (Fig. 3). Each has an effective optical lever arm of about 3 meters. Position shifts corresponding to a wide range of IP parameters can be resolved at these locations.

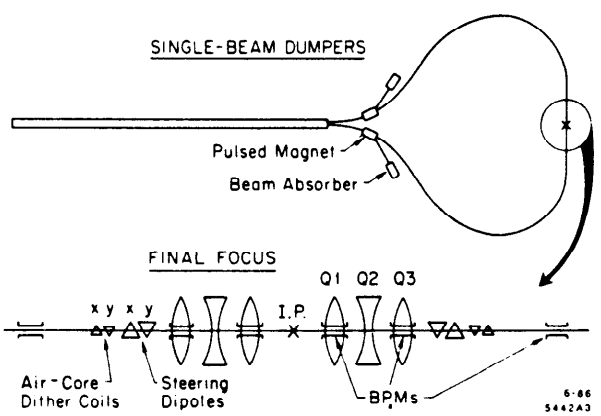

Fig. 3. Schematic of beamline components relevant to the deflection technique.

The useful range of these techniques, i.e., the maximum offset that still gives a measurable deflection, is limited only by the ability of the BPM to resolve beam centroid movements. For example, assume the BPM near Q1 can resolve the centroid position of a single bunch of 5×10^9 particles to a level of 20 μm. It will then be possible to detect relative beam-beam offsets up to a maximum of:

$$\Delta(\mu\text{m}) \simeq 40 \frac{N_T}{5 \times 10^9} . \quad (6)$$

For larger beam currents, it may be possible to do better than the limit indicated in (6), because the BPM resolution also improves with increasing current. By chopping one beam off and on using the single beam dumpers and averaging over many pulses, the resolution can be improved further. Although marginal at low intensity, this beam finding technique should bridge the gap between the usual orbit matching methods which rely on absolute BPM accuracy to steer the beams independently to the IP, and techniques based on luminosity-related signals, such as beamstrahlung,[4] disruption imaging,[2] and the Bhabha scattering rate.

5. Dynamic Errors and Corrections

It is expected that even when the static crossing errors have been corrected as described above, the two beams will not remain centered on each other without an active feedback system. Many sources of drift and jitter that could cause the beams to wander at the IP have been identified. In most cases, these effects can be minimized with careful attention to relevant hardware designs. Magnet power supplies, for example, must be well regulated, and support structures must be rigid. Natural ambient ground vibrations at frequencies above 1 Hz have been shown[5] to be negligible, although some local man-made vibration sources such as reciprocating pumps could cause problems if not isolated. On a slower time scale, thermal effects will cause mechanical support structures to expand, and power supplies to drift enough to adversely effect the luminosity unless steering corrections are made. Studies of feedback schemes for the SLC have focused on simple and relatively slow algorithms, although the BPM electronics, control system, and other key components are being built to allow pulse-by-pulse feedback to accommodate faster or more complex schemes.

A simple feedback algorithm for correcting relatively slow drifts is based on automatically suppressing one beam periodically using the single beam dumper. Of course, the luminosity would be sacrificed on these occasional pulses, but they would enable a steering correction to be computed from the measured position shifts of the outgoing beam. Because each measured deflection can correspond to two possible offsets, the operation has to be carried out frequently enough to ensure that the actual offset does not drift outside the domain of the IP, bounded by the deflection maxima, in the time between updates. This approach is probably adequate to track the thermal expansion of support structures and other mechanical effects.

An approach that does not require sacrificing any beam pulses would be to excite small "dither coil" dipoles (Fig. 3) in a pre-programmed way to induce small periodic offsets at the IP, with an amplitude of a fraction of a standard deviation. In this way, one beam can be made to trace out a pattern such as a small circle at the IP. The deflections of the opposing beam will then project the same pattern at the BPM. When the offset between the beams corresponds to a point on a steeply rising positive slope in Fig. 2 (beyond the 1.6 σ peak on either side), the projection is a magnified image of the dither pattern. When the offset is less than 1.6 σ, the projection is an inverted image of the dither pattern. Synchronous position measurement would then allow a determination of whether the beams were colliding within or beyond 1.6 standard deviations of each other. If necessary, a correction could be applied to bring them back to within one σ. The sign of the deflection would indicate the direction in which to steer. In both these algorithms, corrections are applied using steering correctors immediately upstream of Q3.

Acknowledgements

We wish to thank the members of the SLC Final Focus Group for helpful discussions on this topic, and in particular W. Kozanecki for encouraging us to put this paper together.

References

1. P. Bambade, "Beam-Beam Deflections to Measure Spot Size and Offset at SLC IP," SLAC CN-303, 1985.
2. Mark II Collaboration and SLC Final Focus Group, "Extraction-Line Spectrometers for SLC Energy Measurement," SLAC-SLC-PROP(2), 1986.
3. G. Bowden, Private Communication.
4. G. Bonvicini, C. Field and A. Minten, "Beamstrahlung Monitor for SLC Final Focus Using Gamma Ray Energies," Proceedings of this conference.
5. G. Bowden, "Mechanical Vibrations of the Final Focus," SLAC CN-314, 1985; G.E. Fischer, "Ground Motion and Its Effects in Accelerator Design," SLAC-PUB-3392 Rev., 1985.

A.3 "Observation of Beam-Beam Deflections at the Interaction Point of the Stanford Linear Collider"

In this publication, we report the first measurements of beam-beam deflections at the SLC. The successful application of this method to maintain the beams in collision is described, with a summary of the experimental limitations.

SLAC-PUB-4767
UM-HE-89-2
COLO-HEP-186
January 1989
(A/E)

OBSERVATION OF BEAM-BEAM DEFLECTIONS AT THE INTERACTION POINT OF THE SLAC LINEAR COLLIDER*

P. BAMBADE, [1],[a] R. ERICKSON,[1] W. A. KOSKA,[2] W. KOZANECKI,[1]
N. PHINNEY[1] AND S. R. WAGNER[3]

[1] *Stanford Linear Accelerator Center,*
Stanford University, Stanford, California 94309

[2] *University of Michigan, Ann Arbor, Michigan 48109*

[3] *University of Colorado, Boulder, Colorado 80309*

ABSTRACT

We report the first direct observation of the electromagnetic deflection of high energy electron and positron beams as they pass each other with small impact parameters. Measurements of the deflection amplitude are found in agreement with theoretical expectations. This phenomenon, which is sensitive both to the relative position of the two beams and to their transverse sizes, has been used successfully to optimize and maintain collisions at the interaction point of the SLAC Linear Collider.

Submitted to Physical Review Letters

---

*Work supported by the U. S. Department of Energy under contracts DE-AC02-86ER40253, DE-AC02-84ER01112, and DE-AC03-76SF00515.

The SLAC Linear Collider[1] (SLC) is a novel electron-positron accelerator designed to operate with center-of-mass energies around the mass of the neutral intermediate vector boson (Z^0). The frequency of collisions in linear colliders is limited by power considerations to a few hundred Hertz, typically two or three orders of magnitude lower than in storage rings. At these frequencies, achieving interaction rates useful for physics requires focusing the beams to transverse sizes of at most a few microns, and then establishing and maintaining collisions between beams with impact parameters smaller than the beam sizes themselves. One technique which has been proposed[2] for this purpose is based on measuring the deflections produced in the beam trajectories by the coherent electromagnetic interaction between the beam bunches as they pass near or through each other at the interaction point (IP).

In this letter we report the first observation of beam-beam deflections, which constitutes a crucial step in establishing the viability of the linear collider concept. After deriving the predicted properties of the phenomenon and their dependence on beam parameters, we describe the technique used to measure the deflections. We then turn to a discussion of the experimental results, and conclude with an outline of possible refinements in applying beam-beam deflections to luminosity optimization in linear colliders.

When two oppositely charged, relativistic beams pass each other, they feel an attractive impulse as a result of their electromagnetic interaction. The resulting deflection in their trajectory is given by $\theta = tan^{-1}\ (p_t/p) \approx (p_t/p)$, where p_t is the transverse momentum imparted to one bunch as it passes through the field of the other bunch, and p is the longitudinal momentum of the bunch.

Consider the deflection of a single "probe" particle in the field of an oppositely charged "target" bunch of N_t particles, each with charge q, having a Gaussian charge distribution:

$$G(x,y,z,\sigma_x,\sigma_y,\sigma_z) = \frac{N_t q}{(2\pi)^{3/2}\,\sigma_x\sigma_y\sigma_z}\,\exp\left\{-\frac{x^2}{2\sigma_x^2}-\frac{y^2}{2\sigma_y^2}-\frac{z^2}{2\sigma_z^2}\right\} \quad . \tag{1}$$

The transverse electric field of the bunch is given by:[3]

$$E_{x,y} = -\frac{\partial}{\partial x,y}\left[\frac{N_t q}{\sqrt{\pi}\;4\pi\,\epsilon_0}\int_0^\infty dt\;\frac{\exp\left\{-\frac{x^2}{t+2\sigma_x^2}-\frac{y^2}{t+2\sigma_y^2}-\frac{z^2}{t+2\sigma_z^2}\right\}}{\left(t+2\sigma_x^2\right)^{1/2}\;\left(t+2\sigma_y^2\right)^{1/2}\;\left(t+2\sigma_z^2\right)^{1/2}}\right] \quad . \tag{2}$$

We now solve for the transverse momentum in x and y:

$$p_{x,y} = \int_{\Delta_\tau} qE_{x,y}\,d\tau = \frac{-2N_t\,q^2\Delta_{x,y}}{4\pi\,\epsilon_0 c}\int_0^\infty dt\;\frac{\exp\left\{-\frac{\Delta_x^2}{t+2\sigma_x^2}-\frac{\Delta_y^2}{t+2\sigma_y^2}\right\}}{\left(t+2\sigma_{x,y}^2\right)\;\left(t+2\sigma_x^2\right)^{1/2}\;\left(t+2\sigma_y^2\right)^{1/2}} \quad , \tag{3}$$

where Δ_τ is the length of time the probe charge is in the field of the beam and $\Delta_{x,y}$ is the offset between the probe charge and the center of the bunch. To obtain the right-hand side of Eq. (3), we have made the substitution $c\tau = z$ and performed the integration over z. Equation 3 is valid when disruption effects, where the beams induce size changes in each other during collision, are negligible. Since $p \approx m_e\gamma c$, we may write:

$$\theta_{x,y} = \frac{-2r_e\,N_t\,\Delta_{x,y}}{\gamma}\int_0^\infty dt\;\frac{\exp\left\{-\frac{\Delta_x^2}{t+2\sigma_x^2}-\frac{\Delta_y^2}{t+2\sigma_y^2}\right\}}{\left(t+2\sigma_{x,y}^2\right)\;\left(t+2\sigma_x^2\right)^{1/2}\;\left(t+2\sigma_y^2\right)^{1/2}} \quad , \tag{4}$$

where r_e is the classical radius of the electron.

For the realistic case of a probe beam with a Gaussian charge distribution a convolution with the expression obtained for the deflection of a single particle must be done:

$$\langle\theta_{x,y}\rangle = \int_{-\infty}^{\infty}\int_{-\infty}^{\infty} dxdy\ \tilde{G}(x-\bar{x}_p, y-\bar{y}_p, \sigma_{p,x}\sigma_{p,y})\ \theta_{x,y} \quad , \tag{5}$$

where $\langle\theta_{x,y}\rangle$ is the average deflection angle of the probe bunch (*i.e.*the deflection of the center of gravity of the bunch). The density distribution of the probe beam is $\tilde{G}$, where $\bar{x}_p(\bar{y}_p)$ is the center and $\sigma_{p,x}(\sigma_{p,y})$ is the standard deviation in the $x(y)$ direction. If we assume that the two beam spots are erect ellipses in the transverse plane, then[4]

$$\langle\theta_{x,y}\rangle = \frac{-2r_e\, N_t\, \Delta_{x,y}}{\gamma} \int_0^{\infty} dt\ \frac{\exp\left\{-\frac{\Delta_x^2}{(t+2\Sigma_x^2)} - \frac{\Delta_y^2}{(t+2\Sigma_y^2)}\right\}}{(t+2\Sigma_{x,y}^2)\ (t+2\Sigma_x^2)^{1/2}\ (t+2\Sigma_y^2)^{1/2}} \quad , \tag{6}$$

where $\Delta_x(\Delta_y)$ is now the distance between beam centers and $\Sigma_x^2 = \sigma_{p,x}^2 + \sigma_{t,x}^2$ ($\Sigma_y^2 = \sigma_{p,y}^2 + \sigma_{t,y}^2$) is the sum of the squares of the probe and target beam sizes. The integration in this expression can be performed analytically if we assume that $\Sigma_x = \Sigma_y = \Sigma$ (this includes the case of round probe and target beams). With $\Delta = (\Delta_x^2 + \Delta_y^2)^{1/2}$ the result is:

$$\langle\theta_{x,y}\rangle = \frac{-2r_e\, N_t\, \Delta_{x,y}}{\gamma\Delta} \left(\frac{1-\exp\left\{-\frac{\Delta^2}{2\Sigma^2}\right\}}{\Delta}\right) \quad . \tag{7}$$

Equation 7 shows, as expected, that there is no deflection either when the beams are far from each other or when they are exactly centered. The maximum

deflection for round beams occurs when the impact parameter is approximately 1.6 Σ. During its start up phase, the SLC ran with typical beam intensities of slightly less than 1×10^{10} particles/pulse, and transverse beam sizes at the IP of approximately 5 μm, so the maximum deflections seen in this data should be about 35 μrad. At these sizes and intensities disruption effects are expected to be negligible.

We used four beam position monitors (BPMs), two on either side of the IP, to determine the beam deflection at the IP. These BPMs[5] are captured between quadrupole magnet pole pieces due to space limitations (Fig. 1). The four electrodes in each BPM are carefully impedance-matched and are read out on both ends into custom-designed electronics.[5] This allows us to measure the vertical and horizontal positions of both beams on the same machine pulse, even though the beams are separated by less than 30 nsec in the BPMs closest to the IP. The pulse-to-pulse resolution of these BPMs is measured to be better than 10 μm for beam intensities of $\sim 5 \times 10^9$ particles/pulse, and is expected to improve further as SLC beam intensities increase.

Measuring positions in two BPMs on both sides of the IP independently defines incoming and outgoing beam trajectories at the IP. The information from all four BPMs is used in four separate linear fits which yield the beam position, the incoming beam angle, and the beam deflection angle (all evaluated at the IP) in each plane for both beams on a single beam pulse.[6] While the positions and angles of the beams at the IP are observed to be stable on a pulse-by-pulse basis to a fraction of the measured beam size and angular divergence (typically several hundred μrad), fluctuations of this magnitude in the outgoing beam angle can still be several times larger than the expected maximum deflection. Fitting directly

for the difference between the outgoing and incoming angles of a given beam effectively decouples any angular motion of the incoming beam from the deflection angle measurement. This can also be shown to reduce any static misalignments in the BPMs to a constant offset of the measured deflection angle,[6] which can be ignored for our applications.

In practice, the deflection angles for both beams are measured as a function of the impact parameter as one beam is swept across the other in either the horizontal or the vertical direction. These beam scans are accomplished using small air-core dipole magnets (Fig. 1), which can increment the beam position, between machine pulses, with a resolution of 0.05 μm. Since the beams deflect each other very little when they are far apart, they must first be brought to within a few beam radii of each other. This has been done by steering the beams, one at a time, onto carbon filaments with radii comparable to the beam size, which are inserted into the center of the beam pipe at the IP.[7,8] These filaments produce secondary emission and Bremsstrahlung signals proportional to the fraction of the beam intercepted. The filaments, which are primarily used to measure and optimize transverse beam sizes, stay retracted during deflection measurements.

To get the information necessary to precisely center the beams, one beam is scanned past the other, typically over a range of ± 40 μm in 2 μm steps. The BPM signals are read out on each pulse, processed, and stored by a microcomputer until the scan is finished. The microcomputer also sets and reads back the current in the air-core dipole magnets used to position the beams. When the scan is finished, the microcomputer sends the scan data to a VAX–8800 computer on which the data is analysed and displayed. The results of a typical positron beam scan in x are shown in Fig. 2. The deflection angles parallel ($\langle\theta_x\rangle$) and perpendicular ($\langle\theta_y\rangle$) to the scan

direction as a function of the scanned beam's distance from its original position are shown in Figs. 2(a) and 2(b), respectively. For approximately round beams the data are expected to be described by Eq. (7). For real-time beam centering, fits to the data were approximated using Eq. (7) for the in-plane deflection curve, assuming the beams were aligned in the scanned direction, and by a Gaussian for the out-of-plane curve. As can be seen by the curves shown in Fig. 2, the data is consistent with these approximate functional forms, with the maximum out-of-plane deflection occurring at the zero-crossing of the in-plane deflection curve.

Figure 3 shows a scan with one of the largest maximum deflections measured to date. After centering the beams in x, the e^+ beam was scanned past the e^- beam in the y direction. The beam sizes measured prior to this scan using the carbon filaments were $\sigma_x = 7.2\ \mu$m, $\sigma_y = 3.9\ \mu$m for the electron beam; $\sigma_x = 4.9\ \mu$m, $\sigma_y = 3.9\ \mu$m for the positron beam. The curve derived using these measured beam sizes as input overlays the data. The beam currents, which provide a multiplicative normalization, were adjusted to give the best fit and were found to be consistent with currents measured by other means. The agreement between data and theory indicates that beam-beam deflections are well understood and reliably measured.

Beam-beam deflections are a powerful tool for luminosity optimization at the SLC. Positioning the scanned beam on the zero-crossing of the deflection curve aligns the beams to a small fraction of the beam size. This has been the primary method used to steer the SLC beams into collision. In most cases, the beam spots at the interaction point are approximately round, so that meaningful fits to the deflection data using the form of Eq. (7) can be made. These immediately yield estimates of the beam sizes and intensities. In the future, pulse-to-pulse sampling

of the beam deflection will be made in a feedback microcomputer which will be used to compensate for any slow drifts of the beams relative to each other.

Beam-beam deflections may also be used to minimize the spot size at the IP. Small changes in beam size are signalled by measurable changes in the slope of the deflection curve through the zero-crossing point. This is demonstrated in Fig. 4, which shows the dependence of the slope on the size of the e^- beam in x for several different e^+ beam radii. The electron beam size in y is assumed fixed near its optimal value.

The relationship between the slopes of the deflection curves and the luminosity is:[9]

$$L = \frac{Nf\gamma}{4\pi r_e}\,(S_x + S_y) \quad , \tag{8}$$

where S_x and S_y are the slopes of the deflection curves measured with separate x and y scans after the beams have been centered. The repetition rate of the collider is f. An independent measurement of the number of particles, N, in the deflected beam is also required. The advantage in using the slopes is that they can be accurately measured even when the beams are not round. Optimal luminosity can be achieved by adjusting the focus of the beams to obtain the maximum slopes. Once this has been established, it can be monitored by checking the slopes periodically with short scans across the zero crossing point.

In conclusion, we have presented measurements of the deflections of high-energy electron and positron beams as they pass by each other. These measured deflections agree with theoretical expectations. We have discussed how the deflections have

been used to steer micron-sized beams into collision, and how they will be used for spot size optimization at the SLC.

We would like to thank G. B. Bowden, J.-C. Denard, A. Gromme, J.-L. Pellegrin, and M. Ross, who were responsible for the BPM system. The performance of these devices was critical for the results presented here. We also acknowledge the numerous and invaluable contributions to this experiment by the SLC staff and the Final Focus commissioning group.

REFERENCES

[a] Present adress: Laboratoire de l'Accélérateur Linéaire, Bât. 200, Orsay, France 91405.

1. B. Richter and R. Stiening, in *Proc. of the 1987 Int. Sym. on Lepton and Photon Interactions at High Energies,* Hamburg, July 27–31, 1987, North-Holland, Amsterdam, p. 495.
2. P. Bambade and R. Erickson, in *1986 Linear Accelerator Conf. Proc.,* June 2–6, 1986, SLAC–Report–303, Stanford Linear Accelerator Center, Stanford, California, p. 475.
3. See, for example, K. Takayame, Lett. Cimento **34**, 190 (1982).
4. K. Hirata, Nucl. Instrum. Methods A **269**, 7 (1988).
5. J.-C. Denard *et al.,* in *Proc. of the 1987 IEEE Particle Accelerator Conf.,* Washington, D. C., March 16–19, 1987, p. 686.
6. W. A. Koska and S. R. Wagner, SLAC CN–365 (unpublished), August 1988, Stanford Linear Accelerator Center, Stanford, California.
7. R. Fulton *et al.,* Nucl. Instrum. Methods A **274**, 37 (1989).
8. G. Bowden *et al.,* SLAC–PUB–4744, submitted to Nucl. Instrum. Methods.
9. W. A. Koska, to be published.

FIGURE CAPTIONS

Fig. 1. Schematic of beamline components relevant to the beam-beam deflection measurement.

Fig. 2. A beam-beam deflection scan of the e^+ beam relative to its initial position showing (a) the in-plane deflection, and (b) the out-of-plane deflection. The e^- beam intensity was about 7×10^9 e^-/pulse, and both beams were approximately round with $\sigma = 7$ μm. The beams were approximately 10 μm apart in the out-of-plane direction during this scan.

Fig. 3. An e^+ beam deflection scan in y after alignment in x. The curve overlaying the data is a theoretical calculation using as input the beam sizes as measured by the wire filaments.

Fig. 4. The expected slope of the in-plane deflection curve at the zero-crossing point as a function of the e^- beam σ_x^- with a fixed σ_y^- of 1.5 μm. The solid curve corresponds to a round e^+ beam with $\sigma^+ = 1.5$ μm, the dashed to $\sigma^+ = 3.0$ μm and the dotted to $\sigma^+ = 6.0$ μm. The target beam intensity for these calculations was 1×10^{10}.

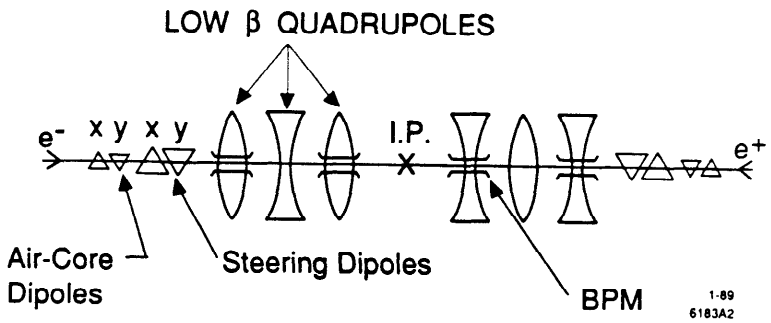
LOW β QUADRUPOLES
e⁻ x y x y
I.P.
e⁺
Air-Core Dipoles
Steering Dipoles
BPM
1-89
6183A2

Fig. 1

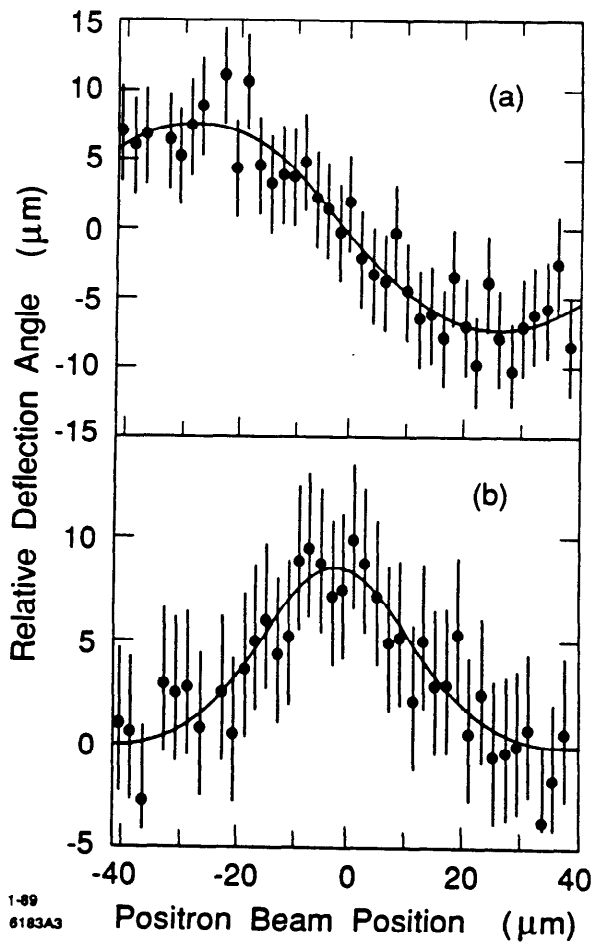
15
10
5
0
-5
-10
-15
(a)
(b)
Relative Deflection Angle (μm)
-40
-20
0
20
40
Positron Beam Position (μm)
1-89
6183A3

Fig. 2

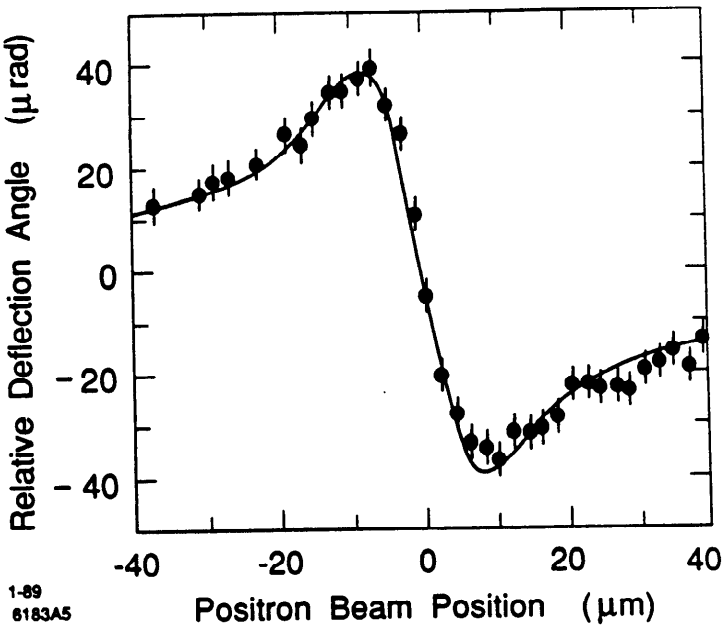
Relative Deflection Angle (μrad)
40
20
0
-20
-40
-40
-20
0
20
40
Positron Beam Position (μm)
1-89
6183A5

Fig. 3

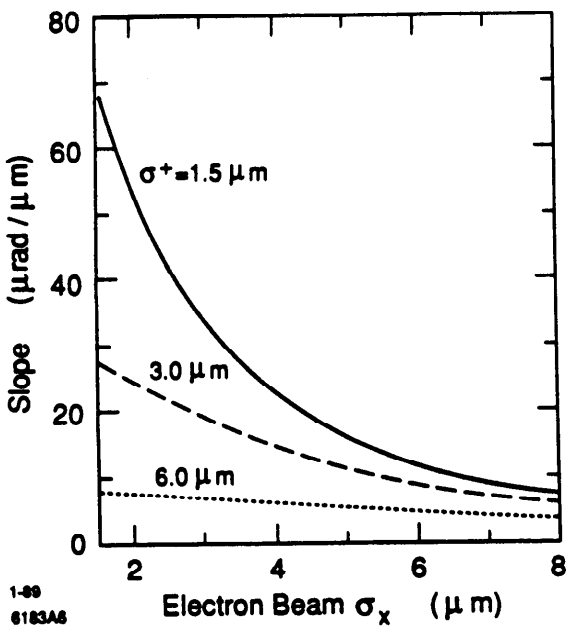
Slope (μrad/μm)
80
60
40
20
0
σ+=1.5 μm
3.0 μm
6.0 μm
2
4
6
8
Electron Beam σx (μm)
1-89
6183A6

Fig. 4

REFERENCES

[1] B. Richter, Nucl. Inst. Meth. **136, 47** (1976).

[2] M. Tigner, Nuovo Cimento **37**, 1228 (1965), and B. Richter, SLAC-PUB-4482 (1987).

[3] M. Sands, SLAC-121-Addendum (1979).

[4] SLAC-REPORT-229 (1980), and SLC *Design Handbook* (1984).

[5] J. C. Sheppard *et al.*, Commissioning of the SLC Injector, *Proceedings of the Particle Accelerator Conference* (Washington, D. C., March 1987).

[6] G. E. Fischer *et al.* A 1.2 GeV Damping Ring Complex for the Stanford Linear Collider, *Proceeding of the Twelfe International Conference on High Energy Accelerators*, FNAL, 37 (1983).

[7] J. T. Seeman *et al.*, Experimental Beam Dynamics in the SLC Linac, *Proceedings of the Particle Accelerator Conference* (Washington, D.C., March 1987).

[8] Fatin Bulos *et al.*, Design of a Hign Yield Positron Source, IEEE Trans. Nucl. Sci. **NS-32,** 1832 (1985), and S. Ecklund, The Stanford Linear Collider Positron Source, *Proceedings of the Workshop on Intense Positron Beams* (Idaho Falls, Idaho, June 1987).

[9] G. E. Fischer *et al.*, Some Experiences from the Commissioning Program of the SLC Arc Transport System, *Proceedings of the Particle Accelerator Conference* (Washington D. C. March 1987).

[10] J. J. Murray *et al.*, The Completed Design of the SLC Final Focus System, *Proceedings of the Particle Accelerator Conference* (Washington, D. C., March 1987).

[11] S. Kheifets *et al.*, SLAC-PUB-4013 (1987).

[12] R. H. Helm and H. Wiedemann, PEP-Note-303 (1979).

[13] K. L. Brown, SLAC-PUB-2257 (1979).

[14] K. L. Brown, SLAC-PUB-4159 (1987), and R. Erickson, SLAC-PUB-4479 (1987).

[15] K. L. Brown *et al.* SLAC-91, Rev. 2, May 1977.

[16] The first of the references in [14].

[17] J. J. Murray and T. Fieguth, MURTLE, Private Program.

[18] K. Bane, Wake-field Effects in a Linear Collider, IEEE Trans. Nucl. Sci. **NS-32**, 1662 (1985).

[19] E. D. Courant and H. S. Snyder, Ann. of Phys. 3, 1-48 (1958)

[20] H. Goldstein, Mécanique Classique, Presse Universitaire de Franse. (1964).

[21] L. Rivkin, Damping Ring for the SLAC Linear Collider, PhD Thesis, CalTech (1986).

[22] See for example: B. Richter et R. Stiening, SLAC-PUB-4376 (1987).

[23] Jacques Haïssinski, A technique for Correcting the Betatron Tunes of the SLC Arcs, Presented at the Particle Accelerator Conference, Chicago (1989).

[24] M. Sands and N. Toge, Private Communication, (Summer 1987)